APPLICATION OF A CLASSICAL VARIATIONAL THEORY OF CHEMICAL REACTION RATES TO THE $F + H_2 \rightarrow FH + H$ AND $F + DH \rightarrow FD(FH) + H(D)$ REACTIONS

by

Irina Rutenburg

A dissertation submitted to the Graduate Faculty in Chemistry in partial fulfillment of the requirements for the degree of Doctor of Philosophy, The City University of New York.

1995

This manuscript has been read and accepted for the Graduate Faculty in Chemistry in satisfaction of the dissertation requirement for the degree of Doctor of Philosophy.

June 20, 1995
Date

Gerald Koerner
Chair of Examining Committee

June 20, 1995
Date

Richard Pike
Executive Officer

Supervisory Committee

The City University of New York

ABSTRACT

APPLICATION OF A CLASSICAL VARIATIONAL THEORY OF CHEMICAL REACTION RATES TO THE $F + H_2 \rightarrow FH + H$ AND $F + DH \rightarrow FD(FH) + H(D)$ REACTIONS

by

Irina Rutenburg

Adviser: Professor Gerald W. Koeppl

The classical variational theory of chemical reaction rates gives the rate as the equilibrium flux of phase points through a trial surface in the phase space of the reaction system. The surface divides phase space into reactant and product regions and is varied to obtain a minimum upper bound for the rate of product formation. For bimolecular reactions of the type $A + BC \rightarrow AB + C$, Koeppl derived expressions for the microcanonical and canonical formulations of this theory which give the energy–dependent mean reaction cross section and canonical rate constant, respectively, for the most general dividing surface defined by configuration space coordinates [J. Chem. Phys. 87, 5746 (1987)]. A numerical method which used the downhill simplex algorithm was developed to evaluate these quantities by determining coefficients (variational parameters) of terms in first, second, and third–order expansions of the dividing surface in the internal coordinates of the reaction system. The variational dividing surface so obtained defines a generalized transition state of the reaction system.

We present results for the application of this theory to the $F + H_2 \rightarrow FH + H$ reaction for a series of potential energy functions in which the relationship between the angle dependent minimum potential energy for reaction and orientation angle of

reactants varies systematically. Results are presented for a series of planar and curved dividing surfaces. The relationship between variational canonical rate constants and features of the potential energy function and features of different formulations of the dividing surface are studied.

We also present results for the first application of this variational theory to a reaction with a heteronuclear diatomic reactant. Several formulations of the dividing surface were used to study the F + DH → FD(FH) + H(D) reactions. The best results were obtained for DS formulations which contain variational parameters which distinguish between reaction at each end of the heteronuclear reactant.

For both reactions, plots of the flux through variational dividing surfaces, that is, reactivity relief maps for transition state configurations of the reaction system, are used to describe the dynamical stereochemistry of the subject reactions. The accuracy of variational results for the variation of reactivity with orientation angle of the transition state is studied by comparing variational and classical mechanical trajectory results.

ACKNOWLEDGEMENTS

There are no words that can express my profound gratitude to my thesis adviser Dr. Gerald Koeppl who greatly assisted me with my research. He has been a tremendous influence to me both personally and professionally and has given me a deeper understanding of science. Dr. Koeppl has exemplified extreme dedication, loyalty and patience in support of my thesis. The arduous task of writing this thesis could not have been accomplished without his guidance, leadership, instruction and most importantly encouragement.

I am very grateful to all of my committee members for their valuable suggestions and constructive discussions which helped to clarify my research. Dr. Richard Pizer has provided continued backing and direction in allowing me to view the physical aspect of science in comparison with the mathematical one. His thoughts and suggestions have been instrumental in the preparation of my thesis. Dr. Johna Leddy, a former committee member, has given much of her time and energy in support of my studies. My relationship with her had a great impact on me both personally and as a scientist. Dr. Gary Quigley unfortunately had to endure the stress and pressure of a short–notice defense date. His ideas are unusual and interesting but most of all appreciated.

Drs. Raymond Disch and Jerome Schulman deserve special acknowledgement for their impressive wisdom and consistent altruism in support of my academic aspirations. I am very grateful for their generosity and patience in sharing their office and microcomputer with me.

I would like to express many thanks to Cordella Stokes for her exceptional organizational skills and personal warmth. I am immensely grateful to Michelle Sedlitz for her enormous help in verifying my English and formatting my thesis. Their laborious efforts proved to be a tremendous asset to me.

I thank John Leong and Rosemary Caruso for their assistance in my work with the VAX minicomputer at Queens College. I thank Lawrence Leung and Steven Tysoe for their help in my work with IBM and Mackintosh microcomputers. I thank Dr. Robert Bittman for teaching me how to conduct literature searches and Gail Ronnermann for assisting me in the most difficult cases. I thank Drs. Arthur Baker and Thomas Strekas for their valuable discussions on different topics in chemistry. I thank Dr. Wilma Saffran for lending me her books, sharing a conference table with me, and personal support. I thank Dr. William Berkowitz for his assistance in my preparation for the second level examinations and a lot of personal help. I thank Randolph Smith for making slides for my seminar.

I would like to thank Judy Waldman of The Graduate School and University Center of The CUNY Library for her patience and flexibility.

In addition, I would like to thank the following people who have given me the confidence as well as personal and professional assistance to complete my academic endeavor:

the entire 1993 – 95 faculty of Department of Chemistry at Queensborough Community College;

the following faculty of Department of Chemistry and Biochemistry at Queens College – Drs. George Axelrad, Maxwell Eidinoff, Robert Engel, Harry Gafney, Norman Goldman, Lawrence Gries, Elie Hayon, David Locke, Marjorie Navidi, Gertrude Rothman, Burton Tropp;

the following staff of Department of Chemistry and Biochemistry at Queens College – Maria Cardenas, Jeanne Deutsch, Charles Ezeude, Diane Fiorito, Thomas Hayden, Leon Katz, Shirley Lichtig, Adrian Robertson;

the following faculty of Queens College – Drs. Martin Braun, Eugene Don, Elliott Mendelson, Nick Metas, Uldis Roze, Alan Sultan, David Tischler, Sol Weintraub;

the following staff of Queens College – Catherine Farley, Kathryn Grosso–Hank, Eleanor Kirstein, Sarah Knecht, Sydney Lefkoe, Elizabeth Mandel, Ellen Rondot;

my fellow students, instructors, and colleagues – Alex Altman, Arthur Barlow, Joel Blickstein, John Boulous, Yael Fuchs, Ross Greenberg, Steve Greenberg, Pauline Hamilton, Sheldon Heber, Isaac Landau, George Lyons, Rose Massiah, Edgar Mendoza, Mitchell Miller, Robert Morgan, Tony Nicolas, Susie Niess, Marina Isakov–Peredo, Dr. Isaac Sasson, Martin Schneiderman, Michael Sommer, Dr. Daniel Sverdlik, Cherryl Tihal, Dr. Catherine Vilcheze, James Vito, Patricia Waters, Phyllis Wilson;

my friends, relatives, and others – Joseph Bambara, Jacqueline Beukelaer, James and Jennie Beukelaer, Jacob and Marina Brusin, Louise Cazuto, Rose Chao, Dr. Arnold Dornberg, Israel and Rita Gitlin, Arkady and Tatiana Katsnelson, Alexander and Anna Lanskoy, Dr. Jacqueline Maier, Elena Neivelt, Charles and Maria Rosenberg, William and Renee Stern, Larisa Surazsky, Michael Surazsky, Sofia Yerikhova, Boris and Helen Zapesochny, Penny Stern and Paul Zarowin, Marianna Zavel, Michael and Raisa Zilberman, my special friends–colleagues from HIAS; and many more.

Special credit should be given to those whose help and encouragement have been invaluable to me:

Dr. Beatrice Arnowich, Joseph Badalamenti, Janine Beukelaer and Declan O'Reilly, Alice Brickman, Joseph DeLuca, Drew Dillon, Richard Francis, Pedro and Patricia Irigoyen, Theresa Johnson, Thomas and Janet Joyce, Claude Masse, Jeffrey and Rosalie Peck, Clair Rosenblatt, Helga De Szalay, David Wilson, Eugene Wolkow, Robert Wurman.

Finally, I would like to express my deepest gratitude to my husband, Lev Rutenburg, for all his support and endurance. Over the years he has been working hard, helping and suffering with me through my entire ordeal.

To the memory of

my mother,

her brother, their parents,

my great aunt, father–in–law,

and Vingi

TABLE OF CONTENTS

LIST OF FIGURES

LIST OF TABLES

CHAPTER 3

CHAPTER 4

CHAPTER 5

INTRODUCTION

The Classical Variational Theory of Chemical Reaction Rates gives the rate as the equilibrium flux of reaction systems through a trial surface. This theory was introduced by Pelzer and Wigner[1], and developed and generalized further by Horiuti[2], Keck[3,4], Marcus[5], Koeppl[6,7], Pechukas[8–10] and Pollak[11], Truhlar and co–workers[12–14], and others[15–17]. The study and development of this theory in its various forms continues to be an active area of research[18–26]. In the most general development of the theory by Keck, the trial surface divides the phase space of the reaction system into reactant and product regions. The trial surface is usually referred to as a dividing surface (DS). In practice, the theory is nearly always applied using a DS which is a function of the internal coordinates of the reaction system, that is, configuration space coordinates. The Transition State Theory (TST) of Chemical Reaction Rates is a special case of the variational theory. The conventional version of TST, developed by Eyring[27] and coworkers[28] and Evans and Polanyi[29] gives the reaction rate for a particular DS[4,30]. This DS passes through a saddle point of the potential energy surface and is perpendicular to the transition state's unbound normal coordinate.

The variational rate, that is, the equilibrium flux of reaction systems through a particular DS, is an upper bound because phase points which start in the reactant region of configuration space can cross and recross the DS regardless of whether they proceed ultimately to the product region. Furthermore, phase points which do not originate in the reactant region, but are present in the equilibrium flux, can cross and recross the DS. Fig. 1 shows how trajectories in an equilibrium sample contribute to the variational rate. Trajectories are shown by horizontal lines. Surfaces in the configuration space of the reaction system are shown by vertical lines. Reactant configurations lie to the left of the surface labeled reactants;

FIGURE 1

Illustration of a sample of trajectories which shows how an equilibrium flux of reaction systems through dividing surface (DS) contributes to the variational rate.

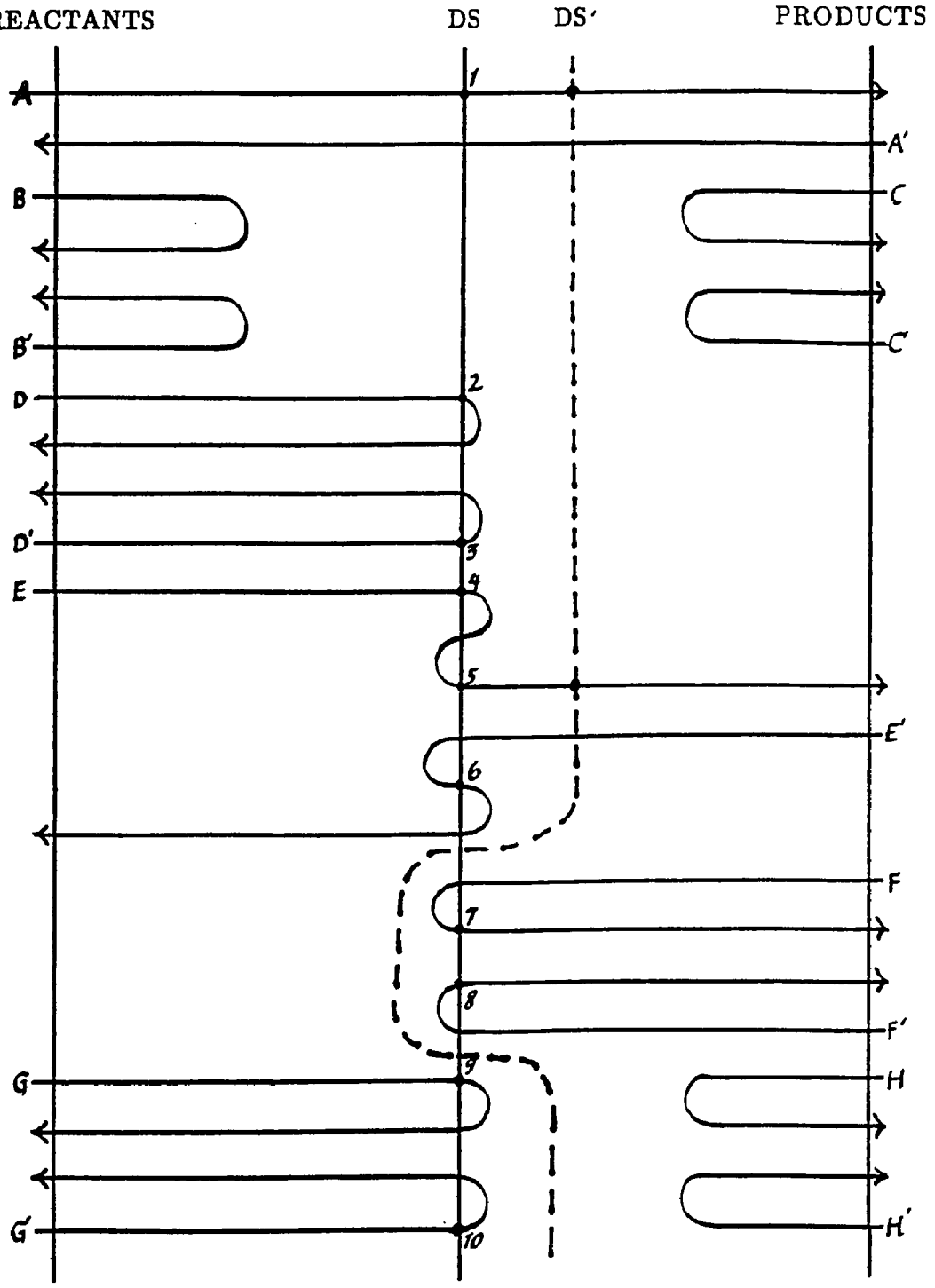

product configurations lie to the right of the surface labeled products. Configurations on the surface labeled DS correspond to generalized transition states of the chemical reaction. Crossings of the DS in the direction of products are numbered. Only two trajectories in the sample (labeled A and E) are reactive; yet there are ten crossings of the DS by trajectories moving toward the product region. Trajectories labeled with a prime represent the microscopic reverse of trajectories with unprimed labels. For the dividing surface labeled DS and sample of trajectories shown, the variational theory overestimates the rate by a factor of 5. Figs. 2 and 3 will help the reader understand Fig. 1. Fig. 2 shows configuration space plots of classical trajectories of types shown in Fig. 1 for the collinear atom–diatom reaction A + BC → AB + C. The trajectories are plotted using Eyring's skewed and scaled coordinates[31]; see Fig. 3. Several potential energy contours are also shown. The reactant (BC) valley is in the lower right hand corner of the potential energy plots.

The DS can be varied to obtain a minimum upper bound for the reaction rate. The variational rate will equal the actual rate of reaction if the DS is crossed only once by all reactive trajectories. For example, the variational rate for the sample of trajectories shown in Fig. 1 for the dividing surface labeled DS′ equals the actual rate. For a classical microcanonical formulation of the variational theory, the reaction rate corresponds to an ensemble of reaction systems of fixed total energy E. It is possible to find DSs at energies up to some value E′ which give the actual rate[32]. For the classical canonical formulation of the variational theory, the rate corresponds to an ensemble of reaction systems for temperature T which contains trajectories with energies above E′; hence, it is impossible to find a DS which gives the actual rate.

The accuracy of the classical variational theory for a given DS can be determined by comparing variational values of the canonical rate constant at a given temperature or energy dependent mean reaction cross section at a given

FIGURE 2

Illustration of types of trajectories shown in Fig.1 plotted on the collinear potential energy surface. See Fig.3 for a description of the coordinate system.

Fig.2a: Direct trajectory of type A

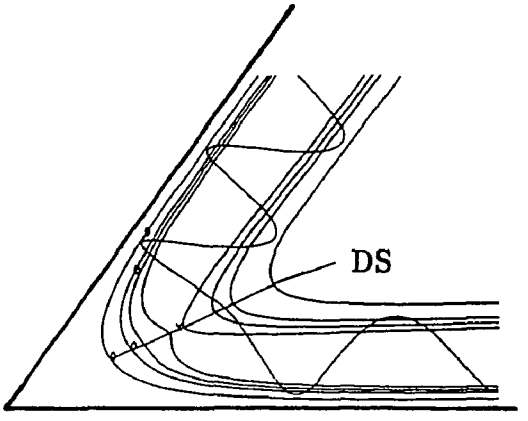

Fig.2b: Reflected trajectory of type B

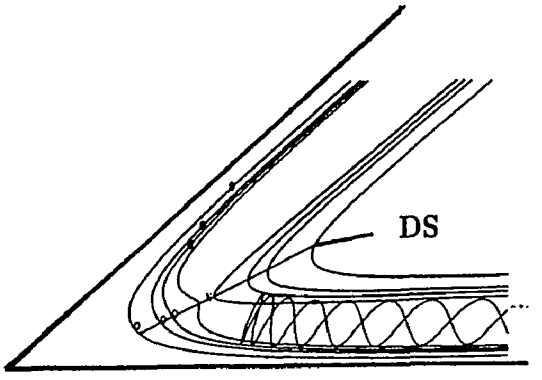

Fig.2c: Reflected trajectory of type D

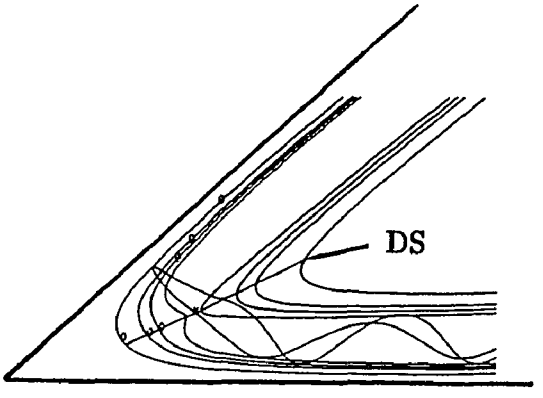

Fig.2d: Indirect reactive trajectory of type E

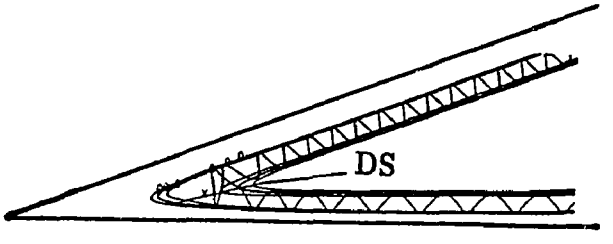

DS – dividing surface

FIGURE 3

Eyring's mass scaled and skewed coordinates for the collinear potential energy surface of a typical $A + BC \rightarrow AB + C$ reaction system. See Ref. 31.

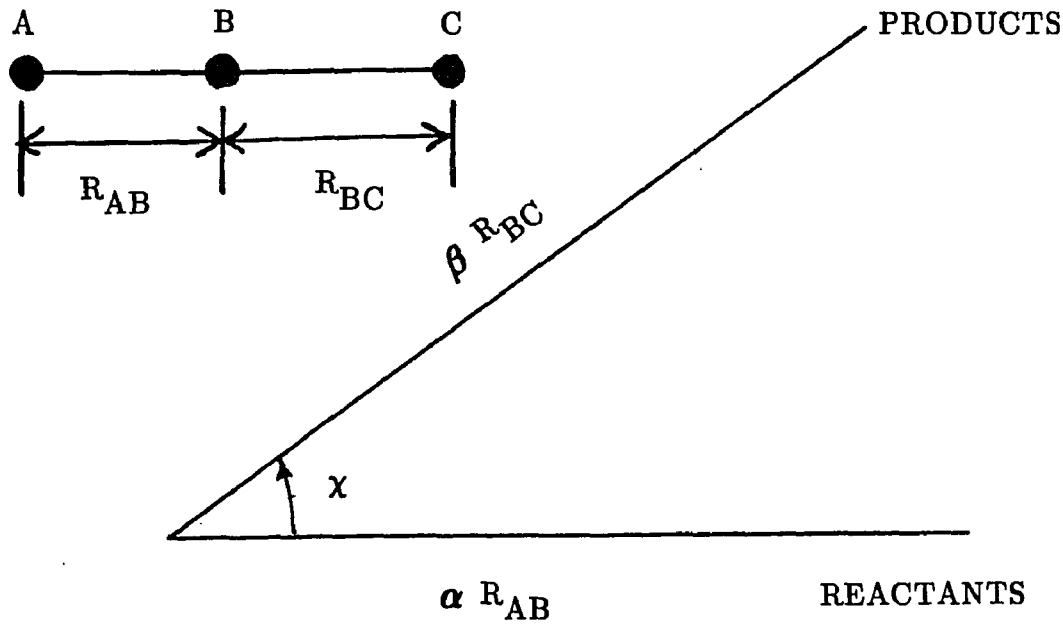

m_A, m_B, and m_C are masses of atoms A, B, and C
R_{AB} – internuclear distance for AB diatomic product
R_{BC} – internuclear distance for BC diatomic reactant

$$\alpha = m_A(m_B+m_C)/M$$
$$\beta = m_C(m_A+m_B)/M$$
$$M = m_A+m_B+m_C$$
$$\cos\chi = \{m_A m_C/[(m_A+m_B)(m_B+m_C)]\}^{1/2}$$

energy with corresponding values calculated by executing a Monte Carlo sample of classical mechanical trajectories. The same Born Oppenheimer potential energy function must be used for the variational and trajectory calculations. Morokuma and Karplus[33] and Koeppl and Karplus[34] were the first to determine the accuracy of TST in this unequivocal manner for collinear reactions and reactions in 3–dimensional space, respectively. In a theory versus experiment test of the accuracy of TST, one cannot be sure whether error is caused by failure of the variational theory or inaccuracy of the potential energy function.

The Born Oppenheimer potential energy function for a given electronic state of the chemical reaction system is often referred to as a potential energy surface (PES). For a collinear atom–diatom reaction, a trajectory can be plotted as a mass point moving on the potential energy surface[31]. In most applications of classical variational and trajectory theories, it is assumed that reaction takes place on the potential energy surface for the electronic ground state of the reaction system, i. e., the electronic state does not change during the chemical reaction.

Koeppl developed a general classical variational treatment for atom–diatom reactions[7]. Koeppl's formulation of the variational theory is based on a method developed by Martin and Raff[35]. He derived expressions for the microcanonical and canonical formulations of this theory which give the energy–dependent mean reaction cross section and canonical rate constant, respectively, for the most general dividing surface defined by configuration space coordinates. A numerical method which uses the downhill simplex algorithm was developed to evaluate these quantities by determining coefficients (variational parameters) of terms in first, second, and third order expansions of the dividing surface in the internal coordinates of the reaction system. Koeppl and Sverdlik applied this treatment to the $H' + HH \rightarrow H'H + H$ and $H + I_2 \rightarrow HI + I$ reactions[36].

In the present work, we apply the general classical variational formulation

developed by Koeppl to the $F + H_2 \rightarrow FH + H$ and $F + DH \rightarrow FD(FH) + H(D)$ reactions.

Levine and co–workers[37,38] and others[39,40] have used the concept of an orientation dependent critical configuration for reaction and other concepts to characterize the dynamic stereochemistry of atom–diatom reactions. Koeppl's power series formulation of the dividing surface contains angle dependent terms, i. e., terms containing the angle θ which the H_2 internuclear axis makes with a line from atom F to the center–of–mass of H_2. These terms make it possible to use the variational theory, instead of the implied DS used by Levine, to characterize the dynamic sterochemistry of atom–diatom reactions in a new and useful way. This can be done by plotting contours of the variational flux through the angle dependent dividing surface. The variational flux can be displayed using contours which depend on internal coordinates θ and R; R is the distance between F and the center of mass of H_2. We call these plots reactivity relief maps. The dynamic stereochemistry can also be characterized by dividing the full range of orientation angle θ (0 to π) into equal intervals and calculating the contribution to the canonical rate constant or energy dependent mean reaction cross section for each interval to show how this quantity varies with θ, i. e., show how the reactivity varies with the orientation angle.

The $F + H_2$ and F + DH reactions were chosen because they have been the subject of many theoretical and experimental studies. Many attempts have been made to calculate an accurate potential energy function for this reaction[41–49]. These attempts represent an ongoing effort to find a potential energy function which can be used to calculate theoretical results which are in agreement with experimental values, for example, variational theory rate constants and more detailed results which can be compared to molecular beam data[50–68]. We performed classical variational calculations for two potential energy functions

developed by Truhlar and co–workers[43] (designated T1 and T2) and one of our own designated KR.

We are not concerned with comparing theoretical and experimental rate constants in the present work. The T1 and T2 potential energy functions cited above yield variational rate and semi–classical trajectory rate constants which are in reasonable agreement with experiment[43,51,52]. We are concerned instead at this stage of our work with the relationship between classical variational results and features of reasonable potential energy functions for the $F + H_2$ reaction, and using the variational theory to characterize the dynamic stereochemistry for these potential energy functions. We are interested in seeing how the subtle differences between potential energy functions are reflected in reactivity relief maps and the variation of reactivity with orientation angle. We are also interested in the relationship between the accuracy of the classical variational theory, i. e., the accuracy of the no recrossing assumption of transition state theory, for a given reasonable potential energy function and the temperature for a canonical ensemble and energy for a microcanonical ensemble of reaction systems. We determine this accuracy in the present work by comparing variational and classical mechanical trajectory results for the same potential energy function. We are also interested in how the accuracy of the classical variational theory and variational portraits of dynamic stereochemistry for atom–diatom reactions depend on features of the potential energy function and different formulations of the dividing surface. We will learn about these matters before we develop and apply a semi–classical formulation of the general variational theory which makes theory and experiment comparisons more meaningful.

We chose the F + DH → FD(FH) + H(D) reactions to apply Koeppl's variational treatment to a reaction with a heteronuclear reactant. We use dividing surfaces of the types used to study the $F + H_2$ reaction and new formulations of the

dividing surface which contain parameters which distinguish between reaction at each end of the reactant. We examine the conditions which must be satisfied to obtain variational energy dependent mean reaction cross sections and practical variational rate constants for reaction at each end of the reactant for a continuous DS which spans the range in θ from 0 to π.

Chapter 1 presents a brief derivation of equations for the canonical rate constant and microcanonical mean reaction cross section for a general configuration space DS. The derivation follows the more detailed derivation given by Koeppl[7].

Chapter 2 presents expressions for dividing surfaces used in the present work and corresponding expressions for the canonical rate constant and energy dependent mean reaction cross section. Expressions for potential energy surfaces are given. The numerical methods used in this work are also described.

Chapter 3 presents canonical variational results for the F + H_2 reaction. Features of the potential energy functions are discussed. Results which describe the relationship between variational rate constants and features of the three potential energy functions are presented. Features of the dividing surface functions are discussed. Results which describe the relationship between variational rate constants for the same potential energy function and different formulations of the dividing surface are presented. Methods used to generate initial vertices for simplex searches are described. The effect of restrictions on variational parameters for quadratic and cubic formulations of the DS is described. Variational results are presented for 300, 1500, and 3000 K.

Chapter 4 presents canonical variational results for the F + DH reactions for the T1 potential energy function, the intermediate potential energy function in the series used in this work. Variational results are presented for the quadratic formulations of the dividing surface which were used to study the F + H_2 reaction, and new quadratic and cubic formulations which contain parameters which

distinguish between reaction at each end of the heteronuclear reactant. Variational rate constants are presented for 300, 600, 1500, and 3000 K.

In Chapter 5, classical variational values of the energy dependent mean reaction cross section are compared with classical trajectory values for the T1 potential energy function to determine the accuracy of the variational theory at several values of the reaction energy. Results are presented for both the $F + H_2$ and F + DH reactions. Energy dependent plots of the distribution of reactivity over θ given by the classical variational and trajectory theories are also compared.

Summary and conclusions are presented in Chapter 6.

Appendices contain variational and least squares fit dividing surface parameters corresponding to the rate constants given in Tables in Chapters 3 and 4. Appendices 1 – 23 contain dividing surface parameters for the $F + H_2$ reaction. Appendices 24 – 40 contain dividing surface parameters for the F + DH reactions.

CHAPTER 1

DERIVATION OF GENERAL EQUATIONS FOR THE CLASSICAL VARIATIONAL CANONICAL RATE CONSTANT AND MICROCANONICAL MEAN REACTION CROSS SECTION

Koeppl[7] applied Keck's classical variational theory of chemical reaction rates to reactions between an atom and a diatomic molecule:

$$A + BC \rightarrow AB + C .$$

A sketch of the derivation of general equations for the canonical rate constant and energy dependent mean reaction cross section is presented in this chapter. These equations were used to calculate results presented in this thesis. See particularly equations 21 and 43. The derivations assume that electronic transitions do not occur during reaction, nuclear motion is governed by the laws of classical mechanics, and the potential energy function is given by the Born–Oppenheimer approximation.

I. CANONICAL FORMULATION

Derivation of the bimolecular rate constant for the generalized dividing surface

The exact classical rate constant is given by[4,8,32,80–83]

$$k_{exact}(T) = Q_{\rho_s}(T)^{-1} \cdot \int d\tau \, \mathbf{v}\cdot\mathbf{n_S} \, \chi_S(\mathbf{q},\mathbf{p}) \, \delta[S(\mathbf{q},\mathbf{p})] \exp[-\beta H(\mathbf{q},\mathbf{p})], \qquad (1)$$

where $Q_{\rho_s}(T)$ is the classical partition function per unit volume for the internal degrees of freedom of the reactants times Planck's constant (h) to the sixth power, T is Kelvin temperature, $\int d\tau$ is an integral operator which sums the flux over the twelve internal (center–of–mass) degrees of freedom of the phase space of the reaction system, $\mathbf{v}$ is the generalized velocity of a phase point, $\mathbf{n_S}$ is the unit vector

normal to the dividing surface, $\chi_S(q,p)$[8,80–82] is the characteristic function defined below, **q** and **p** are the coordinates and momenta of phase space, the delta function $\delta(S)$ restricts the integration to the eleven dimensional phase space surface defined by $S(\mathbf{q},\mathbf{p}) = 0$, $\beta = (k_B T)^{-1}$, where k_B is Boltzmann's constant and T is the Kelvin temperature, $H(\mathbf{q},\mathbf{p})$ is the classical Hamiltonian of the reaction system, $\chi_S(\mathbf{q},\mathbf{p})$ is the characteristic function for the surface: it is +1 for phase points which cross the surface in the direction of products and were on the reactant side of the surface in the asymptotic past, –1 for phase points which cross the surface in the direction of reactants and were on the reactant side in the asymptotic past, and zero otherwise. The critical assumption of variational TST may be expressed as

$$\begin{aligned} \chi_S(\mathbf{q},\mathbf{p}) &= \chi_S^{TST}(\mathbf{q},\mathbf{p}), \\ &= \mathcal{H}(\mathbf{v}\cdot\mathbf{n}_S), \end{aligned} \tag{2}$$

where χ_S^{TST} is the characteristic function of TST and $\mathcal{H}(x)$ is the Heaviside step function, that is, $\mathcal{H}(x) = 1$ for $x > 0$ and $\mathcal{H}(x) = 0$ for $x < 0$. Hence, TST assumes all phase points which move toward products at the dividing surface contribute to the rate. Since the integral operator $\int d\tau\, \delta(S)$ equals $\int d\sigma$ where $d\sigma$ is the eleven–dimensional element of reduced phase space of the surface, substitution of Eq. (2) in (1) gives Keck's expression for the variational rate constant[4] of transition state theory (TST):

$$k(T) = Q_{\rho_S}(T)^{-1} \int d\sigma\, \mathbf{v}\cdot\mathbf{n}_S\, \mathcal{H}(\mathbf{v}\cdot\mathbf{n}_S) \exp[-\beta H(q,p)]. \tag{3}$$

The required integrals may be evaluated by using spherical polar coordinates. The relative Cartesian coordinates of atom C with respect to atom B (Q_1,Q_2,Q_3) and atom A with respect to the center of mass of atoms B and C (Q_4,Q_5,Q_6) define vectors **r** and **R**, respectively. Vectors **r** and **R** are also defined by the spherical polar coordinates (r,θ,ϕ) and (R,Θ,Φ), respectively, shown in Fig. 4; the corresponding conjugate momenta are (P_r,P_θ,P_ϕ) and (P_R,P_Θ,P_Φ). The classical Hamiltonian

FIGURE 4

Spherical polar coordinate system. This figure is Martin and Raff's (Ref.35) Fig.1.

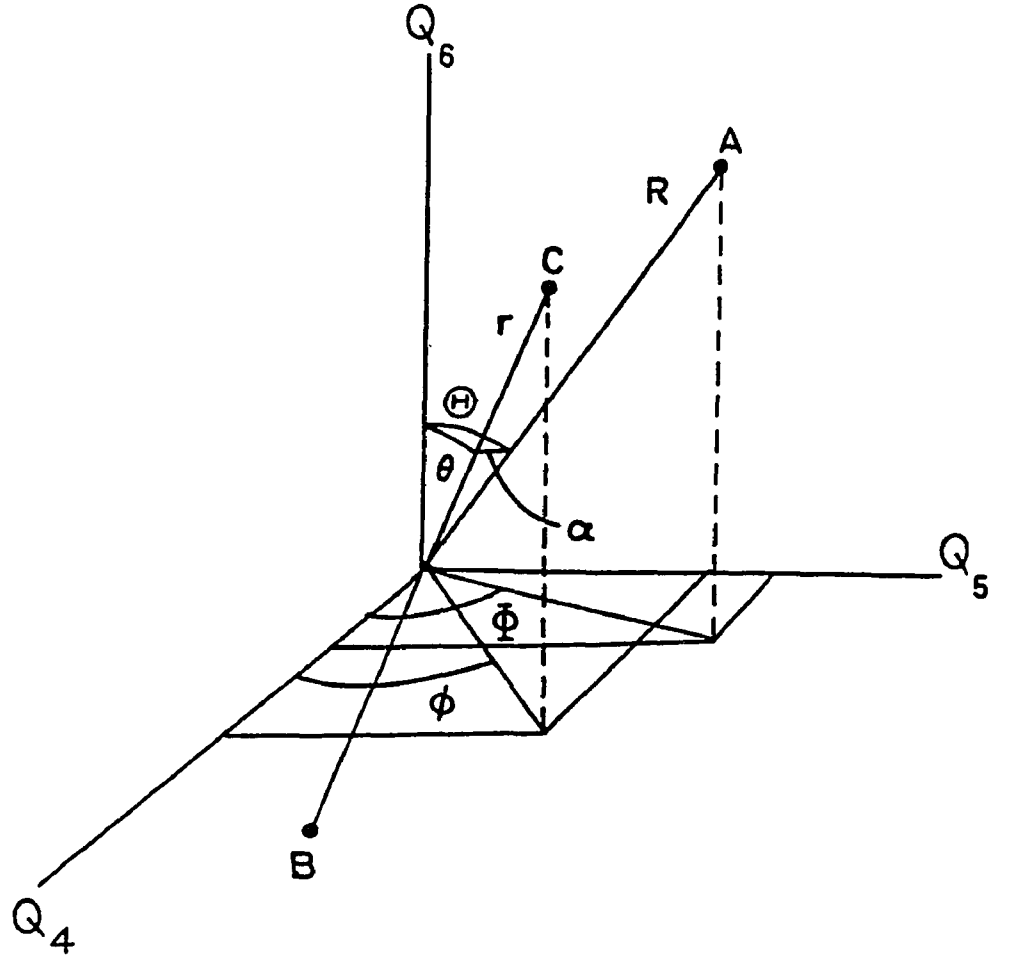

Q_1, Q_2, Q_3 – relative Cartesian coordinates of atom C with respect to the atom B

r, θ, ϕ – corresponding spherical polar coordinates

Q_4, Q_5, Q_6 – relative Cartesian coordinates of atom A with respect to the center of mass of atoms B and C

R, Θ, Φ – corresponding spherical polar coordinates

α – the angle defined by vectors **r** and **R**

expressed in spherical polar coordinates is

$$\begin{aligned} H &= (2\mu_{BC})^{-1} (P_r^2 + P_\theta^2/r^2 + P_\phi^2/r^2\sin^2\theta) \\ &\quad + (2\mu_{A,BC})^{-1} (P_R^2 + P_\Theta^2/R^2 + P_\Phi^2/R^2\sin^2\Theta) + V(r,R,\alpha), \\ &= \mathcal{T} + V(r,R,\alpha), \end{aligned} \tag{4}$$

where μ_{BC} and $\mu_{A,BC}$ are the reduced masses of the (BC) and (A,BC) atom groups, respectively, α is the angle defined by vectors $\mathbf{r}$ and $\mathbf{R}$, $\mathcal{T}$ is the internal kinetic energy of the reaction system, and $V(r,R,\alpha)$ is the potential energy of the reaction system. The classical partition function per unit volume for the internal degrees of freedom of the reactants times Planck's constant to the sixth power is given by

$$Q_{\rho_s}(T) = \gamma^{-1} \int_{\Gamma} \cdots\cdots\cdots \int \exp(-\beta H_{\rho_s}) \prod_{i=1}^{6} dq_i^{sp}\, dp_i^{sp}, \tag{5}$$

where γ is the normalization volume of configuration space, Γ is the volume of the internal phase space of the reactants, H_{ρ_s} is the classical Hamiltonian for the internal degrees of freedom of the reactants on the reaction shell radius (ρ_s), ($\mathbf{q}^{sp},\mathbf{p}^{sp}$) are the spherical polar coordinates and momenta. At the reaction shell radius, the distance between the reactants ($R = \rho_s$) is large enough to ensure that the potential energy of interaction is negligible. The classical Hamiltonian H_{ρ_s} is given by

$$\begin{aligned} H_{\rho_s} &= \mathcal{T}_{\rho_s} + V_{\rho_s}(r) \\ &= (2\mu_{BC})^{-1} (P_r^2 + P_\theta^2/r^2 + P_\phi^2/r^2\sin^2\theta) \\ &\quad + (2\mu_{A,BC})^{-1} (P_{\rho_s}^2 + P_\Theta^2/\rho_s^2 + P_\Phi^2/\rho_s^2\sin^2\Theta) + V_{\rho_s}(r), \end{aligned} \tag{6}$$

where $\mathcal{T}_{\rho_s}$ is the internal kinetic energy of reactants on reaction shell radius, and $V_{\rho_s}(r)$ is large R limit of potential energy for reaction system.

The most general dividing surface may be defined by

$$S(\mathbf{q},\mathbf{p},\boldsymbol{\Omega}) = 0, \tag{7}$$

where S depends on both the configuration (q) and momentum(p) coordinates of phase space and a set of constants and arbitrary variational parameters $(\Omega)^4$. Constants of motion are parameters when the surface depends on momentum as well as configuration coordinates.

We consider the case where the surface depends only on configuration coordinates; that is, the internal coordinates of the reaction system, and is therefore independent of constants of motion in the canonical formulation of the variational theory. A surface defined by internal coordinates depends on the total energy of the reaction system in the microcanonical formulation of the variational theory. The most general surface of this type for the reaction considered here may be expressed as

$$S = r - F(R,\theta) - C = 0, \tag{8}$$

where C is a variational parameter and the function $F(R,\theta)$ depends on additional variational parameters. The internal coordinates that define the dividing surface are shown in Fig. 5. The defining function $F(R,\theta)$ is not completely arbitrary. It must define a surface which provides an unambiguous division of configuration space into reactant and product regions; that is, a surface which is crossed by all reactive trajectories. It is convenient to choose a set of generalized coordinates (q) that makes S a coordinate surface for one of them. Hence we transform from $(r,\theta,\phi,R,\Theta,\Phi)$ space to $(q_*,V,U,\phi,\Theta,\Phi)$ space. The generalized coordinates and their conjugate momenta are

$$q_1 = r - F(R,\theta) = q_*,$$
$$p_1 = P_{q_*}, \tag{9}$$
$$q_2 = R = V,$$
$$p_2 = P_V, \tag{10}$$
$$q_3 = \theta = U,$$

FIGURE 5

Internal coordinates that define dividing surface
for A + BC → AB + C reaction.

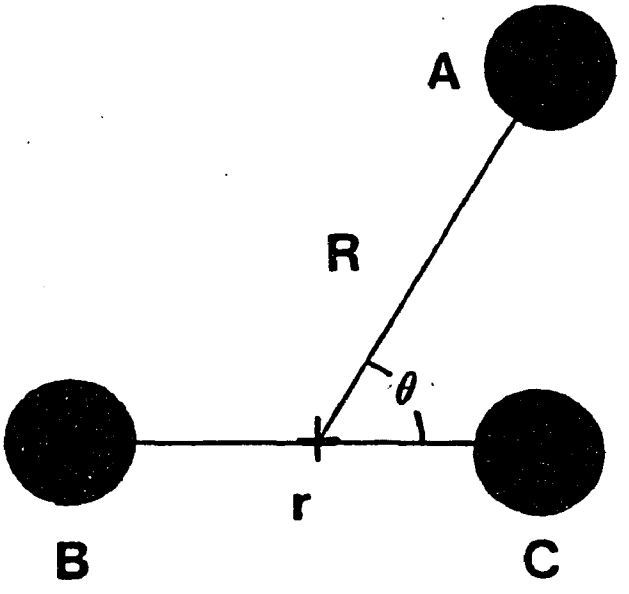

r – internuclear distance for BC molecule

R – distance from atom A to the center of mass (+) of BC molecule

θ – angle of approach of atom A to BC molecule

$$p_3 = P_U, \tag{11}$$

$$q_4 = \phi,$$

$$p_4 = P_\phi, \tag{12}$$

$$q_5 = \Theta,$$

$$p_5 = P_\Theta, \tag{13}$$

$$q_6 = \Phi,$$

$$p_6 = P_\Phi. \tag{14}$$

Coordinate q_* is the generalized reaction coordinate of transition state theory; that is, $q_* = C$ together with $F(R,\theta)$ defines the generalized transition state.

Koeppl used these generalized coordinates and their conjugate momenta to express Eq. (3) as

$$k(T) = Q_{\rho_s}(T)^{-1} \int \cdots\cdots\cdots \int (dq_*/dt)\, \mathcal{K}(dq_*/dt) \exp(-\beta H) \times dV\, dU\, d\phi\, d\Theta\, d\Phi\, dP_{q_*} dP_V\, dP_U\, dP_\phi\, dP_\Theta\, dP_\Phi. \tag{15}$$

The reduced Hamiltonian for the dividing surface is given by

$$\begin{aligned} H = {} & \Big[(2\mu_{BC})^{-1} \{ 1 + [F_U(V,U)/r(q_*,V,U)]^2 \} \\ & + (2\mu_{A,BC})^{-1} F_V(V,U)^2 \Big] P_{q_*}{}^2 \\ & - [F_U(V,U)/\mu_{BC} r(q_*,V,U)^2]\, P_{q_*} P_U - [F_V(V,U)/\mu_{A,BC}]\, P_{q_*} P_V \\ & + (2\mu_{A,BC})^{-1} P_V{}^2 + [2\mu_{BC} r(q_*,V,U)^2]^{-1} P_U{}^2 \\ & + [2\mu_{BC} r(q_*,V,U)^2 \sin^2 U]^{-1} P_\phi{}^2 + (2\mu_{A,BC} V^2)^{-1} P_\Theta{}^2 \\ & + (2\mu_{A,BC} V^2 \sin^2\Theta)^{-1} P_\Phi{}^2 + V[r(q_*,V,U),V,\alpha], \end{aligned} \tag{16}$$

where $F_V(V,U) = F_R(R,\theta)$ and $F_U(V,U) = F_\theta(R,\theta)$ are the partial derivatives of function $F(R,\theta)$ with respect to R and θ, respectively. The function $Q_{\rho_s}(T)$ is given by

$$Q_{\rho_s}(T) = \gamma^{-1} \int_{-\infty}^{+\infty} \int_{-\infty}^{+\infty} \int_{-\infty}^{+\infty} \int_{-\infty}^{+\infty} \int_{-\infty}^{+\infty} \int_{-\infty}^{+\infty} \int_{0}^{2\pi} \int_{0}^{\pi} \int_{0}^{r_{max}^{BC}} \int_{0}^{2\pi} \int_{0}^{\pi} \int_{0}^{\rho_s} \prod_{i=1}^{6} dp_i^{sp}\, dq_i^{sp}$$
$$\times \exp(-\beta H_{\rho_s}), \tag{17}$$

where r_{max}^{BC} is a practical limit for r which is required due to the finite limit for the potential energy of reactant BC at dissociation, the normalization volume γ is

$$\gamma = \int_0^{2\pi} \int_0^{\pi} \int_0^{\rho_s} \sin\Theta\, R^2\, d\Phi\, d\Theta\, dR = (4/3)\pi\, \rho_s^{\,3}. \tag{18}$$

The evaluation of $Q_{\rho_s}(T)$ gives

$$Q_{\rho_s}(T) = 32\, \pi^4\, \beta^{-3}\, (\mu_{BC}\, \mu_{A,BC})^{3/2}\, D_{BC}^{c}(T)\, \sigma_{BC}^{\,-1}, \tag{19}$$

where the canonical reactant integral $D_{BC}^{c}(T)$ is given by

$$D_{BC}^{c}(T) = \int_0^{r_{max}^{BC}} r^2 \exp[-\beta V(r)]\, dr, \tag{20}$$

and σ_{BC} is the symmetry number of BC. Integration over all of the momenta of Eq. (15) and the variables ϕ, Θ, and Φ; the substitutions $V=R$ and $U=\theta$; and use of Eq. (19) give

$$k(T) = (2\pi/\beta)^{1/2}\, (\sigma_{BC}/\sigma_*)\, [N_*^{c}(T)/D_{BC}^{c}(T)], \tag{21}$$

where σ_* is the symmetry number for the reaction system on the dividing surface[4,84,85], and the quantity $N_*^{c}(T)$ is given by

$$N_*^{c}(T) = \int_0^{\pi} \exp\{-\beta V[r(\Omega,R,\theta),R,\theta]\} \sin\theta\, d\theta \int_0^{R_{max}^{S=0}} r(\Omega,R,\theta)^2\, R^2\, dR$$
$$\times \left[\mu_{BC}^{\,-1}\{1+[F_\theta(R,\theta)/r(\Omega,R,\theta)]^2\} + \mu_{A,BC}^{\,-1} F_R(R,\theta)^2\right]^{1/2}, \tag{22}$$

where the quantity $R_{max}^{S=0}$ is a practical limit for the integration over R which is required due to the finite limit for the potential energy as $R \to \infty$ on the dividing surface[35,86,87], and $r(\Omega,R,\theta)$ is the value of r on the DS which is defined by variational parameters (Ω) and the defining function $F(R,\theta)$.

II. MICROCANONICAL FORMULATION

Derivation of the mean reaction cross section for the generalized dividing surface

The canonical rate constant for the reaction A + BC → AB + C given by the collisional theory (CT) of chemical reactions[89–91] is

$$k_{CT}^{qm}(T) = (8\beta^3/\pi\mu_{A,BC})^{1/2}\,[Q_{BC}^{qpf}(T)]^{-1} \times \int_0^\infty \sum_{v,J} f_J\,(2J+1)\,S_r(E-E_{v,J},v,J)\,(E-E_{v,J})\exp(-\beta E)\,dE, \qquad (23)$$

where $Q_{BC}^{qpf}(T)$ is the vibration–rotation quantum partition function (qpf) for the diatomic reactant BC, f_J is the nuclear degeneracy of the state (v,J), E is the total internal energy of the reaction system, $E_{v,J}$ is the energy of the vibration–rotation state with vibrational and rotational quantum numbers v and J, respectively and $S_r(E-E_{v,J},v,J)$ is the total reaction cross section from initial state (v,J) with relative energy $(E-E_{v,J})$ to all possible final states. Eq. (23) was derived using initial–state Boltzmann distributions at temperature T. The designation qm indicates that the internal degrees of freedom of BC were treated quantum mechanically. The degrees of freedom for relative A–BC motion were treated classically.

Morokuma, Eu, and Karplus[89] defined a weighted mean reaction cross section $\bar{S}_r(E)$ and energy density function $\epsilon_{BC}^{qm}(E)$ as

$$\bar{S}_r(E) = [\epsilon_{BC}^{qm}(E)]^{-1} \sum_{v,J} f_J\,(2J+1)\,(E-E_{v,J})\,S_r(E-E_{v,J},\,v,J) \qquad (24)$$

and

$$\epsilon_{BC}^{qm}(E) = \sum_{v,J} f_J\,(2J+1)\,(E-E_{v,J})\,\mathcal{H}(E-E_{v,J}) \qquad (25)$$

where $\mathcal{H}(x)$ is the Heaviside step function

$$\mathcal{H}(x) = 1, \qquad x > 0 \text{ and}$$
$$\mathcal{H}(x) = 0, \qquad x < 0. \qquad (26)$$

Using these quantities, the rate constant may be expressed as

$$k_{CT}^{qm}(T) = (8\beta^3/\pi\mu_{A,BC})^{1/2} [Q_{BC}^{qpf}(T)]^{-1} \times \int_0^\infty \epsilon_{BC}^{qm}(E) \bar{S}_r(E) \exp(-\beta E)\, dE. \quad (27)$$

All of the equations above for the collisional theory rate constant pertain to a quantum mechanical treatment of the diatomic reactant BC. If the degrees of freedom of BC are treated classically, Eqs. (24), (25), and (27) give

$$k_{CT}^{cm}(T) = (8\beta^3/\pi\mu_{A,BC})^{1/2} [Q_{BC}^{cpf}(T)]^{-1} \times \int_0^\infty \epsilon_{BC}^{cm}(E) \bar{S}_r(E) \exp(-\beta E)\, dE, \quad (28)$$

$$\epsilon_{BC}^{cm}(E) = \sigma_{BC}^{-1} h^{-3} \int_{-\infty}^{+\infty}\int_{-\infty}^{+\infty}\int_{-\infty}^{+\infty}\int_0^{2\pi}\int_0^{\pi}\int_0^{\infty} (E-H_{BC})\, \mathcal{H}(E-H_{BC}) \times \prod_{i=1}^{3} dQ_i^{sp}\, dP_i^{sp}, \quad (29)$$

$$\bar{S}_r(E) = [\epsilon_{BC}^{cm}(E)]^{-1} h^{-3} \int_{-\infty}^{+\infty}\int_{-\infty}^{+\infty}\int_{-\infty}^{+\infty}\int_0^{2\pi}\int_0^{\pi}\int_0^{\infty} (E-H_{BC})\, S_r(E-H_{BC}, Q^{sp}, P^{sp}) \times \prod_{i=1}^{3} dQ_i^{sp}\, dP_i^{sp}, \quad (30)$$

where H_{BC}, the classical Hamiltonian for BC, is

$$H_{BC} = (2\mu_{BC})^{-1} \{P_r^2 + P_\theta^2/r^2 + P_\phi^2/r^2\sin^2\theta\} + V_{\rho_s}(r). \quad (32)$$

The classical partition function (cpf) for the internal degrees of freedom of BC is given by

$$Q_{BC}^{cpf}(T) = h^{-3} \int_{-\infty}^{+\infty}\int_{-\infty}^{+\infty}\int_{-\infty}^{+\infty}\int_0^{2\pi}\int_0^{\pi}\int_0^{r_{max}^{BC}} \exp(-\beta H_{BC}) \prod_{i=1}^{3} dQ_i^{sp}\, dP_i^{sp} = h^{-3} (4\pi) (2\pi\mu_{BC}/\beta)^{3/2} D_{BC}^{c}(T)\, \sigma_{BC}^{-1}. \quad (31)$$

The quantity $\epsilon_{BC}^{cm}(E)$ is given by

$$\epsilon_{BC}^{cm}(E) = h^{-3} (64/15) (2)^{1/2} \pi^2 \mu_{BC}^{3/2} \sigma_{BC}^{-1} D_{BC}^{\mu}(E), \quad (33)$$

where the microcanonical reactant integral is given by

$$D_{BC}^{\mu}(E) = \int_0^\infty r^2 [E-V_{\rho_s}(r)]^{5/2}\, \mathcal{H}[E-V_{\rho_s}(r)]\, dr. \quad (34)$$

The designation cm indicates that the internal degrees of freedom of BC were

treated according to classical mechanics.

Koeppl used the rate constant given by variational TST for the generalized dividing surface to evaluate $\bar{S}_r(E)$. He assumed that the rate constant k(T) [Eq. (3)] gives the rate constant $k_{CT}^{cm}(T)$ defined by the collisional theory [Eq. (28)] and obtained

$$Q_{\rho_s}(T)^{-1} \int \mathbf{v}\cdot\mathbf{n}_s \, \mathcal{K}(\mathbf{v}\cdot\mathbf{n}_S) \exp(-\beta H) \, d\sigma$$

$$= (8\beta^3/\pi\mu_{A,BC})^{1/2} [Q_{BC}^{cpf}(T)]^{-1} \int_0^\infty \epsilon_{BC}^{cm}(E) \, \bar{S}_r(E)^{TST} \exp(-\beta E) \, dE. \quad (35)$$

To put the collisional theory rate constant on a completely classical basis, Koeppl introduced

$$Q_{BC}(T) = h^3 \, Q_{BC}^{cpf}(T), \text{ and} \quad (36)$$

$$\epsilon_{BC}(E) = h^3 \, \epsilon_{BC}^{cm}(E). \quad (37)$$

Note that Planck's constant cancels in the numerator and denominator of the equation that defines the classical result for $\bar{S}_r(E)$ (see Eq. (30)). Substitution of Eqs. (36) and (37) in (35) gives

$$\int_0^\infty \epsilon_{BC}(E) \, \bar{S}_r(E)^{TST} \exp(-\beta E) \, dE$$

$$= (\pi\mu_{A,BC}/8\beta^3)^{1/2} [Q_{BC}(T)/Q_{\rho_s}(T)] \int d\sigma \, \mathbf{v}\cdot\mathbf{n}_s \, \mathcal{K}(\mathbf{v}\cdot\mathbf{n}_S) \exp(-\beta H). \quad (38)$$

Substitution of Eqs. (31), (36), and (19) in (38) gives

$$\int_0^\infty \epsilon_{BC}(E) \, \bar{S}_r(E)^{TST} \exp(-\beta E) \, dE$$

$$= (8\pi\mu_{A,BC})^{-1} \int d\sigma \, \mathbf{v}\cdot\mathbf{n}_s \, \mathcal{K}(\mathbf{v}\cdot\mathbf{n}_S) \exp(-\beta H). \quad (39)$$

Koeppl showed that taking the inverse Laplace transform $(\mathcal{L}^{-1})$[92] gives

$$\bar{S}_r(E)^{TST} = [8\pi\mu_{A,BC}\epsilon_{BC}(E)]^{-1} \int d\sigma \, \mathbf{v}\cdot\mathbf{n}_s \, \mathcal{K}(\mathbf{v}\cdot\mathbf{n}_S) \, \delta(E-H), \quad (40)$$

$$= [8\pi\mu_{A,BC}\epsilon_{BC}(E)]^{-1} (256/15) (2^{1/2}) \pi^4 (\mu_{A,BC}\mu_{BC})^{3/2} \times \sigma_*^{-1} N_*^{\mu}(E), \quad (41)$$

where

$$N^{\mu}_{*}(E) = \int_0^{\pi} \sin\theta \, d\theta \int_0^{\infty} r(\Omega,R,\theta)^2 \, R^2 \, [E-V(\Omega,R,\theta)]^{5/2} \, \mathcal{K}[E-V(\Omega,R,\theta)] \, dR$$
$$\times \left[\mu_{BC}^{-1} \{1+[F_{\theta}(\Omega,R,\theta)/r(\Omega,R,\theta)]^2\} + \mu_{A,BC}^{-1} F_R(\Omega,R,\theta)^2 \right]^{1/2}. \quad (42)$$

Substitution of Eqs. (33) and (37) in (41) gives

$$\bar{S}_r(E)^{TST} = (\pi \mu_{A,BC}^{1/2}/2) \, (\sigma_{BC}/\sigma_*) \, [N^{\mu}_{*}(E)/D^{\mu}_{BC}(E)]. \quad (43)$$

The relationship between $\bar{S}_r(E)^{TST}$ and the canonical rate constant can be obtained using Eqs. (3) and (39):

$$k(T) = (8\pi\mu_{A,BC}) \, Q_{\rho_s}(T)^{-1} \int_0^{\infty} \epsilon_{BC}(E) \, \bar{S}_r(E)^{TST} \exp(-\beta E) \, dE. \quad (44)$$

CHAPTER 2

EXPRESSIONS FOR DIVIDING SURFACES, CANONICAL RATE CONSTANTS, MICROCANONICAL MEAN REACTION CROSS SECTIONS, POTENTIAL ENERGY FUNCTIONS AND DISCRIPTION OF NUMERICAL METHODS

This chapter defines dividing surface (DS) functions used in this work. The equations for the canonical rate constant and mean reaction cross section for a general dividing surface derived in Ch. 1 are then used to obtain expressions for these quantities for the particular dividing surfaces used in this work. Expressions for the potential energy functions used in this work are given. Finally numerical methods, computer programs, and plots used to display calculated results are described.

The power series expansion of the dividing surface is described in Sect. I. The dividing surfaces used in this work are defined in Sect. II. Corresponding expressions for the canonical rate constant and microcanonical mean reaction cross section are given in Sects. III and IV, respectively. The potential energy surface (PES) functions used in this work are described in Sect. V. The numerical methods and computer programs used to obtain variational results are described in Sect. VI. The plots used to display dividing surfaces, potential energy contours, reactivity relief maps and angle dependent minimum energy for chemical reaction are described. Finally the method used to obtain parameters for a dividing surface which follows the path of steepest ascent from a set of angle dependent saddle points is described.

I. GENERAL POWER SERIES EXPANSION OF THE DIVIDING SURFACE FUNCTION

The most general dividing surface defined by configuration space variables, i.e., internal coordinates, for A + BC reaction, is

$$S = 0 = r - F(R,\theta) - C. \tag{45}$$

Rearrangement gives

$$r = F(R,\theta) + C \tag{46}$$

where, R and θ are internal coordinates (see Fig. 5) and C is a variational parameter. The function $F(R,\theta)$ contains additional variational parameters.

The function $F(R,\theta)$ may be expanded as a power series in the internal coordinates. Expressions for the rate constant and mean reaction cross section can be obtained by substitution of partial derivatives of function $F(R,\theta)$ in equations 21 and 43, respectively. The flexibility of the surface can be improved systematically by introducing additional terms in a power series expansion of the surface. The surface is defined by

$$S = 0 = r - \sum_{n=0}^{\infty} \frac{1}{n!} \{ (R - R_o) \frac{\partial}{\partial R} + (\theta - \theta_o) \frac{\partial}{\partial \theta} \}^n F(R_o,\theta_o) \tag{47}$$

when the function is expanded about the point (R_o,θ_o), or more simply by

$$S = 0 = r - \left[\sum_{n=1}^{\infty} \frac{1}{n!} \{ R \frac{\partial}{\partial R} + \theta \frac{\partial}{\partial \theta} \}^n F(0,0) \right] - C \tag{48}$$

when the function is expanded about the point (0,0). The constant C is F(0,0). Rearrangement gives

$$r = \left[\sum_{n=1}^{\infty} \frac{1}{n!} \{ R \frac{\partial}{\partial R} + \theta \frac{\partial}{\partial \theta} \}^n F(0,0) \right] + C. \tag{49}$$

II. DIVIDING SURFACE FUNCTIONS

A. Dividing surfaces expressed in terms of coordinates R and θ

1. ***Truncated (TR) DS***

$$r = AR + C \tag{50}$$

where A and C are variational parameters. This DS does not depend on θ. It is the simplest one used in the work reported here. It was introduced by Martin and Raff[35] and used to study the $H + H_2$ and $H + I_2$ reactions.

2. ***Linear Combination of Internal Coordinates (LCIC) DS***

$$r = AR + B\theta + C \tag{51}$$

where A, B, and C are variational parameters. This DS was also introduced by Martin and Raff[35].

3. ***Quadratic (Q) DS*** (designated linear θ in figures and tables when compared with $\sin^2\theta$ DS function which is given in Sect. II B of this chapter)

$$r = AR + B\theta + C + 1/2\,(DR^2 + 2ER\theta + F\theta^2) \tag{52}$$

where A, B, C, D, E and F are variational parameters. This DS was introduced by Sverdlik and Koeppl[36].

4. ***Cubic (C) DS*** (designated linear θ when compared with $\sin^2\theta$)

$$r = AR + B\theta + C + 1/2\,(DR^2 + 2ER\theta + F\theta^2) + 1/6\,(GR^3 + 3HR^2\theta + 3IR\theta^2 + J\theta^3) \tag{53}$$

where A, B, C, D, E, F, G, H, I, and J are variational parameters. This DS was introduced by Sverdlik and Koeppl[36].

B. Dividing surfaces expressed in terms of R and powers of $\sin^2\theta$

1. ***Quadratic DS*** (designated $\sin^2\theta$ in figures and tables)

$$r = AR + B\sin^2\theta + C + 1/2\,(DR^2 + 2ER\sin^2\theta + F\sin^4\theta) \tag{54}$$

where A, B, C, D, E, and F are variational parameters. This DS is introduced here.

2. ***Cubic DS*** (designated $\sin^2\theta$ in figures and tables)

$$r = AR + B\sin^2\theta + C + 1/2\,(DR^2 + 2ER\sin^2\theta + F\sin^4\theta)$$

$$+ 1/6\,(GR^3 + 3HR^2\sin^2\theta + 3IR\sin^4\theta + J\sin^6\theta) \quad (55)$$

where A, B, C, D, E, F, G, H, I and J are variational parameters. This DS is introduced here.

C. Dividing surfaces which differentiate between both ends of a heteronuclear diatomic reactant

1. ***Five–parameter DS***

$$r = AR + BAC(\theta'-\theta) + EAC(\theta'-\theta)R + C \quad (56)$$

for $0 \leq \theta < \theta'$ and

$$r = AR + BAB(\theta-\theta') + EAB(\theta-\theta')R + C \quad (57)$$

for $\theta' < \theta \leq \pi$ where A, BAC, EAC, BAB and EAB are variational parameters. Note that when $\theta = \theta'$, $r = r' = AR' + C$; hence

$$C = r' - AR'. \quad (58)$$

This DS function is introduced in this work and used to study the F + DH → FD(FH) + H(D) reactions. To understand the significance of r', R' and θ', consider the potential energy surface (PES), that is the Born–Oppenheimeir potential energy function $V(r,R,\theta)$, for the F + DH reaction. For the three potential energy surfaces studied in this work a single saddle point was found in r and R coordinate space for all fixed values of θ in the range from 0 to π. The potential energy at the angle dependent saddle point so defined is plotted versus θ in Fig. 35 (which is presented and discussed in Ch.4, Sect. II) for potential energy functions used in this work. The angle dependent saddle point energy corresponds to the minimum energy required for the reaction at a specified value of θ.

BAC and EAC are variational parameters for attack at the C end of BC; BAB and EAB correspond to attack at the B end of BC (see Fig. 5). The value θ' and the values r' and R' correspond to the saddle point of highest energy. The values of r', R' and θ' for the Truhlar 1 PES are 1.9891 and 2.2532 a. u., and 81.5 deg., respectively. The potential energy for this saddle point configuration is 2.31 eV.

When atom B is D and C is H, $\theta < \theta'$ corresponds to attack at the H end of DH and $\theta > \theta'$ corresponds to attack at the D end of DH.

2. *Ten–parameter DS*

$$r = AR + BAC(\theta'-\theta) + EAC(\theta'-\theta)R + 1/2\ \{DR^2 + FAC(\theta'-\theta)^2 + HAC(\theta'-\theta)R^2\} + CC \tag{59}$$

for $0 \leq \theta < \theta'$ and

$$r = AR + BAB(\theta-\theta') + EAB(\theta-\theta')R + 1/2\ \{DR^2 + FAB(\theta-\theta')^2 + HAB(\theta-\theta')R^2\} + CC \tag{60}$$

for $\theta' < \theta \leq \pi$ where A, BAC, EAC, BAB, EAB, D, FAC, HAC, FAB and HAB are variational parameters and

$$CC = r' - AR' - 1/2\ DR'^2. \tag{61}$$

III. EXPRESSIONS FOR THE CANONICAL RATE CONSTANT

Rate constants (k(T)) obtained for different formulations of the dividing surface for atom–diatom reactions are given below. $V[r(\Omega),R,\theta]$ indicates that the potential energy on the dividing surface depends on variational parameters as well as R and θ. k(T) is given by Eq. (21).

A1. *Truncated dividing surface*

$$k(T) = 2\ (2\pi/\beta)^{1/2}\ [D_{BC}^{c}(T)]^{-1}\ (\sigma_{BC}/\sigma_*) \times \int_0^{\pi/2} \exp\{-\beta V[r(\Omega,R,\theta),R,\theta]\}\ \sin\theta\ d\theta \int_0^{R_{max}^{S=0}} r(\Omega,R,\theta)^2\ R^2\ dR \times \left[\mu_{BC}^{-1} + \mu_{A,BC}^{-1}\ A^2\right]^{1/2}, \tag{62}$$

where the variational parameters (Ω) are A and C.

A2. *Linear Combination of Internal Coordinates dividing surface*

$$k(T) = 2\ (2\pi/\beta)^{1/2}\ [D_{BC}^{c}(T)]^{-1}\ (\sigma_{BC}/\sigma_*) \times \int_0^{\pi/2} \exp\{-\beta V[r(\Omega,R,\theta),R,\theta]\}\ \sin\theta\ d\theta \int_0^{R_{max}^{S=0}} r(\Omega,R,\theta)^2\ R^2\ dR$$

$$\times \left[\mu_{BC}^{-1}\{1 + [B/r(\Omega,R,\theta)]^2\} + \mu_{A,BC}^{-1} A^2\right]^{1/2}, \qquad (63)$$

where the variational parameters (Ω) are A, B and C.

A3. ***Quadratic dividing surface*** (linear θ)

$$k(T) = 2(2\pi/\beta)^{1/2}[D_{BC}^{c}(T)]^{-1}(\sigma_{BC}/\sigma_*)\int_0^{\pi/2}\int_0^{R_{max}^{S=0}} [r(\Omega,R,\theta)\,R]^2 \sin\theta \times dR\,d\theta \left[\mu_{BC}^{-1}\{1 + [(B + E\,R + F\,\theta)/r(\Omega,R,\theta)]^2\} + \mu_{A,BC}^{-1}(A + D\,R + E\,\theta)^2\right]^{1/2} \times \exp\{-\beta V[r(\Omega,R,\theta),R,\theta]\}, \qquad (64)$$

where A, B, C, D, E and F are variational parameters (Ω).

A4. ***Cubic dividing surface*** (linear θ)

$$k(T) = 2(2\pi/\beta)^{1/2}[D_{BC}^{c}(T)]^{-1}(\sigma_{BC}/\sigma_*)\int_0^{\pi/2}\int_0^{R_{max}^{S=0}} [r(\Omega,R,\theta)\,R]^2 \sin\theta \times dR\,d\theta \left[\mu_{BC}^{-1}\{1 + [(B + E\,R + F\,\theta + (1/2)(H\,R^2 + 2\,I\,R\,\theta + J\,\theta^2))/r(\Omega,R,\theta)]^2\} + \mu_{A,BC}^{-1}\{A + D\,R + E\,\theta + (1/2)(G\,R^2 + 2\,H\,R\,\theta + I\,\theta^2)\}^2\right]^{1/2} \times \exp\{-\beta V[r(\Omega,R,\theta),R,\theta]\}, \qquad (65)$$

where A, B, C, D, E, F, G, H, I, and J are variational parameters (Ω).

B1. ***Quadratic dividing surface*** ($\sin^2\theta$)

$$k(T) = 2(2\pi/\beta)^{1/2}[D_{BC}^{c}(T)]^{-1}(\sigma_{BC}/\sigma_*)\int_0^{\pi/2}\int_0^{R_{max}^{S=0}} [r(\Omega,R,\theta)\,R]^2 \sin\theta \times dR\,d\theta \left[\mu_{BC}^{-1}\{1 + [(B + E\,R + F\sin^2\theta)(2\sin\theta\cos\theta)/r(\Omega,R,\theta)]^2\} + \mu_{A,BC}^{-1}(A + D\,R + E\sin^2\theta)^2\right]^{1/2} \times \exp\{-\beta V[r(\Omega,R,\theta),R,\theta]\}, \qquad (66)$$

where A, B, C, D, E, and F are variational parameters (Ω).

B2. ***Cubic dividing surface*** ($\sin^2\theta$)

$$k(T) = 2(2\pi/\beta)^{1/2}[D_{BC}^{c}(T)]^{-1}(\sigma_{BC}/\sigma_*)\int_0^{\pi/2}\int_0^{R_{max}^{S=0}} [r(\Omega,R,\theta)\,R]^2 \sin\theta$$

$$\times \mathrm{dR}\, \mathrm{d}\theta \times \Big[\mu_{\mathrm{BC}}^{-1}\{1 + [((B + E\,\mathrm{R} + F \sin^2\theta)\,(2 \sin\theta \cos\theta)$$
$$+ (\sin\theta \cos\theta)\,(H\,\mathrm{R}^2 + 2\,I\,\mathrm{R} \sin^2\theta + J \sin^4\theta))/\mathrm{r}(\boldsymbol{\Omega},\mathrm{R},\theta)]^2\}$$
$$+ \mu_{\mathrm{A,BC}}^{-1}\{A + D\,\mathrm{R} + E \sin^2\theta$$
$$+ (1/2)\,(G\,\mathrm{R}^2 + 2\,H\mathrm{R} \sin^2\theta + I \sin^4\theta)\}^2 \Big]^{1/2}$$
$$\times \exp\{-\beta \mathrm{V}[\mathrm{r}(\boldsymbol{\Omega},\mathrm{R},\theta),\mathrm{R},\theta]\}, \qquad (67)$$

where A, B, C, D, E, F, G, H, I and J are variational parameters ($\boldsymbol{\Omega}$).

C1. ***Five–parameter dividing surface*** (heteronuclear reactant)

When the DS function contains parameters which distinguish between reaction at each end of a heteronuclear reactant, the rate constant is expressed as the sum of contributions $\mathrm{k(T)}^{\mathrm{C}}$ for integration over θ from 0 to θ' and $\mathrm{k(T)}^{\mathrm{B}}$ for integration over θ from θ' to π, i.e., $\mathrm{k(T)} = \mathrm{k(T)}^{\mathrm{C}} + \mathrm{k(T)}^{\mathrm{B}}$ where

$$\mathrm{k(T)}^{\mathrm{C}} = (2\pi/\beta)^{1/2}\,[\mathrm{D}_{\mathrm{BC}}^{\mathrm{c}}(\mathrm{T})]^{-1}\,(\sigma_{\mathrm{BC}}/\sigma_*) \int_0^{\theta'} \int_0^{\mathrm{R}_{\mathrm{max}}^{\mathrm{S}=0}} [\mathrm{r}(\boldsymbol{\Omega},\mathrm{R},\theta)\,\mathrm{R}]^2 \sin\theta$$
$$\times \mathrm{dR}\, \mathrm{d}\theta \Big[\mu_{\mathrm{BC}}^{-1}\,\{1 + [(BAC + EAC\,\mathrm{R}$$
$$+ FAC\,(\theta'-\theta))/\mathrm{r}(\boldsymbol{\Omega},\mathrm{R},\theta)]^2\}$$
$$+ \mu_{\mathrm{A,BC}}^{-1}\,(A + D\,\mathrm{R} + EAC\,(\theta'-\theta))^2 \Big]^{1/2}$$
$$\times \exp\{-\beta \mathrm{V}[\mathrm{r}(\boldsymbol{\Omega},\mathrm{R},\theta),\mathrm{R},\theta]\} \qquad (68)$$

and

$$\mathrm{k(T)}^{\mathrm{B}} = (2\pi/\beta)^{1/2}\,[\mathrm{D}_{\mathrm{BC}}^{\mathrm{c}}(\mathrm{T})]^{-1}\,(\sigma_{\mathrm{BC}}/\sigma_*) \int_{\theta'}^{\pi} \int_0^{\mathrm{R}_{\mathrm{max}}^{\mathrm{S}=0}} [\mathrm{r}(\boldsymbol{\Omega},\mathrm{R},\theta)\,\mathrm{R}]^2 \sin\theta$$
$$\times \mathrm{dR}\, \mathrm{d}\theta \Big[\mu_{\mathrm{BC}}^{-1}\,\{1 + [(BAB + EAB\,\mathrm{R}$$
$$+ FAB\,(\theta-\theta'))/\mathrm{r}(\boldsymbol{\Omega},\mathrm{R},\theta)]^2\}$$
$$+ \mu_{\mathrm{A,BC}}^{-1}\,(A + D\,\mathrm{R} + EAB\,(\theta-\theta'))^2 \Big]^{1/2}$$
$$\times \exp\{-\beta \mathrm{V}[\mathrm{r}(\boldsymbol{\Omega},\mathrm{R},\theta),\mathrm{R},\theta]\} \qquad (69)$$

where A, BAC, EAC, BAB and EAB are variational parameters. $\mathrm{k(T)}^{\mathrm{C}}$ and $\mathrm{k(T)}^{\mathrm{B}}$ give contributions to k(T) for phase points which cross the DS "near" the C and B

ends of the BC reactant, respectively.

C2. ***Ten–parameter dividing surface*** (heteronuclear reactant)

The rate constant k(T) is the sum of $k(T)^C$ and $k(T)^B$ where

$$k(T)^C = (2\pi/\beta)^{1/2} [D^c_{BC}(T)]^{-1} (\sigma_{BC}/\sigma_*) \int_0^{\theta'} \int_0^{R^{S=0}_{max}} [r(\Omega,R,\theta)\, R]^2 \sin\theta \times dR\, d\theta \Big[\mu_{BC}^{-1} \{1 + [(BAC + EAC\, R + FAC\,(\theta'-\theta) + (1/2)\, HAC\, R^2)/r(\Omega,R,\theta)]^2\} + \mu_{A,BC}^{-1} \{A + D\, R + EAC\,(\theta'-\theta) + HAC\, R\,(\theta'-\theta)\}^2 \Big]^{1/2} \times \exp\{-\beta V[r(\Omega,R,\theta),R,\theta]\} \quad (70)$$

and

$$k(T)^B = (2\pi/\beta)^{1/2} [D^c_{BC}(T)]^{-1} (\sigma_{BC}/\sigma_*) \int_{\theta'}^{\pi} \int_0^{R^{S=0}_{max}} [r(\Omega,R,\theta)\, R]^2 \sin\theta \times dR\, d\theta \Big[\mu_{BC}^{-1} \{1 + [(BAB + EAB\, R + FAB\,(\theta-\theta') + (1/2)\, HAB\, R^2)/r(\Omega,R,\theta)]^2\} + \mu_{A,BC}^{-1} \{A + D\, R + EAB\,(\theta-\theta') + HAB\, R\,(\theta-\theta')\}^2 \Big]^{1/2} \times \exp\{-\beta V[r(\Omega,R,\theta),R,\theta]\} \quad (71)$$

where *A, BAC, EAC, BAB, EAB, D, FAC, HAC, FAB* and *HAB* are variational parameters.

IV. EXPRESSIONS FOR THE MICROCANONICAL MEAN REACTION CROSS SECTION

Eq. (43) can be used to obtain expressions for the mean reaction cross section $(\bar{S}_r(E)^{TST})$ for the dividing surfaces described in Sect. II. The results are given below.

A1. ***Truncated dividing surface***

$$\bar{s}_r(E)^{TST} = \pi\,[D^{\mu}_{BC}(E)]^{-1}\,(\sigma_{BC}/\sigma_*) \times \int_0^{\pi/2}\int_0^{\infty} \sin\theta\, r(\Omega,R,\theta)^2\, R^2\, d\theta\, dR \times \{\, E\text{–}V[r(\Omega,R,\theta),R,\theta]\,\}^{5/2}\, \mathcal{K}\{E\text{–}V[r(\Omega,R,\theta),R,\theta]\} \times \left[\,(\mu_{A,BC}/\mu_{BC}) + A^2\,\right]^{1/2}, \tag{72}$$

where A and C are variational parameters.

A2. ***Linear Combination of Internal Coordinates dividing surface***

$$\bar{s}_r(E)^{TST} = \pi\,[D^{\mu}_{BC}(E)]^{-1}\,(\sigma_{BC}/\sigma_*) \times \int_0^{\pi/2}\int_0^{\infty} \sin\theta\, r(\Omega,R,\theta)^2\, R^2\, d\theta\, dR \times \{\, E\text{–}V[r(\Omega,R,\theta),R,\theta]\,\}^{5/2}\, \mathcal{K}\{E\text{–}V[r(\Omega,R,\theta),R,\theta]\} \times \left[\,(\mu_{A,BC}/\mu_{BC})\,\{\,1 + [B\,/\,r(\Omega,R,\theta)]^2\,\} + A^2\,\right]^{1/2}, \tag{73}$$

where A, B and C are variational parameters.

A3. ***Quadratic dividing surface*** (linear θ)

$$\bar{s}_r(E)^{TST} = \pi\,[D^{\mu}_{BC}(E)]^{-1}\,(\sigma_{BC}/\sigma_*) \int_0^{\pi/2}\int_0^{\infty} [r(\Omega,R,\theta)\,R]^2 \sin\theta\, dR\, d\theta \times \{\, E\text{–}V[r(\Omega,R,\theta),R,\theta]\,\}^{5/2}\, \mathcal{K}\{E\text{–}V[r(\Omega,R,\theta),R,\theta]\} \times \Big[(\mu_{A,BC}/\mu_{BC})\{\,1 + [(B + E\,R + F\,\theta)/r(\Omega,R,\theta)]^2\,\} + \{\,A + D\,R + E\,\theta\,\}^2\,\Big]^{1/2}, \tag{74}$$

where A, B, C, D, E and F are variational parameters.

A4. ***Cubic dividing surface*** (linear θ)

$$\bar{s}_r(E)^{TST} = \pi\,[D^{\mu}_{BC}(E)]^{-1}\,(\sigma_{BC}/\sigma_*) \int_0^{\pi/2}\int_0^{R_{max}^{S=0}} [r(\Omega,R,\theta)\,R]^2 \sin\theta\, dR\, d\theta \times \Big[(\mu_{A,BC}/\mu_{BC})\{1+[(B + ER + F\theta + (1/2)\,(HR^2 + 2IR\theta + J\theta^2))/r(\Omega,R,\theta)]^2\} + \{A + D\,R + E\,\theta + (1/2)\,(G\,R^2 + 2H\,R\theta + I\,\theta^2)\}^2\,\Big]^{1/2}$$

$$\times \{ \text{E–V}[\text{r}(\Omega,\text{R},\theta),\text{R},\theta] \}^{5/2} \, \mathcal{K}\{\text{E–V}[\text{r}(\Omega,\text{R},\theta),\text{R},\theta]\}, \tag{75}$$

where A, B, C, D, E, F, G, H, I, and J are variational parameters.

B1. ***Quadratic dividing surface*** $(\sin^2\theta)$

$$\begin{aligned}\bar{S}_r(E)^{TST} = \pi\,[D^{\mu}_{BC}(E)]^{-1}\,(\sigma_{BC}/\sigma_*) \int_0^{\pi/2}\int_0^{\infty} [r(\Omega,R,\theta)\,R]^2 \sin\theta\, dR\, d\theta \\ \times \{ \text{E–V}[\text{r}(\Omega,\text{R},\theta),\text{R},\theta] \}^{5/2} \, \mathcal{K}\{\text{E–V}[\text{r}(\Omega,\text{R},\theta),\text{R},\theta]\} \\ \times \Big[(\mu_{A,BC}/\mu_{BC})\{\,1 + [(B + E\,R + F\sin^2\theta)(2\sin\theta\cos\theta)/r(\Omega,R,\theta)]^2\,\} \\ + \{\,A + D\,R + E\sin^2\theta\,\}^2\Big]^{1/2},\end{aligned} \tag{76}$$

where A, B, C, D, E, and F are variational parameters.

B2. ***Cubic dividing surface*** $(\sin^2\theta)$

$$\begin{aligned}\bar{S}_r(E)^{TST} = \pi\,[D^{\mu}_{BC}(E)]^{-1}\,(\sigma_{BC}/\sigma_*) \int_0^{\pi/2}\int_0^{R_{max}^{S=0}} [r(\Omega,R,\theta)\,R]^2 \sin\theta\, dR\, d\theta \\ \times \Big[(\mu_{A,BC}/\mu_{BC})\{1+[((B + ER + F\sin^2\theta)(2\sin\theta\cos\theta) \\ + (\sin\theta\cos\theta)\,(HR^2 + 2IR\sin^2\theta + J\sin^4\theta))/r(\Omega,R,\theta)]^2\} \\ + \{A + D\,R + E\sin^2\theta \\ + (1/2)\,(G\,R^2 + 2H\,R\sin^2\theta + I\sin^4\theta)\}^2\Big]^{1/2} \\ \times \{ \text{E–V}[\text{r}(\Omega,\text{R},\theta),\text{R},\theta] \}^{5/2} \, \mathcal{K}\{\text{E–V}[\text{r}(\Omega,\text{R},\theta),\text{R},\theta]\},\end{aligned} \tag{77}$$

where A, B, C, D, E, F, G, H, I and J are variational parameters.

C1. ***Five–parameter dividing surface*** (heteronuclear reactant)

The mean reaction cross section $\bar{S}_r(E)^{TST}$ is the sum of $\bar{S}_r(E)^{C}$ and $\bar{S}_r(E)^{B}$, i. e., $\bar{S}_r(E)^{TST} = \bar{S}_r(E)^{C} + \bar{S}_r(E)^{B}$ where

$$\begin{aligned}\bar{S}_r(E)^{C} = \pi/2\,[D^{\mu}_{BC}(E)]^{-1}\,(\sigma_{BC}/\sigma_*) \int_0^{\theta'}\int_0^{\infty} [r(\Omega,R,\theta)\,R]^2 \sin\theta\, dR\, d\theta \\ \times \{ \text{E–V}[\text{r}(\Omega,\text{R},\theta),\text{R},\theta] \}^{5/2} \, \mathcal{K}\{\text{E–V}[\text{r}(\Omega,\text{R},\theta),\text{R},\theta]\} \\ \times \Big[(\mu_{A,BC}/\mu_{BC})\{\,1 + [(BAC + EAC\,R \\ + FAC\,(\theta'-\theta))/r(\Omega,R,\theta)]^2\,\} \\ + \{\,A + D\,R + EAC\,(\theta'-\theta)\,\}^2\Big]^{1/2}\end{aligned} \tag{78}$$

and

$$\bar{s}_r(E)^B = \pi/2\,[D^{\mu}_{BC}(E)]^{-1}\,(\sigma_{BC}/\sigma_*)\int_{\theta'}^{\pi}\int_0^{\infty}[r(\Omega,R,\theta)\,R]^2\sin\theta\,dR\,d\theta$$
$$\times\{\,E\text{–}V[r(\Omega,R,\theta),R,\theta]\,\}^{5/2}\,\mathcal{K}\{E\text{–}V[r(\Omega,R,\theta),R,\theta]\}$$
$$\times\Big[(\mu_{A,BC}/\mu_{BC})\{\,1+[(BAB+EAB\,R$$
$$+FAB\,(\theta\text{–}\theta'))/r(\Omega,R,\theta)]^2\,\}$$
$$+\{\,A+D\,R+EAB\,(\theta\text{–}\theta')\,\}^2\Big]^{1/2} \qquad (79)$$

where A, BAC, EAC, BAB and EAB are variational parameters. $\bar{s}_r(E)^C$ and $\bar{s}_r(E)^B$ give contribution to $\bar{s}_r(E)^{TST}$ for phase points which cross DS near the C and B ends of the BC reactant, respectively, i.e., $\bar{s}_r(E)^C$ corresponds to $0 \le \theta < \theta'$ and $\bar{s}_r(E)^B$ to $\theta' < \theta \le \pi$.

C2. ***Ten–parameter dividing surface*** (heteronuclear reactant)

The mean reaction cross section $\bar{s}_r(E)^{TST}$ is the sum of $\bar{s}_r(E)^C$ and $\bar{s}_r(E)^B$, i. e., $\bar{s}_r(E)^{TST} = \bar{s}_r(E)^C + \bar{s}_r(E)^B$ where

$$\bar{s}_r(E)^C = \pi\,[D^{\mu}_{BC}(E)]^{-1}\,(\sigma_{BC}/\sigma_*)\int_0^{\theta'}\int_0^{R^{S=0}_{max}}[r(\Omega,R,\theta)\,R]^2\sin\theta\,dR\,d\theta$$
$$\times\Big[(\mu_{A,BC}/\mu_{BC})\{1+[(BAC+EAC\,R+FAC(\theta'\text{–}\theta)$$
$$+(1/2)\,HAC\,R^2)/r(\Omega,R,\theta)]^2\}$$
$$+\{A+D\,R+EAC\,(\theta'\text{–}\theta)+HAC\,R(\theta'\text{–}\theta)\}^2\Big]^{1/2}$$
$$\times\{\,E\text{–}V[r(\Omega,R,\theta),R,\theta]\,\}^{5/2}\,\mathcal{K}\{E\text{–}V[r(\Omega,R,\theta),R,\theta]\} \qquad (80)$$

and

$$\bar{s}_r(E)^B = \pi\,[D^{\mu}_{BC}(E)]^{-1}\,(\sigma_{BC}/\sigma_*)\int_{\theta'}^{\pi}\int_0^{R^{S=0}_{max}}[r(\Omega,R,\theta)\,R]^2\sin\theta\,dR\,d\theta$$
$$\times\Big[(\mu_{A,BC}/\mu_{BC})\{1+[(BAB+EAB\,R+FAB(\theta\text{–}\theta')$$
$$+(1/2)\,HAB\,R^2)/r(\Omega,R,\theta)]^2\}$$

$$+ \{A + D\,\mathrm{R} + EAB(\theta-\theta') + HAB\,\mathrm{R}(\theta-\theta')\}^2 \Big]^{1/2}$$
$$\times \{\,\mathrm{E-V[r(\Omega,R,\theta),R,\theta]}\,\}^{5/2}\ \mathcal{A}\{\mathrm{E-V[r(\Omega,R,\theta),R,\theta]}\} \qquad (81)$$

where *A, BAC, EAC, BAB, EAB, D, FAC, HAC, FAB* and *HAB* are variational parameters.

V. POTENTIAL ENERGY SURFACE FUNCTIONS

Extended London–Eyring–Polanyi–Sato (LEPS) PES

In 1929 London[93] proposed the following potential energy function:

$$\mathrm{E}(r_1,r_2,r_3) = Q_1 + Q_2 + Q_3 - (J_1^2 + J_2^2 + J_3^2 - J_1J_2 - J_2J_3 - J_1J_3), \qquad (82)$$

where r_1, r_2, r_3 are internuclear separations of AB, BC and AC molecules, Q_1, Q_2, Q_3 are Coulomb integrals of AB, BC and AC molecules, J_1, J_2, J_3 are exchange (resonance) integrals of AB, BC and AC molecules.

Later Eyring and Polanyi proposed a method of evaluating the Coulomb and exchange integrals for the constituent diatomic molecules using spectroscopic data[94].

Sato introduced a factor 1/(1+k) in the above equation, where k is often referred as the overlap parameter[95]. In the extended form of the equation developed by Kuntz et al[96], k is replaced by overlap parameters a, b and c for each diatomic constituent of the system, AB, BC and AC, respectively.

$$\mathrm{E}(r_1,r_2,r_3) = Q_1/(1+a) + Q_2/(1+b) + Q_3/(1+c) - \{J_1^2/(1+a)^2 + J_2^2/(1+b)^2$$
$$+ J_3^2/(1+c)^2 - J_1J_2/[(1+a)(1+b)] - J_2J_3/[(1+b)(1+c)]$$
$$- J_1J_3/[(1+a)(1+c)]\}. \qquad (83)$$

The potential energy functions used in the present work are described below.

1. *Extended LEPS PES for* F + HH *reaction developed by Muckerman*[51,57]

Koeppl did some preliminary work with a PES developed by Muckerman which is known as the Muckerman 5 (M5) PES. The overlap parameters are 0.167

for FH and 0.106 for HH.

2. ***Extended LEPS PES for*** **F + HH** ***reaction developed by Truhlar and co–workers***[43]

This function is designated Truhlar 1 (T1) PES. The overlap parameters are 0.175 for FH and 0.104 for HH.

3. ***Extended LEPS PES for*** **F + HH** ***reaction with angle dependent overlap parameter developed by Truhlar and co–workers***[43]

This function is designated Truhlar 2 (T2) PES. The overlap parameter for HH is 0.104. The overlap parameter for FH was varied with the orientation angle θ defined in Fig. 5 using the piecewise function defined below.

0.175	for θ from 0° to 10°
$0.175 + 1.15\text{x}10^{-4}(\theta-10)^2 - 6\text{x}10^{-6}(\theta-10)^3$	for θ from 10° to 20°
$0.191 + 5\text{x}10^{-4}(\theta-41)$	for θ from 20° to 60°
$0.17569 + 3.308\text{x}10^{-2}\sin^2\theta$	for θ from 60° to 90°

4. ***Extended LEPS PES for*** **F + HH** ***reaction with angle dependent overlap parameter developed by Koeppl and Rutenburg***

We developed and used a PES designated KR. The overlap parameter for HH was 0.104. The overlap parameter for FH is varied with the orientation angle θ using the piecewise function defined below.

0.175	for θ from 0° to 10°
$0.175 - 1.15\text{x}10^{-4}(\theta-10)^2 + 6\text{x}10^{-6}(\theta-10)^3$	for θ from 10° to 20°
$0.159 - 5\text{x}10^{-4}(\theta-41)$	for θ from 20° to 60°
$0.17431 - 3.308\text{x}10^{-2}\sin^2\theta$	for θ from 60° to 90°

Note that the expression for the FH overlap parameter for the KR PES contains the same terms as the T2 expression, however, the signs of the angle dependent terms are reversed.

VI. NUMERICAL METHODS

Variational calculations were performed using FORTRAN programs on the VAX 6420 minicomputer at Queens College. Sets of trial variational parameters were generated using the methods of Sverdlik and Koeppl[36]. The downhill simplex algorithm was used to find the values of the variational parameters that minimize the canonical rate constant or mean reaction cross section[97,98]. The integrals of functions $N_\beta(T)$ and $N_\beta(E)$ were evaluated using Simpson's Rule (reported in tables) and simple quadrature.

The two dimensional integrals require integration over R and θ. For the F + HH reaction, the θ integration was from 0 to $\pi/2$; the resulting value of the integral is doubled to obtain the flux for reaction at both ends of the HH molecule. For the F + DH reactions, the θ integration was from 0 to π for the 6–parameter DS which does not distinguish between reaction at each end of DH. For the five– and ten–parameter DSs which distinguish between reaction at each end of DH, the integrals for $N^*_c(T)$ and $N^*_\mu(T)$ are obtained by adding the integrals for the ranges 0 to θ' (H end of DH) and θ' to π (D end of DH). Appropriate limits for R were found by trial and error. For both reactions the integration range for R was usually 1.0 to 7.0 a.u..

A grid of 280 (R) by 180 (θ) points was usually used for the F + HH reaction to calculate $N^c_*(T)$. A grid of 560 (R) by 720 (θ) points was usually used for the F + DH reactions. The quantity $D^c_{BC}(T)$ in the denominator of the expression for k(T) was usually calculated using 500 points. The value used for r^{BC}_{max} was usually 7.00 a.u. (see Eq. (20)).

It should be noted that the simplex search algorithm finds a local minimum, not the absolute minimum. Hence many searches which started with different sets of trial parameters were often made in attempts to find the global minimum for a given DS and PES. Note that it is impossible to prove that an extremum found in this way is a global extremum.

A FORTRAN program running on an IBM microcomputer is used to plot the intersections of a given DS with the r and R coordinate plane for a specified value of θ. Potential energy contours are also plotted for the two–dimensional r and R coordinate space for the specified value of θ on the same graph. The BC reaction valley is at the lower right corner of the plot. A series of two–dimensional DS and PES plots are made for specified values of θ to characterize the angular dependence of the DS and PES. A set of plots for the F + HH reaction is shown in Fig. 6.

Such plots were analyzed in order to determine whether the DS found by a variational search was acceptable, i.e., to verify that there are no "holes" in it. Holes are made by trajectories which originate in the reactant region of configuration space and reach to the product region without crossing the DS. If a DS was unacceptable, we repeated the variational search with restrictions imposed on the DS which ensured that it would not have holes.

The simplex is a geometric figure with one more vertex than the parameter space in which it is embedded[97], e.g., a 6–parameter DS corresponds to a simplex with 7 vertices. The value of k(T) or $\overline{S}_r(E)$ for a given vertex is called the response. A set of parameter values gives the response at a vertex. The search algorithm manipulates the simplex vertices according to a set of rules to find the lowest response. If a vertex is generated during the search that corresponds to DS parameters which violate a restriction on their values, the search algorithm assigns a large value to the response and the search moves away from the region of parameter space that violates the restriction.

We use another FORTRAN program for an IBM microcomputer to produce plots of the integrands of $N_*^c(T)$ and $N_*^\mu(E)$. The variables of the integrands are R and θ. The value of the integrand at particular values of R and θ is proportional to the flux through the DS at R and θ. Hence contour plots of the integrand in R and θ coordinate space show how the variational transition state theory reactive flux is

FIGURE 6

Illustration of a series of 2–dimensional contour plots of potential energy surface and dividing surface as intersection with potential energy surface for several values of angle θ. This is a plot of Truhlar 1 potential energy surface and linear combination of internal coordinates dividing surface (dashed line) for 300 K for F + HH reaction. Contours of potential energy surface are in eV.

Fig.6a

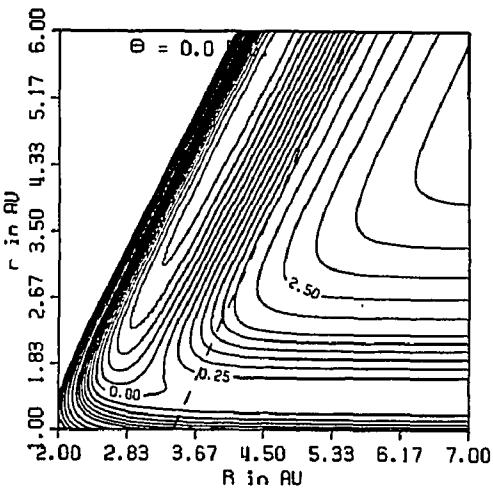

Fig.6b

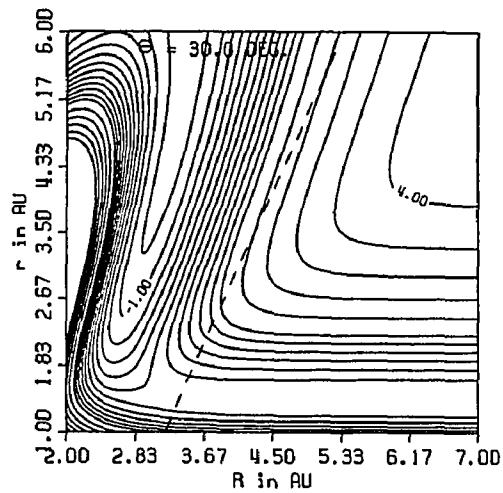

Fig.6c

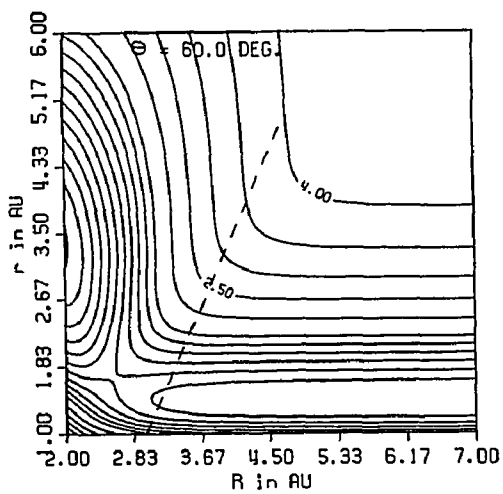

Fig.6d

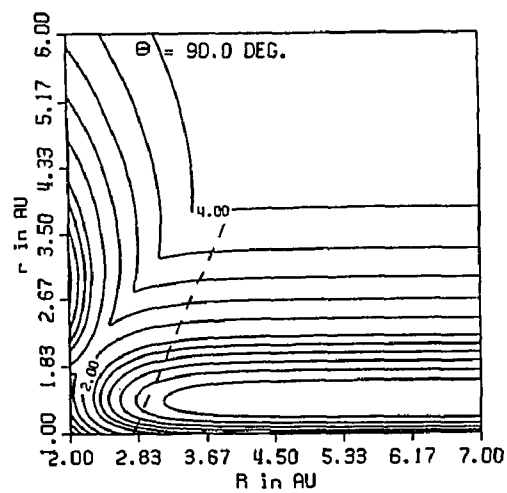

distributed on the DS. We refer to such plots as reactivity relief maps. Reactivity relief maps are plotted using R and θ Cartesian axes and also the polar representation of these coordinates (see Figs. 7a and 7b, respectively).

A FORTRAN program that runs on an IBM microcomputer was used to find the angle (θ) dependent potential energy saddle points in r and R coordinate space for the F + HH and F + DH reactions. Plots of potential energy contours for r and R coordinate space at fixed θ for all of the PES studied in this work show a single saddle point for θ on the range 0 to π, i.e., no basins were found. The saddle point locations and energies were found using the downhill simplex algorithm. At each value of θ, the saddle point energy corresponds to the minimum energy required for reaction at the specified θ. Plots of the minimum energy for chemical reaction (angle dependent barrier for chemical reaction) versus θ for the F + HH and F + DH reactions are shown in Figs. 8 and 35 in Chs. 3 and 4, respectively.

If potential energy alone determined the location of the best variational DS, the DS would intersect (pass through) the angle dependent saddle points, i.e., the DS would span high energy regions of configuration space as well as possible. At all values of θ, the intersection of the DS with the r and R coordinate plane would pass through the saddle point and lie on the path of steepest ascent from it in both directions. However, entropic factors as well as potential energy determines the location of the DS of lowest reactive flux. Nevertheless we developed a method to find such a steepest ascent DS to compare with the variational DS and sometimes use as the basis for a simplex search to find the best variational DS. PES plots were made for a set of θ values. On each plot, a line was drawn through the saddle point which followed the path of steepest ascent from it. Points were read from the line and in this way sets of points were found at each θ that lie on the steepest ascent DS. The downhill simplex algorithm together with a least squares fit was used to find the parameters of a DS (designated LS DS) which fits the points so generated.

FIGURE 7

Illustration of reactivity relief maps, contour maps of integrands of the integral in the numerator of the expression of the canonical rate constant. The plots are for quadratic dividing surface obtained with slope restriction and Truhlar 2 potential energy surface for 300 K for F + HH reaction. Contours are in arbitrary units.

Fig.7a: Cartesian plot

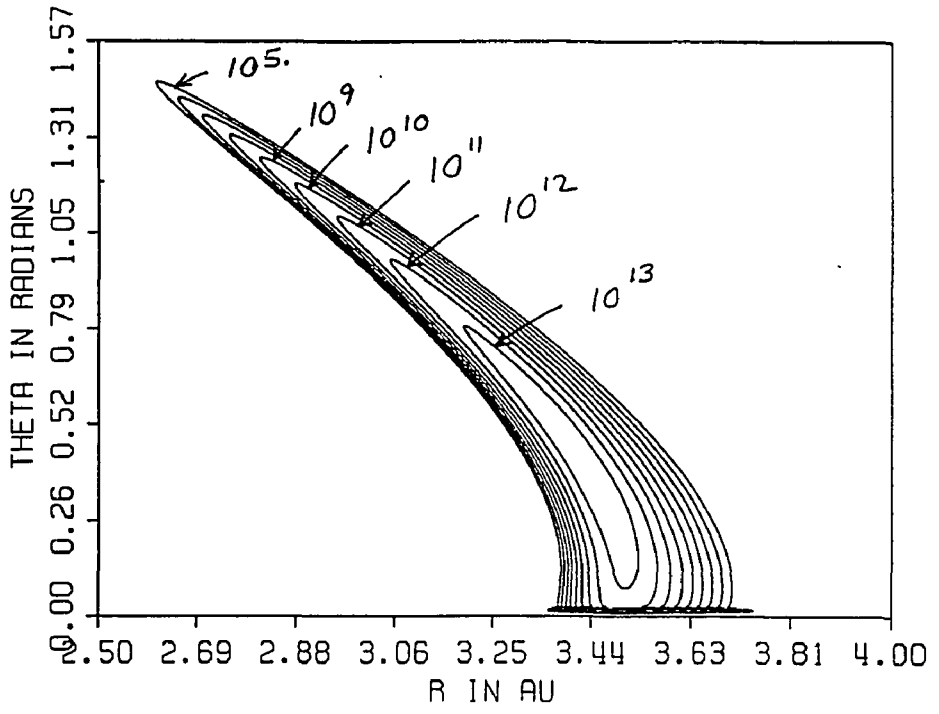

Fig.7b: Polar plot

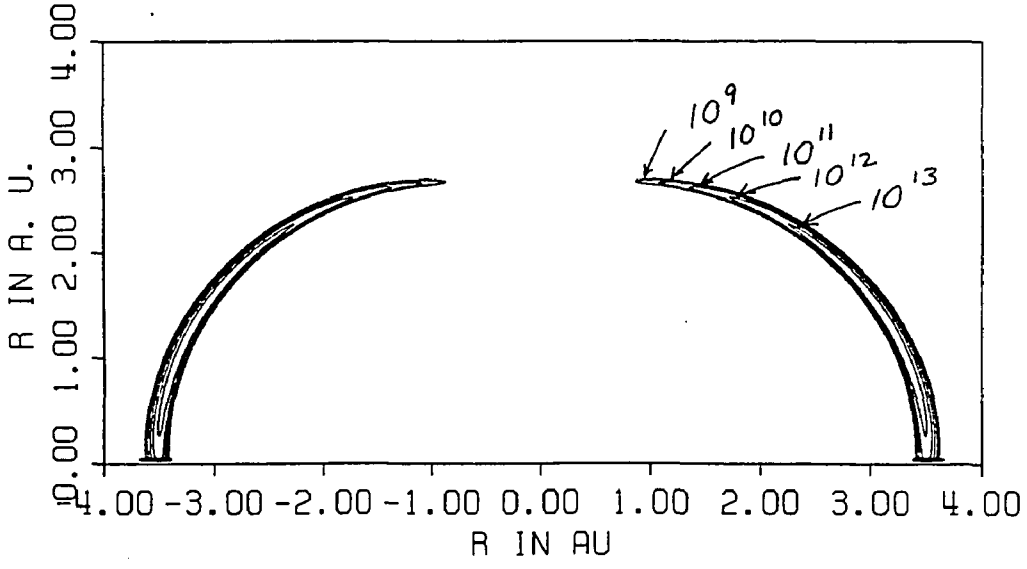

CHAPTER 3

CANONICAL VARIATIONAL RATE CONSTANTS FOR F + HH → FH + H REACTION

In this chapter, canonical rate constants, reactivity relief maps, and angular distributions of rates are presented for the reaction F + HH → FH + H. Results are presented for three potential energy surface (PES) functions and three dividing surface (DS) functions described in Ch. 2, Sects. V and II, respectively, using the methods described in Ch. 2, Sect. VI. Simplex searches were initiated to obtain variational canonical rate constants at temperatures of 300, 1500, and 3000 K. Values of the DS parameters for some DS types were determined subject to restrictions, which will be discussed later in this chapter. Tables in this chapter give values of canonical rate constants (k(T)); corresponding DS parameters are given in Appendices 1 – 23. DSs which were chosen to be presented on plots are marked with ← in the tables.

I. THE EFFECT OF POTENTIAL ENERGY SURFACE FUNCTION ON RATE CONSTANT

The expressions for the three PESs used in this project are given in Ch. 2, Sect. V. The overlap parameters of the Truhlar 1 (T1) potential energy function for FH and H_2 do not depend on orientation angle θ (see Ch. 2, Sect. V 3). The FH overlap parameter for the Truhlar 2 (T2) and Koeppl/Rutenburg (KR) potential energy functions depend on θ (see Ch. 2, Sects. V 4 and 5, respectively). Plots of potential energy contours for fixed θ in r and R coordinate space showed a single saddle point and no basins for $0 \leq \theta \leq \pi/2$ for these potential energy functions. The energy at the saddle point varies with θ. The saddle point energy (barrier height) at

θ is the minimum potential energy required for chemical reaction at angle θ. The variation of the angle dependent minimum energy for reaction with θ for the potential energy surfaces used in this work and the Muckerman 5 (M5) PES is shown in Fig. 8. For a given θ the barrier height shows an increasing trend in the PES series T2 → T1 → KR. The increase in barrier height with θ is steeper for T1 than for T2, and the barrier height profile for KR is steeper than T1 to about the same degree that T1 is steeper than T2. We will sometimes use the term floppy to describe the steepness of the barrier height versus θ profile. The "floppiness" of the three potential energy functions increases in the series KR → T1 → T2.

The variational theory can be used to characterize the dynamical stereochemistry of the F + HH reaction for the three potential energy functions. One can readily compute the contribution to the variational canonical rate constant for specified increments of θ. See Eqs. (21) and (22) of Ch. 1. Fig. 9 shows contributions to the canonical variational rate constant for 16 equal increments of θ from 0 to $\pi/2$ for KR, T1 and T2 PESs. The θ range from 0 to $\pi/2$ was divided into 5.625 deg. intervals. These results were obtained using the same type of quadratic DS (slope restriction) which will be described later in this chapter. The angular distributions of the rate constant are plotted as histograms centered on each 5.625 deg. interval. The largest contribution to the rate constant corresponds to the angular range 11.2 to 16.9 deg. for KR PES, 16.9 to 22.5 deg. for T1 PES, and 22.5 to 28.1 deg. for T2 PES. Contributions to the rate constant undergo a dramatic shift towards larger θ as the PES becomes floppier. Note that the sum of the contributions gives the rate constant. The rate constant for T2 is the largest because the barrier height versus θ profile shown in Fig. 8 lies lowest; more reaction systems have enough energy to surmount the barrier at all angles. Note also that the largest contribution to the rate constants does not occur for the increment 0 to 5.6 deg. near $\theta = 0$ where the potential energy is the lowest because the "volume

FIGURE 8

Relationship between minimum potential energy for F + HH reaction (barrier height) and orientation angle θ (see Fig. 5) for potential energy surfaces used in this work.

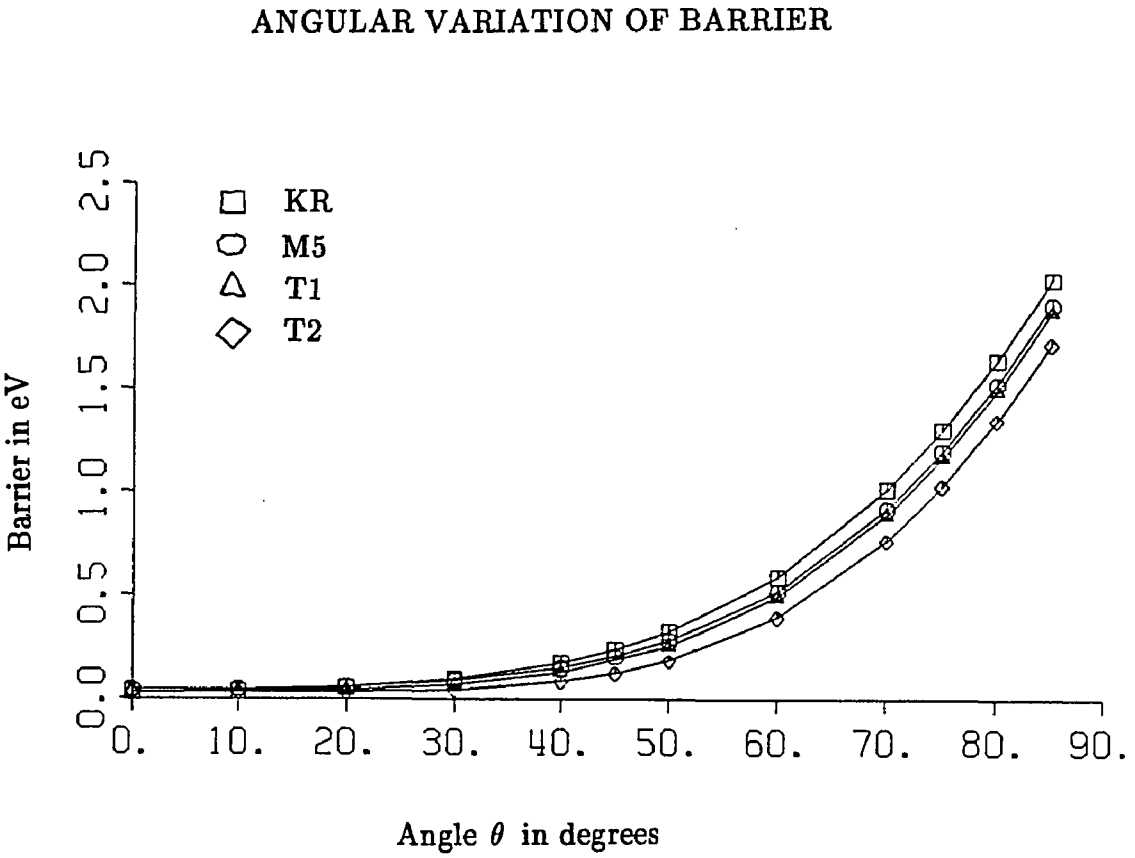

Potential energy surfaces

KR – Koeppl/Rutenburg
M5 – Muckerman 5
T1 – Truhlar 1
T2 – Truhlar 2

FIGURE 9

Contribution from 16 equal angular increments from $\theta = 0$ to $\pi/2$ to canonical rate constant (k(T)) for F + HH reaction for 300 K temperature (T) for quadratic dividing surfaces obtained with slope restriction and potential energy surfaces used in this work. Rate constants (rates) are in 10^{12} $cm^3/mol \cdot s$.

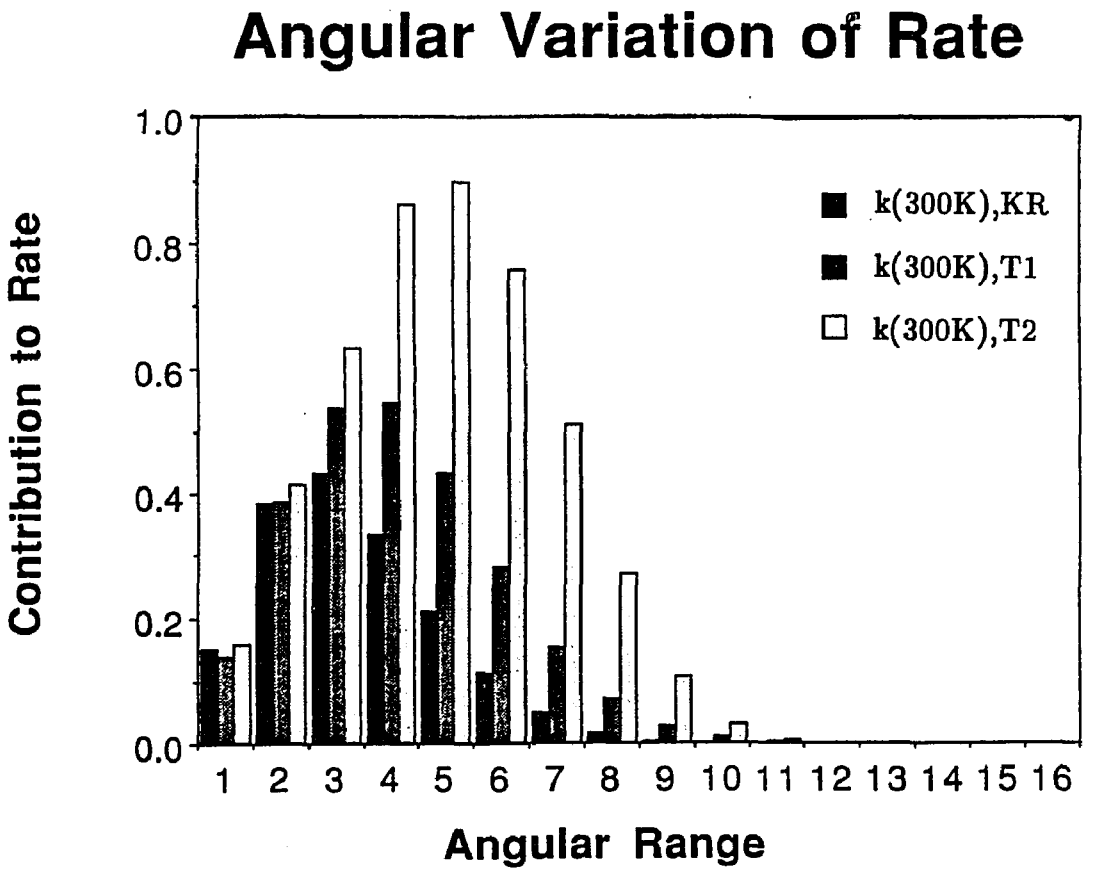

Potential energy surfaces

KR – Koeppl/Rutenburg
T1 – Truhlar 1
T2 – Truhlar 2

element" for the integral $N_*^c(T)$ contains the factor $\sin\theta$.

Rate constants were compared for the PES series keeping temperature and DS type fixed to study the relationship between PES and variational results. Table 1 presents rate constants for three PESs, three DSs and three temperatures. The results for PESs are tabulated in columns; results for the DSs are tabulated in rows; the type of restriction imposed on DS parameters is indicated in parenthesis beside k(T). In order to see how rate constant depends on the PES for the same DS, the table should be traversed horizontally along its rows. The rate constant increases in the PES series KR → T1 → T2 for each DS and each temperature.

Fig. 10 shows contours of the reactivity relief maps, i. e., contours of $N_*^c(T)$ (Ch. 1, Eq. (22)), in terms of Cartesian R and θ coordinates for the quadratic slope restriction DS at 300 K for KR and T2 PESs. It is easy to see that the area spanned by the same contour is larger for the "floppier" T2 PES and that the region of high reactivity extends to smaller R and larger θ. Fig. 11 provides an alternative representation of these reactivity relief maps in polar coordinates R and θ. The highest contour (10^{13} arbitrary units) extends to $\theta = 30$ deg. for KR PES and to 45 deg. for T2 PES. The rate constant increases for a PES as the barrier profile (see Fig. 8) "drops" because more reaction systems have enough energy to surmount the barrier at all angles of approach.

II. THE EFFECT OF DIVIDING SURFACE FUNCTION ON RATE CONSTANT

The expressions for each of the DSs used in this work are given in Ch. 2, Sect. II. The truncated (TR) DS is planar and has no angular dependence (see Ch. 2, Sect. II A1). The linear combination of internal parameters (LCIC) DS is planar and depends on angle θ (see Ch. 2, Sect. II A2). Quadratic (Q) and cubic (C) DSs are both angle dependent and curved and have 6 and 10 parameters, respectively

TABLE 1

Comparison of canonical variational rate constants (k(T)) for F + HH reaction for a series of dividing surfaces (DS) and potential energy surfaces (PES) for several temperatures (T). Rate constants are in $10^{12}cm^3/mol \cdot s$. ← marks the k(T) for which DSs are plotted in Fig. 12.

Dividing surfaces	Potential energy surfaces		
	KR	T1	T2
	k(300K)		
TR	4.163	6.775	13.99 ←
LCIC	3.764	5.605	9.941 ←
Q	3.331(S)	4.986(E)	8.828(E) ←
	k(1500K)		
TR	109.1	142.5	190.6
LCIC	81.03	101.1	129.6
Q	74.78(E)	93.78(S)	119.9(E)
	k(3000K)		
TR	302.0	353.3	414.9
LCIC	222.1	256.9	300.0
Q	207.9(E)	240.7(ES)	281.8(E)

PES

KR – Koeppl/Rutenburg
T1 – Truhlar 1
T2 – Truhlar 2

DS

TR – truncated
LCIC – linear combination of internal coordinates
Q – quadratic
E – energy limit
S – slope
ES – energy limit and slope
SD – second derivative

FIGURE 10

Comparison of reactivity relief maps in Cartesian coordinates for quadratic dividing surfaces obtained with slope restriction and two potential energy surfaces (PES) for 300 K. Contours are in arbitrary units.

Fig.10a

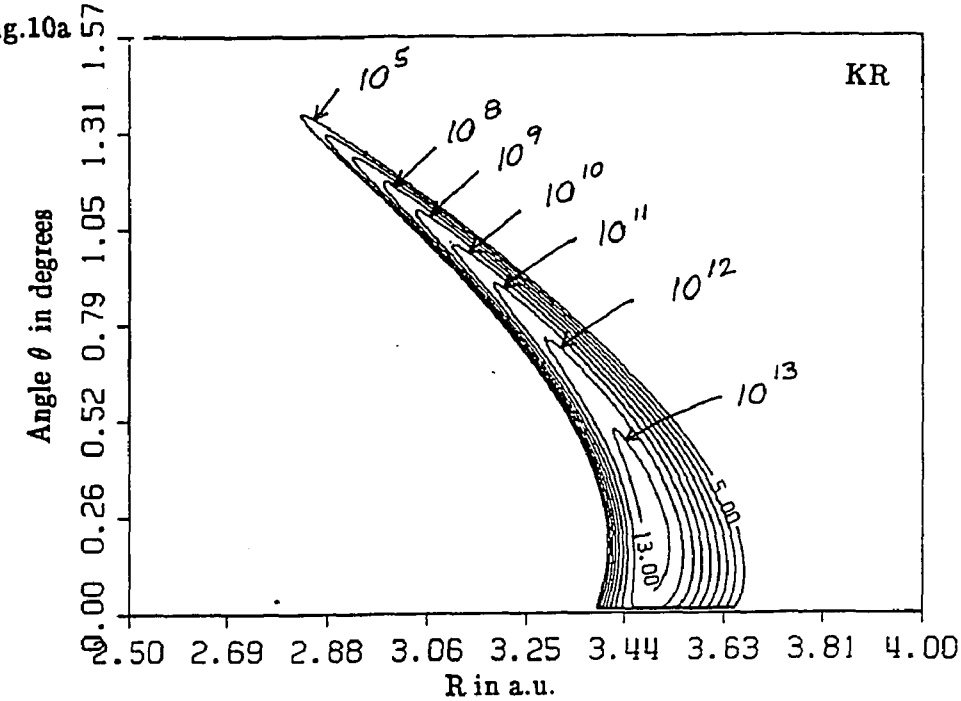

Fig.10b

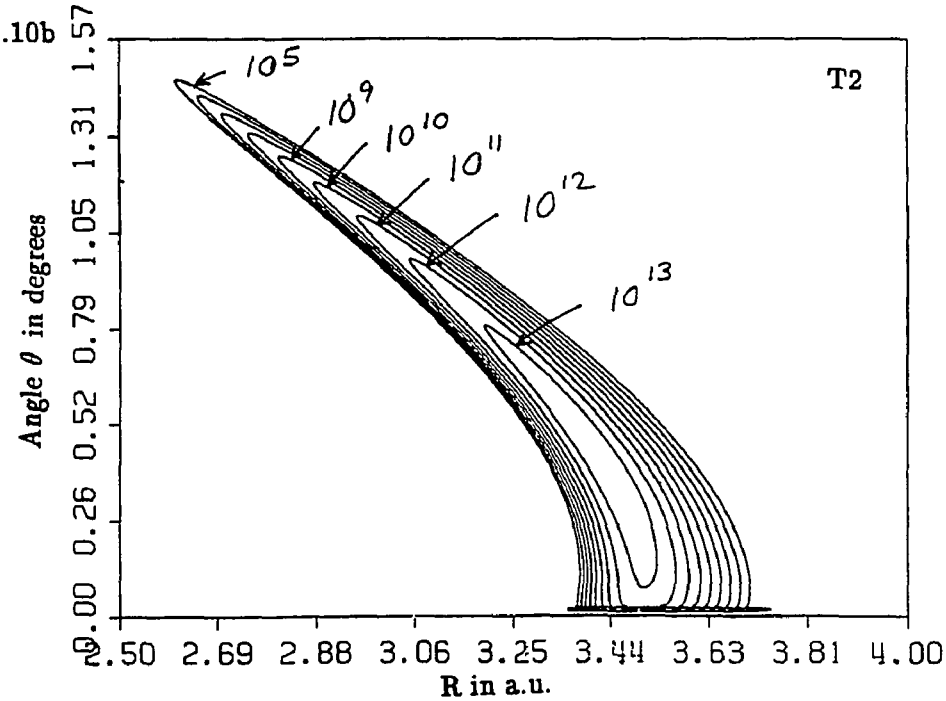

PES: KR – Koeppl/Rutenburg T2 – Truhlar 2

FIGURE 11

Comparison of reactivity relief maps in polar coordinates for quadratic dividing surfaces obtained with slope restriction and two potential energy surfaces (PES) for 300 K. Contours are in arbitrary units.

Fig.11a

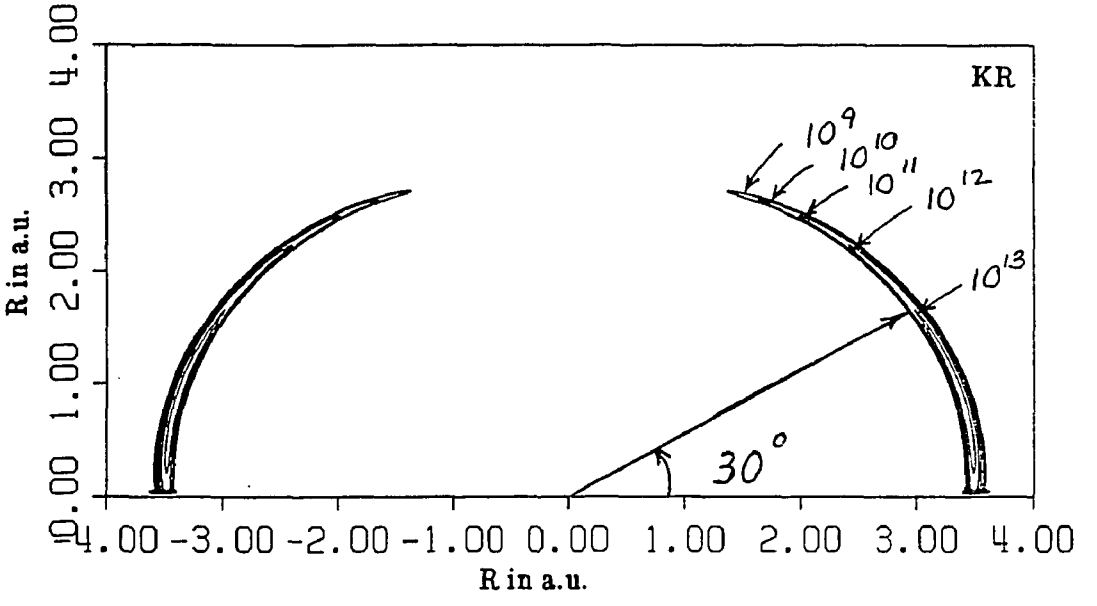

Fig.11b

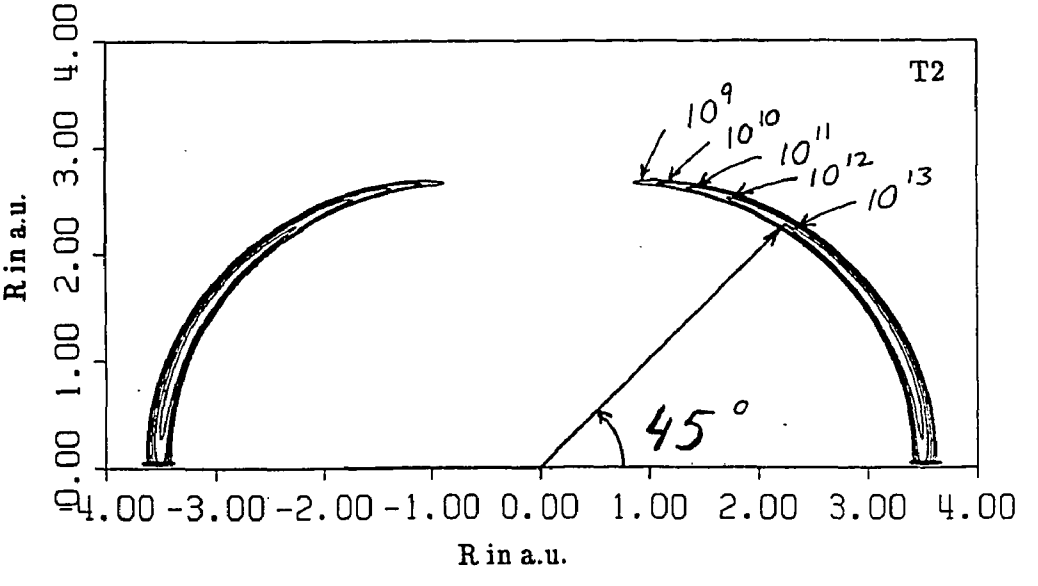

PES: KR – Koeppl/Rutenburg T2 – Truhlar 2

(see Ch. 2, Sect. II A3 and A4). For the discussion below Q and C DSs are not differentiated from each other, but rather contrasted to planar DSs as curved DSs. So, Q is used to represent any curved DS in the sense of this discussion. A discussion of the Q vs C DS formulation is given in Sect. VII of this chapter. Fig.12 shows the intersection of TR, LCIC and Q DSs at 300 K with the r and R coordinate plane for the T2 PES for four values of θ. Two quadratic DSs, obtained with different restrictions imposed on DS parameters, are shown. The detailed discussion of the restrictions is provided in Sect. IV of this chapter. At this point note that the Q DS obtained with energy (E) limit restriction is shown because it gave the lowest value of k(T) for this PES and temperature. The Q DS obtained with slope (S) restriction is shown because it was chosen to be the standard for variational calculations (as explained in Sect. IV of this chapter), although for this PES and temperature it did not give the lowest k(T).

Results were studied for a series of DSs keeping PES and temperature fixed. The lowest rate constants for each type of DS, PES, and temperature are presented in Table 1 as described above. In order to see how rate constants vary with the DS for the same PES, the table should be traversed vertically. The variational results decrease monotonically with the order of expansion of the DS for each PES and each temperature, i. e., the rate constants decrease in the DS series TR → LCIC → Q. Fig. 13 shows reactivity relief maps for TR, LCIC and Q(E) DSs at 300 K for T2 PES. Fig. 14 shows maps for TR, LCIC and Q(S) DSs. Contours of the same value span smaller regions in the TR → LCIC → Q series in Figs. 13 and Fig. 14 regardless of the type of the restriction imposed on the Q DS. For TR DS some contours with low values do not separate in the two quadrants. The separation is achieved for the LCIC DS and increases for the Q DS.

TR DSs, which do not use θ for variational optimization, have the highest rate. The rate constants improve significantly for the angle dependent LCIC and Q

FIGURE 12

Four dividing surfaces for Truhlar 2 potential energy surface and 300 K for values of θ equal to 0, 30, 60, and 90 deg.. Contours of potential energy surface are in eV.

Fig.12a

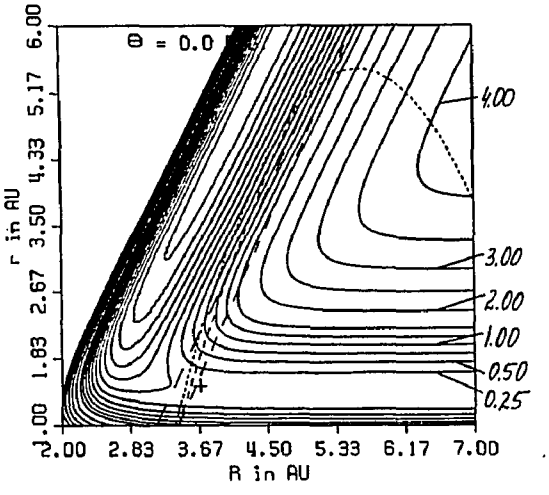

Fig.12b

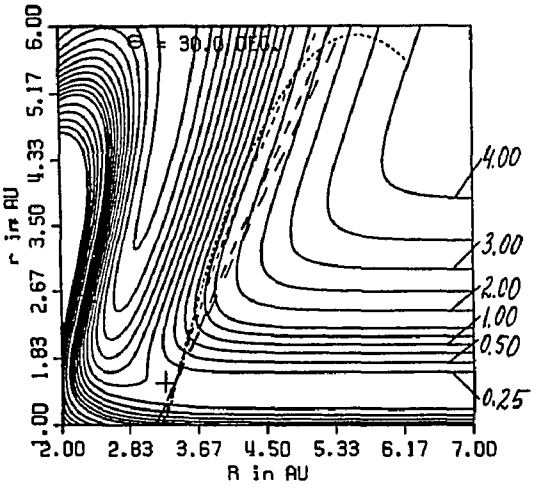

Fig.12c

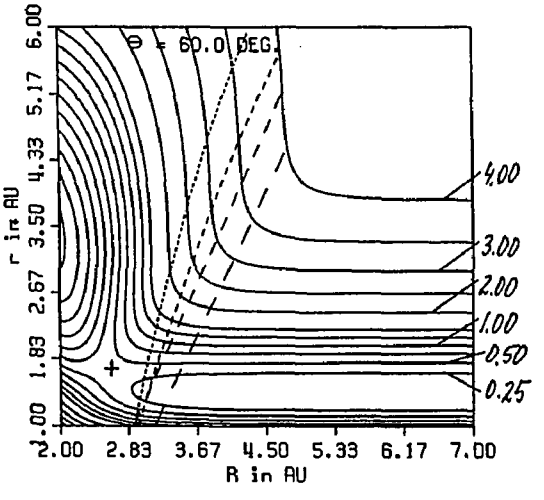

Fig.12d

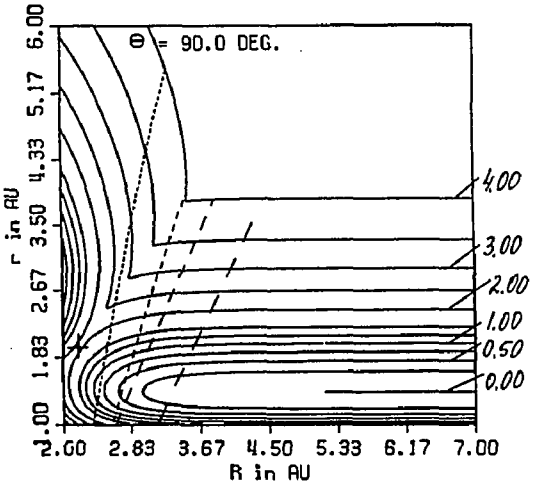

Dividing surfaces

truncated

linear combination of internal coordinates

quadratic obtained with slope restriction

quadratic obtained with energy limit restriction

Potential energy surface

saddle point

FIGURE 13

Reactivity relief maps for three dividing surfaces (DS) (see Fig.12) for Truhlar 2 potential energy surface and 300 K. Contours are in arbitrary units.

Fig.13a

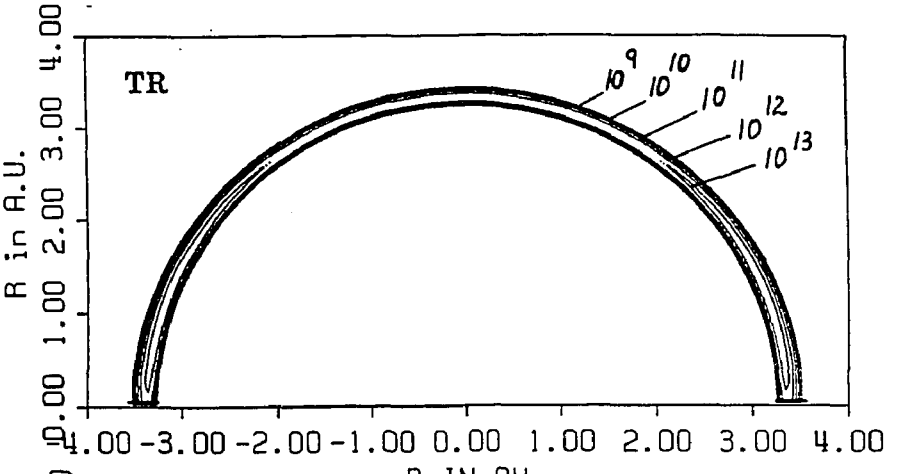

Fig.13b

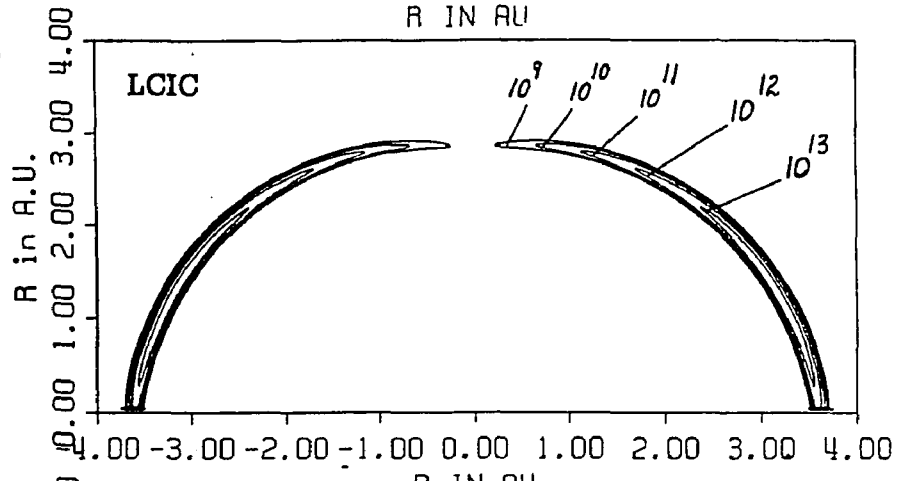

Fig.13c

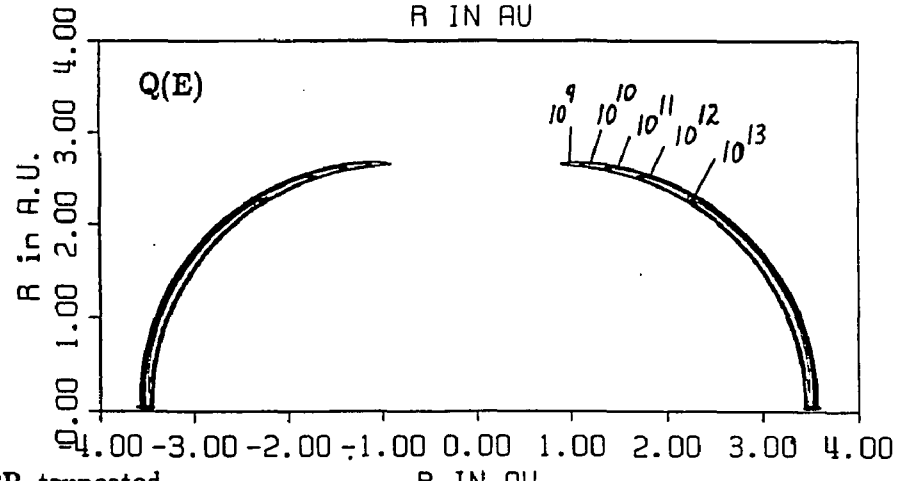

DS: TR–truncated,
LCIC–linear combination of internal coordinates, Q(E)–energy limit quadratic

FIGURE 14

Reactivity relief maps for three dividing surfaces (DS) (see Fig.12) for Truhlar 2 potential energy surface and 300 K. Contours are in arbitrary units.

Fig.14a

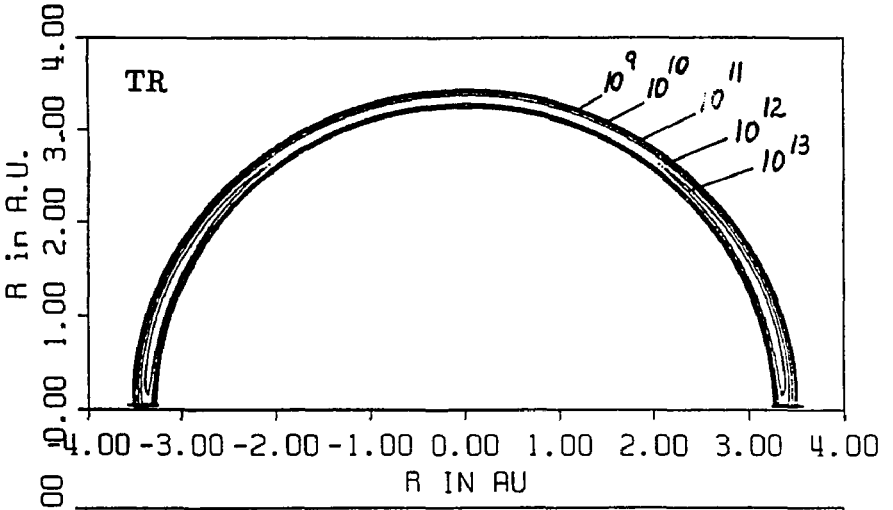

Fig.14b

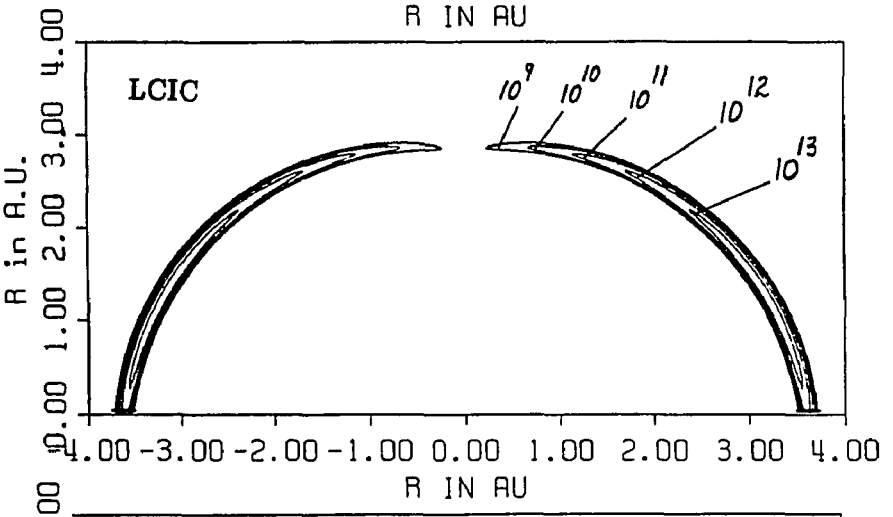

Fig.14c

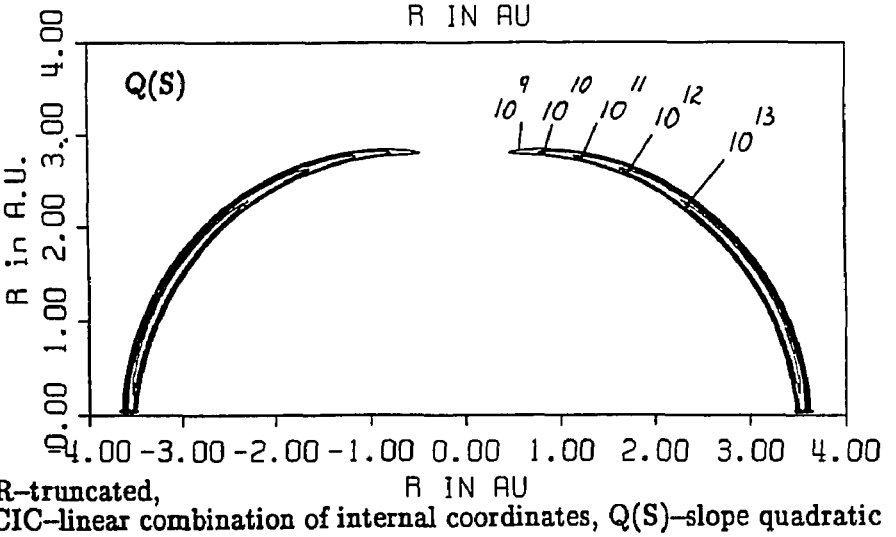

DS: TR–truncated,
LCIC–linear combination of internal coordinates, Q(S)–slope quadratic

DSs versus the angle independent TR DS. TR DSs vary neither their positions nor slopes with θ, whereas other DSs which include θ for variational optimization do (see Fig. 12). The angle dependent DSs have more flexibility and can avoid multiple crossings of the DS and minimize the value of the flux integral more successfully than TR DSs. There was also improvement of rate constants obtained using Q DSs vs LCIC DSs. This can be explained using the same reasoning: Q DSs are curved, planar LCIC DSs are flat. Curved DSs have more flexibility than planar DSs; hence, curved DSs can avoid multiple crossings of the DS by trajectories and minimize the value of the flux integral more successfully than planar DSs.

Table 2 presents ratios of rate constants given in Table 1. The columns of the table tabulate ratios of rate constants for the same type of PES as in Table 1, the rows of the table give ratios of rate constants for different types of DS (higher/lower). Note that the improvement in the rate constant obtained by using the angle dependent DSs (i.e., LCIC and Q vs TR) increases in the PES series KR → T1 → T2. These results can be understood in terms of the angular dependence of the position of the energy barrier. Fig. 15 shows the pronounced variation of R at the saddle point with θ. The improvement obtained by using angle dependent DSs is greatest when the barrier–angle profile is lowest because the ability of the DS to remain closer to the saddle point over a large angular range is more important for minimizing the equilibrium flux through the DS.

Table 3 is similar to Table 1. It presents k(T) for TR, LCIC and Q DSs. In Table 1 results are given for the Q DSs which gave the lowest k(T) no matter which restriction was imposed on the Q DS. Table 3 gives rate constants for quadratic DSs determined with the slope (S) restriction. Q(S) DSs were chosen to be our variational standard for Q DSs (see Sect. IV of this Chapter). Table 4 presents ratios for k(T) from Table 3 in the same manner as Table 2 presents ratios for Table 1. Ratios in Table 4 for Q(S) DSs are sometimes smaller than ratios in Table 2

TABLE 2

Ratios of canonical variational rate constants (k(T)) for F + HH reaction for a series of dividing surfaces (DS) and potential energy surfaces (PES) for several temperatures (T) (see Table 1).

Dividing surfaces	Potential energy surfaces		
	KR	T1	T2
	ratios of k(300K)		
TR/Q	1.250	1.359	1.585
TR/LCIC	1.106	1.209	1.407
LCIC/Q	1.130	1.124	1.126
	ratios of k(1500K)		
TR/Q	1.459	1.519	1.590
TR/LCIC	1.346	1.409	1.471
LCIC/Q	1.084	1.078	1.081
	ratios of k(3000K)		
TR/Q	1.453	1.468	1.472
TR/LCIC	1.360	1.375.	1.383
LCIC/Q	1.068	1.067	1.065

PES

KR – Koeppl/Rutenburg
T1 – Truhlar 1
T2 – Truhlar 2

DS

TR – truncated
LCIC – linear combination of internal coordinates
Q – quadratic

FIGURE 15

Decreasing trend in the value of R at the saddle point as orientation angle θ increases for potential energy surfaces studied in this research.

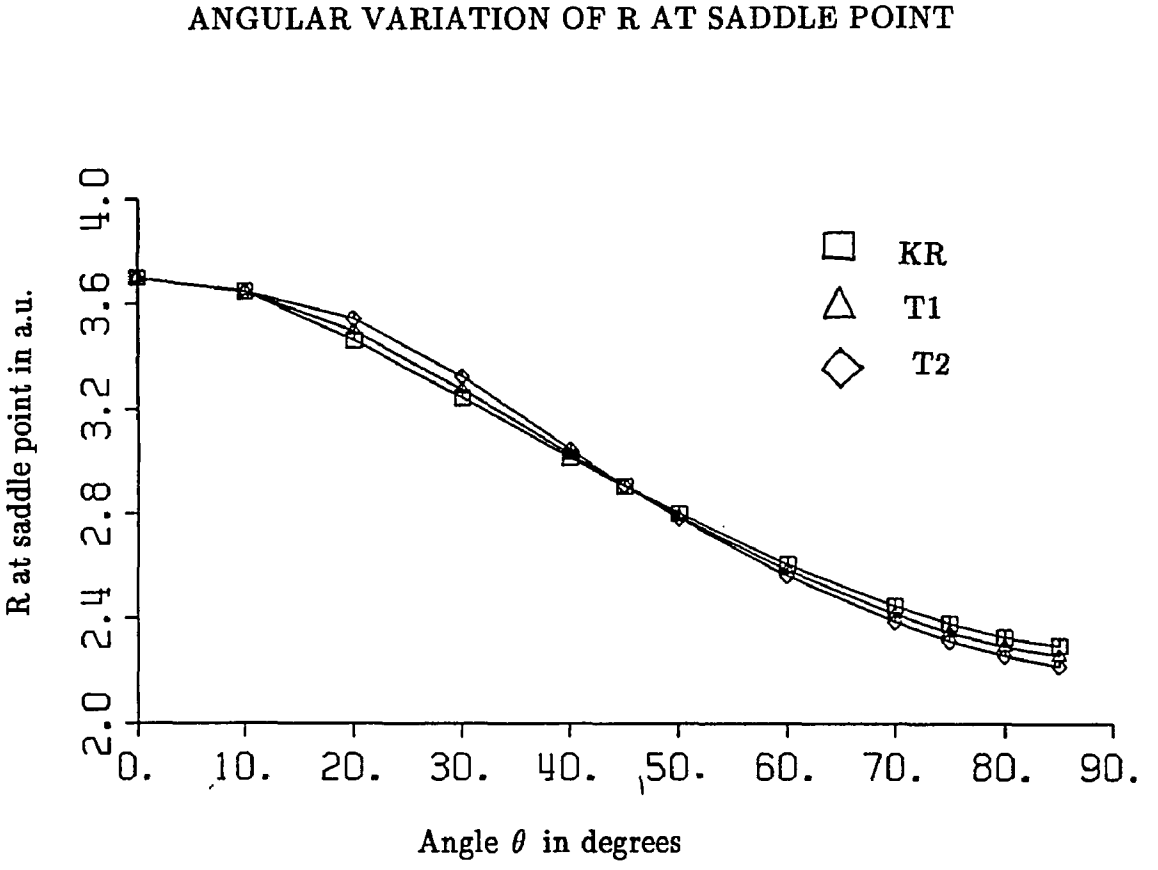

Potential energy surfaces

KR – Koeppl/Rutenburg
T1 – Truhlar 1
T2 – Truhlar 2

TABLE 3

Comparison of canonical variational rate constants (k(T)) for F + HH reaction for a series of dividing surfaces (DS) and potential energy surfaces (PES) for several temperatures (T). Rate constants are in $10^{12}cm^3/mol \cdot s$.
← marks k(T) for which DSs are plotted in Fig. 12.

Dividing surfaces	Potential energy surfaces		
	KR	T1	T2
		k(300K)	
TR	4.163	6.775	13.99 ←
LCIC	3.764	5.605	9.941 ←
Q(S)	3.331	5.021	9.178 ←
		k(1500K)	
TR	109.1	142.5	190.6
LCIC	81.03	101.1	129.6
Q(S)	75.54	93.78	120.5
		k(3000K)	
TR	302.0	353.3	414.9
LCIC	222.1	256.9	300.0
Q(S)	209.0	242.0	283.4

PES

KR – Koeppl/Rutenburg
T1 – Truhlar 1
T2 – Truhlar 2

DS

TR – truncated
LCIC – linear combination of internal coordinates
Q – quadratic
S – slope
SD – second derivative

TABLE 4

Ratios of canonical variational rate constants (k(T)) for F + HH reaction for a series of dividing surfaces (DS) and potential energy surfaces (PES) for several temperatures (T) (see Table 3).

Dividing surfaces	Potential energy surfaces		
	KR	T1	T2
	ratios of k(300K)		
TR/Q	1.250	1.349	1.524
TR/LCIC	1.106	1.209	1.407
LCIC/Q	1.130	1.116	1.083
	ratios of k(1500K)		
TR/Q	1.444	1.519	1.582
TR/LCIC	1.346	1.409	1.471
LCIC/Q	1.073	1.078	1.075
	ratios of k(3000K)		
TR/Q	1.445	1.460	1.464
TR/LCIC	1.360	1.375.	1.383
LCIC/Q	1.063	1.062	1.059

PES

KR – Koeppl/Rutenburg
T1 – Truhlar 1
T2 – Truhlar 2

DS

TR – truncated
LCIC – linear combination of internal coordinates
Q – quadratic

since Q(S) DSs are not necessarily the ones which give the lowest rate constants among Q DSs. But the general trends in effect of order of DS expansion in Tables 3 and 4 are similar to the trends in Tables 1 and 2.

III. THE EFFECT OF TEMPERATURE ON RATE CONSTANT

Variational rate constants were obtained for each type of DS and each type of PES at 300, 1500 and 3000 K (see Tables 1 and 3). The rate constants were compared for these temperatures keeping the DS and PES fixed (see Tables 1 and 2, and 3 and 4). The rate constants increase with increasing temperature for each DS and PES. Fig. 16 shows Q(S) DSs for the T2 PES at 300, 1500 and 3000 K. The values of k(T) are given in Table 3. Fig. 17 shows reactivity relief maps for the DSs shown in Fig. 16. Fig. 18 shows an enlarged map for 300 K. The area spanned by contours of the same value increases with temperature. The map at 300 K has an "island" which will be discussed in detail in Sect. IV of this chapter.

Fig. 19 shows the angular distribution of reactivity from $\theta = 0$ to $\pi/2$ for the Q(S) DS and T2 PES at three temperatures. Contributions to the rate constant for 16 equal increments of θ are plotted. Each contribution to the rate constant increases with temperature and the peak contribution moves to larger θ for the series 300 → 1500 → 3000 K.

Fig. 20 shows the effect of temperature on rate constant for Q(S) DSs for the PESs studied in this work. Rate constants increase with temperature for each PES, with T2 PES always having the highest and KR the lowest value. Note that as the temperature decreases the variation of the rate constant with PES increases. The relative increase of rate constant with temperature is largest for the KR PES, which has the steepest energy barrier – angle profile.

FIGURE 16

Quadratic dividing surfaces obtained with slope restriction for 300, 1500, and 3000 K for Truhlar 2 potential energy surface for values of θ equal to 0, 30, 60, and 90 deg.. Contours of potential energy surface are in eV.

Fig.16a

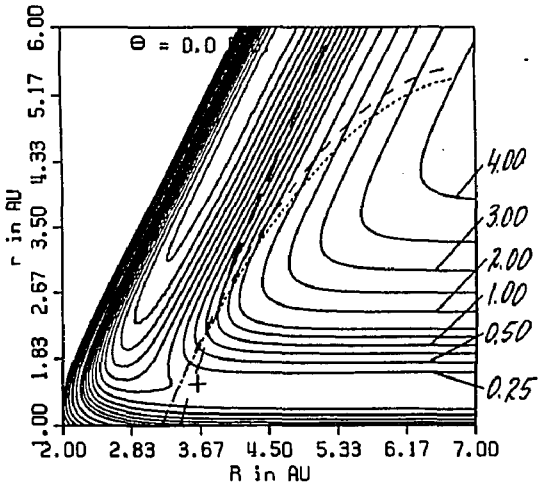

Fig.16b

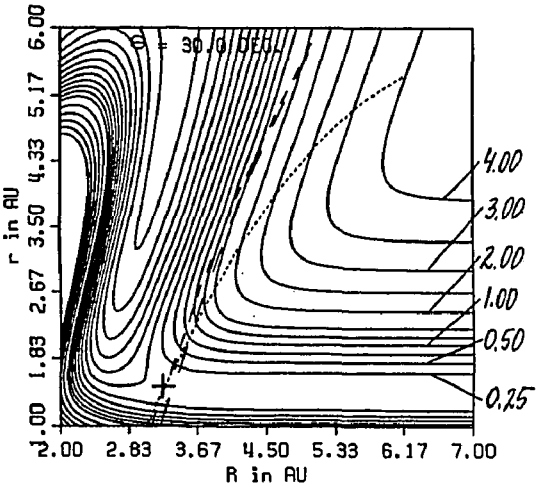

Fig.16c

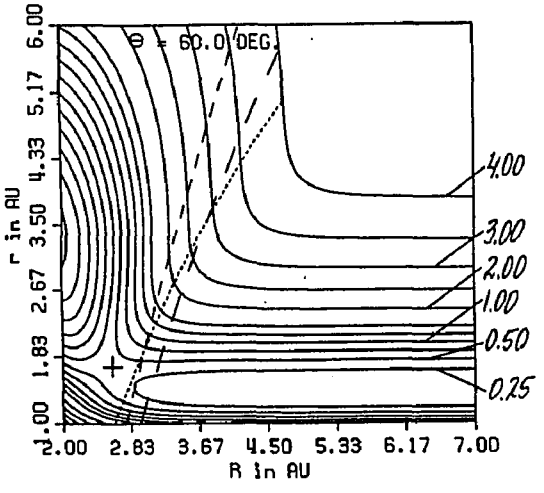

Fig.16d

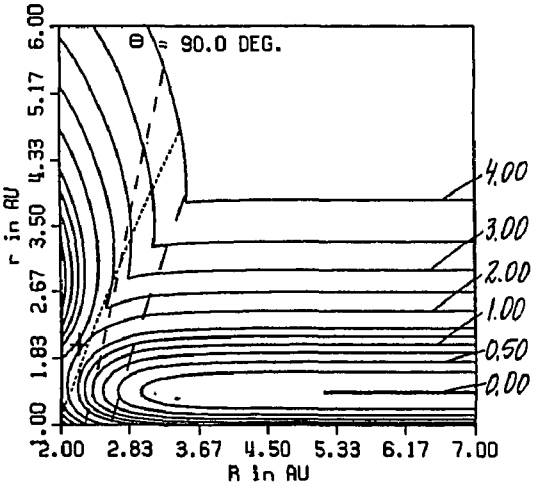

Dividing Surfaces

300 K

1500 K

3000 K

Potential energy surface

saddle point

FIGURE 17

Reactivity relief maps for quadratic dividing surfaces obtained with slope restriction for 300, 1500, and 3000 K for Truhlar 2 potential energy surface. See Fig. 16. Contours are in arbitrary units.

Fig.17a

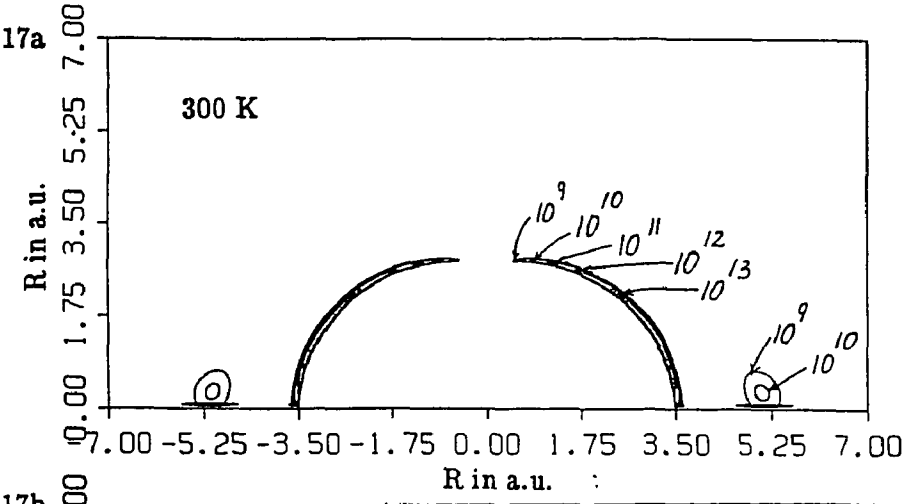

Fig.17b

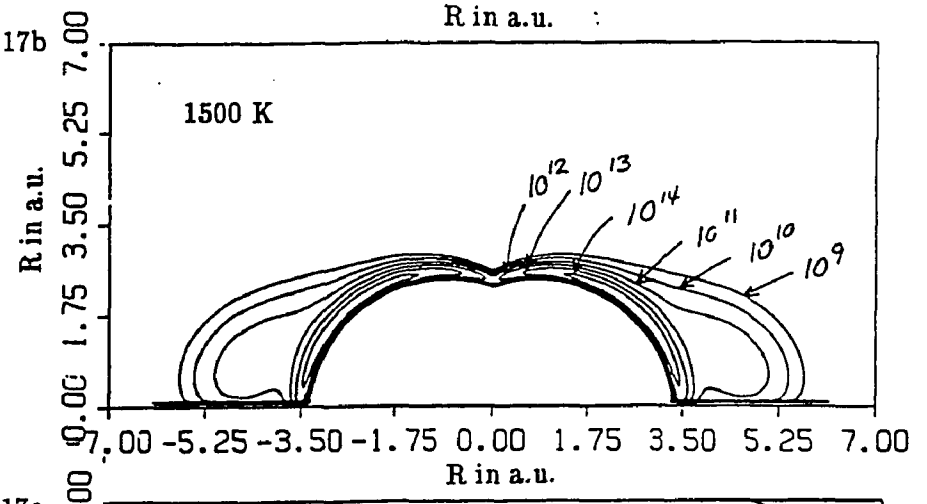

Fig.17c

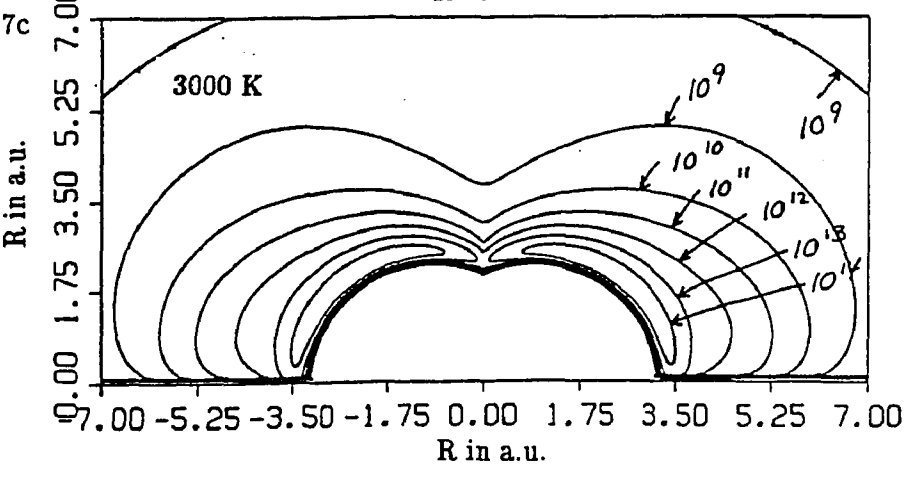

FIGURE 18

Reactivity relief map for quadratic dividing surface obtained with slope restriction for Truhlar 2 potential energy surface and 300 K. See Figs. 16 and 17.

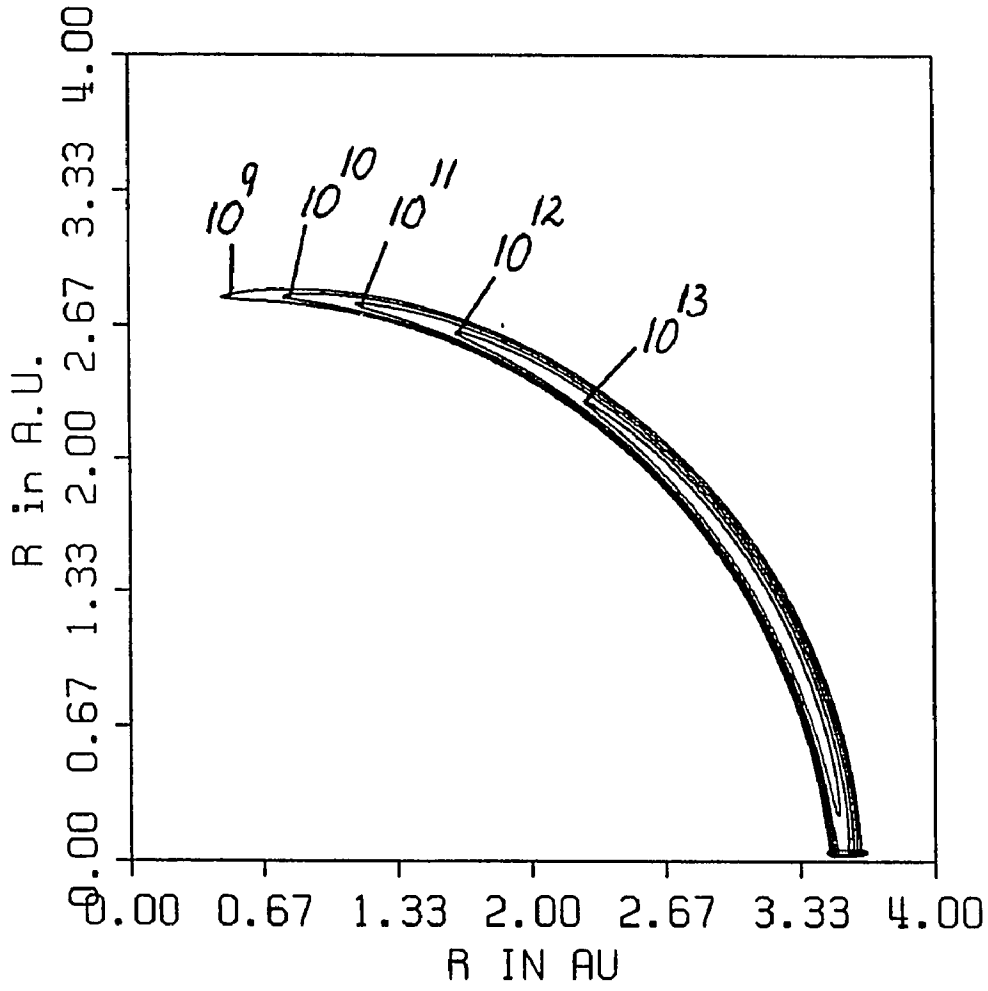

FIGURE 19

Contribution from 16 equal angular increments for $\theta = 0$ to $\pi/2$ to canonical rate constant (k(T)) for quadratic dividing surfaces obtained with slope restriction for Truhlar 2 potential energy surface for three temperatures (T). Contributions to rate constant (rate) are in 10^{12} $cm^3/mol \cdot s$.

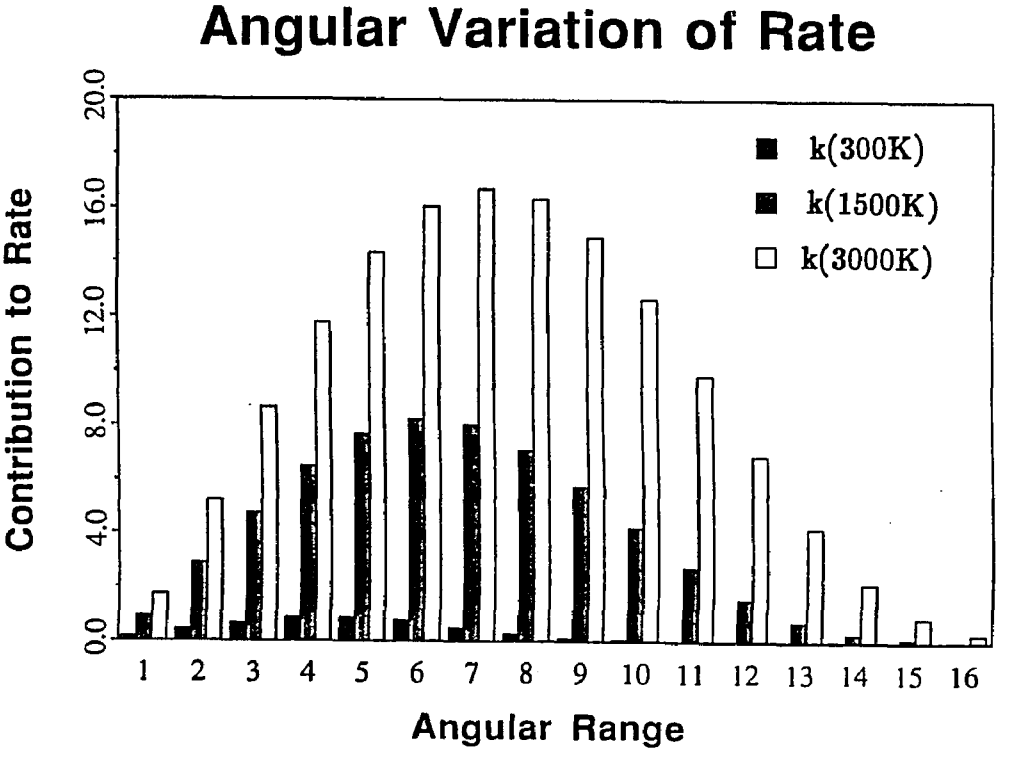

FIGURE 20

Canonical rate constants (k(T)) for quadratic dividing surfaces obtained with slope restriction for three temperatures (T) for potential energy surfaces used in this work. Rate constants (rates) are in 10^{12} $cm^3/mol \cdot s$.

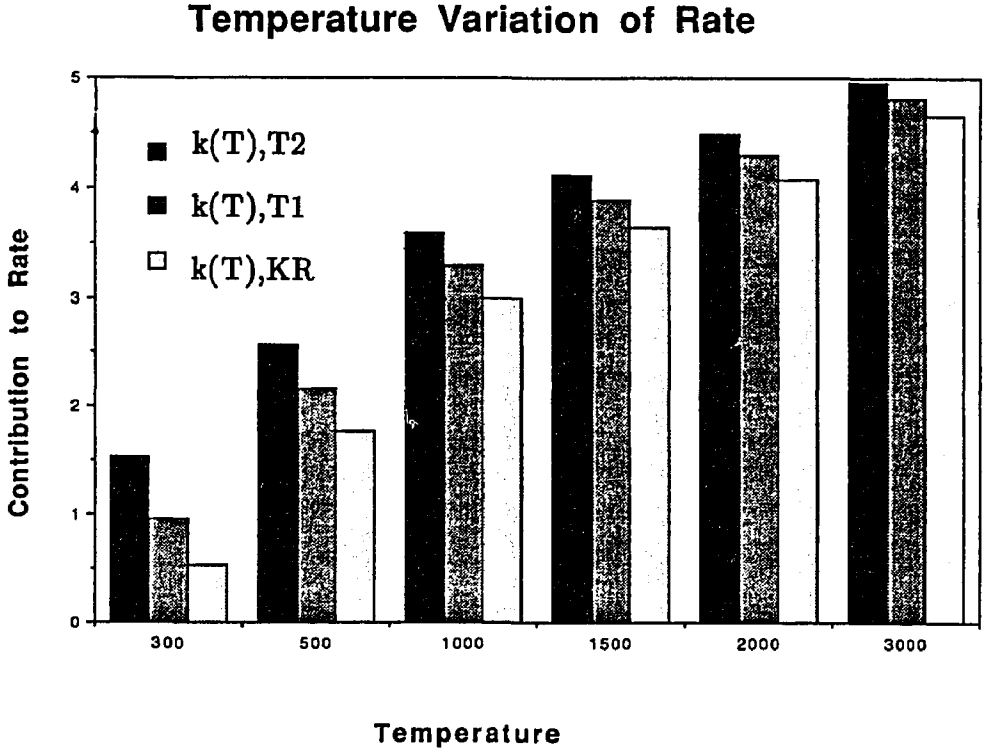

Potential energy surfaces

T2 – Truhlar 2
T1 – Truhlar 1
KR – Koeppl/Rutenburg

IV. RESTRICTED AND NON-RESTRICTED METHODS USED IN VARIATIONAL SEARCHES

In order to qualify as a DS, the DS should start in a high energy region of the PES at the left bottom corner of a plot of the intersection of the DS with the r, R coordinate plane at a given value of θ where the flux through it is negligible. It should then proceed to a region of low energy, the region of high reactive flux near the saddle point. It should then proceed further to another high energy region, in the upper right corner of the plot where the flux through it is negligible. Otherwise the DS will have a hole, i.e., it will not be crossed by all reactive trajectories. In order to ensure this requirement, plots of DSs must be made and examined. Consider what this means in terms of the evaluation of the flux integral $N_*^c(T)$. At all values of θ the integral should be vanishingly small for small R; it should become large as R increases and become vanishingly small again at large R. To determine whether this requirement was satisfied, integrands, i.e., reactivity relief maps, were plotted and examined.

To ensure that the requirement described above was satisfied, we imposed restrictions on parameters which define the DS. These restrictions were applied during the simplex search.

1. Planar dividing surfaces: TR and LCIC

For all DSs we required R be no less than a certain value at the integration limit. The limit 7 a.u. was tried first for TR and LCIC DSs, then calculations were repeated for 4 a.u.. It was observed that the rate constants did not differ for these values: no trajectories, which proceed from reactants toward products were missed. This confirmed that 7 a.u. was big enough to ensure the passage of DSs to high energy regions where the flux was negligible.

2. Quadratic dividing surfaces

Quadratic DSs are more complicated. They can bend toward the product or

reactant valleys. Quadratic and cubic variational DSs determined with no restrictions on variational parameters bend toward the product valley and then curve abruptly back into the reactant valley for low values of θ. See the intersection of the DS labeled non–restricted with the r – R plane at $\theta = 0$ in Fig. 21. It is possible for low energy trajectories which originate in the reactant region to cross this DS two or more times. It is also possible for high energy trajectories to pass from the reactant valley to the product valley without crossing the DS. A DS which bends toward the product and reactant valley could yield "islands" of flux, i. e., local maxima, in reactivity relief maps.

Consider the following procedure. First find the quadratic variational DS using a search with no restrictions on parameters. Plot the DS at a set of θ values, and find the value of R where the DS starts bending toward the reactant valley, then use this as the upper integration limit for R. If the energy is high enough at this value of R, extra crossings of the DS in the reactant valley will not contribute to the flux. But if the DS bends too soon, i. e., before it ascends from the saddle point region to the high energy region in the upper right corner of the PES plot, then some trajectories which contribute to the flux, will not be counted. The DS will not be crossed by all reactive trajectories. The calculation will not yield a legitimate variational rate constant if the value of the integration limit for R is too small because the DS has a hole.

Before the behavior described above was clearly understood quadratic DSs were found using a restriction applied by Sverdlik and Koeppl to the $H + I_2 \rightarrow HI + I$ reaction. The second partial derivative of r with respect to R was required to be positive, i.e., variational parameter $D > 0$ (see Eq. (52)) and R = 7 a.u. for the limit of this variable. This was done in order to prevent the DS from being concave down, i.e., from bending toward reactant valley. This restriction "straigtened" the DS because DSs in this work tend to bend toward the reactant

FIGURE 21

Quadratic dividing surfaces for Truhlar 2 potential energy surface and 300 K for values of θ equal to 0, 30, 60, and 90 deg.. Contours of potential energy surface are in eV.

Fig.21a

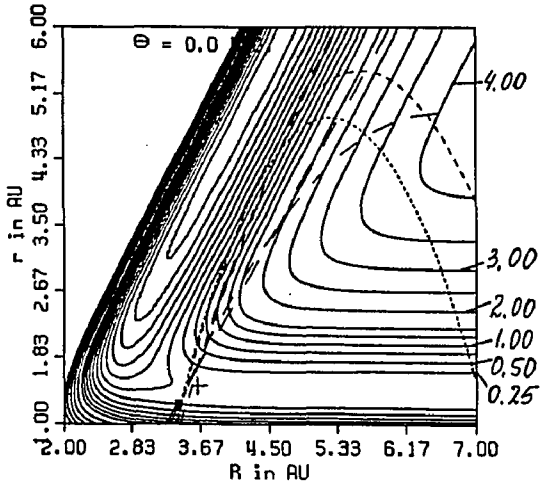

Fig.21b

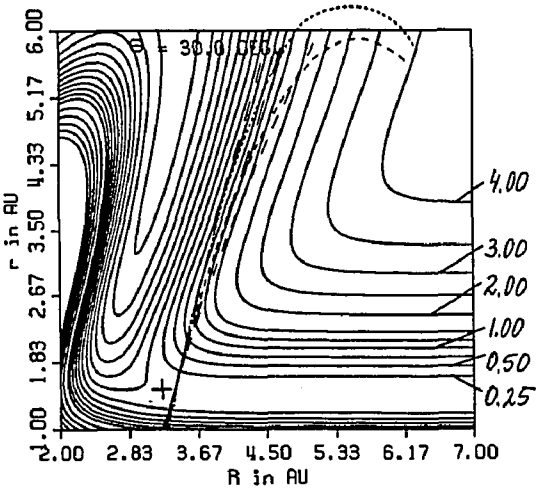

Fig.21c

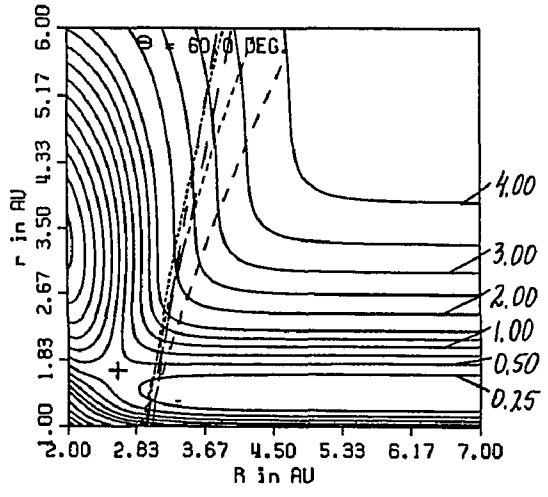

Fig.21d

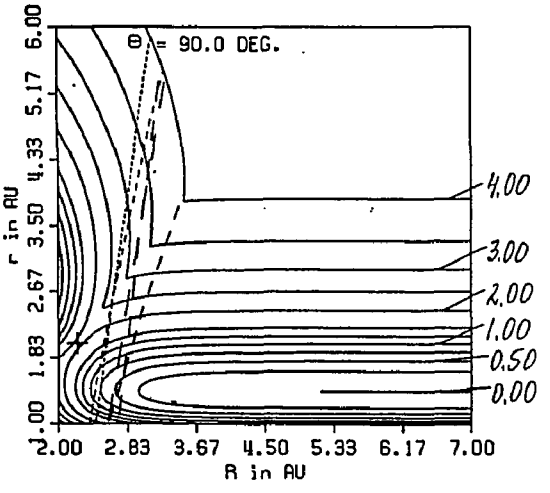

Dividing Surfaces

— — — second derivative restriction
— — — — energy limit and slope restriction
— — — — — slope restriction
- - - - - - - energy limit restriction
---------- no restriction

Potential energy surface

+ saddle point

and not the product valley. The intersection of such a DS with the r and R coordinate plane at fixed θ is a straight line. These DSs are identified by SD (second derivative) in figures and tables.

We became aware of the unusual behavior of the quadratic DS described above when we performed unrestricted variational searches for the F + HH reaction. These DSs, identified by N (non–restricted) in tables and figures, and their reactivity relief maps were plotted and studied. The N DSs curved toward the reactant valley and some did so too soon. The N DSs gave the lowest rate constants for each PES and temperature (see Tables 5 and 6). However these low results do not correspond to rigorous upper bounds for the reaction rate because these DSs are not crossed by all trajectories which originate in the reactant region. We decided to try to find acceptable DSs by performing searches with a number of different restrictions imposed on variational parameters. These restrictions are defined below.

a. ***Restrictions for quadratic dividing surfaces applied in this work***

1. Second derivative (SD) restriction described above.
2. First derivative, slope (S), restriction: the first partial derivative of r with respect to R was required to be positive ($A + D\mathrm{R} + E\theta > 0$ (see Eq. (52)). This condition ensures that r will be the increasing function of R and will prevent the DS from bending backwards toward the reactant valley.
3. Energy (E) limit restriction: the potential energy was required to be 4.0 eV at the limit of integration over R (see Fig. 21). This will ensure that the DS will proceed toward and terminate in a high energy region.
4. Combined restrictions 3 and 2 (ES).
5. Either restriction 3 or 2 (E/S). These DSs were obtained by accident. The computer program was meant to use restriction 4 (ES) but by mistake was programed for E/S restriction.

TABLE 5

Canonical variational rate constants (k(T)) for F + HH reaction for quadratic dividing surfaces (DS) for 300 and 1500 K temperatures (T) for a series of potential energy surfaces (PES). Rate constants are in $10^{12}cm^3/mol \cdot s$.
← marks k(T) for which DSs are plotted in Figs. 16 and 21.

Potential energy surfaces		
KR	T1	T2
k(300K)		
4.272 (E)	5.473 (E)	11.16 (E)
3.597 (SD)	5.453 (E)	10.15 (E)
3.446 (ES)	5.449 (E)	9.314 (SD) ←
3.387 (S)	5.301 (SD)	9.285 (S)
3.341 (E)	5.128 (S)	9.178 (S) ←
3.332 (E)	5.123 (SD)	9.060 (E)
3.331 (S)	5.057 (ES)	8.980 (ES) ←
3.222 (N)	5.021 (S)	8.828 (E) ←
	4.986 (E)	8.706 (N) ←
	4.910 (N)	
k(1500K)		
86.07 (E)	100.8 (ES)	124.9 (E)
80.96 (E/S)	100.2 (E/S)	123.9 (ES)
78.57 (ES)	96.66 (E)	122.4 (SD)
76.73 (SD)	96.62 (E)	122.2 (S)
75.54 (S)	96.54 (ES)	121.4 (S)
74.78 (E)	95.61 (SD)	120.5 (S) ←
74.22 (N)	95.17 (E)	119.9 (E)
	94.05 (E)	119.9 (E)
	93.86 (ES)	119.7 (N)
	93.78 (S)	
	92.85 (N)	

PES

KR – Koeppl/Rutenburg
T1 – Truhlar 1
T2 – Truhlar 2

DS

E – energy limit
S – slope
ES – energy limit and slope
E/S – energy limit or slope
SD – second derivative
N – no restrictions

TABLE 6

Canonical variational rate constants (k(T)) for F + HH reaction for quadratic dividing surfaces (DS) for 3000 K temperature (T) for a series of potential energy surfaces (PES). Rate constants are in $10^{12}cm^3/mol \cdot s$.
← marks k(T) for DS which is plotted in Fig. 16.

Potential energy surfaces		
KR	T1	T2
k(3000K)		
230.5 (E)	253.3 (E)	295.8 (E)
214.9 (E/S)	247.8 (E)	287.7 (SD)
213.2 (SD)	247.2 (E/S)	287.4 (ES)
210.6 (S)	246.7 (SD)	284.8 (S)
210.5 (S)	245.9 (S)	283.4 (S) ←
209.7 (ES)	245.5 (ES)	282.4 (E)
209.0 (S)	242.0 (S)	281.8 (E)
208.4 (ES)	241.5 (E)	280.7 (N)
207.9 (E)	240.7 (ES)	
206.9 (N)	239.7 (N)	

PES

KR – Koeppl/Rutenburg
T1 – Truhlar 1
T2 – Truhlar 2

DS

E – energy limit
S – slope
ES – energy limit and slope
E/S – energy limit or slope
SD – second derivative
N – no restrictions

b. *Discussion of rate constants and appearance of quadratic restricted DSs*

See Tables 5 and 6 and Figs. 21 – 26.

The SD restriction gave higher rate constants than other restrictions. This can be explained in view of the previous discussion. Because this restriction gives a DS with parameter D = 0, these DSs appear as straight lines in the r and R plane at fixed θ. DSs obtained with restrictions 2, 3, 4 and 5 are curved in the r and R plane at fixed θ. SD DSs have less flexibility than other curved DSs to avoid multiple crossings. Some E DSs and other curved DSs were found which gave higher rate constants than SD DSs. They correspond to local minima to which the simplex converges before finding lower minima during a particular search. See the discussion in Ch. 2, Sect. VI and also Sverdlik and Koeppl[36].

Each type of restriction creates a specific appearance of DS (see Fig. 21). SD DSs appear as straight lines in the r and R plane at fixed θ. All S DSs have some undesirable feature. They have higher slopes at small R than other quadratic DSs, and extend toward low energy regions of the product valley more than others. E DSs do not extend toward the product valley as much as S DSs. These DSs make a sharp curve just before they end in the high energy region. ES DSs have the most "reasonable" appearance: they descend from a high energy region to the saddle point region and ascend to a high energy region without making an abrupt bend. They avoid the product valley more than other Q DSs.

S and E DSs give about the same values for the rate constants. ES rate constants overall tend to be slightly higher, although some are comparatively low. This can be explained by the fact that although they are curved and flexible, there are two restrictions to be satisfied. Since E/S DSs were obtained by mistake, they were abandoned when the mistake was discovered and there were no attempts to find lower minima for them. Actually these DSs are either E or S. Note that it was difficult to find a set of initial vertices (variational parameters) which satisfy the

FIGURE 22

Reactivity relief maps for quadratic dividing surface obtained with second derivative restriction for Truhlar 2 potential energy surface and 300 K. See Fig. 21. Contours are in arbitrary units.

Fig.22a

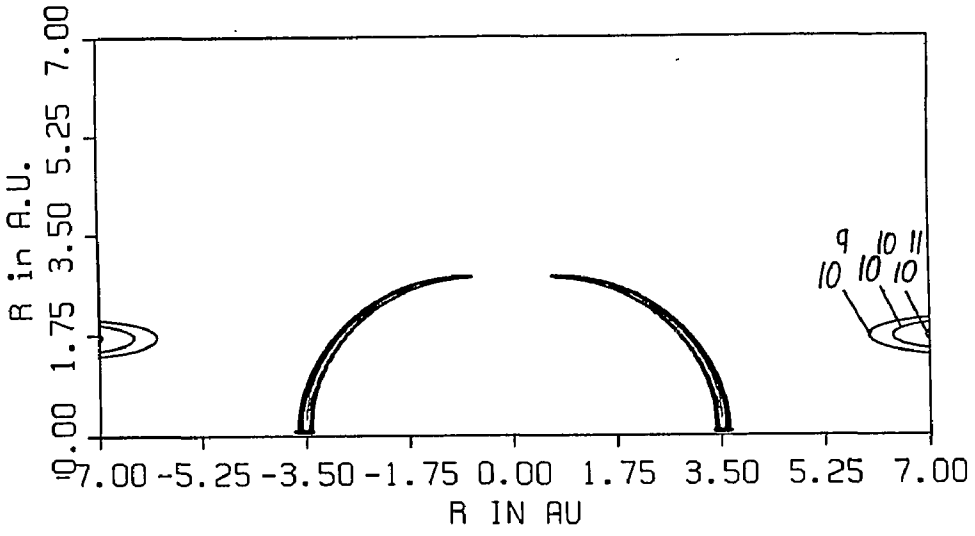

Fig.22b

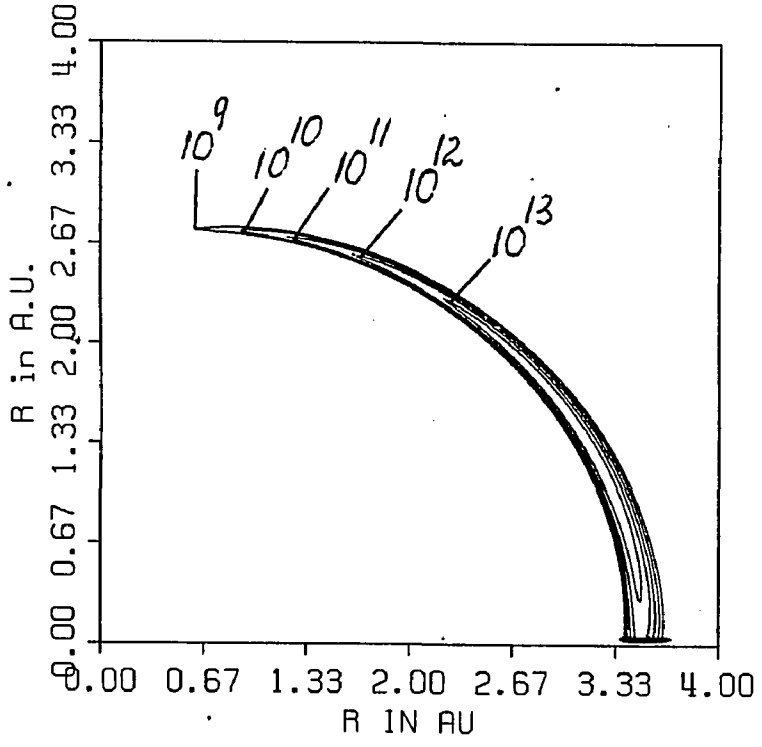

FIGURE 23

Reactivity relief maps for quadratic dividing surface obtained with energy limit and slope restriction for Truhlar 2 potential energy surface and 300 K. See Fig. 21. Contours are in arbitrary units.

Fig.23a

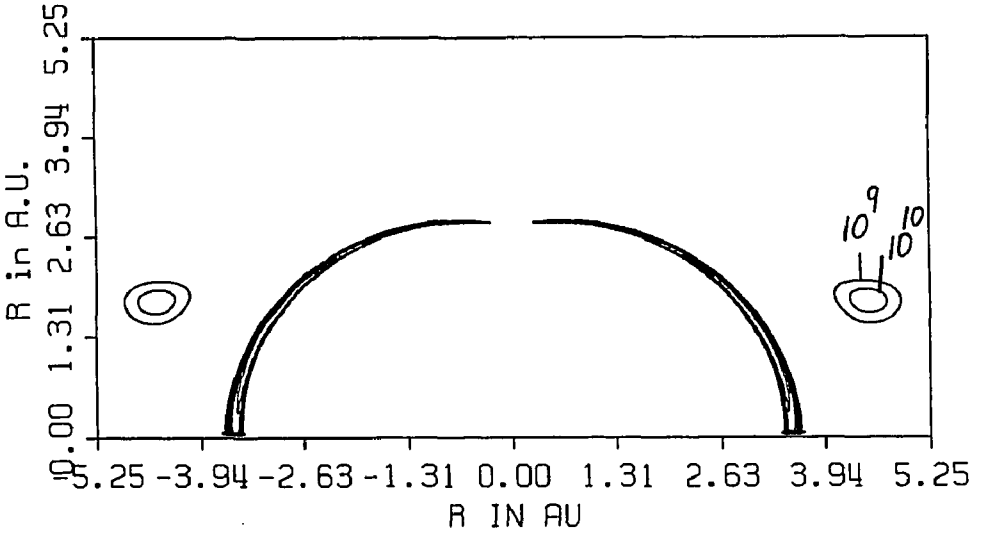

Fig.23b

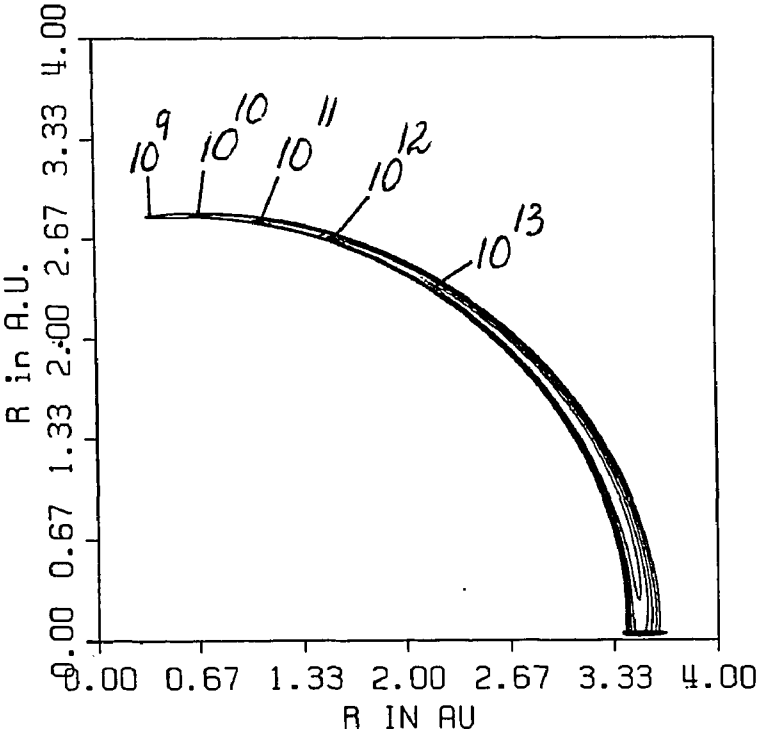

FIGURE 24

Reactivity relief maps for quadratic dividing surface obtained with slope restriction for Truhlar 2 potential energy surface and 300 K. See Fig. 21.
Contours are in arbitrary units.

Fig.24a

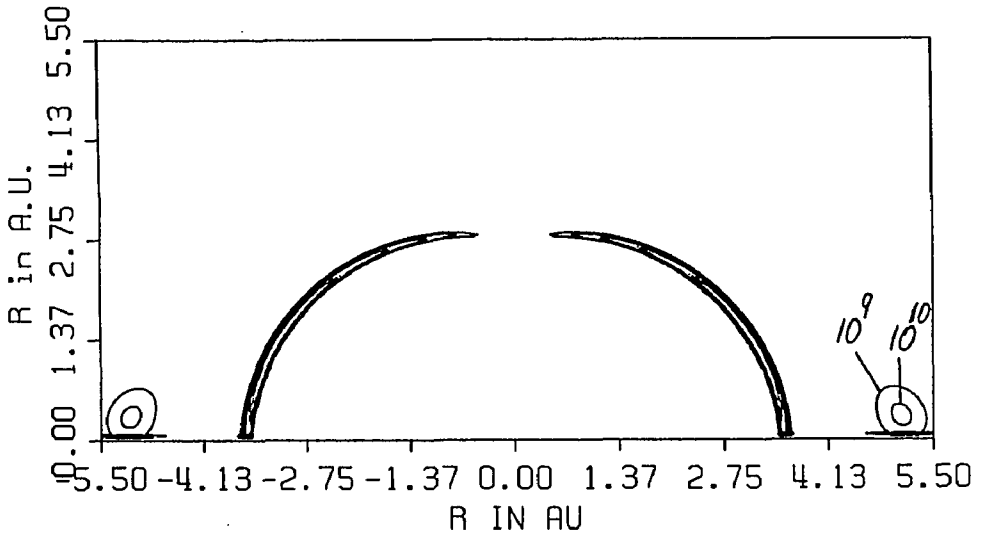

Fig.24b

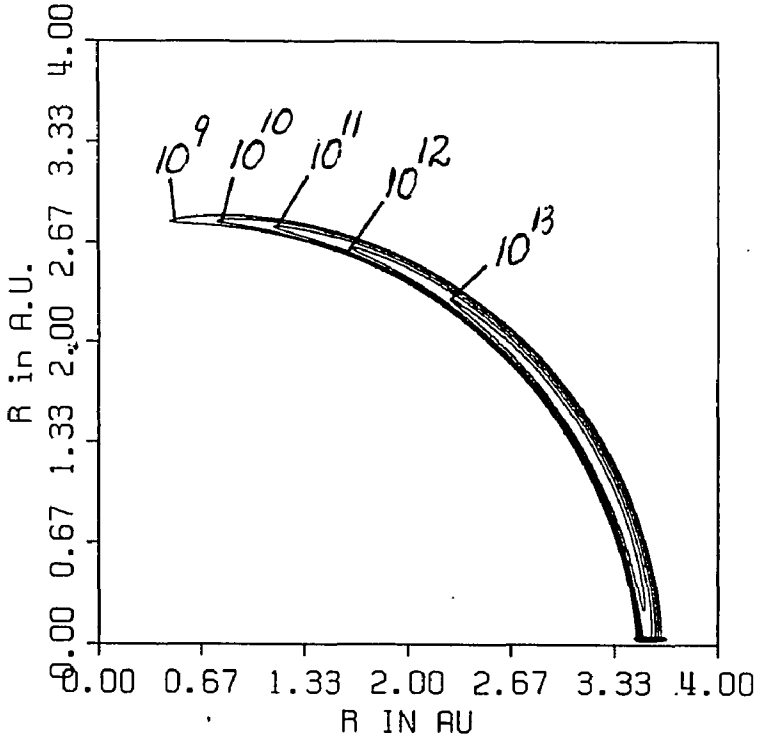

FIGURE 25

Reactivity relief maps for quadratic dividing surface obtained with energy limit restriction for Truhlar 2 potential energy surface and 300 K. See Fig. 21. Contours are in arbitrary units.

Fig.25a

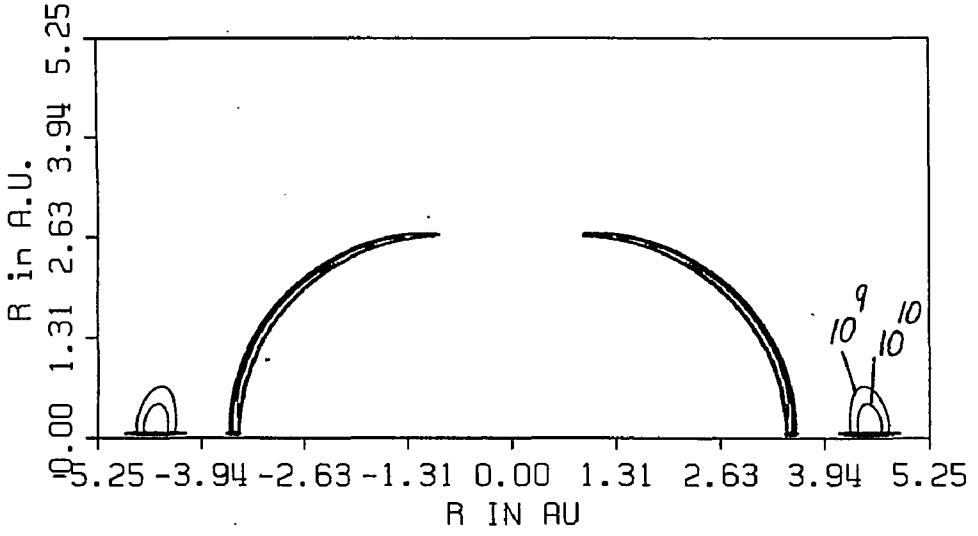

Fig.25b

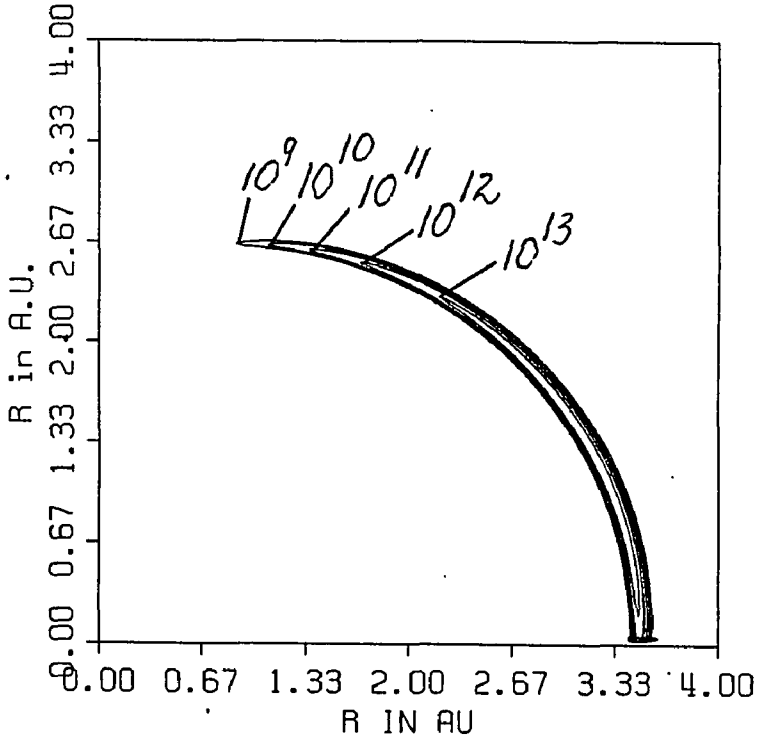

FIGURE 26

Reactivity relief maps for quadratic dividing surface obtained with no restriction for Truhlar 2 potential energy surface and 300 K. See Fig. 21. Contours are in arbitrary units.

Fig.26a

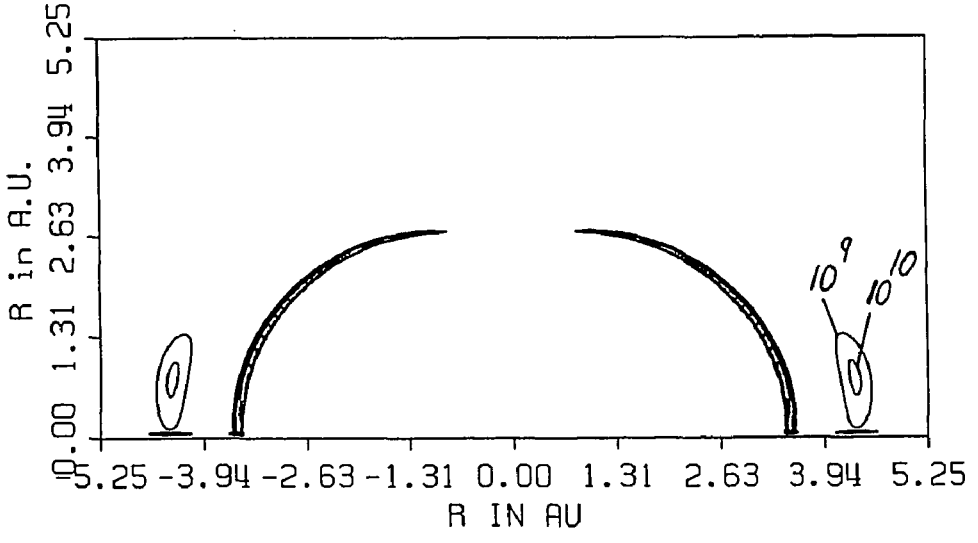

Fig.26b

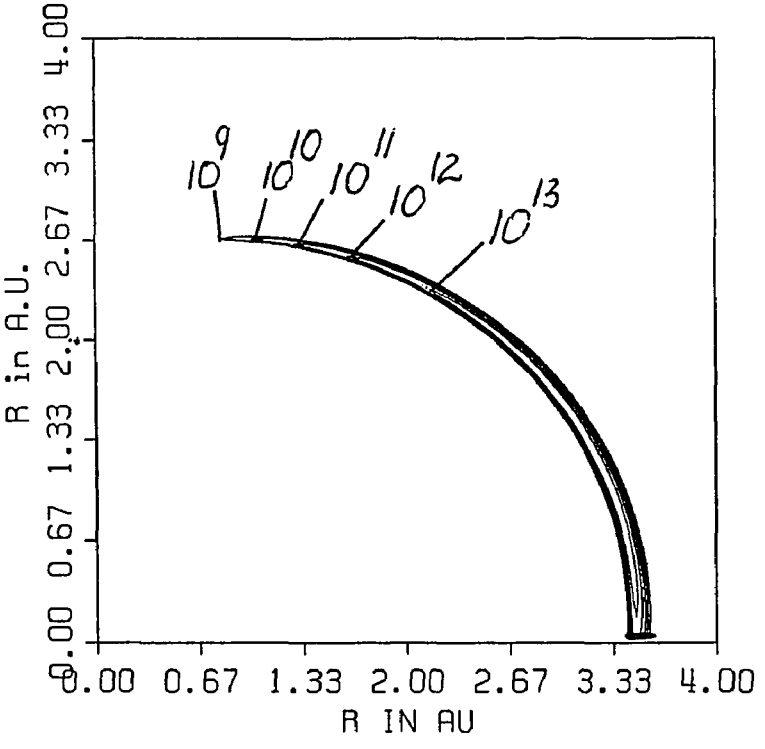

energy limit restriction whereas initial vertices for slope restriction DSs can be easily obtained as discussed in Sect. VI of this chapter. Also it should be stated that the differences in k(T) values for quadratic DSs obtained with different restrictions imposed on the DS are not large. Note that the value of k(T) for the S DS is higher than that for the E DS for the T2 PES at 300. See Figs. 21 – 26. However for other PESs and temperatures there are S DSs and DSs with other types of restriction which give smaller values of k(T) than E DSs. See Tables 5 and 6.

c. ***Discussion of islands in reactivity relief maps***

It happened that almost every Q DS used in this work is inclined to move toward the product valley to minimize the variational flux. There may therefore be a significant contribution to the variational flux from trajectories which originate in the product valley. This possibility is shown on reactivity relief maps; they all show small islands of flux through the DS near the product valley. See Figs. 22 – 26. The Q DSs were all obtained with an upper limit of integration of 7 a.u. for R. In order to show that an island makes a negligible contribution to the rate, we calculated the rate constant for each DS which gives an island using a different upper limit of integration for R (R_{max}). The new value of the limit was in the range 4 – 7 a.u.. For each DS, the value of R_{max} was found by examining the reactivity relief map, i. e., the value of R just before the island appears. Both rate constants were almost the same. For example for the T2 PES at 300K, see the rate constants given below:

	k(T) for R_{max} = 7.00 a.u.	k(T) for R_{max} = lower value
SD	9.314×10^{12} $cm^3/mol\cdot s$	9.311×10^{12} $cm^3/mol\cdot s$, R_{max} = 6.00 a.u.,
S	9.178×10^{12} $cm^3/mol\cdot s$	9.176×10^{12} $cm^3/mol\cdot s$, R_{max} = 4.58 a.u..

Figs. 22 and 24 for SD and S DSs were used to determine the lower values for the

upper limit of integration over R.

It was impossible to perform this procedure for any DS which used the energy limit restriction: E, ES, or E/S, because when the upper limit of integration over R was lowered from 7.00 to the value obtained from the reactivity relief map, the restriction on energy was not satisfied. Since the only DS types which could be shown by this procedure to yield a negligible contribution from islands correspond to SD and S restrictions and since the former DS gives higher rates than the latter, the S DS was chosen as the standard quadratic DS for this work. Although Q(E) DSs could not be proven by direct calculations to have insignificant islands, we did not discard them. We consider proof of insignificance of islands for Q(S) DSs and Q(SD) DSs as indirect proof of insignificance of islands for Q(E) DSs and others since the islands for all DSs show contours of the same order of magnitude – 10^{10} and 10^{9}.

Finally, it is possible that although the N DSs found in this work do not divide configuration space into unambiguous reactant and product regions, they may nevertheless yield practical variational values of the rate constant. This can be demonstrated using an approach similar to the one described above to show that islands of flux in reactivity relief maps for Q SD and S DSs make insignificant contributions. The rate constant should be calculated using N DS parameters and an R integration limit which corresponds to the value where the potential energy on the DS is a maximum at $\theta = 0$. Plots of N DSs show that the potential energy at this value of R is as large or larger for $\theta > 0$; hence if the potential energy is large enough at the limit for R at $\theta = 0$ to give negligible flux, the calculated rate constant corresponds to a practical variational result.

V. ANOTHER FUNCTION FOR DIVIDING SURFACE: FORMULATION IN TERMS OF R AND $SIN^2\theta$

We expected that variational DSs would pass close to the angle dependent saddle points of the PES, at least for θ values where the potential energy is low at the saddle point. This behavior was expected because of the important $e^{-\beta V(r^*,R,\theta)}$ factor in the integrand of $N^c_*(T)$. When the DS passes on either side of the saddle point and enters the reactant or product valley, the potential energy is lower and $e^{-\beta V(r^*,R,\theta)}$ is larger. Hence consideration of the effect of potential energy on the variational rate causes one to expect that a good DS will pass close to the angle dependent saddle points and should have the flexibility to do this. However, all variational DSs found in this work missed saddle points by large distances at large values of θ. The contribution to the reactive flux is large at low values of θ and small at high values of θ; hence the position of DS at high values of θ is not as important as at low values of θ. Still it was desirable to try to find a DS which could pass closer to saddle points at all values of θ.

We considered a power series expansion of the DS with terms in coordinate R as before and $\sin^2\theta$ instead of θ. The expression for the function is given in Ch. 2, Sect. II B. The new function is designated as $\sin^2\theta$ and old one as linear θ in figures and tables. We performed variational searches using quadratic DSs for the new function for KR and T2 PESs at 300, 1500 and 3000 K. Only one cubic DS was found using this function at 300 K. We did not find a significant improvement in rate constant values or in the appearance of the DS as explained above. See Table 7 and Figs. 27 –31. The $\sin^2\theta$ DSs, like the linear θ DSs, "miss" the angle dependent saddle points. Q(S) and Q(E) DSs for linear θ and $\sin^2\theta$ functions for the T2 PES at 300 K are plotted in Fig. 27. The DSs can almost be superimposed for the same type of restriction at θ values of 0 and 30 deg.. Figs. 28 – 29 show reactivity relief

TABLE 7

Comparison of canonical variational rate constants (k(T)) for F + HH reaction obtained with quadratic, linear θ and $\sin^2\theta$, dividing surface (DS) functions for two potential energy surfaces (PES) for several temperatures (T).
Rate constants are in $10^{12}cm^3/mol \cdot s$. ← marks DSs plotted in Fig. 27.

Dividing surfaces	Potential energy surfaces	
	KR	T2
	k(300K)	
linear θ	3.597 (SD)	9.314 (SD)
	3.446 (ES)	9.178 (S) ←
	3.332 (E)	8.980 (ES)
	3.331 (S)	8.828 (E) ←
	3.222 (N)	8.706 (N)
$\sin^2\theta$	3.931 (ES)	10.43 (ES)
	3.582 (SD)	9.212 (SD)
	3.359 (S)	9.041 (S)
	3.295 (E)	9.016 (S)
	3.138 (N)	9.000 (E) ←
		8.921 (S) ←
		8.770 (N)
	k(1500K)	
linear θ	75.54 (S)	120.5 (S)
	74.78 (E)	119.9 (E)
$\sin^2\theta$	75.20 (S)	121.3 (S)
	75.16 (E)	120.5 (E)
	k(3000K)	
linear θ	209.0 (S)	283.4 (S)
	207.9 (E)	281.8 (E)
$\sin^2\theta$	211.4 (S)	288.1 (E)
	209.3 (E)	284.7 (S)

PES
KR – Koeppl/Rutenburg
T2 – Truhlar 2

DS
SD – second derivative
ES – energy limit and slope
E – energy limit
S – slope
N – no restrictions

FIGURE 27

Comparison of quadratic dividing surfaces, linear θ and $\sin^2\theta$, for Truhlar 2 potential energy surface and 300 K for values of θ equal to 0, 30, 60, and 90 deg.. Contours of potential energy surface are in eV.

Fig.27a

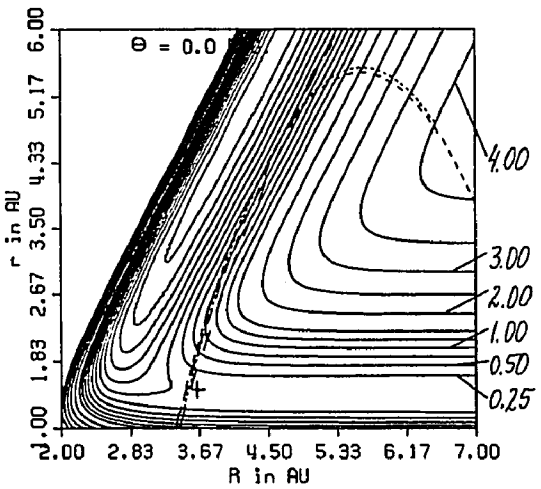

Fig.27b

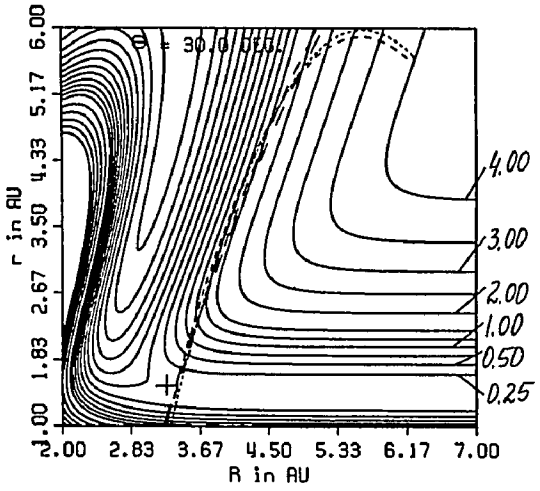

Fig.27c

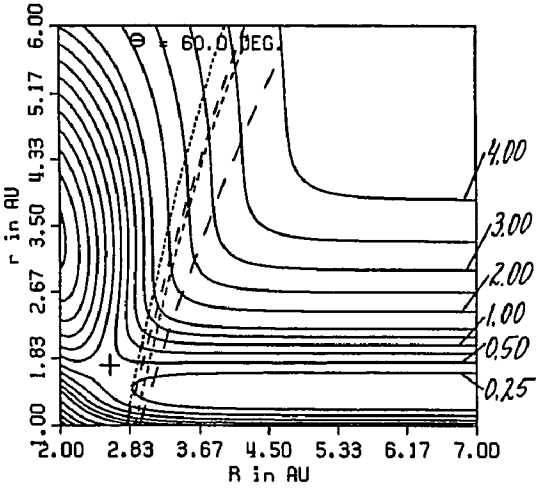

Fig.27d

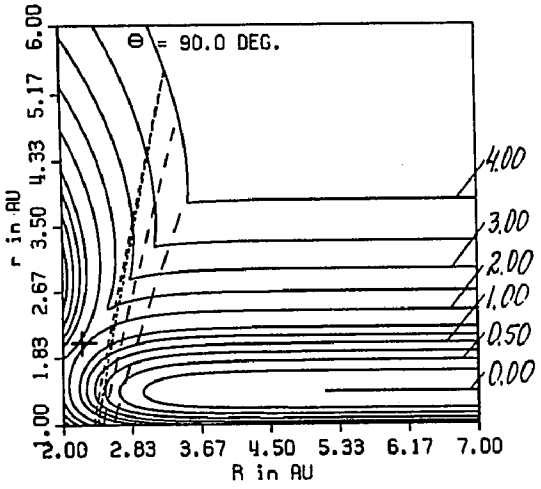

Dividing Surfaces

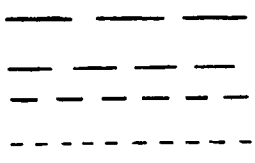

linear θ obtained with slope restriction

$\sin^2\theta$ obtained with slope restriction

linear θ obtained with energy limit restriction

$\sin^2\theta$ obtained with energy limit restriction

Potential energy surface

saddle point

FIGURE 28

Comparison of reactivity relief maps for quadratic dividing surfaces, linear θ and $\sin^2\theta$, obtained with slope restriction for Truhlar 2 potential energy surface and 300 K. See Figs. 27 and 29. Contours are in arbitrary units.

Fig.28a

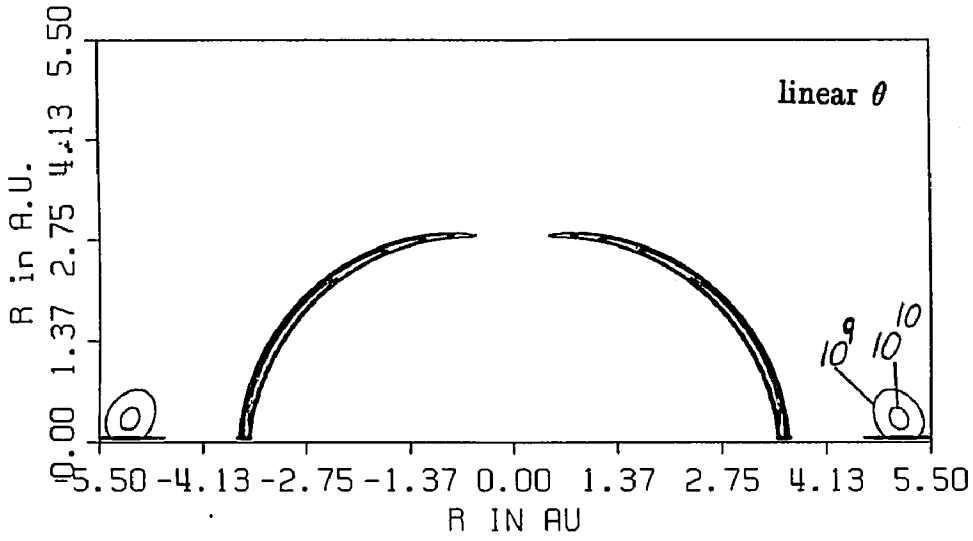

Fig.28b

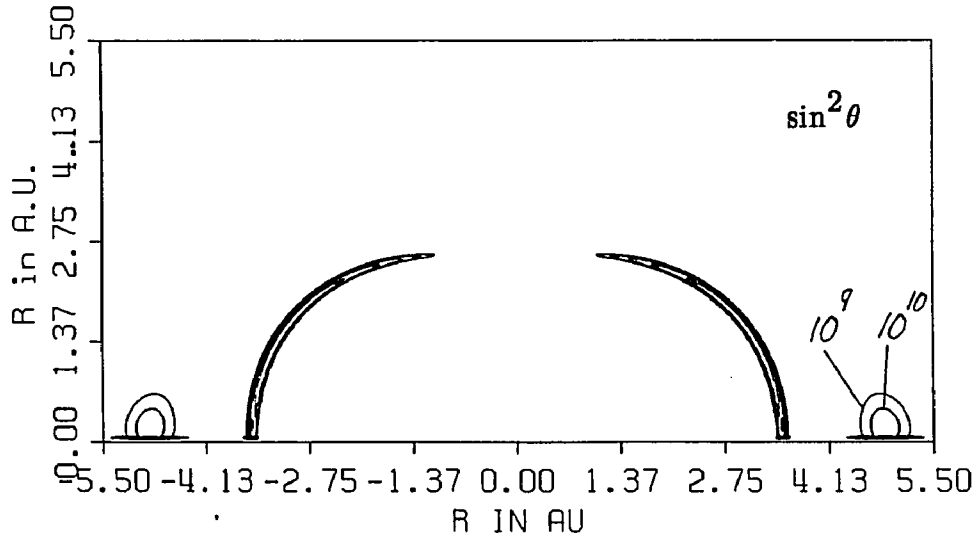

FIGURE 29

Comparison of reactivity relief maps for quadratic dividing surfaces, linear θ and $\sin^2\theta$, obtained with slope restriction for Truhlar 2 potential energy surface and 300 K. See Figs. 27 and 28. Contours are in arbitrary units.

Fig.29a

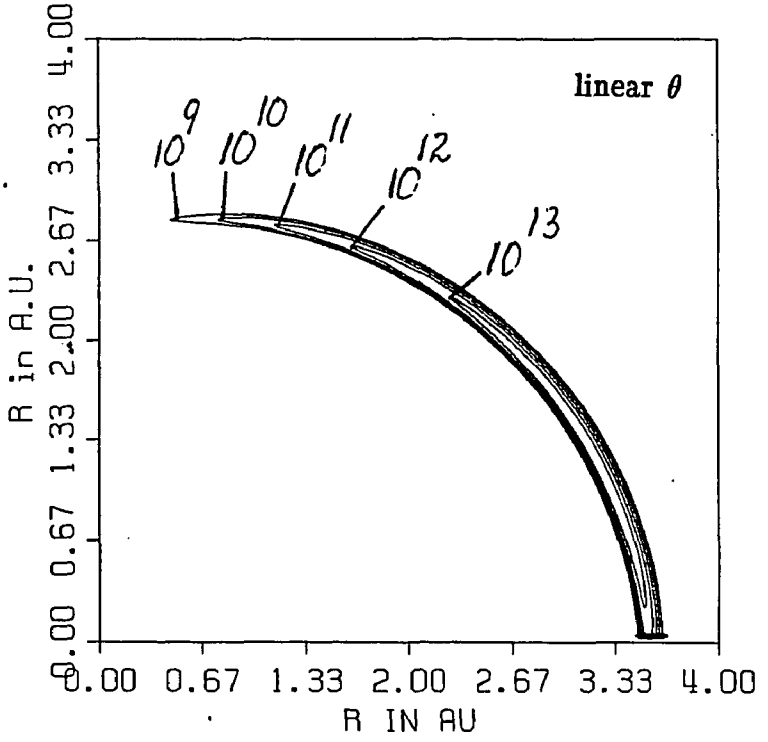

Fig.29b

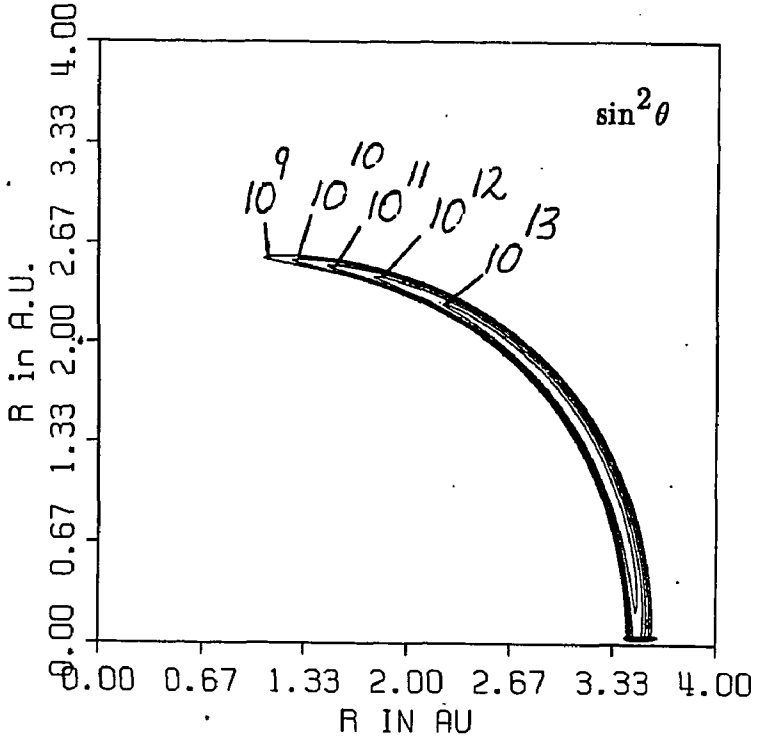

FIGURE 30

Comparison of reactivity relief maps for quadratic dividing surfaces, linear θ and $\sin^2\theta$, obtained with energy limit restriction for Truhlar 2 potential energy surface and 300 K. See Figs. 27 and 31. Contours are in arbitrary units.

Fig.30a

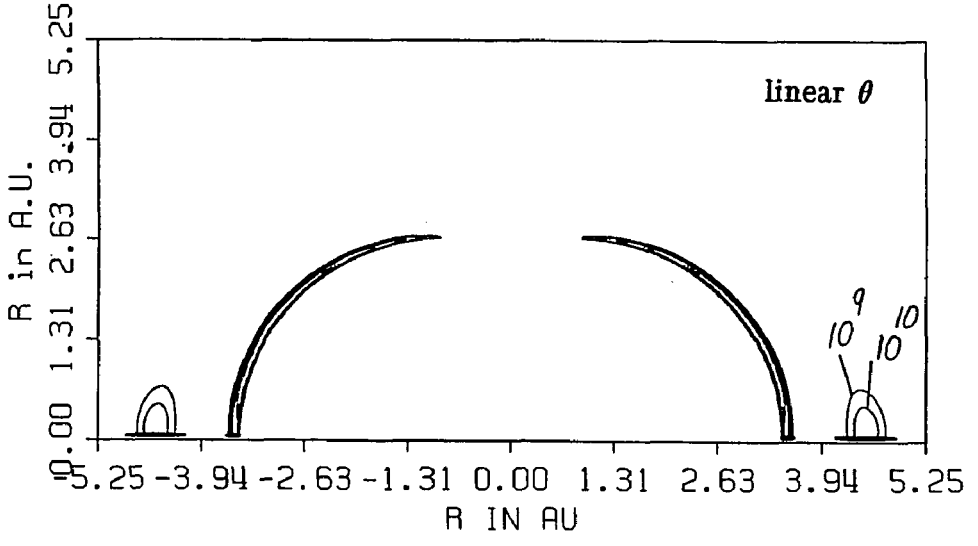

Fig.30b

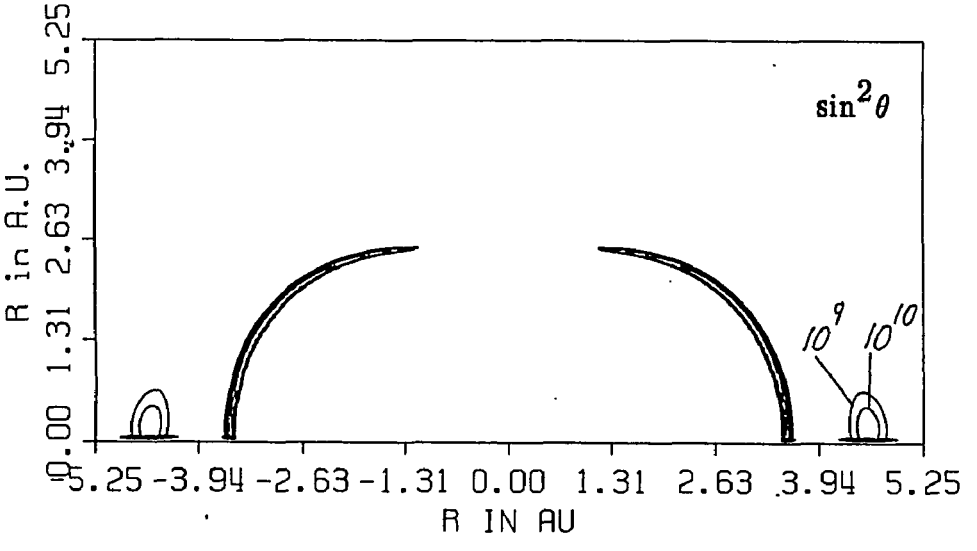

FIGURE 31

Comparison of reactivity relief maps for quadratic dividing surfaces, linear θ and $\sin^2\theta$, obtained with energy limit restriction for Truhlar 2 potential energy surface and 300 K. See Figs. 27 and 30. Contours are in arbitrary units.

Fig.31a

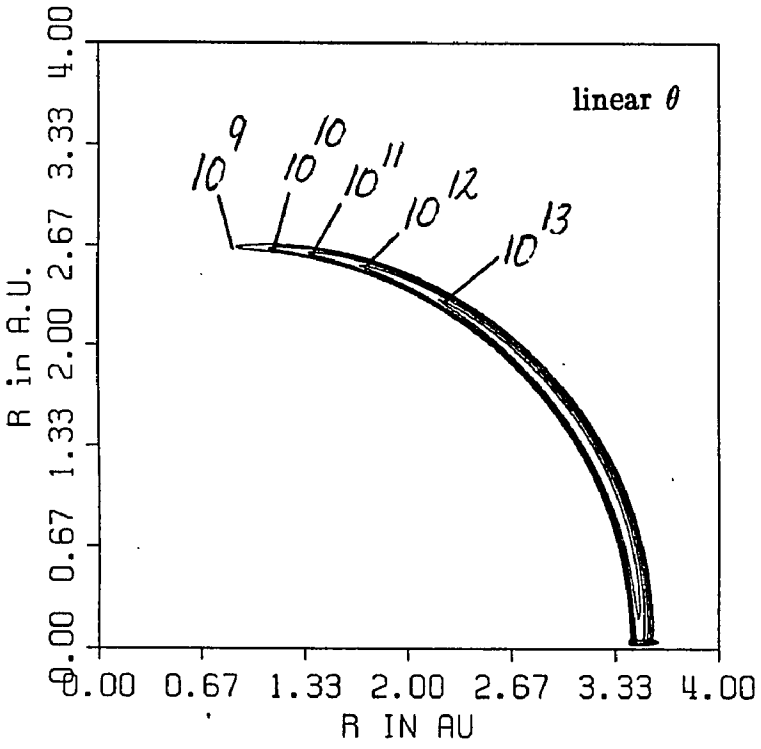

Fig.31b

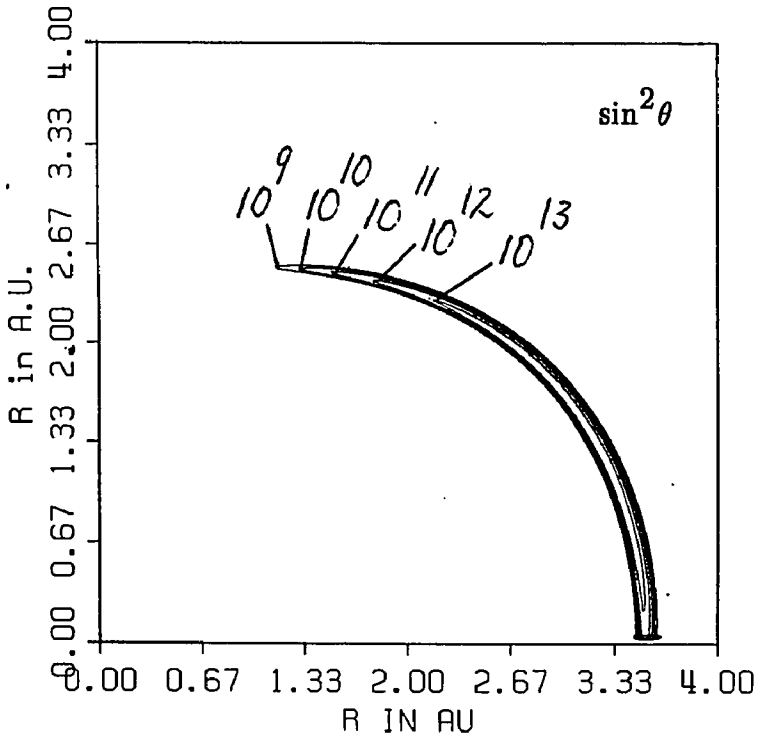

maps for Q(S) linear θ and $\sin^2\theta$ DSs. Figs. 30 – 31 show reactivity relief maps for Q(E) linear θ and $\sin^2\theta$ DSs. Although contours "fall off" faster with increasing θ for the $\sin^2\theta$ DS, the highest contour (10^{13}) extends to the same value of θ for both the S and E DS independent of whether the DS function is of the linear θ or $\sin^2\theta$ type. See Figs. 29 and 31. There is no pattern in rate constants for the linear θ versus $\sin^2\theta$ DSs. The rate constants are lower for the Q(S) $\sin^2\theta$ DS than for the Q(S) linear θ DS and the rate constants are lower for the Q(E) linear θ DS than for the Q(E) $\sin^2\theta$ DS for the DSs plotted in Fig. 27. The rate constants are lower for the Q(E) linear θ DS than for the Q(E) $\sin^2\theta$ DS for the T2 PES and for the Q(E) $\sin^2\theta$ DS than for the Q(E) linear θ DS for the KR PES at 300 K. The rate constants are lower for the Q(E) linear θ DS than for the Q(E) $\sin^2\theta$ DS for the T2 PES at 1500 K and for the KR PES at 3000 K (see Table 7). Also note that the rate constants are different only in the third (sometimes second) significant figure.

So the new function did not move DSs closer to the angle dependent saddle points at all values of θ. We did not see the need to examine other functions because of the fact that the DSs stay near saddle points at values of θ where the contribution to the reactive flux is large and move away from the saddle points at values of θ where the contribution to the flux is small.

VI. LEAST SQUARES FIT DIVIDING SURFACES

It was expected that DSs would not only pass near saddle points but would also follow the path of steepest descent to the saddle point from the small R high potential energy region of PES and the path of the steepest ascent from saddle point to large R high potential energy region. Our DSs not only moved away from saddle points but also proceeded from the saddle point region toward the product valley (a low energy region) and gave islands in reactivity relief maps as described in Sect. IV of this chapter.

We developed a method to determine parameters for Q DSs that followed the angle dependent steepest descent – saddle point – steepest ascent path for θ in the range 0 to $\pi/2$. We used points read from these paths on PES contour plots and a least squares method to find the variational parameters. This method is described in Ch. 2, Sect. VI. These DSs were found using mostly quadratic and some cubic, mostly linear θ and some $\sin^2\theta$ functions, and are designated as least squares (LS) fit DSs in figures and tables.

The rate constants calculated for LS DSs were larger than those for variational DSs. Tables 8 and 9 give rate constants for representative variational and LS DSs. Fig. 32 shows variational Q(S) and LS DSs for the T2 PES at 300 K. The LS DS stays near saddle point for all values of θ while the variational DS stays near saddle points only at values of θ near 30 deg.. Note that although the LS DS does pass close to angle dependent saddle points, it does not take the path of steepest ascent from the saddlepoint at low values of θ. See Fig. 32. Figs. 33 and 34 show reactivity relief maps for both DSs. In Fig. 34 we indicate saddle point locations and the value of θ at which high value flux contours "diverge" from saddle point locations for the variational DS. Flux contours for the LS DS follow the saddle points until the flux falls to a negligible value at 58 deg.. The variational DS flux contours stay close to the saddle points up to about 30 deg. where the contribution to the reactive flux is the highest for the T2 PES (see Fig. 9), and move away from the saddle points at 35 deg. before even the 10^{13} contour falls off. The area over which the contours are high is dramatically larger for the LS DS.

LS DSs have smaller slopes (see Fig. 32) and hence do not extend toward the product valley as variational DSs do. Since LS DSs do not extend toward the product valley they do not show islands in reactivity relief maps. All LS DSs gave higher rate constants than any of the variational Q DSs. We explain this the following way. The major contribution to the reactive flux comes from the low

TABLE 8

Comparison of canonical variational rate constants with least squares (LS) fit rate constants for F + HH reaction. Rate constants (k(T)) were obtained using the quadratic linear θ dividing surface (DS) function for two potential energy surfaces (PES) for several temperatures (T). Rate constants are in $10^{12}cm^3/mol \cdot s$. ← marks DSs plotted in Fig. 32.

	Potential energy surfaces	
	KR	T2
	k(300K)	
Variational k(T)	3.446 (ES) 3.332 (E) 3.331 (S)	9.178 (S) ← 8.980 (ES) 8.828 (E)
LS k(T)	5.988 5.573	15.04 ← 13.81
	k(1500K)	
Variational k(T)	75.54 (S) 74.78 (E)	120.5 (S) 119.9 (E)
LS k(T)	131.3 101.9	164.6 159.3
	k(3000K)	
Variational k(T)	209.0 (S) 207.9 (E)	283.4 (S) 281.8 (E)
LS k(T)	506.2 252.4	360.4 341.8

PES

KR – Koeppl/Rutenburg
T2 – Truhlar 2

DS

ES – energy limit and slope
E – energy limit
S – slope

TABLE 9

Comparison of canonical variational rate constants with least squares (LS) fit rate constants for F + HH reaction. Rate constants (k(T)) were obtained using the quadratic $\sin^2\theta$ dividing surface function for Koeppl/Rutenburg potential energy surface for several temperatures (T). Rate constants are in $10^{12}cm^3/mol \cdot s$.

	k(300K)
Variational k(T)	3.931 (ES) 3.359 (S) 3.295 (E)
LS k(T)	4.799
	k(1500K)
Variational k(T)	75.54 (S) 74.78 (E)
LS k(T)	101.9
	k(3000K)
Variational k(T)	211.4 (S) 209.3 (E)
LS k(T)	261.1

Dividing surfaces

ES – energy limit and slope
S – slope
E – energy limit

FIGURE 32

Comparison of quadratic linear θ variational and quadratic linear θ least squares fit dividing surfaces for Truhlar 2 potential energy surface and 300 K for values of θ equal to 0, 30, 60, and 90 deg.. Contours of potential energy surface are in eV.

Fig.32a

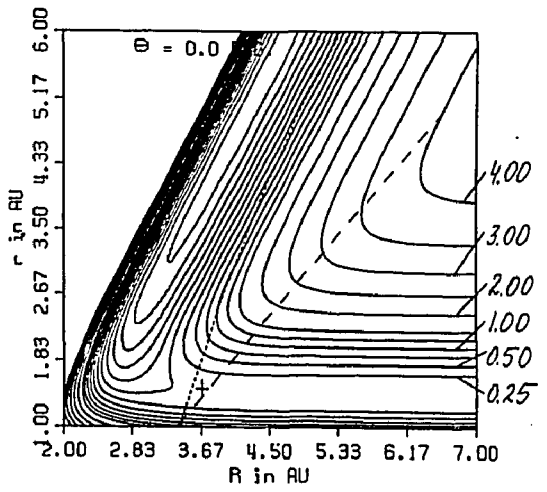

Fig.32b

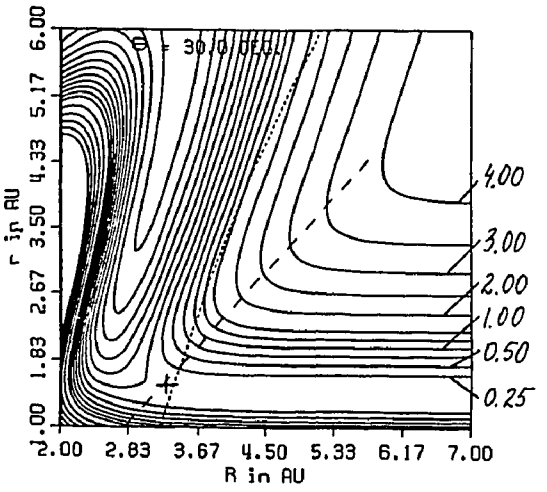

Fig.32c

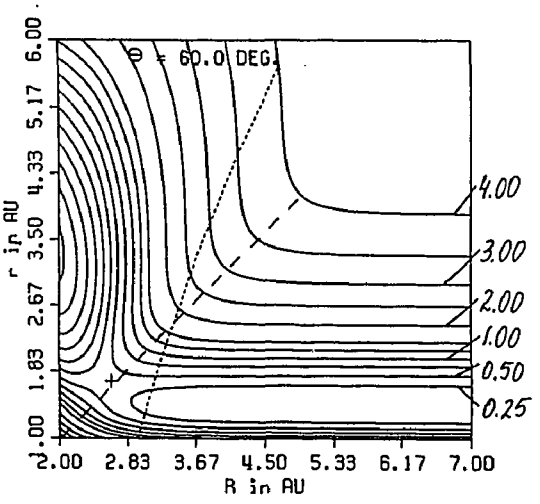

Fig.32d

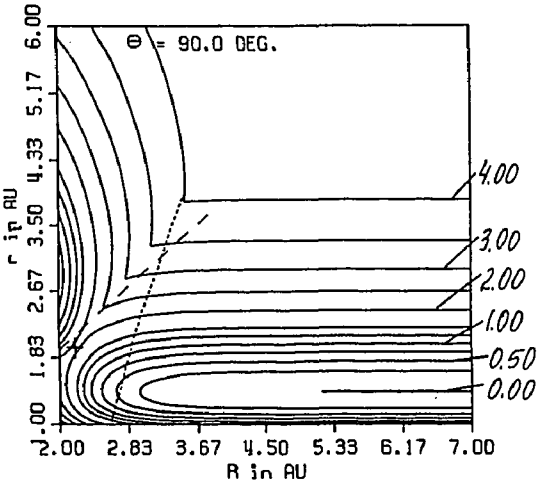

Dividing Surfaces

— — — — least squares fit
---------- variational obtained with slope restriction

Potential energy surface

+ saddle point

FIGURE 33

Comparison of reactivity relief maps for quadratic linear θ variational dividing surface obtained with slope restriction and quadratic linear θ least squares (LS) fit dividing surface for Truhlar 2 potential energy surface and 300 K. See Figs. 32 and 34. Contours are in arbitrary units.

Fig.33a

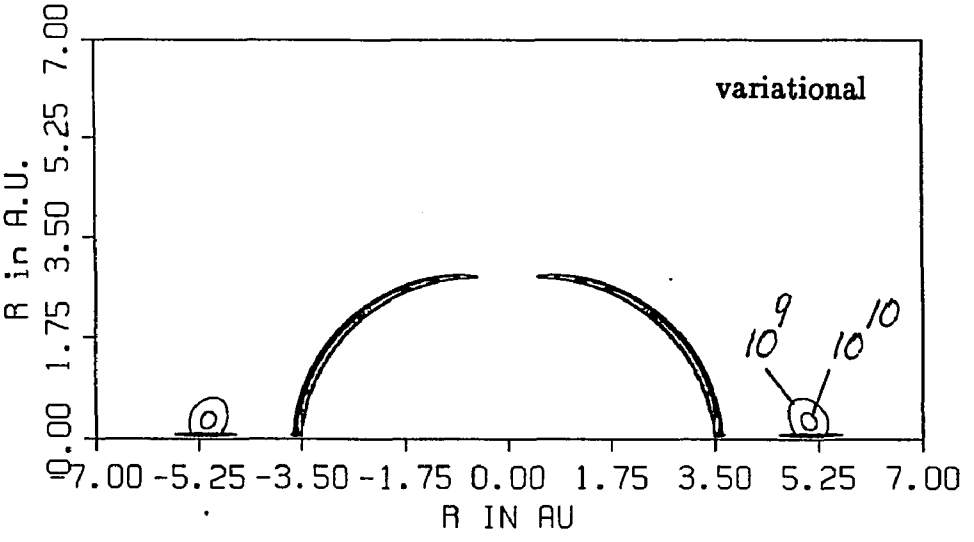

Fig.33b

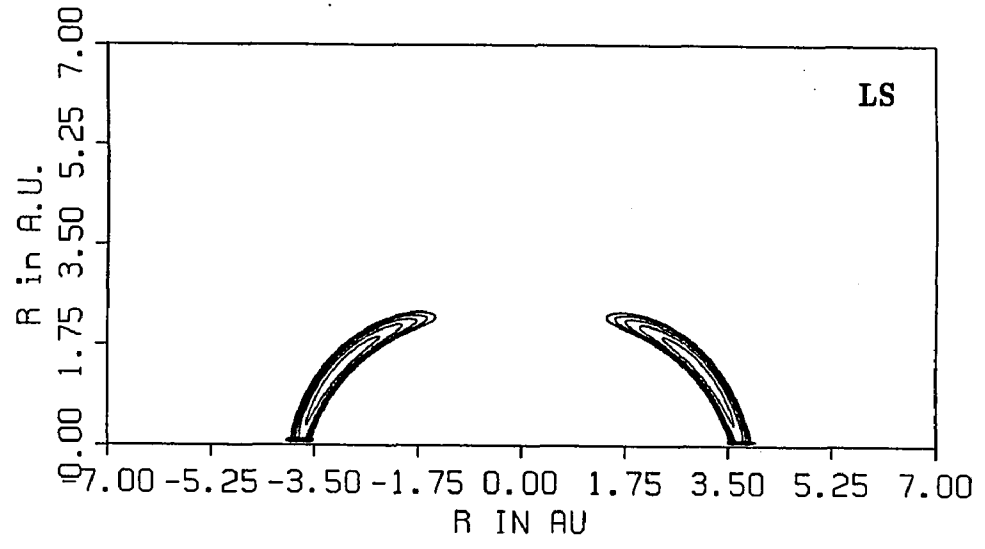

FIGURE 34

Comparison of reactivity relief maps for quadratic linear θ variational dividing surface obtained with slope restriction and quadratic linear θ least squares (LS) fit dividing surface for Truhlar 2 potential energy surface and 300 K. See Figs. 32 and 33. Contours are in arbitrary units.

Fig.34a

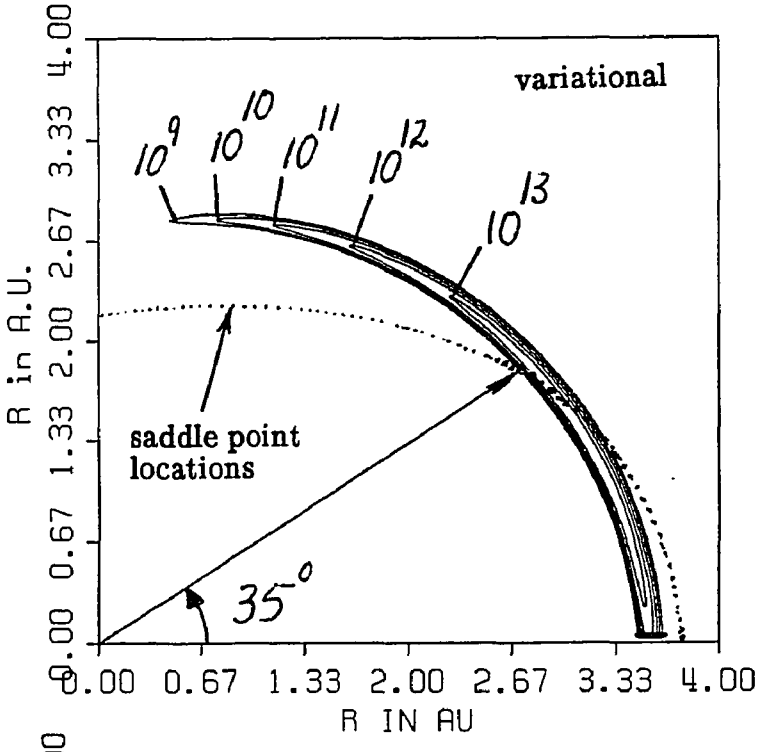

Fig.34b

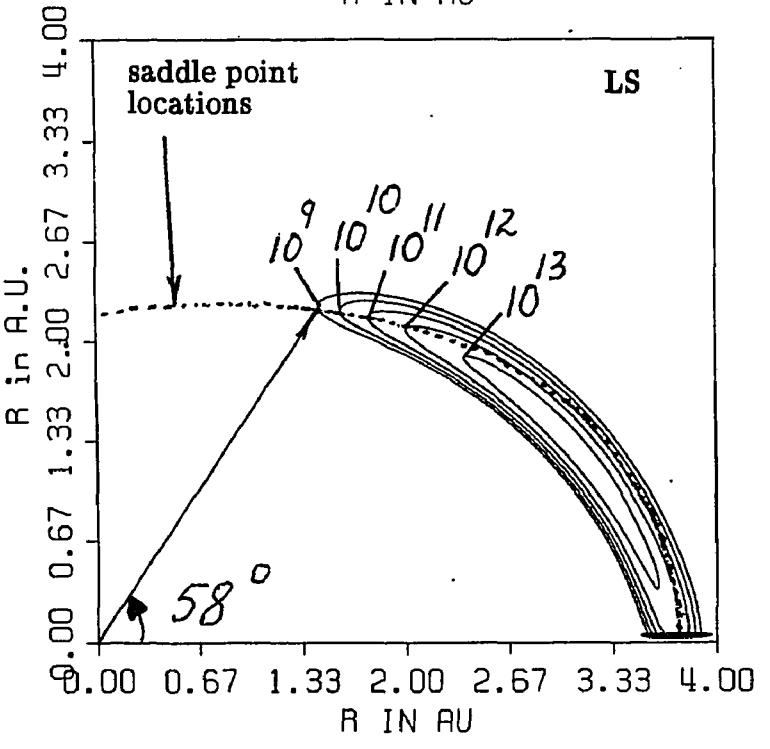

energy region near saddle points and LS DSs with their low slopes have a longer section of the DS in this region; hence, the rate constants are larger. Variational DSs have higher slopes and smaller areas of the DS in the low energy region and hence lower rate constants. It is speculated further that the above explanation could help explain why variational DSs extend toward the product valleys. They take this high slope path at least in part to keep areas of the DS in low energy regions small. In order for them to avoid the product valley they must change their slopes abruptly. This is difficult to do; hence, they pass close to the product valley. Contribution to the flux in this region appears as an island on the reactivity relief map. The contribution to the flux from islands has been shown, as stated in Sect. IV of this chapter, to be negligible.

We did calculations to try to learn whether a numerically determined LS DS was near a DS which yields a local minimum of the rate constant. We did this by using sets of variational parameters based on the LS DS parameters to define vertices for the simplex search algorithm. The variational parameters did not satisfy the energy limit restrictions but searches were possible with the slope restriction. Variational DSs moved into their usual positions eventually and gave the same rate constants as before. At this point it made no sense to use alternative LS DSs to initiate searches. Many unsuccessful attempts to find even a local minimum in the rate constant for a DS which passed through angle dependent saddle points and followed the path of steepest ascent from these saddle points convinced us that entropic factors as well as the potential energy play an important role in determining the position of the variational DS.

VII. CUBIC DIVIDING SURFACES

It was expected that the cubic (C) DSs, being more flexible, would give lower rates than quadratic ones. Variational calculations were done for selected cubic DSs

at 300 K. It was not worthwhile to do more work with cubic DSs, since they did not give significant improvement in calculated rate constants compared to quadratic DSs calculated with the same restriction, and required much more computer time.

Using the linear θ DS function and T1 PES, we obtained variational rate constants at 300 K for the Q(SD) DS of 5.301 and C(SD) DS of 5.302 and 5.319 × 10^{12} $cm^3/mol \cdot s$. For the linear θ DS function and T2 PES, we found variational rate constants at 300 K for the Q(S) and C(S) DSs of 9.178 and 8.908 × 10^{12} $cm^3/mol \cdot s$., respectively. However, the variational rate constant for C(S) DS and T2 PES at 300 K is larger than that for the Q(E) DS and T2 PES at 300 K which is 8.828 × $10^{12} cm^3/mol \cdot s$. Furthermore, again for the T2 PES, the $\sin^2\theta$ DS function at 300 K gave variational rate constants for Q(S) and C(S) DSs of 8.921 and 8.962 × $10^{12} cm^3/mol \cdot s$, respectively. The latter result should have been smaller than the former result because of the greater flexibility of the C DS; it is likely that the two results correspond to different relative minima.

LS C DSs followed the same pattern as LS Q DSs: they gave higher rate constants than variational C DSs. Only a selected few LS C DSs were found. Using the linear θ DS function and T2 PES, we obtained rate constants at 300 K for the variational C(S) DS of 8.908 and LS C DS of 13.67 × $10^{12} cm^3/mol \cdot s$. The $\sin^2\theta$ DS function gave rate constants for the variational C(S) DS of 8.962 and LS C DS of 11.80 × $10^{12} cm^3/mol \cdot s$.

It should be noted that the decrease of rate constants was the most significant from TR to LCIC DS, and then less from LCIC to Q DS (see Tables 1, 2, 3, and 4), and less or no improvement from Q to C DSs according to the results shown above. The cubic function should always give a lower variational rate constant than the corresponding quadratic function for the same type of DS because of its greater flexibility. When this is not found in practice, it is because the cubic search either has converged to a different (higher) local minimum or was not continued long

enough for complete convergence to the minimum. The cubic search requires more time than quadratic because more terms and parameters are introduced into DS formulation when the order of expansion increases. There is only a small improvement in cubic versus quadratic DS rate constants because the quadratic DS function is flexible enough to produce a value which is close to the global minimum of the rate constant.

VIII. INITIAL VALUES FOR VARIATIONAL PARAMETERS

The method used to generate initial vertices for variational searches for planar DSs was described by Sverdlik and Koeppl[36]. Variational parameters for planar DSs were used to generate initial vertices for quadratic and cubic DSs assigning initial values of 0.01 to the additional variational parameters which appear in Q and C DSs. Also low temperature (300 K) variational DS parameters were used to generate initial vertices for variational searches at higher temperatures. The procedure we used was not as systematic as it could have been. We decided that for future work we should always use LS DS parameters to generate initial vertices. The increments in variational parameters used to generate initial vertices correspond to 10 % of the value for each variational parameter. See Sverdlik and Koeppl[36].

IX. LIMITS OF INTEGRATION FOR θ AND R AND GRID SIZE

For the F + HH reaction we integrated from zero to $\pi/2$ for θ since the diatomic reactant is homonuclear and the potential energy is symmetric about $\pi/2$. The values of the rate constant were doubled to obtain the overall rate.

The lower limit of integration for R was 1.0 a.u.. The choice of the lower limit of integration for R is based on the value of equilibrium internuclear separation of FH molecule. The choice of the upper limit of integration for R has to

ensure that it is large enough compared to the equilibrium internuclear separation of the FH molecule to represent infinite separation of F and H nuclei. To determine whether the choice of the integration limits for R was reasonable we calculated the value of the rate constant for each DS with new limits of integration for R. The upper limit was increased many times by an increment of 0.1 a.u.. We were looking for a sudden increase in the rate constant at values close to 7.0 a.u. This would indicate that we had not integrated over all R values where the flux is significant. Sudden increases were not found. The value of R where a small increase in rate constant occurred was usually as high as $10 - 11$ a.u. and sometimes as low as 9.0 a.u.. Also the upper limit was decreased by the same increment and the procedure was repeated. We were looking now for a sudden decrease in rate constant. This happened only below 4.0 a.u.. We conclude that $R_{max} = 7.0$ a.u. was an acceptable value for the R integration limit.

The choice of the grid size for integration over θ and R was also studied. The grid should be chosen to be fine enough to give an accurate rate constant. We tested a grid size of 280 by 180 points for inner integration over R and outer integration over θ, respectively, to calculate the integral $N_*^c(T)$ (see Eq. (22)). 500 points were used for the integration over r to calculate the integral $D_{BC}^c(T)$ (see Eq. (20)). In order to determine, whether the 280 by 180 grid was acceptable we calculated rate constants for each DS with finer grids, increasing the number of points each time by a factor of 4. We looked for a change in the value of the rate constant. There was essentially no change in rate constant for finer grids.

We repeated the work done to study the effect of using different integration limits for R with different girds. For a 280 by 180 point grid rate constants fluctuated in value at the fourth or fifth decimal position when the upper limit of R integration was increased by increments of 0.1 a.u.. When the grid was increased by a factor of 4 to 560 by 360 points, the rate constants fluctuated in the fifth or sixth

decimal positions when the R upper limit was incremented. For further increase of the grid by a factor of 4 to 1120 by 720 points, the rate constant retained 7 decimal place agreement. The fluctuations for a 280 by 180 point grid were not large enough to make us redo the previous work for the F + HH reaction, but it was decided that a 560 by 360 point grid would be used for future work.

X. COMPUTER TIME REQUIRED FOR VARIATIONAL CALCULATIONS

The computer time required for variational calculations depends on the following factors:

1. Type of DS used, i.e., number of variational parameters. The larger the number of variational parameters, the longer it takes for the simplex to converge.
2. Size of grid. The finer the grid the longer it takes to converge.
3. Number of significant figures required for convergence. The more significant figures we want the longer it takes to converge. We performed variational searches until convergence was obtained to six significant figures.

It took from 30 minutes to 1 hour for TR and LCIC DS calculations with the grid specified above and convergence to six significant figures. It took from 2 to 5 hours to obtain the same convergence for quadratic linear θ and $\sin^2\theta$ DSs. Cubic searches were abandoned because a great deal of computer time was required.

CHAPTER 4

CANONICAL VARIATIONAL RATE CONSTANTS FOR F + DH → FD(FH) + H(D) REACTIONS

In this chapter, canonical rate constants, reactivity relief maps, and angular distributions of rates are presented for the reactions: F + DH → FD(FH) + H(D). Results are presented for the same 6–parameter quadratic dividing surface (DS) function used to study the F + HH reaction and for 5 and 10–parameter DS functions which contain parameters which distinguish between reaction at each end of the heteronuclear reactant. The 6–parameter quadratic DS is described in Ch. 2, Sect. II A3; 5– and 10– parameter DSs are described in Ch. 2, Sect. II C1 and C2, respectively. For the 6–parameter DS, variational values are reported for the total reaction rate constant, i. e., the sum of rates for reaction at both ends of DH, for 300, 600, 1500, and 3000 K. The conditions which must be satisfied to obtain practical variational rate constants for reaction at each end of a heteronuclear reactant are described. The 5 and 10–parameter DS formulations are used to obtain practical variational rate constants for reaction at each end of DH for temperatures of 300, 600, and 1500 K.

All of the results in this chapter were calculated for the Truhlar 1 potential energy surface (PES) function described in Ch. 2, Sect. V 3.

Tables in this chapter give values of canonical rate constants (k(T)); corresponding DS parameters are given in Appendices 24 – 40. DSs which were chosen to be presented on plots are marked with ← in the tables.

I. PROCEDURE FOR FINDING VARIATIONAL RATE CONSTANTS

Experience gained in our study of the F + HH reaction culminated in the

following procedure:

1. Plot PES contours for θ values of 10, 20, 30, ..., 180 deg..

2. Use the plots to obtain estimates for r and R coordinates at the angle dependent saddle points.

3. Obtain accurate saddle point values of r and R for each θ value using the estimated values and the simplex search described in Ch. 2, Sect. VI.

4. Use the approach described in Ch. 2, Sect. VI to find the least squares (LS) fit values of parameters for a DS which passes close to angle dependent saddle points and takes the path of steepest ascent from these points.

5. Plot the LS DSs on PES contour maps and select the ones to use in this work.

6. Using the parameters of the chosen LS DSs to define initial vertices for simplex searches, obtain variational rate constants.

7. Plot variational DSs on PES contour maps.

8. Study the PES contour plots to make sure the DSs proceed directly to high energy regions of PES and do not bend toward product or reactant valleys.

9. If a DS bends toward the product valley before it reaches the high energy region or bends back into the reactant valley, repeat the variational search with restrictions on the DS. Search for lower relative minima which correspond to a DS which does not have undesirable features.

10. Obtain reactivity relief maps for each DS.

11. Study the maps to determine whether "islands" are present. An island appears when a DS passes close to a reactant or product valley of PES as explained in Ch. 3, Sect. IV B.

12. If an island is present, determine the value of R where the island appears on the reactivity relief map.

13. Calculate rate constants for DSs which have islands using the limits for R determined in step 12.

14. Compare rate constants obtained in step 13 with the ones obtained in step 6. If there is a negligible difference in rate constant values then the islands do not make a significant contribution to the variational rate constant. If an island is not negligible, make additional searches to find a more acceptable DS.
15. Repeat steps 6 – 14 for higher temperatures.

II. POTENTIAL ENERGY SURFACE AND ANGLE DEPENDENT POTENTIAL ENERGY BARRIER

Although the Truhlar 2 (T2) PES is in better agreement with accurate *ab initio* potential energy functions for the F + HH system[48,50] than the Truhlar 1 (T1) PES, we elected to use the T1 instead of T2 PES for three reasons: its features are in good qualitative agreement with the best *ab initio* surface available at this time; it is the intermediate PES in the series studied in this work; and it is easier to evaluate the analytical derivatives of the potential energy function with respect to internuclear separations which are required to calculate classical mechanical trajectories.

The variation of the angle dependent minimum energy for reaction with orientation angle θ is shown in Fig. 35. The barrier has a maximum value of 2.31 eV at $\theta = 81.5$ deg.. For reaction at total reaction system energies less than 2.31 eV, reaction to form FH occurs in a cone defined by an angle less than 81.5 deg., and reaction to form FD occurs in a cone defined by an angle greater than 81.5 deg.. The high barrier for sidewise approach of DH divides the reactivity of the DH molecule into FH + D and FD + H product channels.

III. QUADRATIC DS VARIATIONAL RATE CONSTANTS

We decided to use the 6–parameter quadratic DSs for our work on the F + DH reactions since during the work on the F + HH reaction this DS proved to be

FIGURE 35

Relationship between minimum potential energy for F + DH reactions (barrier height) and orientation angle θ for Truhlar 1 potential energy surface.

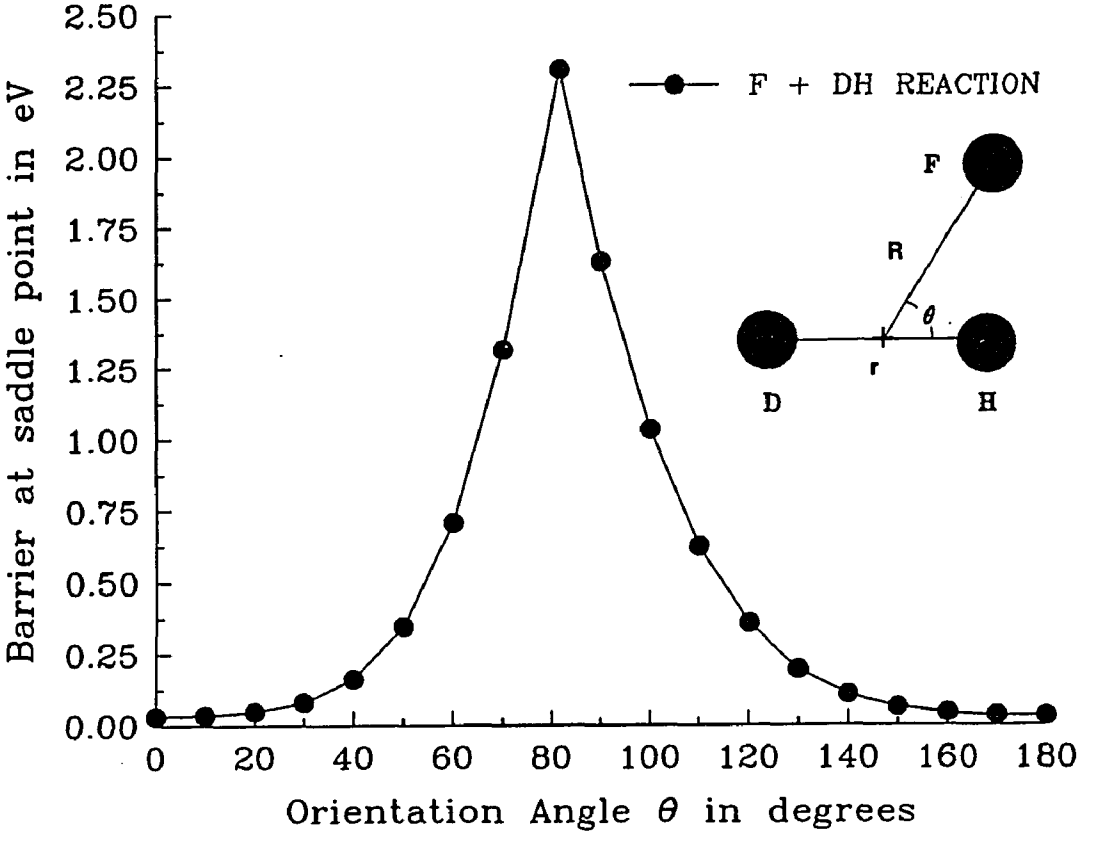

the most effective with respect to rate constant values (versus truncated (TR) and linear combination of internal coordinates (LCIC) DSs) and also from the point of view of saving computer time (versus cubic DS). We had no further interest in studying the effect of different degrees of expansion of the dividing surface on rate constant value. We did not study $\sin^2\theta$ formulations of DS because a significant improvement was not expected.

Fig. 36 shows contributions to the canonical variational rate constant for 18 equal increments of θ from 0 to π for 300, 600, 1500, and 3000 K. The θ range from 0 to π was divided into 10 deg. intervals. These results were obtained using the 6–parameter quadratic slope restriction DS and T1 PES. The angular distributions of the rate constant should be plotted as histograms; however, for the sake of clarity, the incremental contributions are plotted as points centered on each 10 deg. interval. The largest contribution to the rate constants for reactions at the H and D ends of DH is given below.

	Reaction at the H end of DH	Reaction at the D end of DH
300 K	10 – 20 deg.	160 – 170 (10 – 20) deg.
600 K	10 – 20 deg.	150 – 160 (20 – 30) deg.
1500 K	20 – 30 deg.	150 – 160 (20 – 30) deg.
3000 K	20 – 30 deg.	140 – 150 (30 – 40) deg.

Althought the 6–parameter DS is not acceptable for reasons which will be explained later in this chapter, this DS does illustrate the general trend described with respect to Fig. 9 in Ch. 3, Sect. I: the largest contribution to the rate constant does not occur for the increment 0 to 10 deg. near $\theta = 0$ where the potential energy is the lowest because the "volume element" for the integral $N^c_*(T)$ contains the factor $\sin\theta$.

LS DSs were found, plotted and used to formulate initial vertices for variational searches. All quadratic variational and LS DS rate constants for 300, 600, 1500, and 3000 K are presented in Table 10. Rate constants are much higher

FIGURE 36

Contribution from 18 equal angular increments from $\theta = 0$ to 180 deg. to canonical rate constant (k(T)) for F + DH reactions for four temperatures (T) for quadratic dividing surfaces obtained with slope restriction and Truhlar 1 potential energy surface. Rate constants (rates) are in 10^{12} $cm^3/mol \cdot s$.

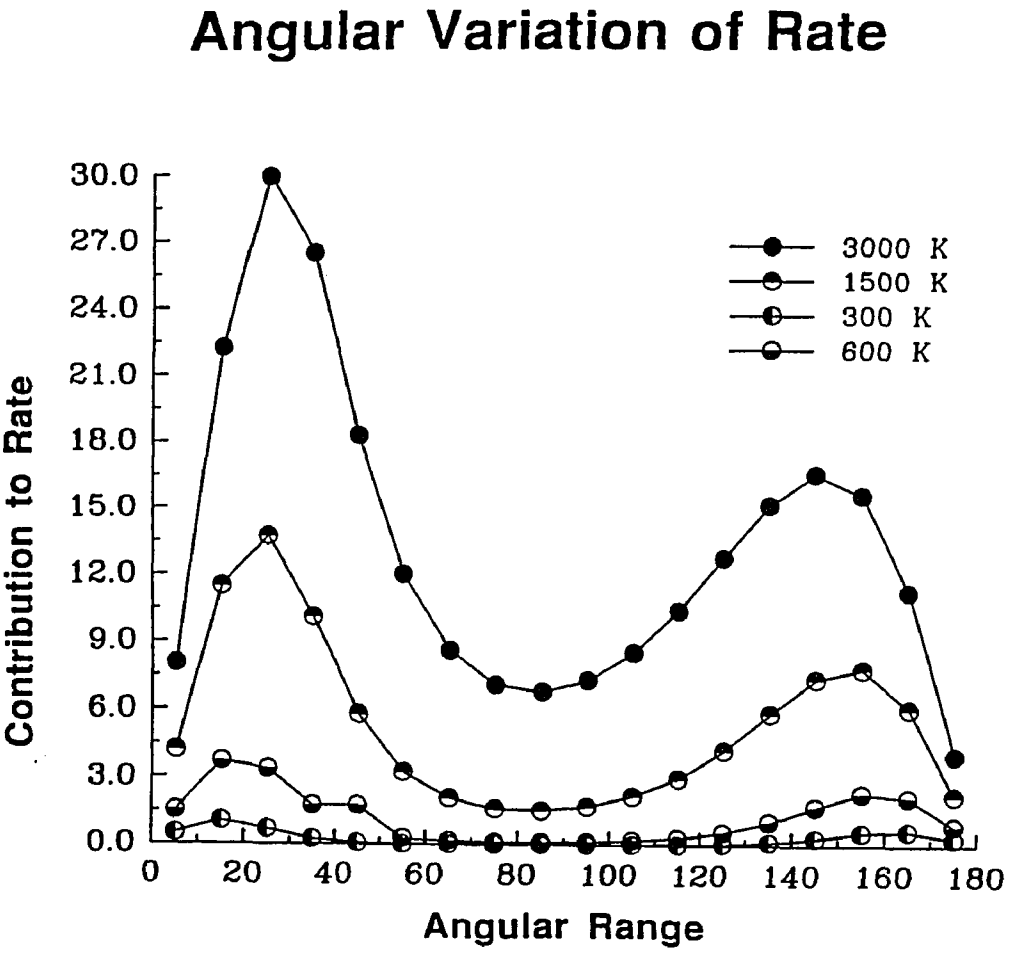

TABLE 10

Canonical least squares (LS) fit and variational total rate constants (k(T)) for F + DH reactions for quadratic dividing surfaces (DS) for several temperatures (T). LS DSs were used to generate vertices for variational searches. Rate constants are in $10^{12}cm^3/mol \cdot s$. ← marks k(T) for which DSs are plotted in Figs. 37 and 38.

k(300K)	k(600K)	k(1500K)	k(3000K)
15.09 (LS)	49.60 (LS)	154.6 (LS)	323.3 (LS)
5.734 (N) *			
5.711 (S)	20.69 (S) ←	91.61 (S) ←	235.5 (S) ←
16.69 (LS) ←	51.87 (LS)	154.5 (LS)	313.7 (LS)
4.991 (N) * ←	21.87 (N) *	93.77 (N) *	239.8 (N) *
4.991 (S)			
27.11 (LS)			
4.524 (N)			
4.795 (S)			
5.008 (SD)			
19.95 (LS)	57.73 (LS)	163.8 (LS)	328.3 (LS)
4.523 (N)	21.87 (N) *	93.77 (N) *	239.8 (N) *
4.952 ** ←			
4.729 (S)			
23.51 (LS)	63.03 (LS)	175.0 (LS)	353.7 (LS)
4.521 (N)			
4.645 (S)	20.74 (S)	91.61 (S)	235.6 (S)
5.150 (SD)			
84.07 (LS)			
4.521 (N)			
4.635 (S) ←			
	20.98 (S) GK	94.37 (S) GK	241.73 (S) GK
	20.92 (S) IR	91.73 (S) IR	236.00 (S) IR

DS:
- N – non–restricted, * marks acceptable DSs
- S – slope
- ** – acceptable intermediate value of 4.523(N) with no islands
- SD – second derivative
- GK – Koeppl's values obtained with rougher grid of 180 by 280 points
- IR – Rutenburg's values obtained with finer grid of 360 by 720 points used in this work and Koeppl's values were used to generate vertices for IR searches

for LS DSs than for variational DSs: by a factor of 2.6 – 5.1 for 300K, 2.4 – 3.1 for 600K, 1.6 – 1.9 for 1500K, and 1.3 – 1.5 for 3000K. Rate constants increase monotonically with increasing temperature as expected.

First variational DSs were obtained for 300 K with no restrictions (N) imposed on DS parameters. See Figs. 37 – 41. Some of these curve into the reactant valley before they reach the high energy region. These DSs are not strictly acceptable as explained in Ch. 3, Sect. IV B. But two N DSs, marked with an asterisk in Table 10, did not curve into the reactant valley. See Figs. 37 and 38. The rate constants for these DSs are relatively high. The rate for one of these DSs is particularly high; this DS could correspond to a high local minimum. These DSs are acceptable. Such dividing surfaces were not found during work on the F + HH reaction. No strictly acceptable N DSs were found for the F + HH reaction. Variational searches were then performed with the slope (S) restriction. All S DSs gave rate constants which were lower than those for the acceptable N DSs. Two DSs were found with the second derivative (SD) restriction which repeated the pattern observed for the F + HH reaction: these DSs gave higher rate constants than other quadratic DSs as described in Ch. 3, Sect. IV.

Variational searches usually required 20 hours of computer time. If the rate constant did not converge to enough significant figures during this time, the search was continued in further calculations until convergence was obtained to 6 significant figures. Occasionally we plotted intermediate DSs found in a search in order to see the trend in DS position on the way to convergence. During such work an intermediate N DS was plotted. This DS was acceptable; it did not curve "too soon" into the reactant valley (see Figs. 37 and 38) and islands did not appear on the reactivity relief map (see Fig. 40). The value of the rate constant for this intermeduate N DS was higher than for S DSs but lower than for acceptable converged N DSs found in other searches. This behavior is another demonstration

FIGURE 37

Three quadratic dividing surfaces for 300 K for values of θ equal to 0, 30, 150, and 180 deg.. Contours of potential energy surface are in eV.

Fig.37a

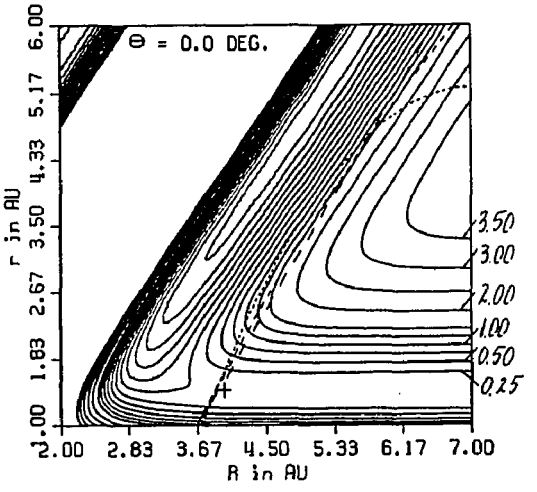

Fig.37b

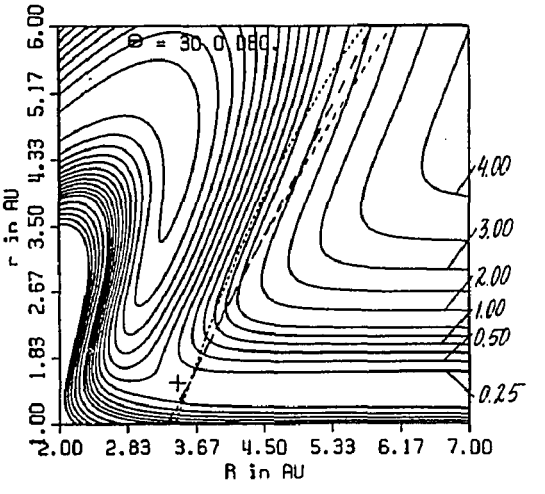

Fig.37c

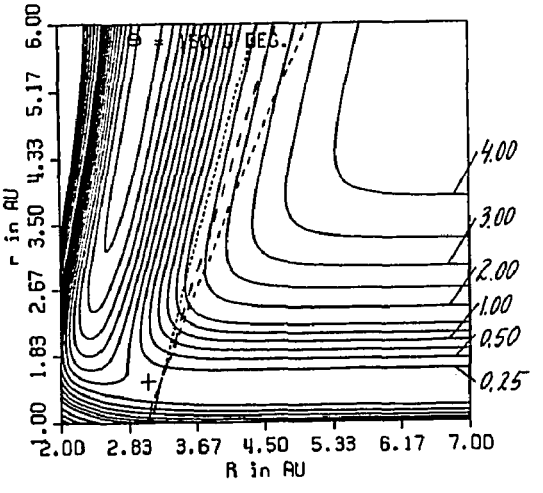

Fig.37d

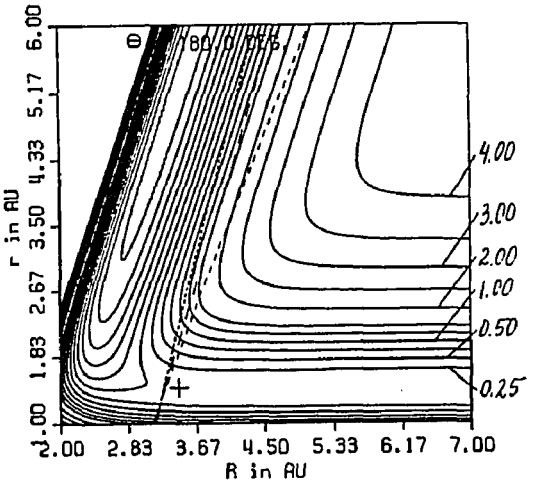

Dividing surfaces

— — — — obtained with no restriction
— — — — — — intermediate value of the above without islands (see Fig. 40)
---------- obtained with slope restriction

Potential energy surface

\+ saddle point

FIGURE 38

Three quadratic dividing surfaces for 300 K for values of θ equal to 60, 81.5, 90, and 120 deg.. Contours of potential energy surface are in eV.

Fig.38a

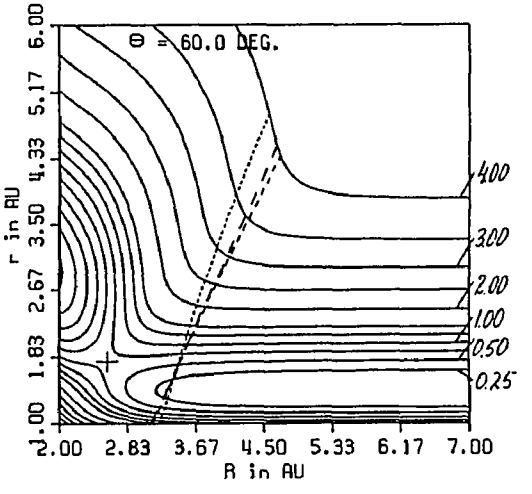

Fig.38b

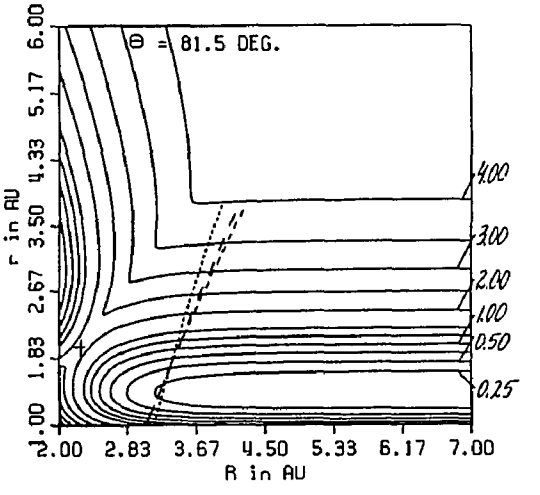

Fig.38c

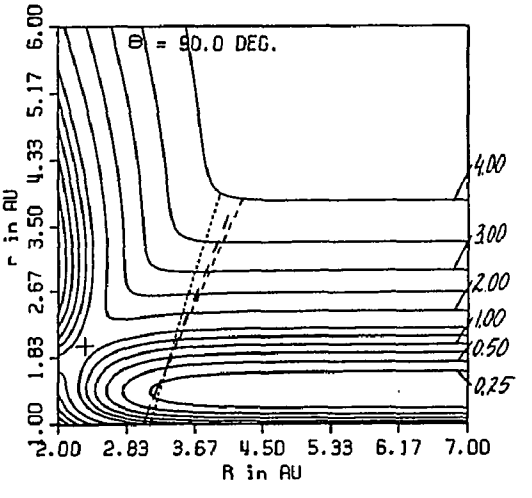

Fig.38d

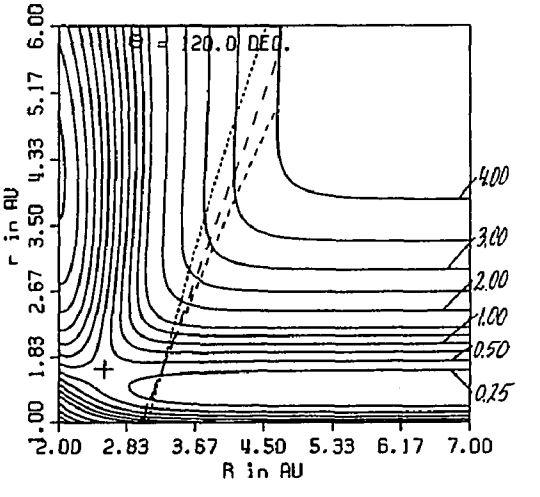

Dividing surfaces

— — — — obtained with no restriction

— — — — — intermediate value of the above without islands (see Fig. 40)

---------- obtained with slope restriction

Potential energy surface

+ saddle point

FIGURE 39

Reactivity relief maps for quadratic dividing surface obtained with no restriction for 300 K. See Figs. 37 and 38. Contours are in arbitrary units.

Fig.39a

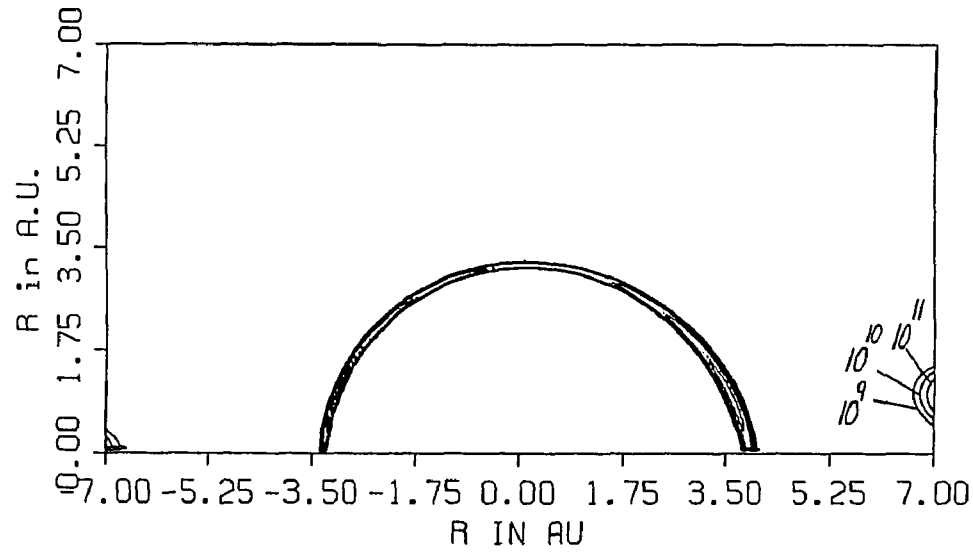

Fig.39b

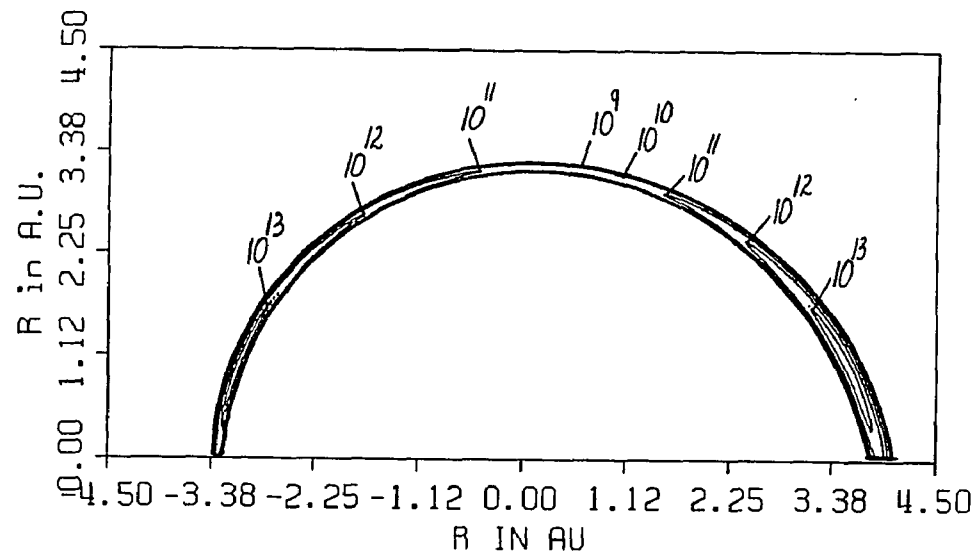

FIGURE 40

Reactivity relief maps for intermediate value of quadratic dividing surface obtained with no restriction for 300 K. See Figs. 37 and 38. Contours are in arbitrary units.

Fig.40a

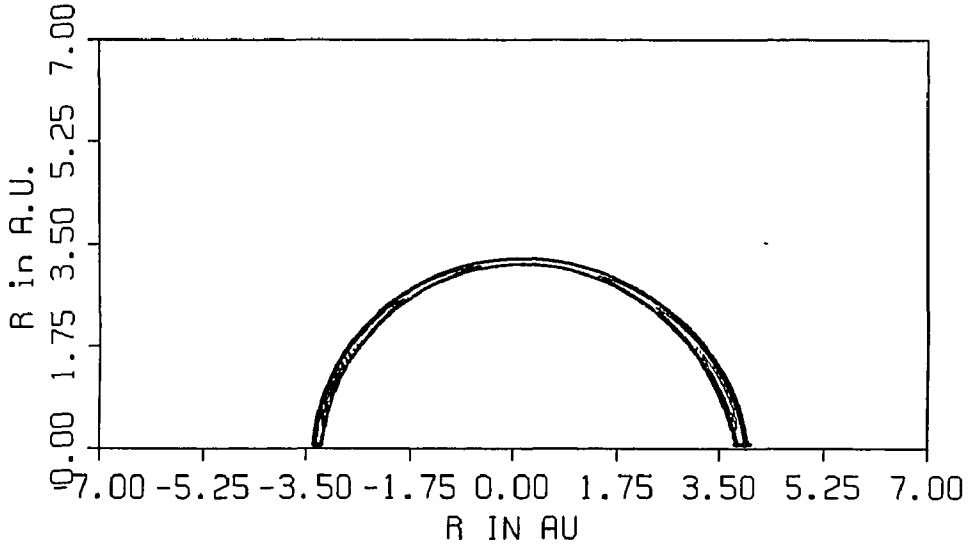

Fig.40b

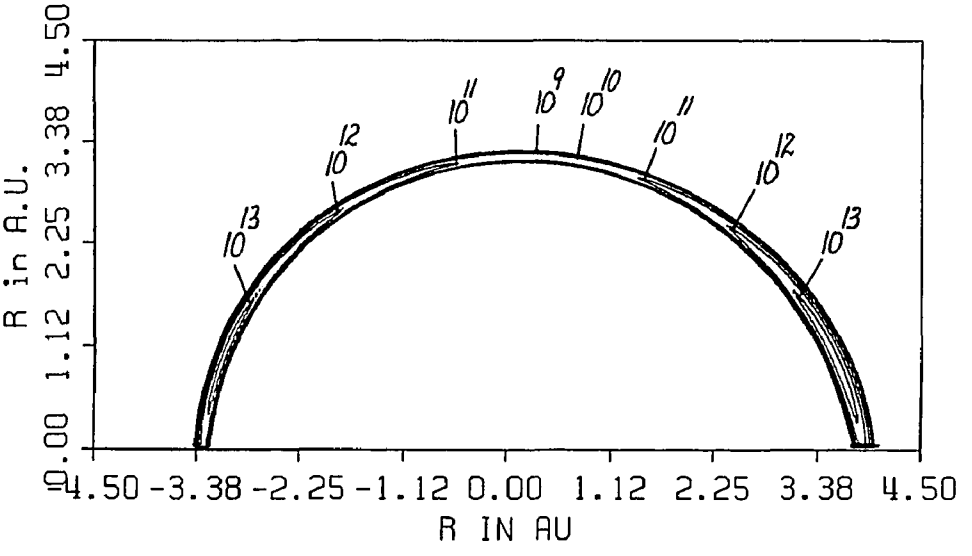

FIGURE 41

Reactivity relief maps for quadratic dividing surface obtained with slope restriction for 300 K. See Figs. 37 and 38. Contours are in arbitrary units.

Fig.41a

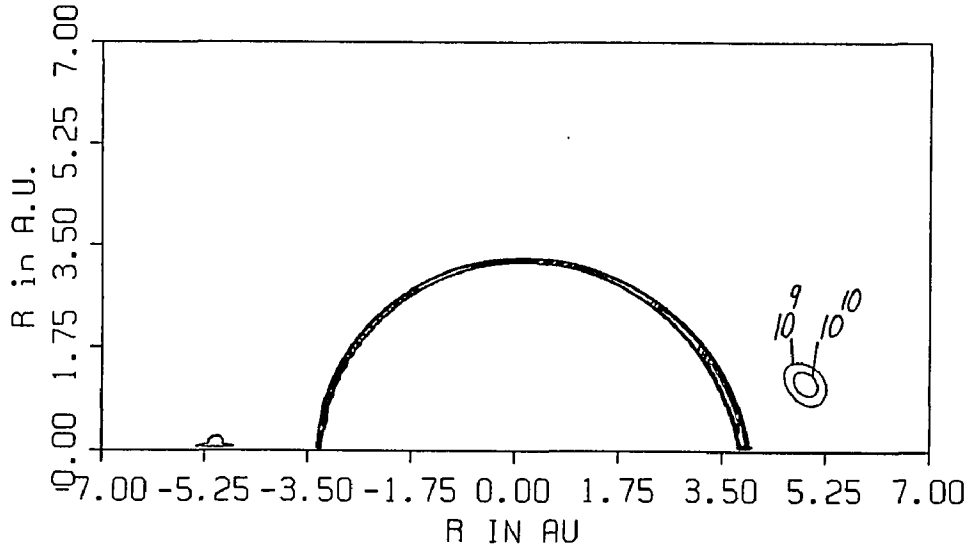

Fig.41b

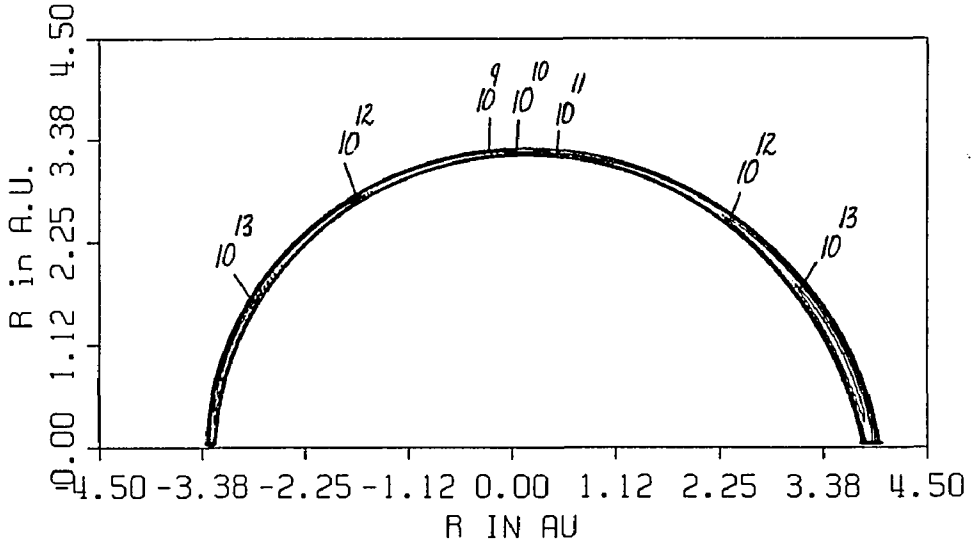

that islands which appear in reactivity relief maps are not significant. When the search was continued, the DS curved into the reactant valley too soon and was not strictly acceptable. All the other DSs have islands in reactivity relief maps. See Figs. 39 and 41. The acceptable N DSs have islands with contours in the range 10^9 – 10^{11} arbitrary units; the 10^{11} contour may make a significant contribution to the rate constant. S DSs have islands with contours in the range 10^9 – 10^{10} arbitrary units.

Two acceptable N DSs and two S DSs were found for temperatures higher than 300 K using the same initial search vertices as for 300 K. They repeated the pattern of 300 K: S DSs gave lower rate constants than acceptable N DSs. Figs. 42 and 43 show plots of S DSs for 300, 600, 1500, and 3000 K. Figs. 44 – 46 show corresponding reactivity relief maps. The contours "expand" as the temperature increases. The highest contour shown on the reactivity relief maps for 300 and 600 K corresponds to 10^{13} arbitrary units and it extends to higher θ values for 600 K. The highest contour shown on reactivity relief maps for 1500 and 3000 K corresponds to 10^{14} arbitrary units; it is not present at 1500 K for high values of θ and is present for 3000 K. The reactivity relief map for 300 K has an island with highest contour 10^{10} arbitrary units, and the reactivity relief map for 600 K has an island with highest contour 10^{11} arbitrary units. Note that at any temperature contours span a larger area in the first quadrant than in the second quadrant. Islands appear in the first quadrant which is associated with the formation of FH.

IV. NEW DIVIDING SURFACE FUNCTION

All of the reactivity relief maps discussed above have an undesirable feature at all temperatures: the contours do not fall to "negligible" values near 81.5 deg. where the minimum energy required for reaction is large (see Fig. 35). The reactivity relief maps resemble those for planar TR and LCIC DSs found for the F + HH

FIGURE 42

Quadratic dividing surfaces obtained with slope restriction for four temperatures for values of θ equal to 0, 30, 150, and 180 deg.. Contours of potential energy surface are in eV.

Fig.42a

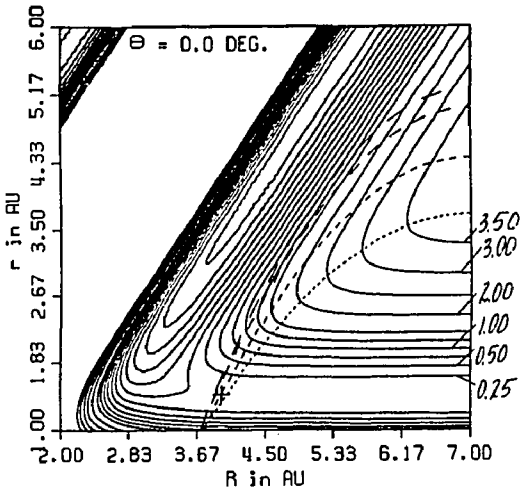

Fig.42b

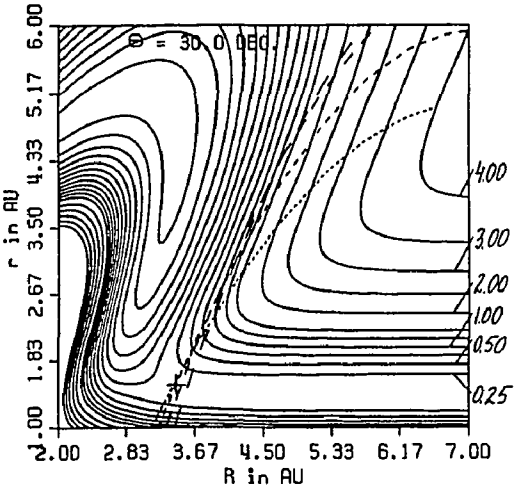

Fig.42c

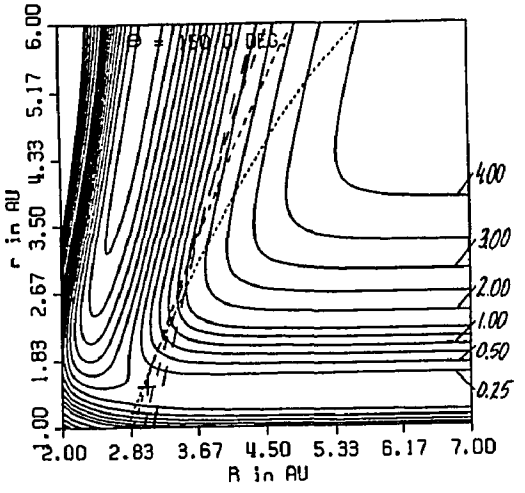

Fig.42d

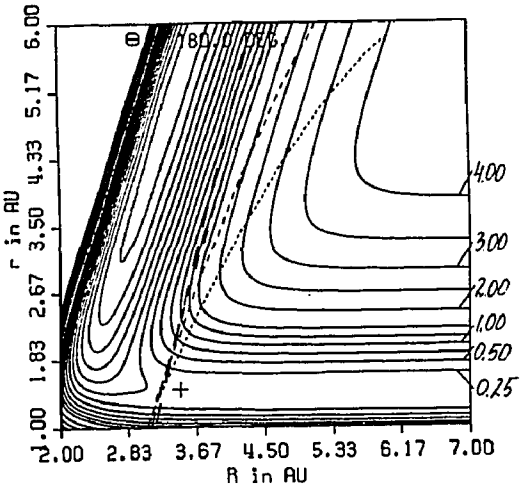

Dividing surfaces

300 K
600 K
1500 K
3000 K

Potential energy surface

saddle point

FIGURE 43

Quadratic dividing surfaces obtained with slope restriction for four temperatures for values of θ equal to 60, 81.5, 90, and 120 deg.. Contours of potential energy surface are in eV.

Fig.43a

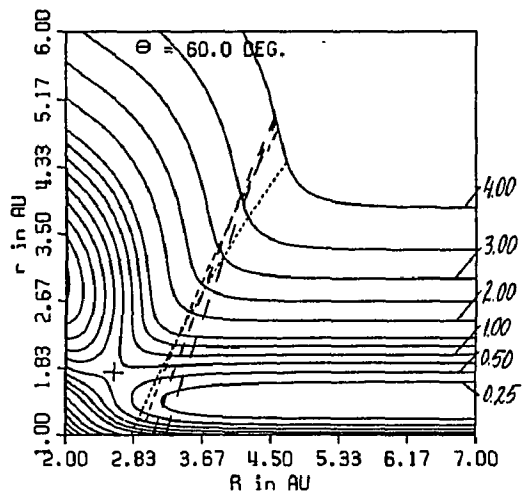

Fig.43b

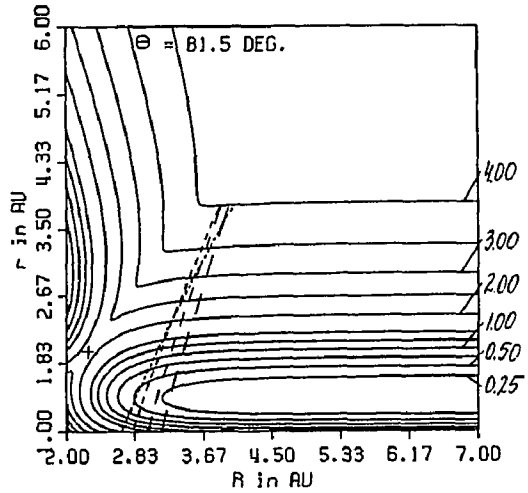

Fig.43c

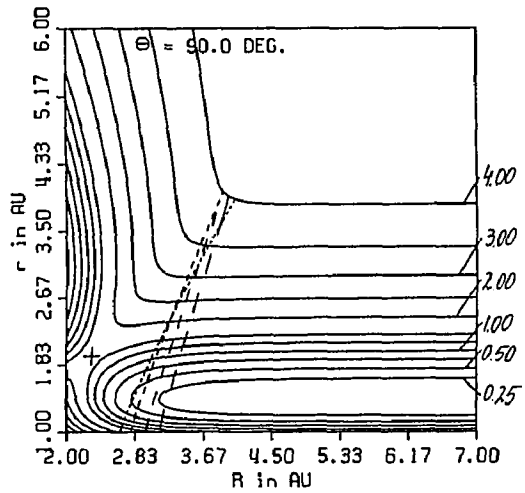

Fig.43d

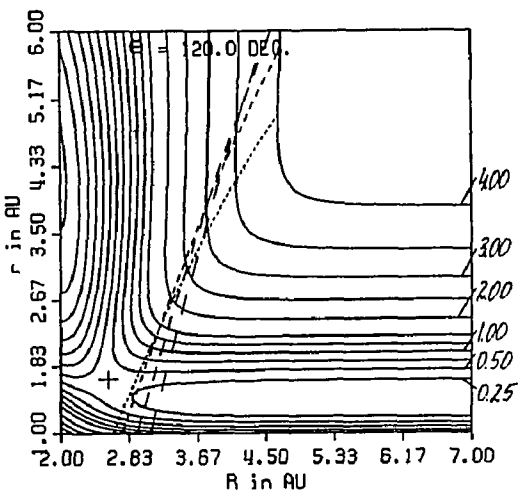

Dividing surfaces

300 K

600 K

1500 K

3000 K

Potential energy surface

saddle point

FIGURE 44

Reactivity relief maps for quadratic dividing surface obtained with slope restriction for two temperatures. See Figs. 42, 43, and 45. Contours are in arbitrary units.

Fig.44a

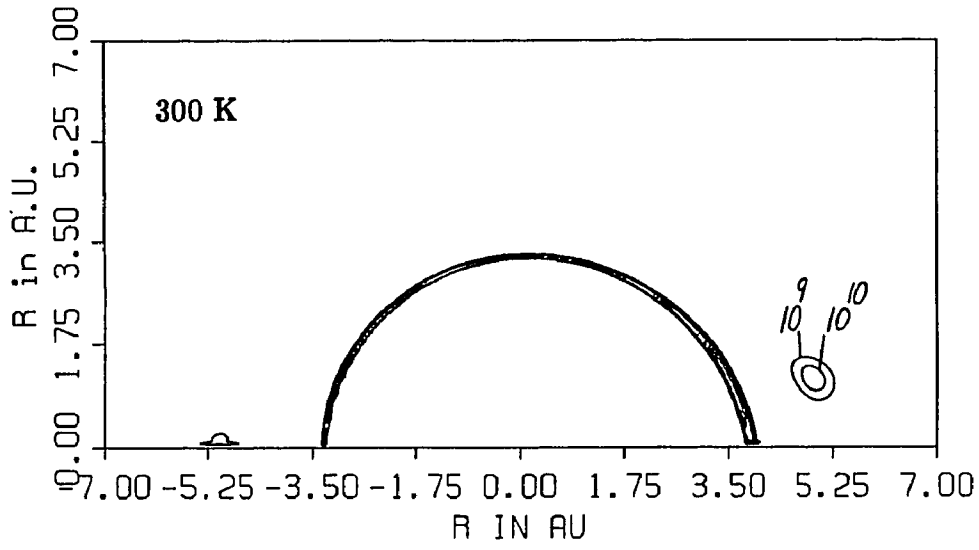

Fig.44b

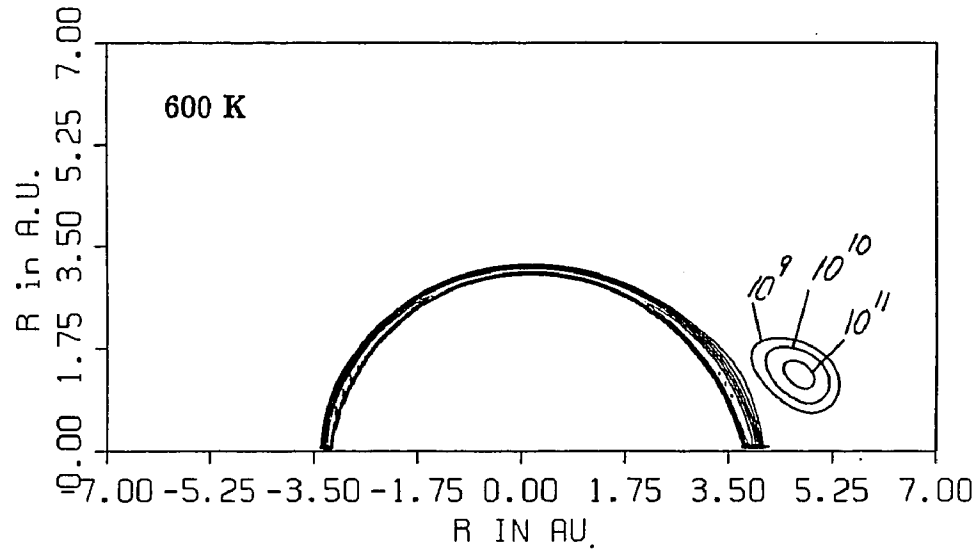

FIGURE 45

Reactivity relief maps for quadratic dividing surface obtained with slope restriction for two temperatures. See Figs. 42, 43, and 44. Contours are in arbitrary units.

Fig.45a

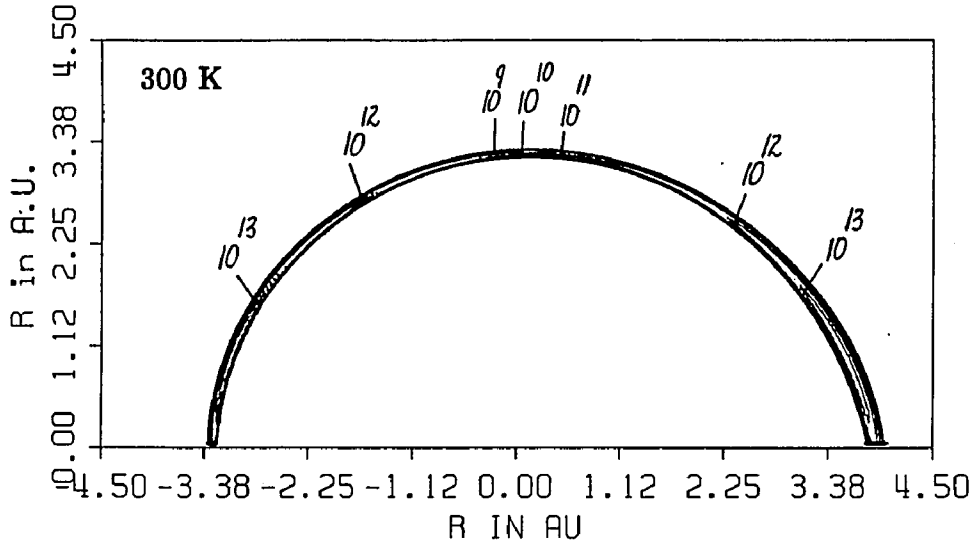

Fig.45b

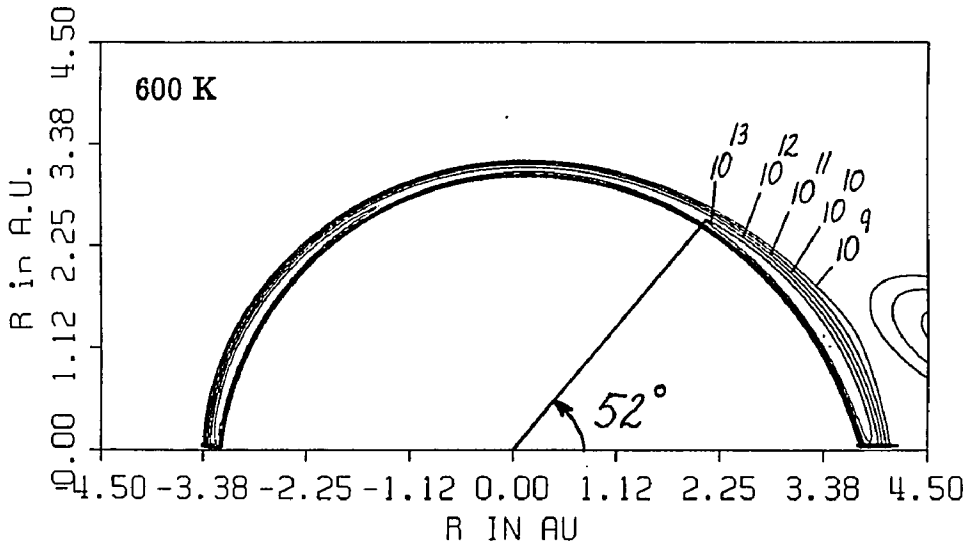

FIGURE 46

Reactivity relief maps for quadratic dividing surface obtained with slope restriction for two temperatures. See Figs. 42 and 43. Contours are in arbitrary units.

Fig.46a

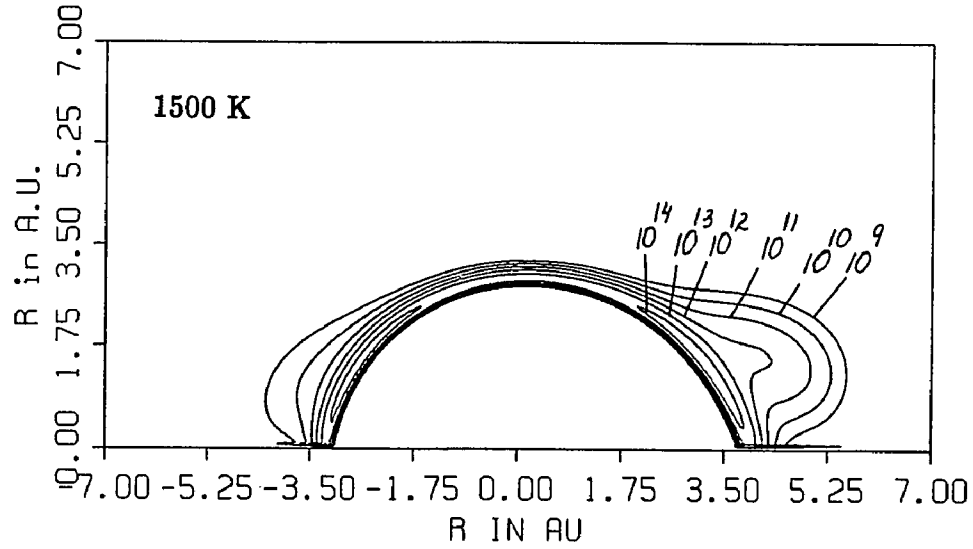

Fig.46b

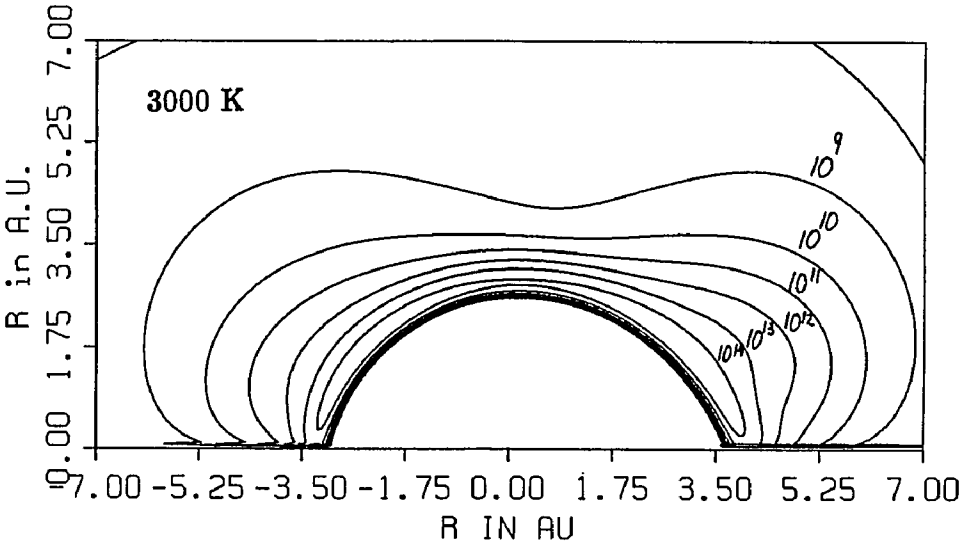

reaction. So we developed new 5– and 10–parameter functions which contain parameters which differentiate between reaction at each end of the diatomic reactant. The 5–parameter function is described in Ch. 2, Sect. I C1. The intersection of the 5–parameter DS with the r and R coordinate plane at given θ is a straight line; this DS is not curved. This DS resembles the LCIC DS and quadratic second derivative (SD) DS, i. e., when a search with this restriction yields zero for variational parameter D. The 10–parameter DSs are presented in Ch. 2, Sect. I C2. The intersection of this DS with the r and R plane at a given θ is a curve. Because of this curvature, the 10–parameter DS is comparable to the quadratic DS used to study the F + HH reaction; however, parameters are present to distinguish between reaction at each end of the diatomic reactant.

Table 11 presents quadratic, 5– and 10–parameter variational rate constants for 300, 600, 1500 and 3000 K.

1. Five–parameter DS rate constants

Twelve LS DSs were chosen to generate initial vertices for unrestricted (N) variational searches for 300 K and all twelve converged to the same value of the rate constant. This seemed impossible at first. But then it was realized that all the initial vertices were chosen on the same basis. The parameters for the LS DSs were all determined using points on straight lines through the r and R coordinate saddle points for a set of θ values so as to approximate the path of steepest ascent at different orientation angles. This was done in 12 different ways. So even if there were twelve LS DSs, all of the initial vertices were similar to each other. Four different sets of initial vertices were used for variational searches for 600 K: three calculations done with slope (S) restriction converged to the same value of the rate constant and one gave a higher rate constant with no restrictions imposed on the DS function. The last result corresponds to a higher local minimum. The same four sets of initial vertices were used to do variational searches for 1500 and 3000 K with

TABLE 11

Comparison of canonical variational rate constants (k(T)) for F + DH reactions obtained using quadratic, 5–parameter, and 10–parameter dividing surfaces for several temperatures (T). Rate constants are in $10^{12}cm^3/mol \cdot s$.

k(300K)	k(600K)	k(1500K)	k(3000K)
	Lowest values of k(T) for quadratic DS		
4.635 (S)	20.69 (S)	91.61 (S)	235.5 (S)
	k(T) for 5–parameter DS		
5.105 (N) *	23.47 (N) 21.98 (S) **	90.60 (S) **	225.6 (S) ***
	k(T) for 10–parameter DS		
4.564 (S) 4.363 (E3.0) 4.374 (E3.5)	19.76 (S) 19.13 (E3.0)	84.07 (S) 83.00 (E3.0) 82.61 (E3.5)	215.4 (S) 212.4 (E3.0)

Dividing surfaces

S – slope
N – non–restricted
E – energy limit (values 3.0 and 3.5 are in eV)
* – twelve different initial conditions converged to the same value
** – three different initial conditions converged to the same value
*** – four different initial conditions converged to the same value

the S restriction and all of them converged to the same value of the rate constant at each temperature. The slope restriction condition was introduced for 5–parameter 600, 1500, and 3000 K searches; however, examination of computer outputs showed the restriction was not actually applied during searches. So all 5–parameter DSs for all cited temperatures are actually unrestricted.

Figs. 47 and 48 show plots of 5–parameter DSs for the cited temperatures; Figs. 49 – 51 show the corresponding reactivity relief maps. The 5–parameter DSs do a much better job than the Q DSs of separating the reactive flux for reaction at each end of reactant DH; at θ values near 81.5 deg., negligible contours are present for 300 and 600 K and the highest contours present for 1500 and 3000 K at this angle have values that are 5 and 3 orders of magnitude smaller, respectively, than the values of the highest contour. At 300 and 600 K the reactivity relief maps have small islands at the very end of integration limit for R (7 a.u.). The area enclosed by each contour increases dramatically with temperature. The area enclosed by each contour for each temperature is larger in the first quadrant than in the second quadrant, indicating higher rates for FH product.

5–parameter DSs gave higher rate constants than quadratic DSs at 300 and 600 K. 5–parameter DSs gave lower rate constants than quadratic DSs at 1500 and 3000 K. Fig. 36 shows that at low temperatures the contribution to the rate is large at low values of θ; at these values the position of DS is particularly important. Compare the plots of quadratic DSs and 5–parameter DS at the cited temperatures for low values of θ. See Figs. 42 and 47, respectively. Both quadratic and 5–parameter DSs are within about the same distance from the saddle points of the PES. But quadratic DSs are curved and 5–parameter DSs are "straight"; hence 5–parameter DSs have less flexibility to avoid extra crossings by trajectories and thus to minimize reactive flux. The result is higher rate constants for 5–parameter DSs. This is the same argument which was used to account for higher rates for SD

FIGURE 47

Five–parameter dividing surfaces for four temperatures for values of θ equal to 0, 30, 150, and 180 deg.. Contours of potential energy surface are in eV.

Fig.47a

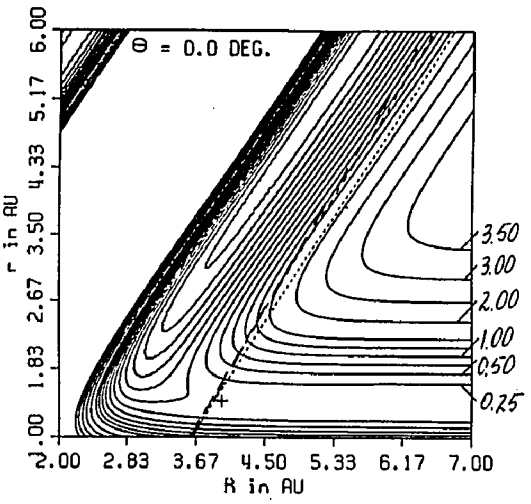

Fig.47b

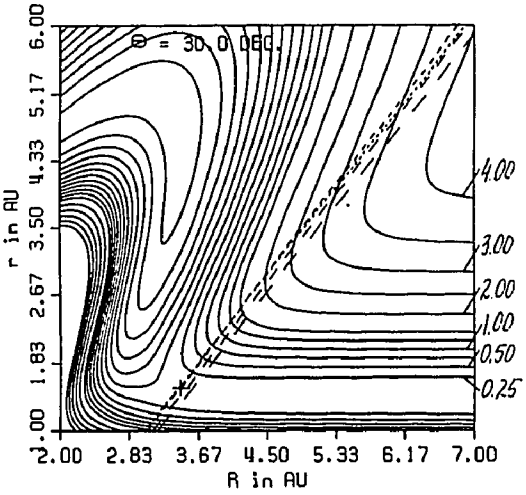

Fig.47c

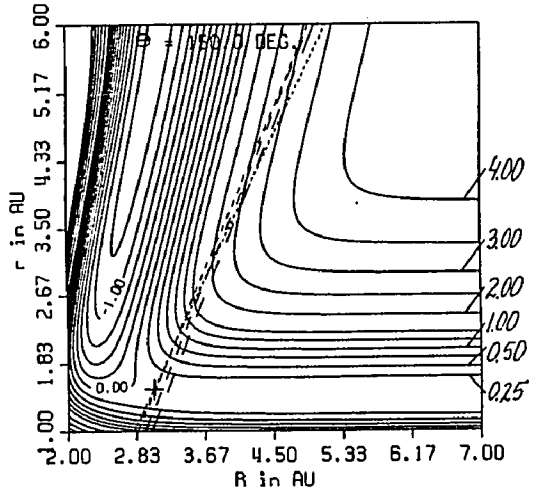

Fig.47d

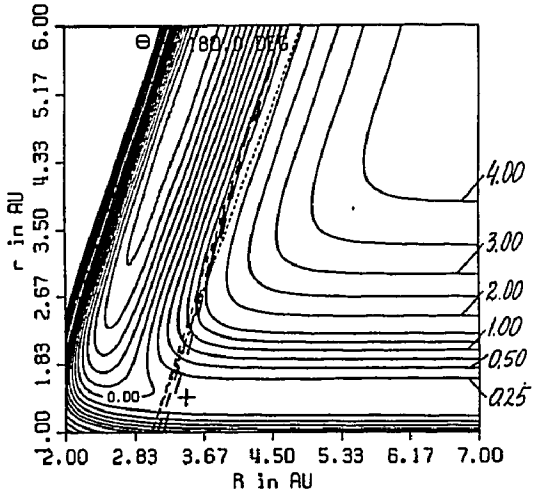

Dividing surfaces

300 K

600 K

1500 K

3000 K

Potential energy surface

saddle point

FIGURE 48

Five–parameter dividing surfaces for four temperatures for values of θ equal to 60, 81.5, 90, and 120 deg.. Contours of potential energy surface are in eV.

Fig.48a

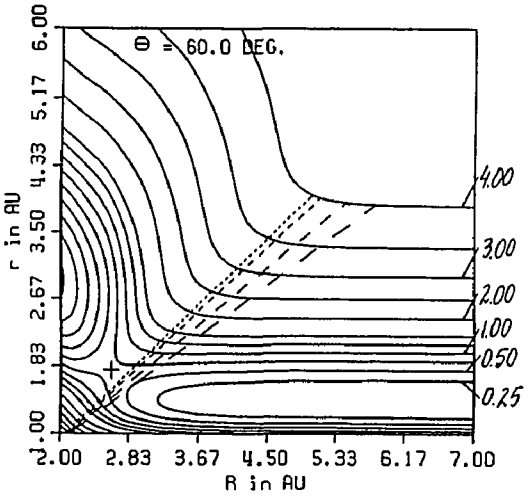

Fig.48b

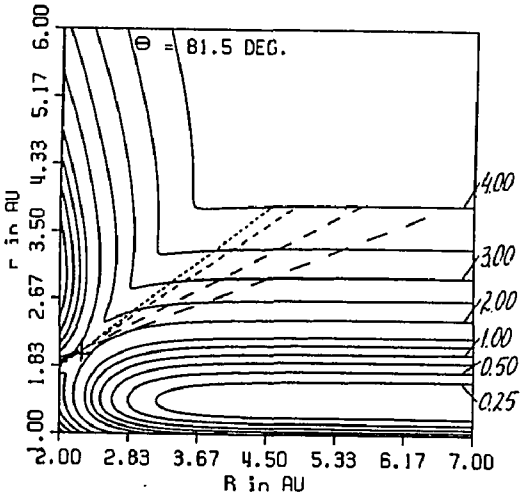

Fig.48c

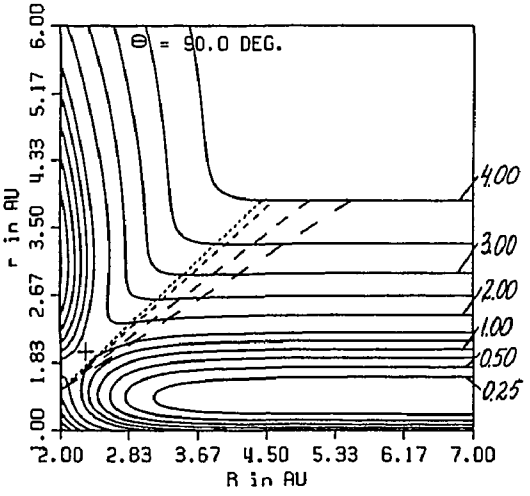

Fig.48d

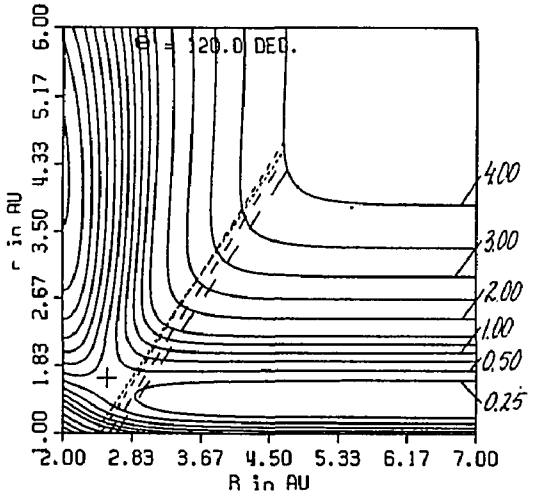

Dividing surfaces

300 K

600 K

1500 K

3000 K

Potential energy surface

saddle point

FIGURE 49

Reactivity relief maps for 5–parameter dividing surface for two temperatures. See Figs. 47, 48, and 50. Contours are in arbitrary units.

Fig.49a

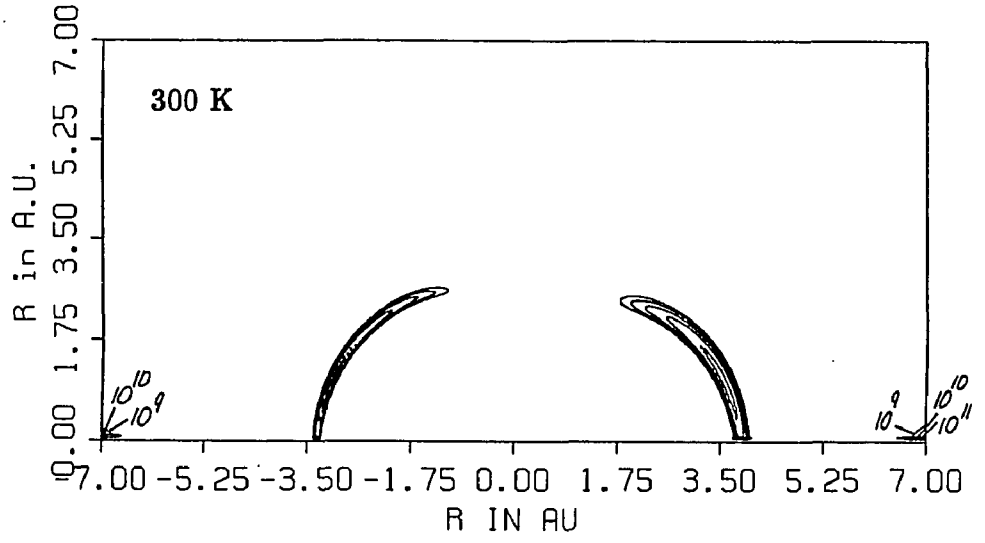

Fig.49b

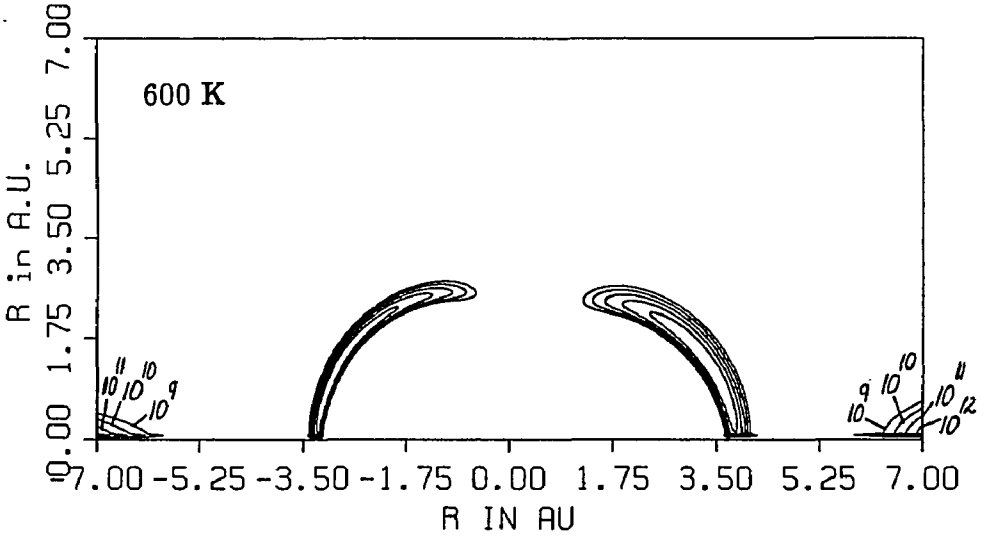

FIGURE 50

Reactivity relief maps for 5–parameter dividing surface for two temperatures. See Figs. 47, 48, and 49. Contours are in arbitrary units.

Fig.50a

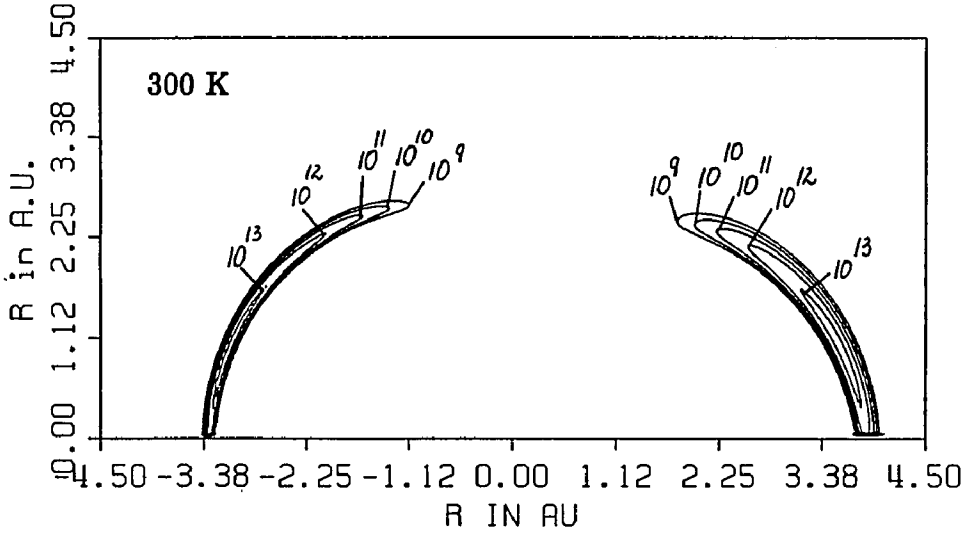

Fig.50b

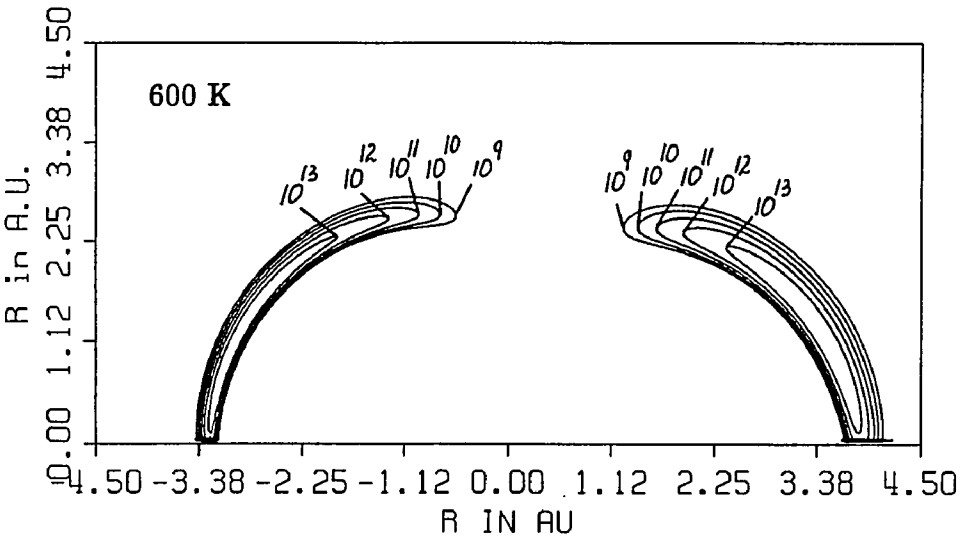

FIGURE 51

Reactivity relief maps for 5–parameter dividing surface for two temperatures. See Figs. 47 and 48. Contours are in arbitrary units.

Fig.51a

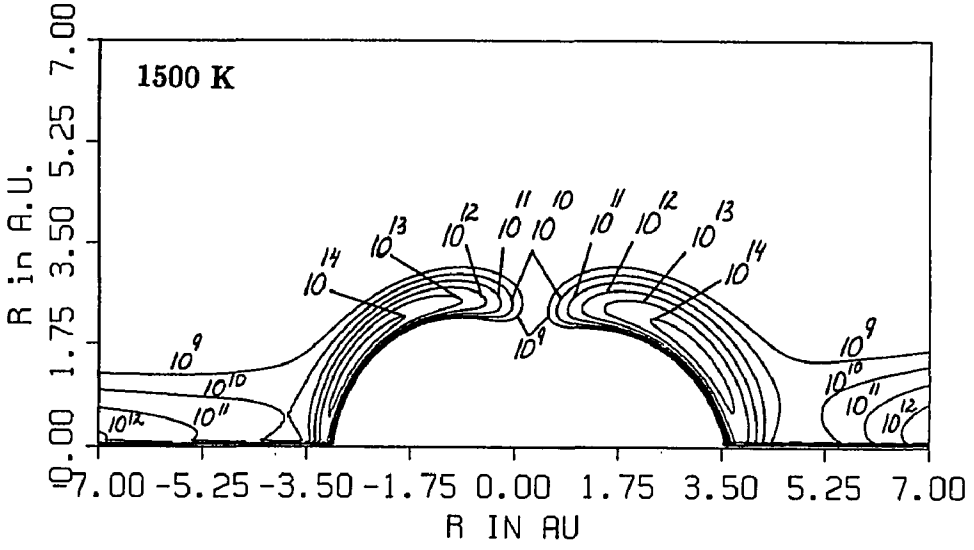

Fig.51b

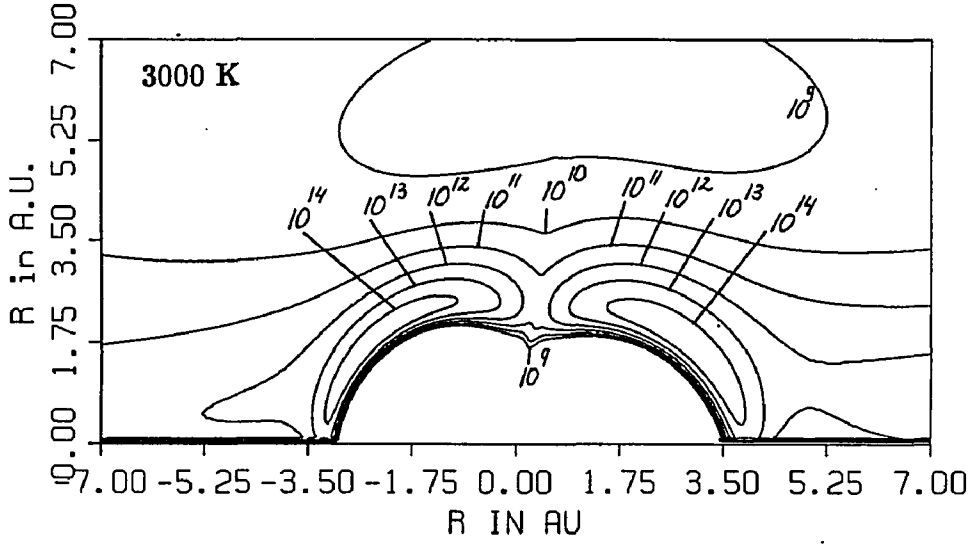

restriction DSs in Ch. 3, Sect. IV. In order to account for lower rate constants for 5–parameter than quadratic DSs at 1500 and 3000 K, Figs. 43 and 48 should be compared. They show plots of quadratic and 5–parameter DSs at high values of θ, respectively. The 5–parameter DSs are closer to saddle points than quadratic DSs at high values of θ. From Fig. 36 it is clear that at high temperatures there is a much larger contribution to the rate for high values of θ. So at high values of θ at high temperatures the ability of the DS to stay close to the saddle points is more important for minimization of the reactive flux. The 5–parameter DSs do a better job than quadratic DSs and give lower rate constants at 1500 and 3000 K.

Rate constants increase monotonically with temperature for 5–parameter DSs as expected and follow the same pattern as for quadratic DSs. This can be seen in the reactivity relief maps for quadratic (Figs. 44 – 46) and 5–parameter (Figs. 49 – 51) DSs.

2. Ten–parameter DS rate constants

First we obtained 10–parameter LS DSs. Then we attempted to find variational 10–parameter DSs using 10–parameter LS DSs to specify sets for initial vertices for simplex searches. This took too much time. Since the work for 5–parameter DSs preceded the work for 10–parameter DSs we used 5–parameter variational DSs to generate sets of initial vertices for 10–parameter DS searches at the same temperature. It took much less time to converge from vertices based on a 5–parameter DS to the 10–parameter DS than from vertices based on a 10–parameter LS DS. Small values, e.g., 0.001 were assigned to parameters of the 10–parameter DS which are absent for the 5–parameter DS. It was decided to use the slope restriction directly taking into account previous experience that all the variational curved unrestricted DSs studied bent only toward the reactant valley, if at all, and that in Ch. 3, Sect. IV B the slope restriction was adopted as the standard restriction. We also considered that if DSs did not require the slope

restriction, it would not be used. Only one set of initial vertices was used to find 10–parameter DSs at each temperature.

As already stated rate constants for 10–parameter DSs are presented in Table 11 together with these for 5–parameter DSs and the best quadratic DSs. 10–parameter DSs gave the lowest rate constants for all DSs at all cited temperatures as expected. 10–parameter DSs evidently have the advantage of both worlds: they are curved like quadratic DSs; hence, they have flexibility to minimize the reactive flux. Furthermore they differentiate between two ends of the heteronuclear reactant like 5–parameter DSs and have the ability to stay close to saddle points at high as well as at low values of θ when this is advantageous in terms of minimizing the flux. Figs. 52 and 53 present plots of 10–parameter DSs at the cited temperatures obtained with slope (S) restriction. The position of 10–parameter DSs with respect to saddle points is similar to 5–parameter DSs. Compare Figs. 52 and 53 with Figs. 47 and 48, respectively.

Figs. 54 – 56 show reactivity relief maps for 10–parameter S DSs at the cited temperatures. As in case of 5–parameter DSs the lobes of the relief maps for reaction at each end of DH are "separate" and tilt toward 81.5 degrees; the FH lobe is bigger than the FD lobe, contours are of the same order of magnitude at the same temperatures, contours of the same order of magnitude extend to higher values of θ at higher temperatures. Compare Figs. 49 – 51 with Figs. 54 – 56, respectively. Rate constants increase monotonically with temperature for 10–parameter DSs as expected and follow the same pattern as quadratic DSs and 5–parameter DSs. This can be seen in the reactivity relief maps for quadratic (Figs. 44 – 46) and 5–parameter (Figs. 49 – 51) DSs.

The total rate constant k(T) is the sum of $k(T)^C$ and $k(T)^B$; $k(T)^C$ gives the contribution to the rate constant for the θ range 0 to θ' and $k(T)^B$ gives the contribution for the range θ' to π. $k(T)^C$ gives the contribution for flux through

FIGURE 52

Ten–parameter dividing surfaces obtained with slope restriction for four temperatures for values of θ equal to 0, 30, 150, and 180 deg.. Contours of potential energy surface are in eV.

Fig.52a

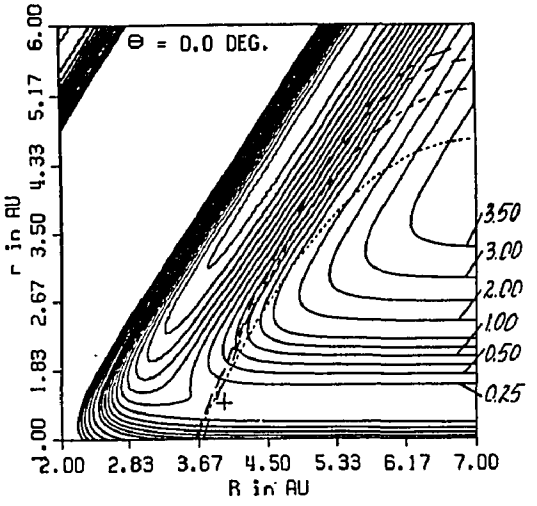

Fig.52b

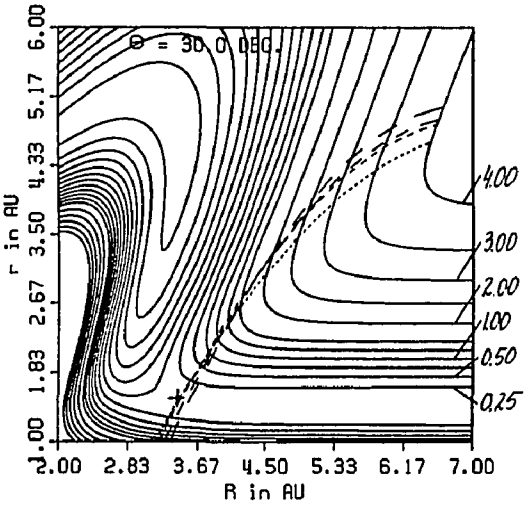

Fig.52c

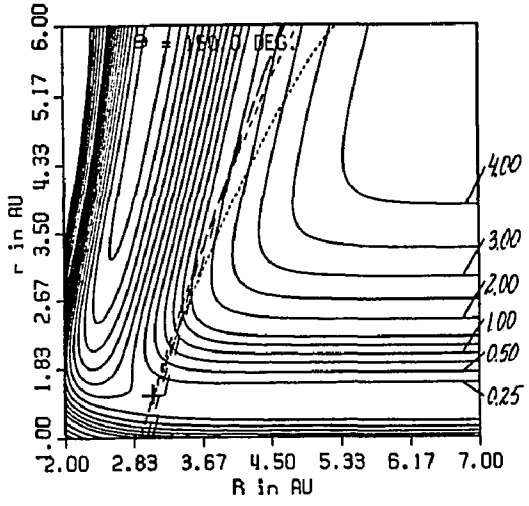

Fig.52d

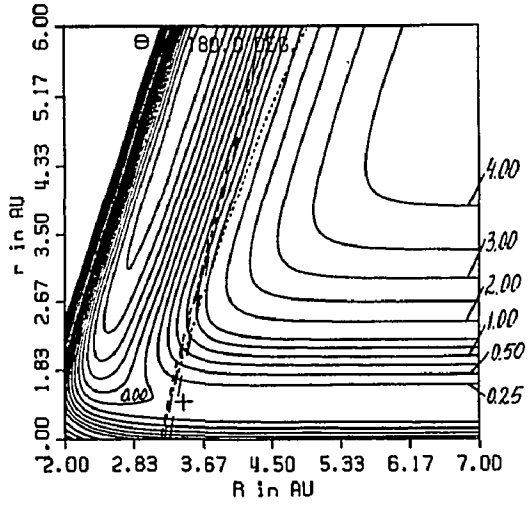

Dividing surfaces

300 K

600 K

1500 K

3000 K

Potential energy surface

saddle point

FIGURE 53

Ten–parameter dividing surfaces obtained with slope restriction for four temperatures for values of θ equal to 60, 81.5, 90, and 120 deg.. Contours of potential energy surface are in eV.

Fig.53a

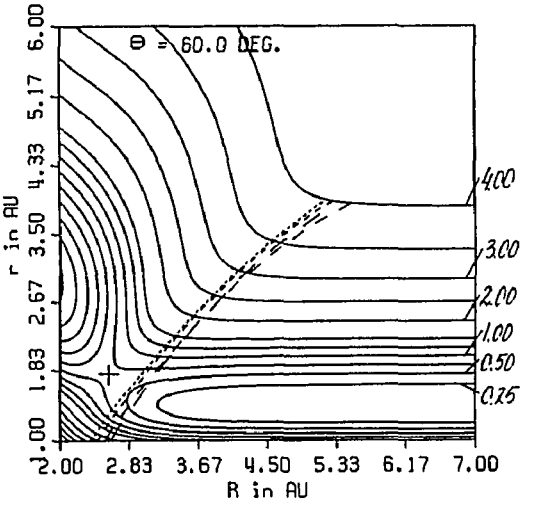

Fig.53b

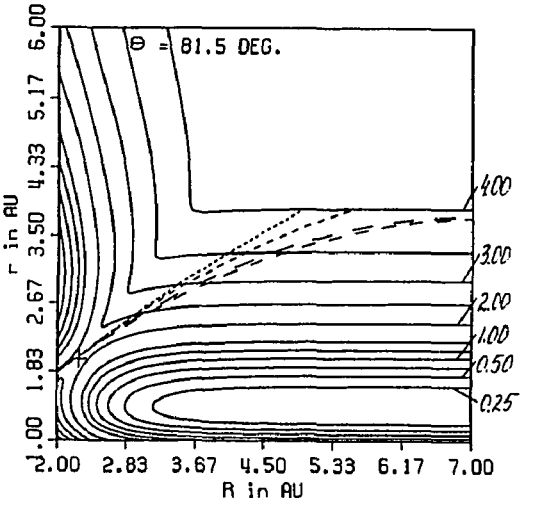

Fig.53c

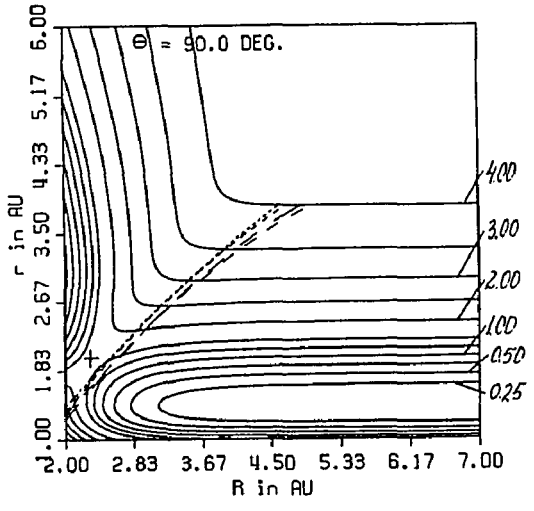

Fig.53d

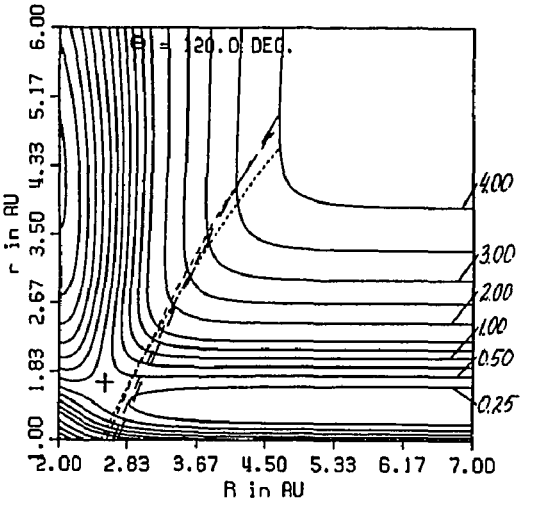

Dividing surfaces

300 K

600 K

1500 K

3000 K

Potential energy surface

saddle point

FIGURE 54

Reactivity relief maps for 10–parameter dividing surface obtained with slope restriction for two temperatures. See Figs. 52, 53, and 55. Contours are in arbitrary units.

Fig.54a

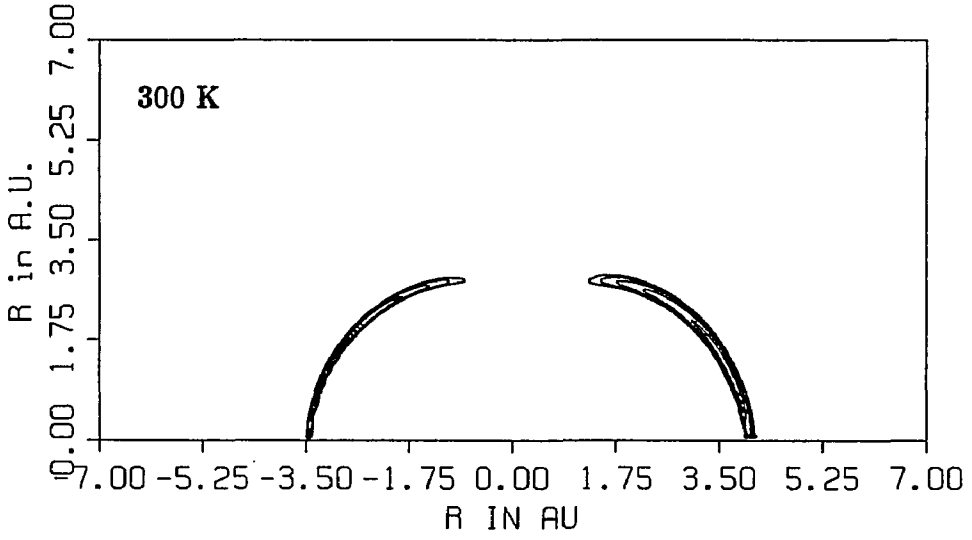

Fig.54b

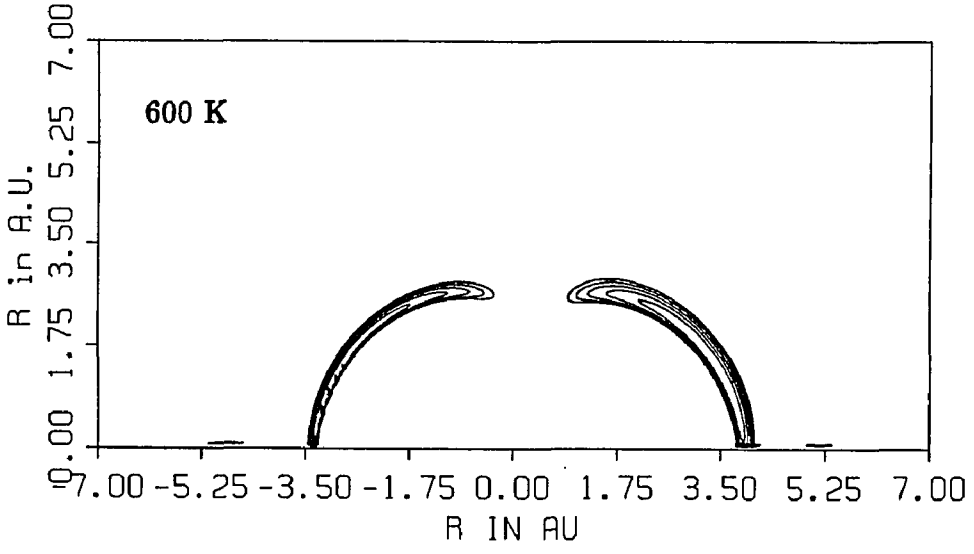

FIGURE 55

Reactivity relief maps for 10–parameter dividing surface obtained with slope restriction for two temperatures. See Figs. 52, 53, and 54. Contours are in arbitrary units.

Fig.55a

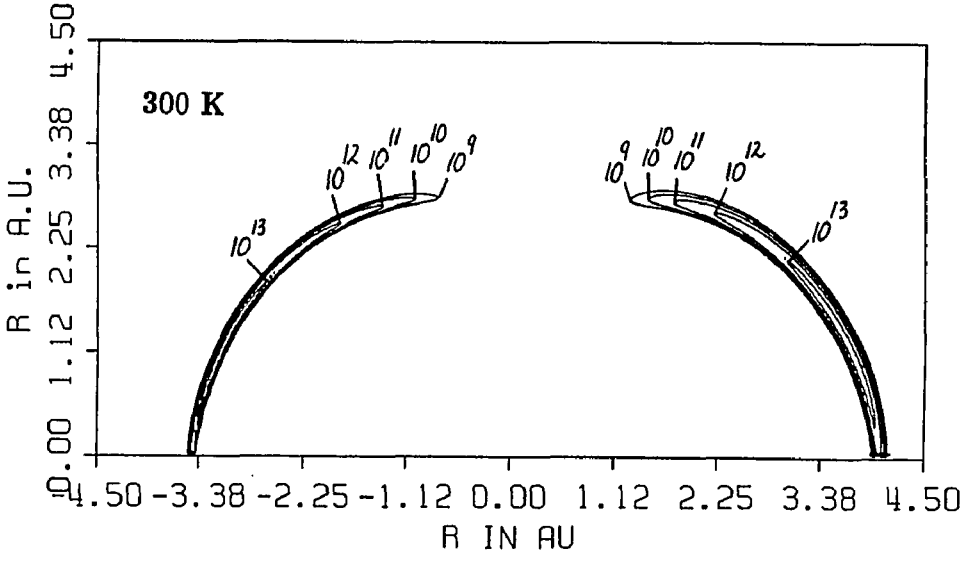

Fig.55b

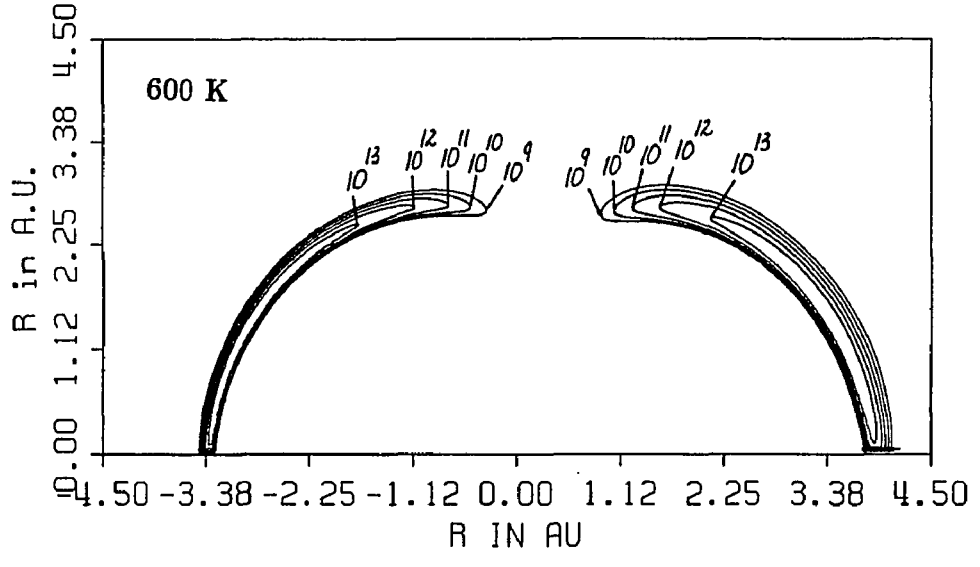

FIGURE 56

Reactivity relief maps for 10–parameter dividing surface obtained with slope restriction for two temperatures. See Figs. 52 and 53. Contours are in arbitrary units.

Fig.56a

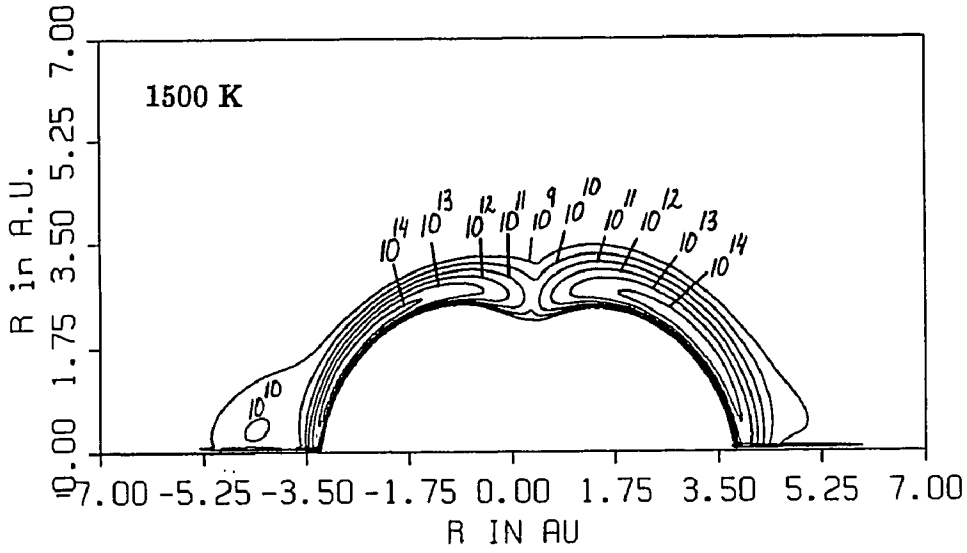

Fig.56b

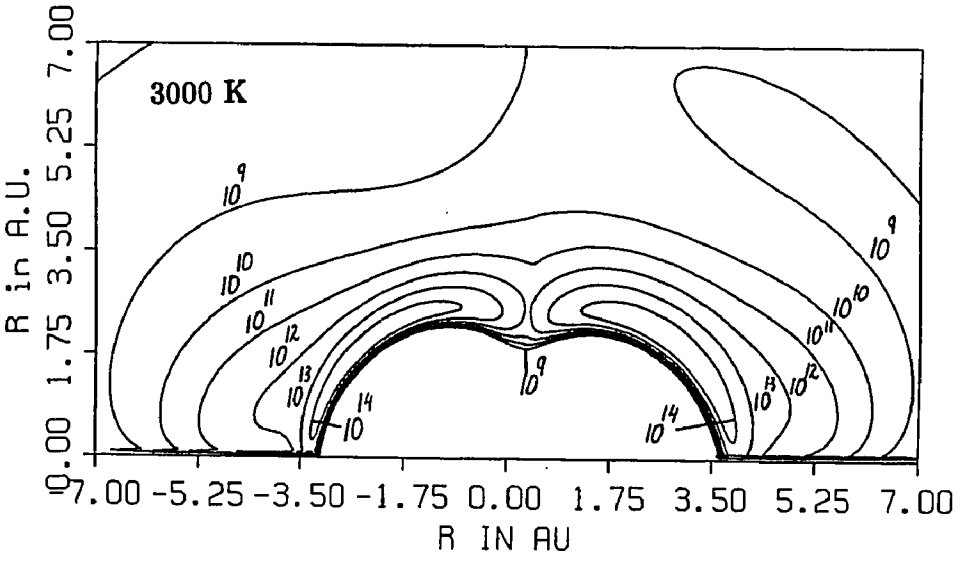

the DS near the C end of reactant BC and $k(T)^B$ gives the contribution for flux through the DS near the B end of BC. See Eqs. 68 and 69 of Ch. 2. For the F + DH reaction, we let B correspond to D and C correspond to H. The quantities $k(T)^H$ and $k(T)^D$ are given in Tables 12 and 13 for the 6 parameter Q(S) DS and 5 and 10–parameter DSs, respectively.

It is important to recognize that these quantities do not correspond to rigorous variational rate constants for reaction at each end of BC. It is in fact impossible to divide k(T) using θ' as we have done to obtain variational results for reaction at each end of the reactant. It is possible to divide the mean energy dependent reaction cross section for reaction at both ends of BC into contributions for reaction at each end of the reactant up to a certain value of the total energy of the reaction system. Since the canonical rate includes flux through the DS for all energies, including energies above the value up to which the flux can be separated for reaction at each end of the reactant, one cannot rigorously divide the flux to obtain canonical variational results for reaction at each end of the reactant. However, the 5 and 10–parameter DSs pass through the angle dependent saddle point at $\theta = 81.5$ deg.; the energy at this point is 2.31 eV for the T1 PES. The reactivity maps of Figs. 50 and 51 show that for 300, 600 and 1500K, the flux for reaction at each end of DH is separated by the high barrier at $\theta = 81.5$ deg.; hence although the $k(T)^H$ and $k(T)^D$ values in Tables 12 and 13 for 5 and 10 parameter DSs are not rigorous variational results as explained, these values represent practical variational values since the flux at energies above 2.31 eV makes a negligible contribution to the reaction rate for temperatures of 300, 600, and 1500 K. Tables 12 and 13 also give the fractions $k(T)^H/k(T)$ and $k(T)^D/k(T)$. The FH rate constants are larger than the FD rate constants for all temperatures. The fraction of FH (and FD) product does not vary much with temperature for the 5 and 10–parameter DSs; the fractions of FH product for 300, 600, and 1500 K for the

TABLE 12

Canonical variational rate constants for total reaction (k(T)), FD ($k(T)^D$), and FH ($k(T)^H$) products obtained using quadratic and 5–parameter dividing surfaces (DS) for several temperatures (T). Rate constants are in $10^{12}cm^3/mol \cdot s$.

k(T)	$k(T)^D$ ($k(T)^D/k(T)$)	$k(T)^H$ ($k(T)^H/k(T)$)	type of restriction
	k(300K) for quadratic DSs		
4.991	2.149 (0.4305)	2.842 (0.5695)	S
4.795	1.987 (0.4143)	2.808 (0.5856)	S
4.645	2.100 (0.4521)	2.545 (0.5479)	S
4.635	2.071 (0.4468)	2.564 (0.5531)	S
	k(300K) for 5–parameter DSs		
5.105	2.115 (0.4143)	2.990 (0.5857)	N
	k(600K) for 5–parameter DSs		
21.98	9.069 (0.4126)	12.91 (0.5873)	S
	k(1500K) for 5–parameter DSs		
90.60	37.50 (0.4139)	53.09 (0.5860)	S
	k(3000K) for 5–parameter DSs		
225.6	95.07 (0.4214)	130.5 (0.5785)	S

DS: N – non–restricted
S – slope

TABLE 13

Canonical variational rate constants for total reaction (k(T)), FD ($k(T)^D$) and FH ($k(T)^H$) products obtained using 10–parameter dividing surfaces (DS) for several temperatures (T). Rate constants are in $10^{12} cm^3/mol \cdot s$.

k(T)	$k(T)^D$ ($k(T)^D/k(T)$)	$k(T)^H$ ($k(T)^H/k(T)$)	type of restriction
	k(300K)		
4.564	1.992 (0.4365)	2.572 (0.5635)	S
4.363	1.942 (0.4451)	2.421 (0.5549)	E3.0
4.374	1.942 (0.4440)	2.432 (0.5560)	E3.5
	k(600K)		
19.76	8.519 (0.4311)	11.24 (0.5688)	S
19.13	8.326 (0.4352)	10.80 (0.5646)	E3.0
	k(1500K)		
84.07	35.69 (0.4245)	48.38 (0.5755)	S
83.00	35.58 (0.4287)	47.42 (0.5713))	E3.0
	k(3000K)		
215.4	92.05 (0.4273)	123.3 (0.5724)	S
212.4	90.87 (0.4278)	121.6 (0.5725)	E3.0

DS: S – slope
E3.0 – energy limit = 3.0 eV
E3.5 – energy limit = 3.5 eV

5–parameter DS are 0.5857, 0.5873, and 0.5860, respectively; the corresponding values for the 10–parameter DS are 0.5560, 0.5646, and 0.5713, respectively. The variation of $k(T)^H/k(T)$ for the 6–parameter Q(S) DS is much larger, a result which is reasonable since this DS does not do a good job of separating the flux for reaction at each end of the reactant.

Several workers have measured the branching ratio for the reaction between a fluorine atom $F(^2P)$ and DH molecule. The branching ratio, which is also referred to as an intramolecular isotope effect, corresponds to the ratio of the rates of the $F + DH \rightarrow FH + D$ and $F + DH \rightarrow FD + H$ reactions. It is unreasonable to expect the ratio of classical rate constants $k(T)^H/k(T)^D$ obtained in this work to agree with experimental values of this isotope effect. The difference found in such a comparison could be the result of inaccuracy of the potential energy surface, recrossing of the DS, quantum versus classical distributions of phase points on the DS, and the absence of a quantum correction for barrier penetration. Nevertheless, we make this comparison below.

Persky[52] used bulk kinetic methods to measure the intramolecular kinetic isotope effect $k(T)^H/k(T)^D$ defined above. At temperatures of 159, 298, and 412 K, he found values of this isotope effect of $1.55\pm.03$, $1.45\pm .03$, and $1.33\pm.03$, respectively. Berry[53] used a chemical laser experiment to measure this isotope effect; he found $1.42\pm.10$ at 297 K. Tsukiyama et al[59] used a two laser method to obtain $1.51\pm.23$. The classical variational theory values of this isotope effect at 300 K for the 5 and 10–parameter DS functions used in our work are 1.41 and 1.25, respectively. See Tables 12 and 13. The values of this isotope effect for the 5–parameter DS for 300, 600, and 1500 K are 1.41, 1.42, and 1.41, respectively; the corresponding values for the 10–parameter DS are 1.25, 1.30, and 1.33, respectively. It is not surprising that the experimental and classical isotope effect show opposite trends with increasing temperature. Kinetic isotope effects are largely determined

by the quantum mechanical behavior of the reaction system.

For the 5– and 10–parameter DSs, reactivity relief maps do not show prominent islands at any temperatures; however, these DSs extend toward the low energy region of the product valley. It was decided to attempt to improve this undesirable feature, i. e., the tendency of DSs to extend to the low energy region near the product valley. It was decided to find 10–parameter energy (E) limit DSs using 5–parameter DSs to generate initial vertices for a simplex search as it had been done for 10–parameter S DSs. None of the initial vertices used to obtain S DSs satisfied the energy limit restriction at the beginning of the search. Recall that it was difficult to obtain E DSs in the work on the F + HH reaction. See Ch. 3, Sect. IV B. We attempted to use S DSs to generate initial vertices to find E DSs. The initial vertices failed again. The value used for the energy limit has been 4.0 eV for the work presented to this point. Since this value was impossible to use it was decided to lower the value gradually. The highest value which permitted us to do energy limit searches was 1.5 eV. But these DSs at some point in variational searches started bending towards the reactant valley in the same fashion as non–restricted DSs. So we took intermediate DSs obtained after each 20 hours of variational search with energy limit of 1.5 eV and attempted to continue them (use them as initial vertices) for searches with the energy limit increased by 0.5 eV. If the restriction failed, we continued the search with the previous energy limit until we could increase the energy limit. By using this methodology we obtained E DSs for 3.0 and 3.5 eV. We could not obtain DSs with an energy limit of 4.0 eV.

Figs. 57 and 58 show plots of 10–parameter E DSs. The E DSs did not eliminate the undesirable feature of S DSs. They also extend toward the product valley. The tendency is explained the same way as for S DSs. A DS prefers to take the shortest path in the vicinity of the saddle point, the low energy region where the flux is large. By doing so the flux is minimized in the region where there is the

FIGURE 57

Ten–parameter dividing surfaces obtained with energy (E) limit restriction for four temperatures for values of θ equal to 0, 30, 150, and 180 deg.. Contours of potential energy surface are in eV.

Fig.57a

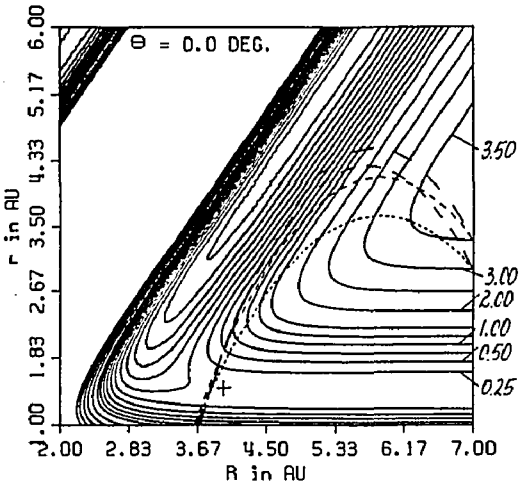

Fig.57b

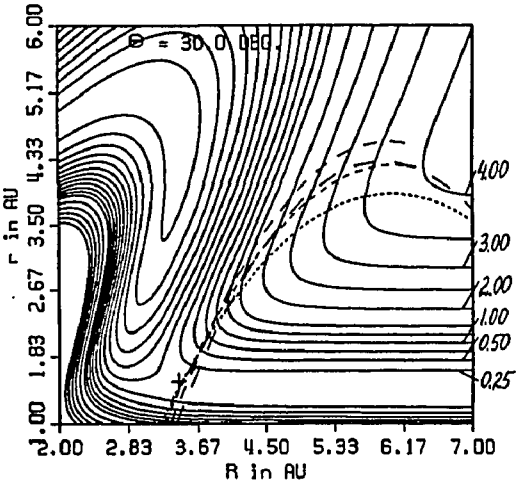

Fig.57c

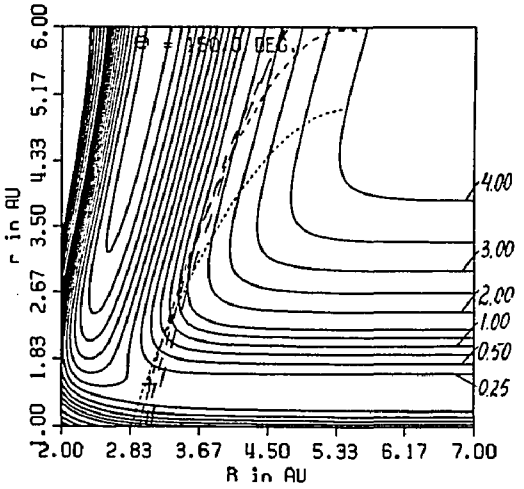

Fig.57d

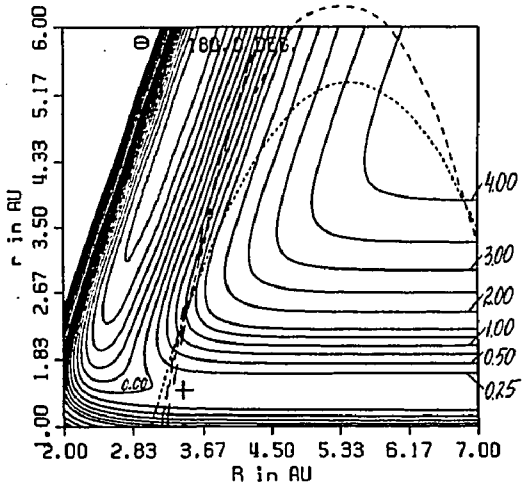

Dividing surfaces

300 K with E = 3.5 eV
600 K with E = 3.0 eV
1500 K with E = 3.5 eV
3000 K with E = 3.0 eV

Potential energy surface

saddle point

FIGURE 58

Ten–parameter dividing surfaces obtained with energy limit (E) restriction for four temperatures for values of θ equal to 60, 81.5, 90, and 120 deg.. Contours of potential energy surface are in eV.

Fig.58a

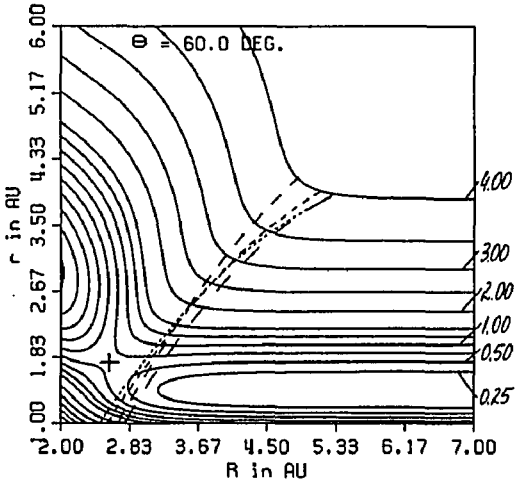

Fig.58b

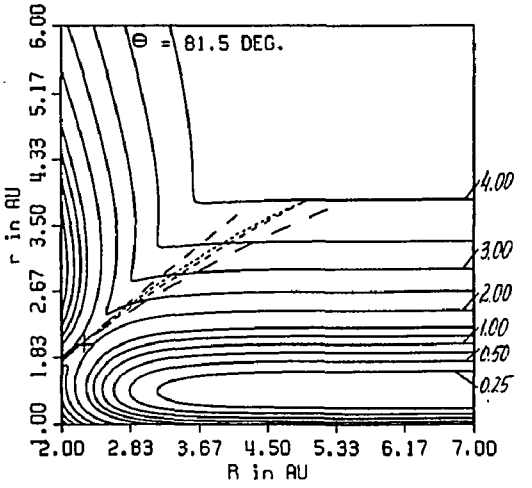

Fig.58c

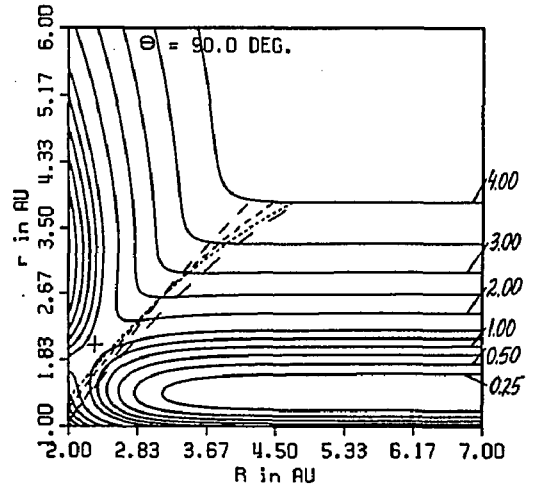

Fig.58d

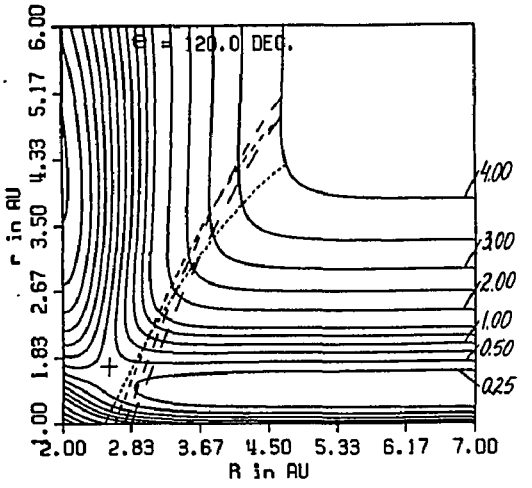

Dividing surfaces

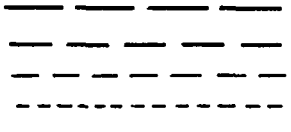

300 K with E = 3.5 eV
600 K with E = 3.0 eV
1500 K with E = 3.5 eV
3000 K with E = 3.0 eV

Potential energy surface

saddle point

major contribution to it. The DS has a high slope in the saddle point region and can not turn "fast enough" to avoid the product valley as it proceeds to the high energy region. This phenomenon was discussed in Ch. 3, Sect. VI with regard to variational DSs vs LS DSs. There was one more opportunity to improve the appearance of DSs, i.e., to find energy and slope restricted (ES) DSs. It was difficult to get variational calculations running with the energy limit restriction, to get them running with both the energy limit and slope restriction was even more difficult. At this point we realized that we were repeating the work for the F + HH study: we were attempting to obtain DSs with different restrictions. It was decided that there was no need to repeat the work already done during the F + HH study for the sake of appearance only.

Figs. 59 – 61 show reactivity relief maps for 10–parameter E DSs. Note that always at the right and often at the left top corners of the plots, contours are present. These plots use polar coordinates. We integrate over R up to 7.0 a.u. to obtain $N_*^c(T)$. The plot shows 7 a.u. in horizontal and vertical directions, but in the diagonal direction on the plot the value of $R > 7$ a.u.; at values of $R > 7$ a.u. DSs curve into the reactant valley and show a superfluous contribution to the reactive flux which appears in the top corners of reactivity relief maps. The E DSs at 300 K have small islands in the reactivity relief maps (see Fig. 59). There was no need to prove insignificance of the islands since this has been proven many times before by different approaches. Also this time we obtained S DSs with no islands which incidentally gave higher rate constants than the E DSs with islands which is yet another indication that islands are insignificant. Nevertheless, we decided to use a new approach inspired by the fact that we found an intermediate value of acceptable quadratic N DS with no islands. See Sect. III of this chapter. We took advantage of the fact that 10–parameter searches required a lot of computer time. We plotted the intermediate DSs obtained after each 20–hour search, and continued the search.

FIGURE 59

Reactivity relief maps for 10–parameter dividing surface obtained with energy limit restriction for two temperatures. See Figs. 57, 58, and 60. Contours are in arbitrary units.

Fig.59a 300 K

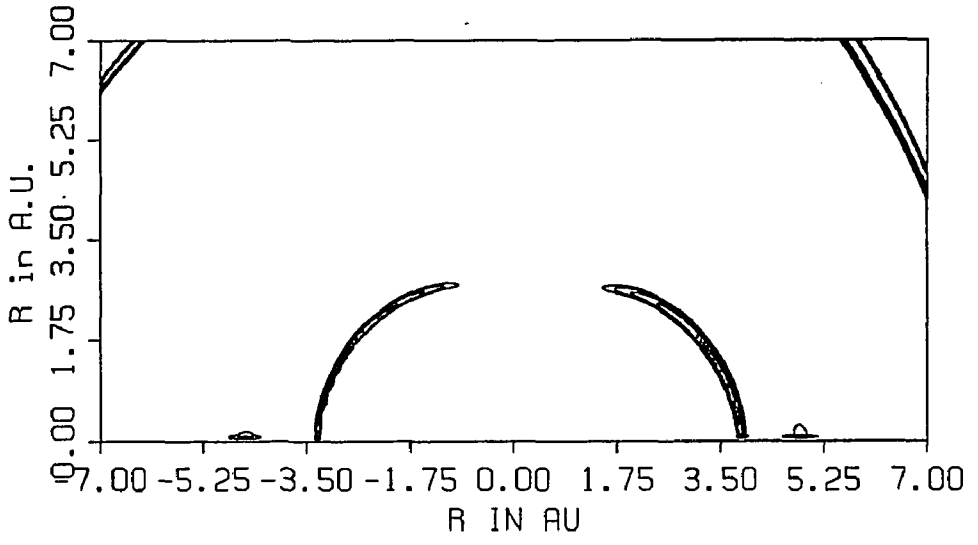

Fig.59b 600 K

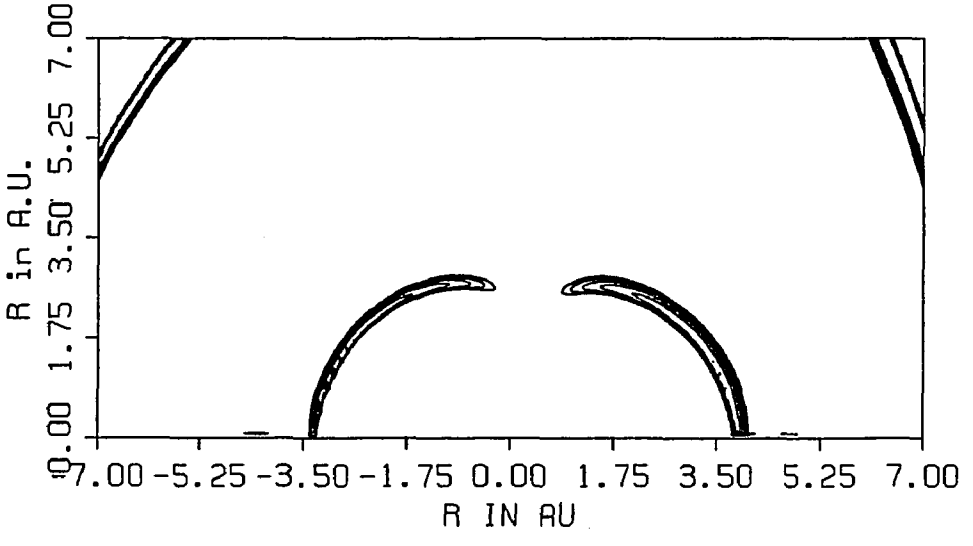

FIGURE 60

Reactivity relief maps for 10–parameter dividing surface obtained with energy limit restriction for two temperatures. See Figs. 57, 58, and 59. Contours are in arbitrary units.

Fig.60a 300 K

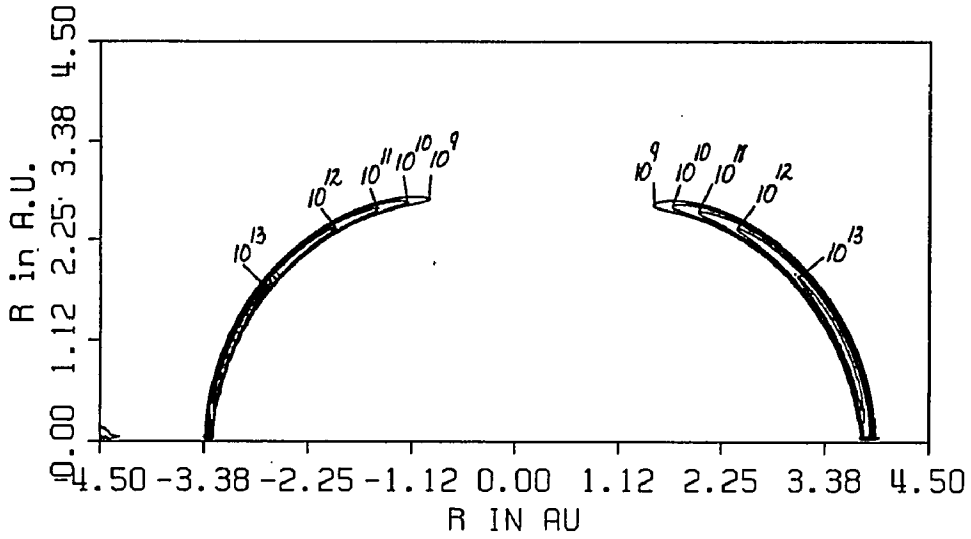

Fig.60b 600 K

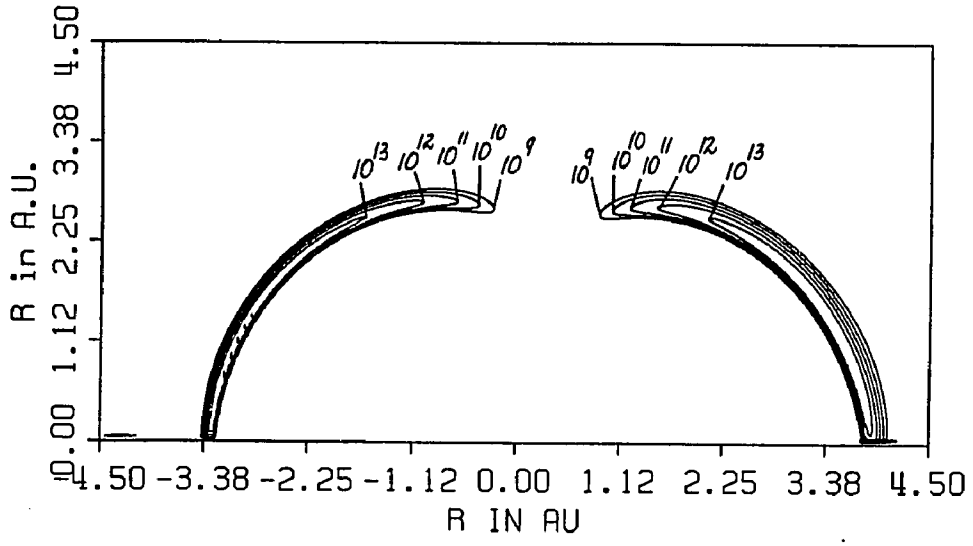

FIGURE 61

Reactivity relief maps for 10–parameter dividing surface obtained with energy limit restriction for two temperatures. See Figs. 57 and 58. Contours are in arbitrary units.

Fig.61a 1500 K

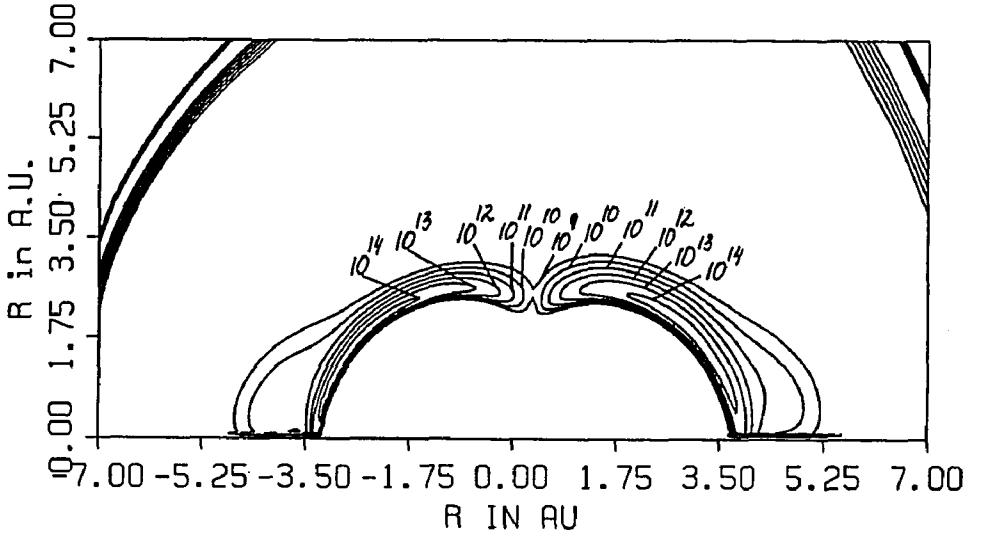

Fig.61b 3000 K

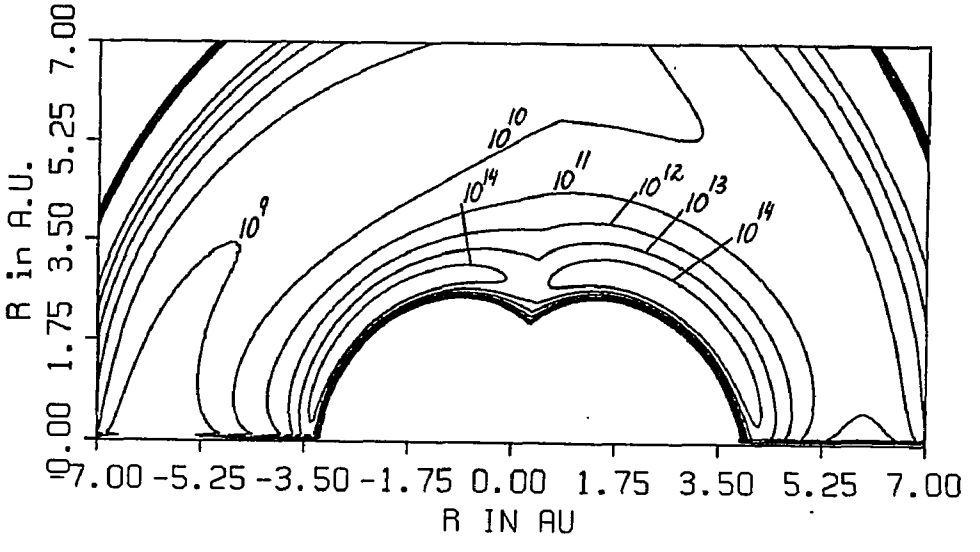

The values of the rate constants decreased gradually. But the appearance of islands was absolutely erratic. They were appearing and disappearing, getting bigger and smaller without any distinct pattern. Some intermediate DSs did not have islands but subsequent DSs with a smaller rate constant showed islands. We feel that we have provided adequate demonstration that such islands are insignificant.

10–parameter E DSs followed the pattern of all previously obtained DSs: monotonic increase of rate constant with temperature, similar orders of magnitude for reactivity contours at different temperatures, tilt of the reactivity relief map lobes towards 81.5 degrees, bigger area of contours in the first quadrant and appearance of islands in the first quadrant. 10–parameter E DSs gave lower rate constants than S DSs, the lowest for all DSs used for the F + DH reaction. For that reason alone we consider them to be the best results for F + DH reaction in spite of the difficulties encountered in obtaining them, the sharp curve at the top of the DSs, and tiny islands at 300 K. But because of the difficulties in obtaining them we would not recommend their use; the more amenable S DSs are preferable.

V. LIMITS OF INTEGRATION AND GRID SIZE

The limits of integration over R are the same as for the F + HH project: from 1.0 a.u. to 7.0 a.u.. The limits of integration over θ are from 0 to π.

As stated in Ch. 3 the grid was quadrupled for the F + DH study: 360 for θ by 560 points for R. The number of points for integration over θ was doubled again because the integration was performed for values of θ from 0 to π for the F + DH reaction versus $\pi/2$ for the F + HH reaction. So, the grid consisted of 720 by 560 points for θ and R, respectively. $D^{c}_{BC}(T)$ for DH was evaluated using 500 points.

VI. COMPUTER TIME REQUIRED FOR F + DH PROJECT

Since we doubled the R grid and quadrupled the θ grid it took a long time for

a variational search to converge to 6 significant figures (as in the F + HH project) especially at low temperatures. The quadratic DS took from 40 to 140 hrs to converge to 6 significant figures for 300 K, 20 – 40 hrs for 600 K, and 20 hrs for 1500 and 3000 K. 5–parameter searches took from 20 to 80 hrs to converge to 6 significant figures for 300 K, from 20 to 40 hrs for 600, 1500 and 3000 K. For 10–parameter DSs we could not obtain convergence to 6 significant figures no matter how long we searched. We obtained convergence to 4 significant figures in most cases which is reported in the tables. We did not run any search longer than 200 hrs. It should be noted that if we attempted to run searches to obtain convergence to 6 significant figures, the previously obtained convergence to 4 significant figures could change. Note that since E DSs were run using S DSs to generate initial vertices, E DSs required less time than S DSs to converge. It should be noted that from the point of view of computer time as well as the number of parameters used (actually because of the number of parameters used) 10–parameter DSs are comparable to the cubic DSs used to study F + HH reaction. We believe that the fine grid size we used would be excessive to recommend for routine work: the last two lines in Table 10 present rate constants obtained by Koeppl with a much rougher grid (180 points for θ and 280 points for R) which were refined by Rutenburg with the grid used for the work on the F + HD reaction (720 points for θ and 560 points for R). The 600 K results agree to 3 significant figures but the high temperature agreement is only in 1 significant figure.

CHAPTER 5

ACCURACY OF THE CLASSICAL VARIATIONAL THEORY

In this chapter, the accuracy of the classical variational theory is studied by comparing values of the energy dependent mean reaction cross section with classical mechanical trajectory values. We chose to use quadratic rather than cubic formulations of the dividing surface (DS) for the accuracy study because of the small cubic versus quadratic gain in accuracy and the relative ease of a quadratic variational search. We chose to determine the accuracy of the variational theory for quadratic rather than more restricted formulations of the DS because we want to know the accuracy when the rate constant or mean reaction cross section is close to its minimum value. Calculations were performed for the Truhlar 1 (T1) potential energy surface (PES) function because it is the intermediate potential energy function in the series studied in this work and it was easier to obtain analytical derivatives of the potential energy function with respect to internuclear separations which are required for accurate trajectory calculations. We determined the accuracy of the variational theory by comparing variational and trajectory mean reaction cross sections rather than rate constants because the former can be calculated with a much smaller error than the latter in Monte Carlo calculations of the same number of trajectories. The accuracy of the variational theory was also studied by comparing angular distributions of contributions to the energy dependent mean reaction cross section with trajectory distributions. The trajectory results were calculated by G. W. Koeppl.

I. RESULTS FOR THE $F + H_2$ REACTION

Variational values of the mean reaction cross section were calculated for the slope (S) restriction, energy (E) limit restriction, and unrestricted (N) quadratic (Q) DSs for energies of 0.1, 0.25, 0.5, 0.75, 1.0, and 1.5 eV. The results are given in Table 14. Note that the energy limit and unrestricted values of the mean reaction cross section are the same. The energy limit used was not 4.0 eV, the value used for most of the canonical calculations, but rather the energy of the microcanonical ensemble. This restriction is easy to satisfy; three variational searches performed with this restriction converged to results obtained for unrestricted searches. We therefore refer to the energy limit results of Table 14 as unrestricted in the text which follows. The value of R_{max} used in the microcanonical calculations was the same as that used for canonical calculations, i. e., 7.0 a.u.. Values of the mean reaction cross section calculated using the slope restriction are slightly larger than the unrestricted values as expected. The errors cited for the trajectory results correspond to a confidence level of 68 percent. Fig. 62 shows plots of unrestricted variational and trajectory mean reaction cross sections versus energy. The difference between these results increases with energy as expected; however the difference at 1.0 and 1.5 eV amounts to only 18 and 25 percent, respectively. These energies are very high in the sense that the probability that reaction systems have these energies at temperatures commonly used in the study of gas phase reactions is extremely small.

The difference between variational theory ($<S_r(E)>^{VT}$) and classical mechanical trajectory ($<S_r(E)>^{CMT}$) values can be expressed as a fraction ($\chi(E)$) which is referred to as the conversion coefficient[83].

$$\chi(E) = \frac{<S_r(E)>^{CMT}}{<S_r(E)>^{VT}} \qquad (84)$$

TABLE 14

Comparison of classical mechanical trajectory (CMT) and variational theory (VT) mean reaction cross sections ($\langle S_r(E)\rangle$) for the $F + H_2$ reaction

E (eV)	$\langle S_r(E)\rangle^{CMT}$ (a. u.)	$\langle S_r(E)\rangle^{VT}$ dr/dR >0 (a. u.)	$\langle S_r(E)\rangle^{VT}$ unrestricted (a. u.)	$\langle S_r(E)\rangle^{VT}$ E limit (a. u.)
0.10	1.08± .08	1.249		1.216
0.25	5.62± .32	6.316	6.185	6.185
0.50	11.81± .37	13.109	12.956	12.956
0.75	15.82± .57	18.567	18.500	18.500
1.0	19.76± .53	23.397		23.362
1.5	25.27± .65	31.812		31.700

FIGURE 62

Plots of trajectory and variational mean reaction cross sections versus energy (E) for the $F + H_2 \rightarrow FH + H$ reaction. Variational results correspond to the quadratic unrestricted dividing surface.

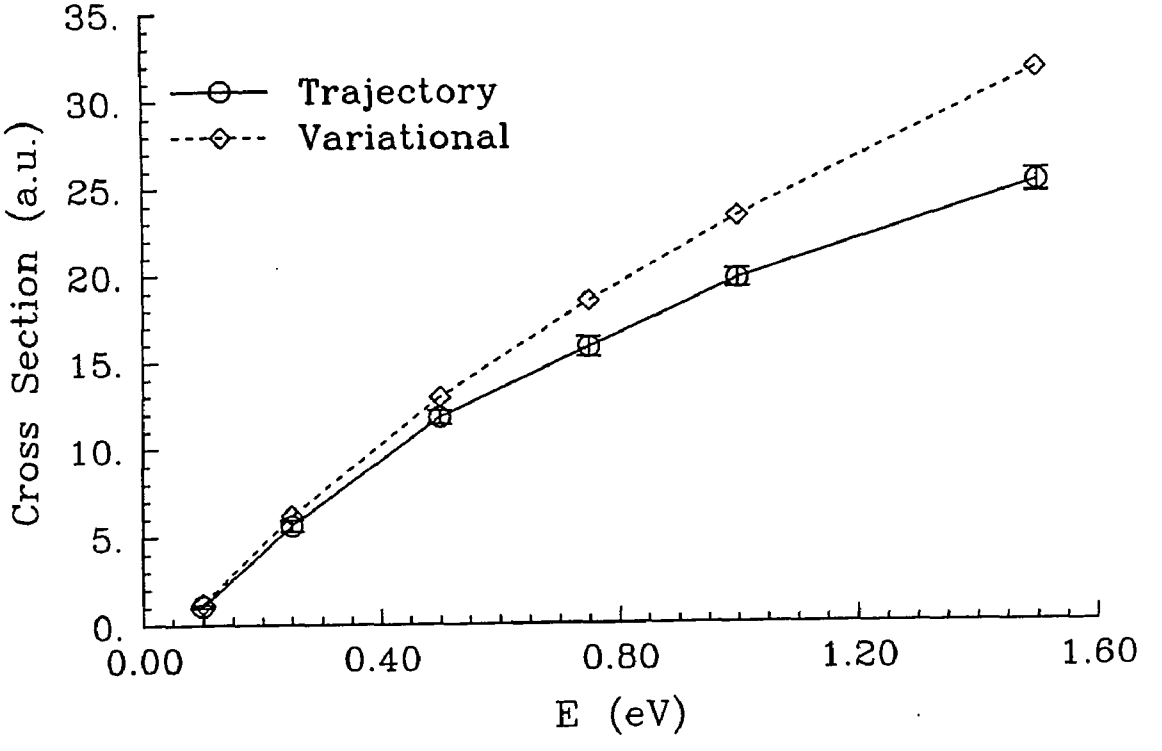

The correction factor $\chi(E)$ may be applied to the variational mean reaction cross section to obtain the trajectory mean reaction cross section, i. e., the actual value of this quantity.

$$\langle S_r(E)\rangle^{CMT} = \chi(E)\,\langle S_r(E)\rangle^{VT} \tag{85}$$

We further describe the difference between variational and trajectory values of the mean reaction cross section by expressing the conversion coefficient as the product of two factors, the transmission coefficient ($\kappa(E)$) and product coefficient ($\rho(E)$):

$$\chi(E) = \kappa(E)\,\rho(E) \tag{86}$$

where these factors are defined by

$$\kappa(E) = \frac{\langle S_r(E)\rangle^{CMT}}{\langle S_r(E)\rangle^{R\ddagger}} \quad \text{and} \tag{87}$$

$$\rho(E) = \frac{\langle S_r(E)\rangle^{R\ddagger}}{\langle S_r(E)\rangle^{VT}}. \tag{88}$$

The quantity $\langle S_r(E)\rangle^{R\ddagger}$ is defined in the following paragraph.

Many chemists believe that a correction, the transmission coefficient, must be applied to transition state theory because some trajectories which originate in the reactant region cross the DS and subsequently recross it and return to the reactant region. The quantity $\langle S_r(E)\rangle^{R\ddagger}$ is the energy dependent mean cross section for all reaction systems on the DS that correspond to trajectories which originate in the reactant region and are moving toward products at the DS, regardless of whether the reaction system ultimately reaches the product region. All crossings of the DS from the reactant to the product side which correspond to trajectories which originate in the reactant region contribute to $\langle S_r(E)\rangle^{R\ddagger}$. The factor $\kappa(E)$ provides a correction for multiple crossings of the DS by trajectories which originate in the reactant region. This factor corrects for trajectories which are reflected after crossing the DS and return to the reactant region and for trajectories which are

ultimately reactive but cross and recross the DS an odd number of times on their way to the product region.

Another factor ($\rho(E)$) must be applied to correct the variational value of the mean reaction cross section. Fig. 1 shows that transition state theory must also be corrected because trajectories which originate in the product region, which are present in the equilibrium flux of reaction systems through DS, can cross and recross the DS and contribute (incorrectly) to the reaction rate, i. e., k(T) and $<S_r(E)>^{VT}$ should correspond to the rate of reaction in the absence of products. Hence the variational theory must also be corrected by applying the product factor $\rho(E)$. Note that the product factor is unity if trajectories which originate in the product region do not contribute to the variational flux.

To gain a clear understanding of the correction factors defined above, the reader should examine Fig. 1 and note that for the sample of trajectories shown: $\chi = 2/10$; $\kappa = 2/7$; $\rho = 7/10$; $S_r^{CMT} \sim 2/8 \sim 2$ DS crossings; $S_r^{R\ddagger} \sim 7/8 \sim 7$ DS crossings; and $S_r^{VT} \sim 10/8 \sim 10$ DS crossings.

Trajectory and variational results for the unrestricted quadratic DS are summarized in Table 15. The quantity $<S_r(E)>^{R\ddagger}$ is determined by calculating the function that defines configurations on the DS ($r - F(R,\theta) - C = 0$) for each time step of each trajectory to detect crossings of the DS by trajectories which contribute to this quantity. Plots of the transmission, product, and conversion coefficient versus energy are given in Fig. 63. The values of the coefficients are given in Table 15. Note that the deviation between variational and trajectory values of the mean reaction cross section for energies of 0.1, 1.0, and 1.5 eV caused by trajectories which start in the reactant region and cross the DS more than once is smaller than the deviation caused by trajectories which originate in the product region, i. e., $\kappa(E) > \rho(E)$ for these energies. For the energy 0.5 eV, $\kappa(E)$ is approximately equal to $\rho(E)$.

TABLE 15

Classical mechanical trajectory (CMT) results for the $F + H_2$ reaction

E eV	b_{max} a.u.	Number of traject.	$\langle S_r \rangle^{CMT}$ a.u.	$\langle S_{R\neq} \rangle^{CMT}$ a.u.	κ	ρ	χ
0.10	3.0	18000	1.08±.08	1.12±.08	0.965	0.919	0.887
0.25	4.0	6000	5.62±.32				0.909
0.50	4.0	9000	11.81±.37	12.45±.39	0.949	0.960	0.910
0.75	4.5	6000	15.82±.57				0.855
1.0	4.5	9000	19.76±.53	21.20±.57	0.932	0.908	0.846
1.5	5.0	9000	25.27±.65	27.29±.70	0.926	0.861	0.797

FIGURE 63

Plots of transmission, product, and conversion coefficients versus energy (E) for the $F + H_2 \rightarrow FH + H$ reaction. Coefficients were calculated for the quadratic unrestricted dividing surface.

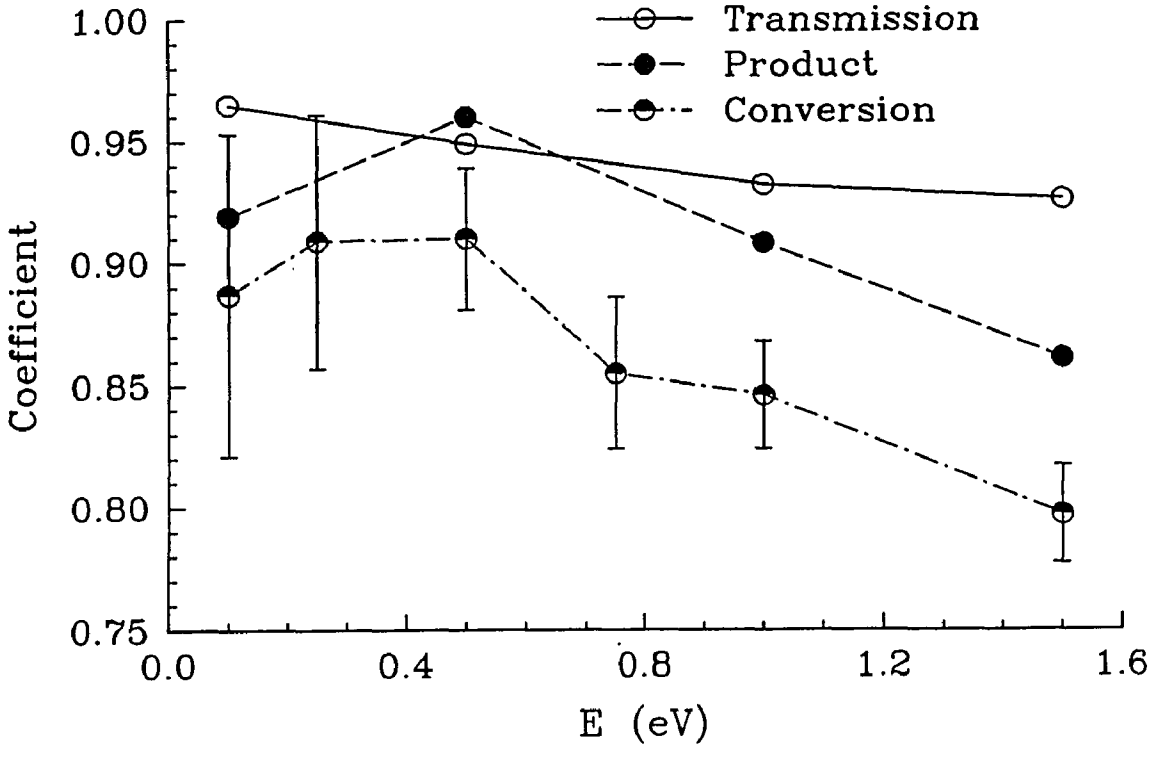

Fig. 64 shows how contributions to the variational mean reaction cross section for 18 equal θ intervals depend on θ for a reaction energy of 0.5 eV. The θ range from 0 to $\pi/2$ was divided into 5 deg. intervals. The contribution for each interval was doubled to obtain the contribution for reaction at both ends of the H_2 molecule. Results are shown for four dividing surfaces: truncated (TR) unrestricted, linear combination of internal coordinates (LCIC) unrestricted, quadratic slope (Q(S)) restriction, and quadratic unrestricted (Q(N)); values of the corresponding mean reaction cross sections are 20.03, 14.15, 13.11, and 12.96. The angular distributions of the mean reaction cross section should be plotted as histograms; however, for the sake of clarity, the incremental contributions are plotted as points centered on each 5 deg. interval. The angular distribution of reactivity for the TR DS differs markedly from that for the Q DSs over most of the θ range. The distribution for the LCIC DS is markedly different from the Q DS distributions for the θ range from 0 to 45 deg.. The distributions for the two Q DSs are in good agreement.

Fig. 65 shows angular distributions of reactivity for the Q(N) DS for energies of 0.1, 0.5, 1.0, and 1.5 eV. Fig. 66 shows angular distributions of reactivity for the canonical rate constant at 300, 1500, and 3000 K for the Q(S) DS. The intervals for the maximum contribution to $<S_r(E)>^{VT}$ for energies 0.1, 0.5, and 1.0 eV are centered on 17.5, 32.5, and 37.5 deg., respectively. The intervals for the maximum contribution to k(T) for temperatures of 300, 1500, and 3000 K are also centered at 17.5, 32.5, and 37.5 deg., respectively. We chose to study the accuracy of the variational theory by comparing variational and trajectory values of mean reaction cross sections for the reason explained earlier. Comparison of the reactivity distributions shown in Figs. 65 and 66 suggests that the accuracy of canonical rate constants at 300, 1500, and 3000 K will be comparable to the accuracy of mean reaction cross sections at 0.1, 0.5, and 1.0 eV; the accuracies of the latter values for the Q(N) DS expressed as the percentage difference between variational and

FIGURE 64

Plots of energy dependent variational angular reactivity distributions for the truncated (TR) unrestricted, linear combination of internal coordinates (LCIC) unrestricted, quadratic unrestricted Q(N) and slope restriction Q(S) dividing surfaces (DS) for energy 0.5 eV.

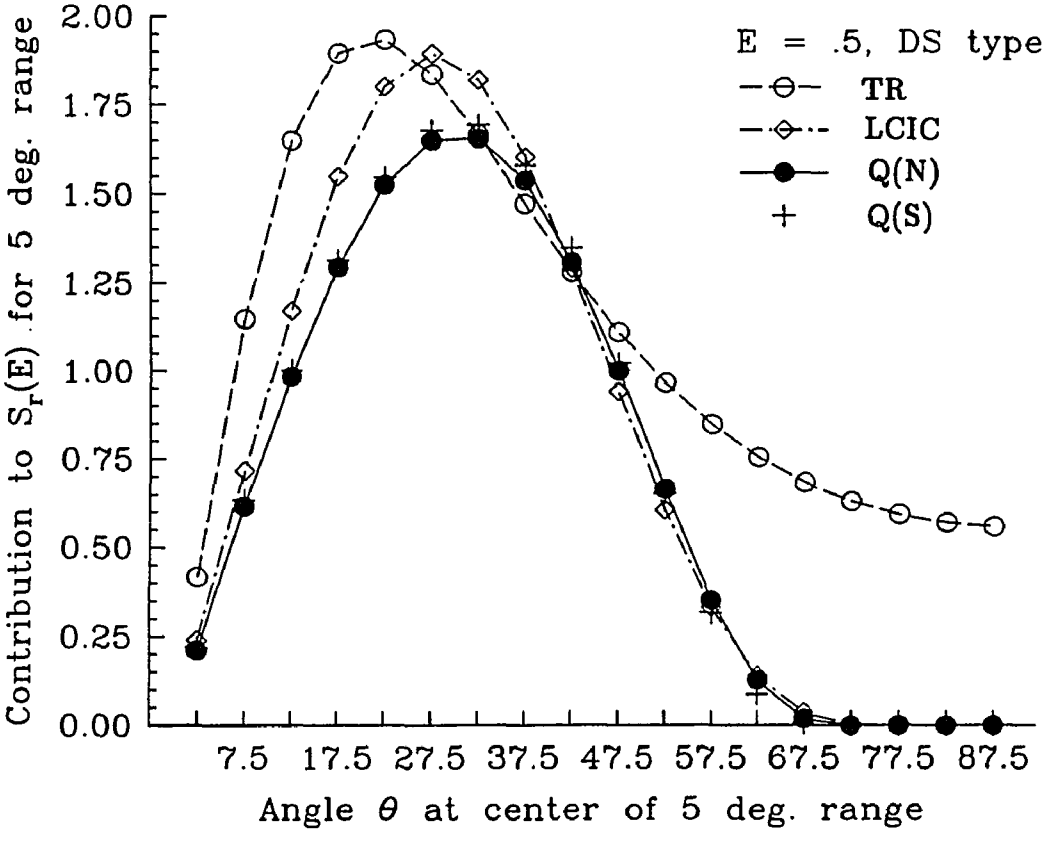

FIGURE 65

Plots of energy dependent variational angular reactivity distributions for quadratic unrestricted dividing surface for energies 0.1, 0.5, 1.0, and 1.5 eV.

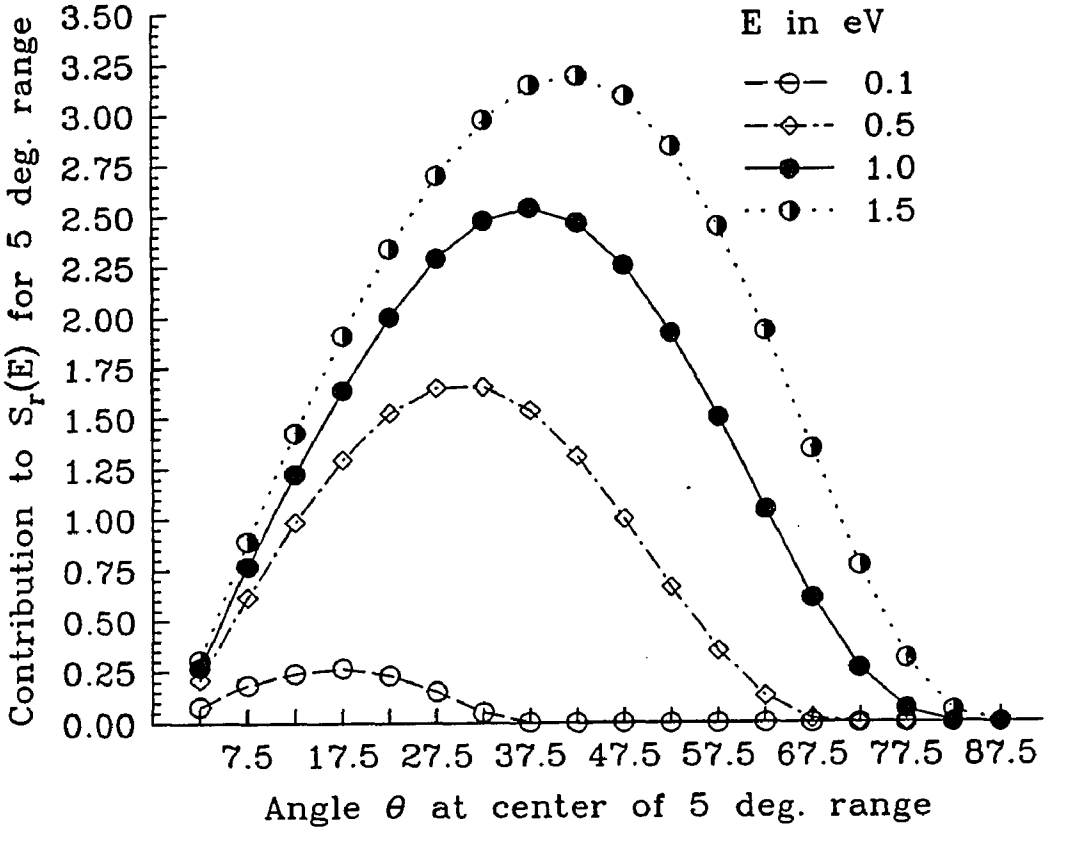

FIGURE 66

Plots of canonical variational angular reactivity distributions for temperatures of 300, 1500, and 3000 K for the quadratic slope restriction dividing surface.

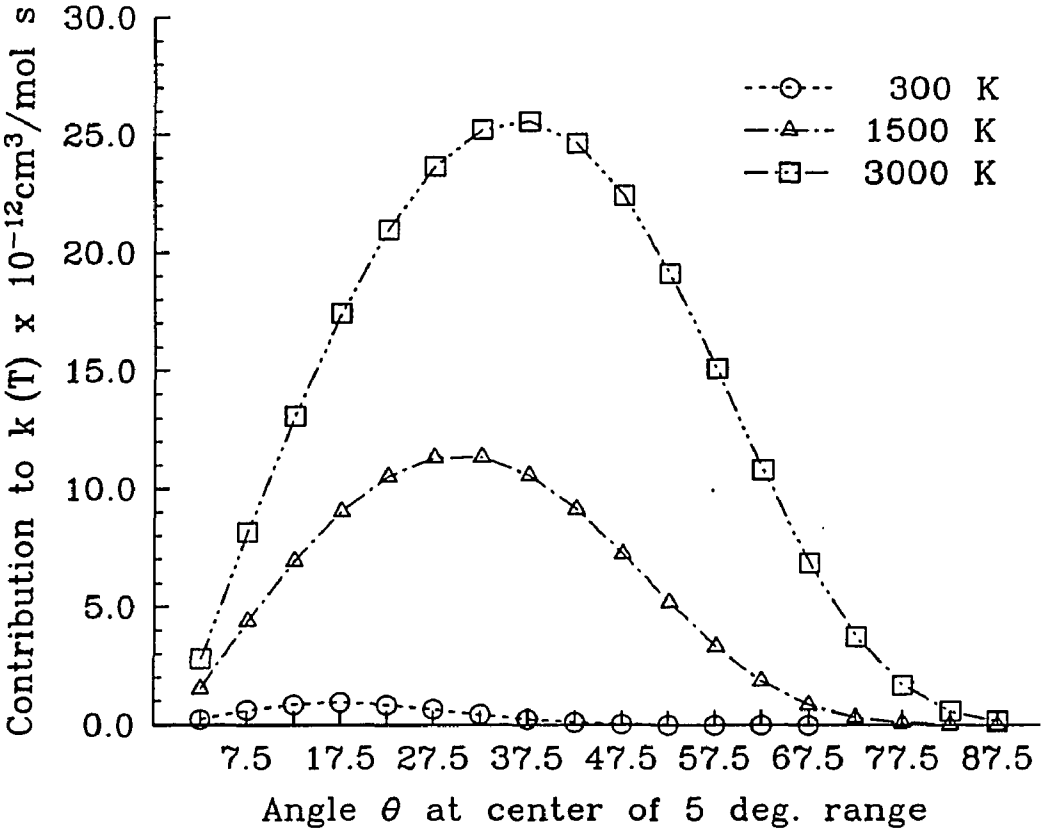

trajectory values are 12.0, 9.0, and 18.2 percent, respectively.

The accuracy of the no–recrossing assumption of transition state theory for collinear atom–diatom reactions has been the subject of many studies[33,87,99–104]. The application of a DS formulation which includes terms in θ makes it possible to determine how the accuracy of the no–recrossing assumption depends on the orientation angle. Figs. 67, 68, 69, and 70 show angular distributions of reactivity for both variational and trajectory theories for energies 0.1, 0.5, 1.0, and 1.5 eV. The variational distributions correspond to the Q(N) DS. The distributions labeled "Reactant ‡" correspond to all reaction systems on the DS for trajectories which originate in the reactant region and are moving toward the products at the DS. The sum of contributions for this distribution is $\langle S_r(E)\rangle^{R\ddagger}$. The ratio of contributions for the trajectory and "Reactant ‡" distributions for a given interval corresponds to $\kappa(E)$ for this interval. The ratio of contributions for the "Reactant ‡" and variational distributions for a given interval correspond to $\rho(E)$ for this interval. The distributions of Figs. 67, 69, and 70 for energies 0.1, 1.0, and 1.5 eV clearly show that the factors $\kappa(E)$, $\rho(E)$, and their product $\chi(E)$ for 5 deg. θ intervals are the lowest, indicating the largest deviations from the variational theory value of $\langle S_r(E)\rangle$ for the interval, for intermediate values of θ. The accuracy of the no–recrossing assumption is lowest for intermediate values of θ. Furthermore, $\kappa(E)$ is clearly greater then $\rho(E)$ for intermediate values of θ. For collinear atom–diatom reactions, the correction factors decline more rapidly with increasing energy than for reaction in 3–dimensional space. On this basis, one expects deviations from the variational flux, i. e., small correction factors, to be skewed toward low values of θ. Only the distribution at the lowest energy, 0.1 eV, appears to be skewed in this sense toward low values of θ.

Fig. 71 shows variational and trajectory angular distributions of reactivity at 0.5 eV for the quadratic energy limit (Q(E)) $\sin^2\theta$ DS. The energy limit restriction

FIGURE 67

Plots of trajectory and variational angular reactivity distribtions for unrestricted quadratic dividing surface for energy 0.1 eV.

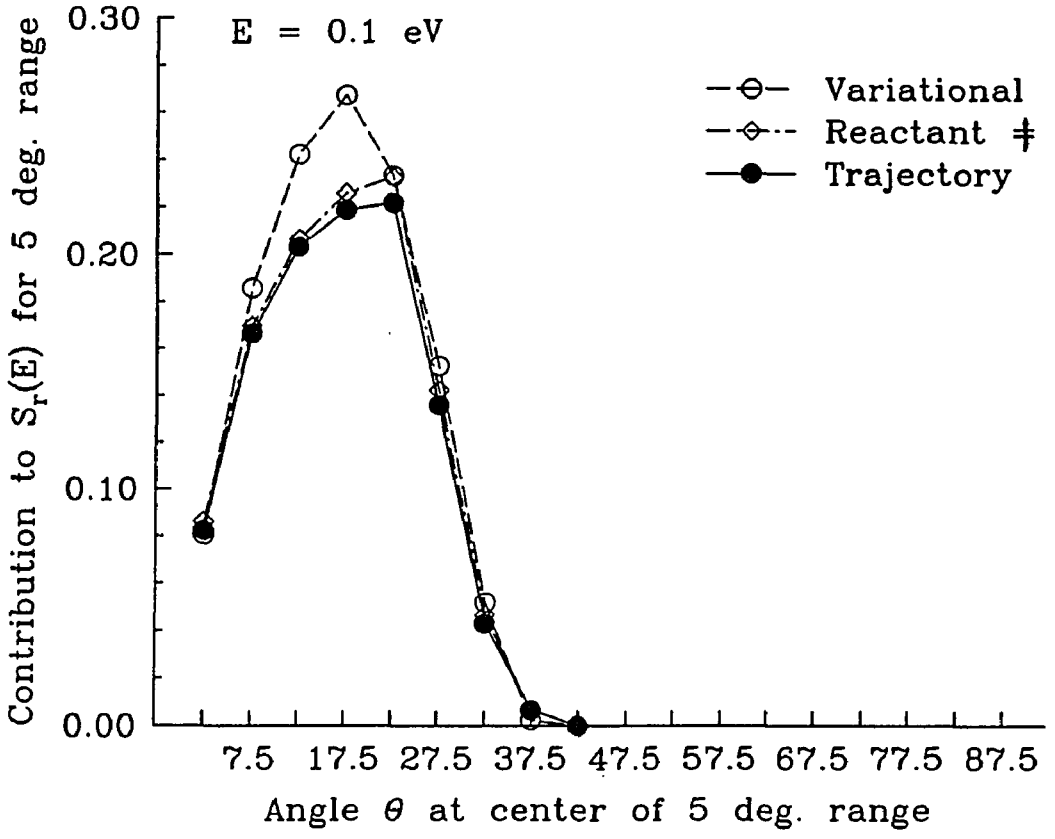

FIGURE 68

Plots of trajectory and variational angular reactivity distributions for unrestricted quadratic dividing surface for energy 0.5 eV.

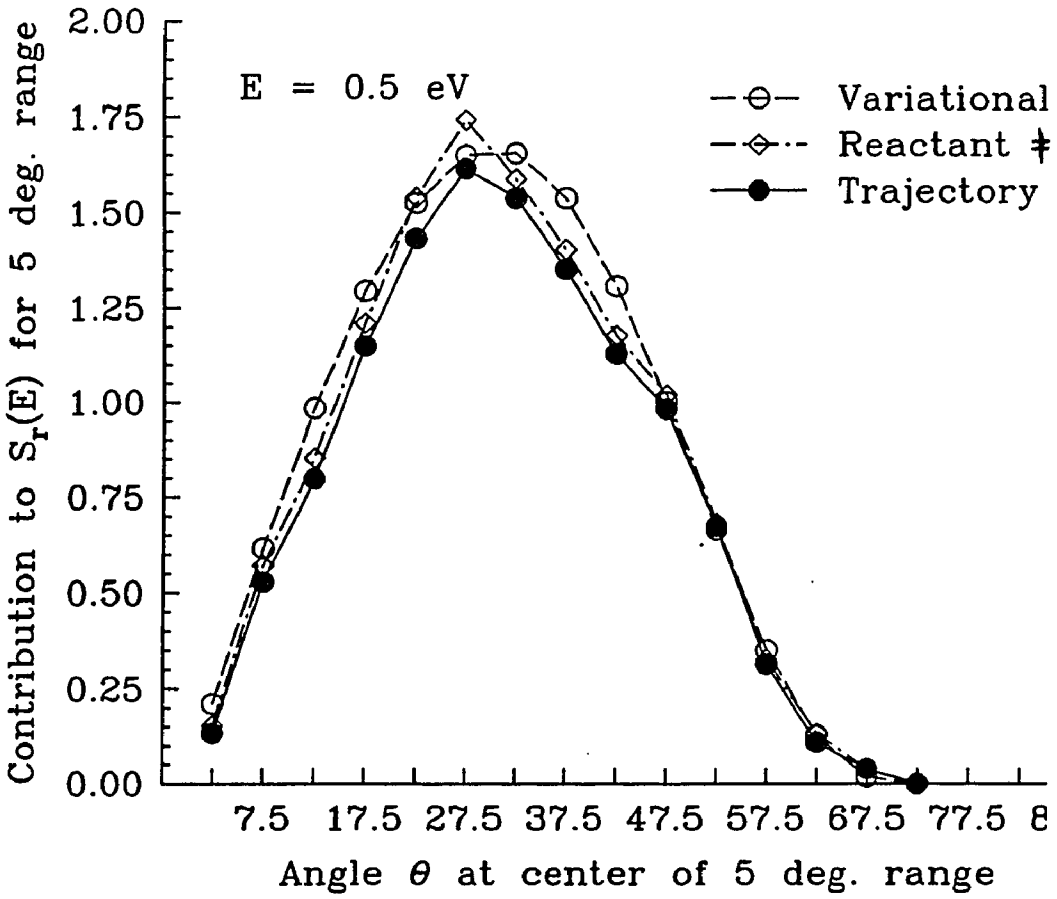

FIGURE 69

Plots of trajectory and variational angular reactivity distributions for unrestricted quadratic dividing surface for energy 1.0 eV.

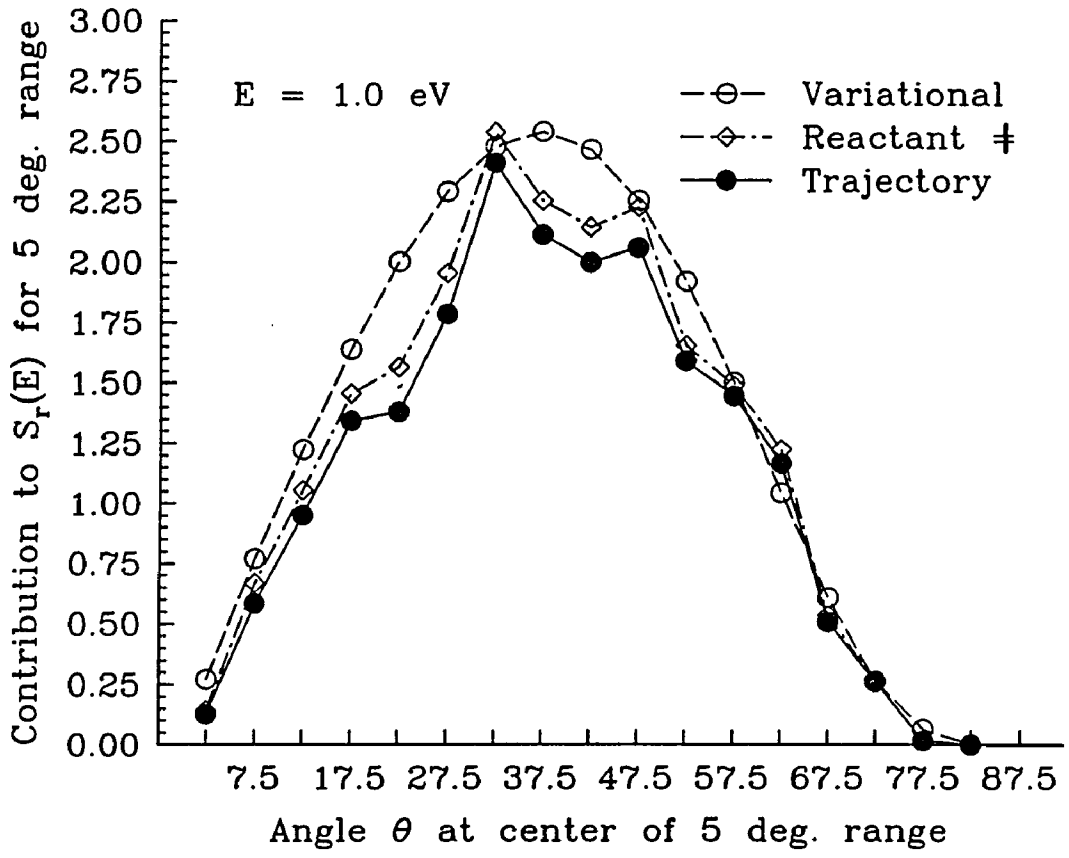

FIGURE 70

Plots of trajectory and variational angular reactivity distributions for unrestricted quadratic dividing surface for energy 1.5 eV.

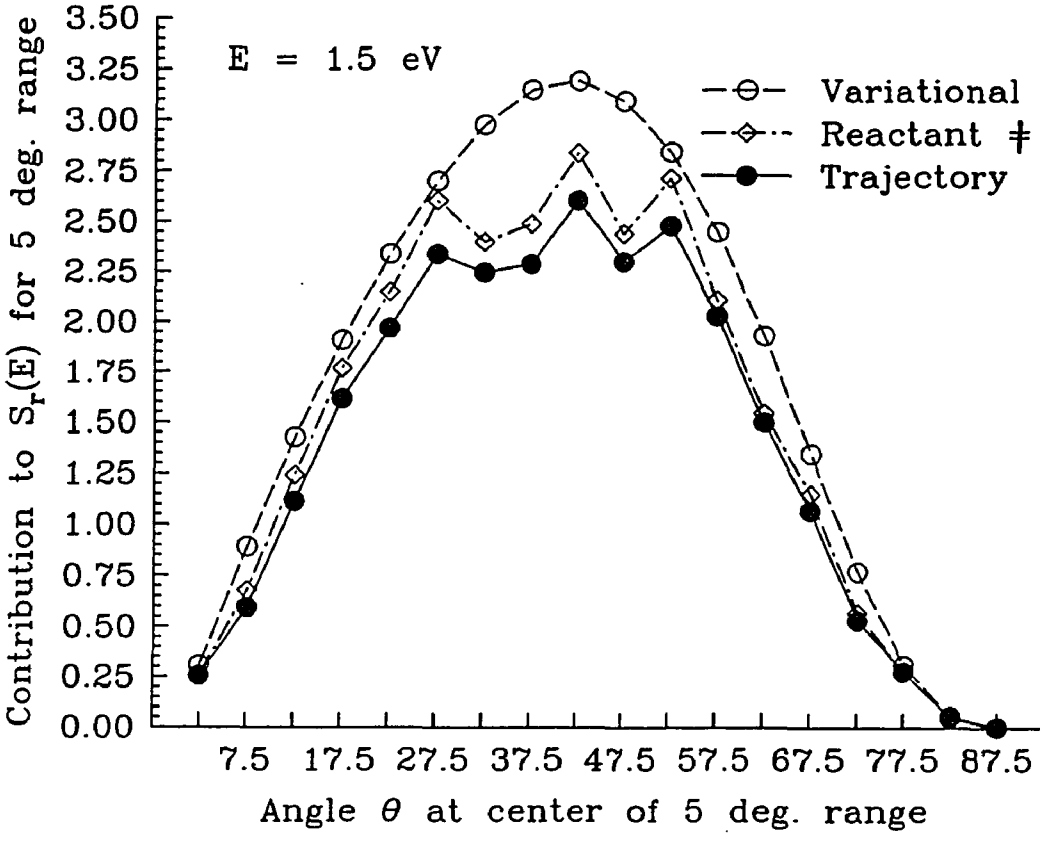

FIGURE 71

Plots of trajectory and variational angular reactivity distributions for unrestricted quadratic $\sin^2\theta$ dividing surface for energy 0.5 eV.

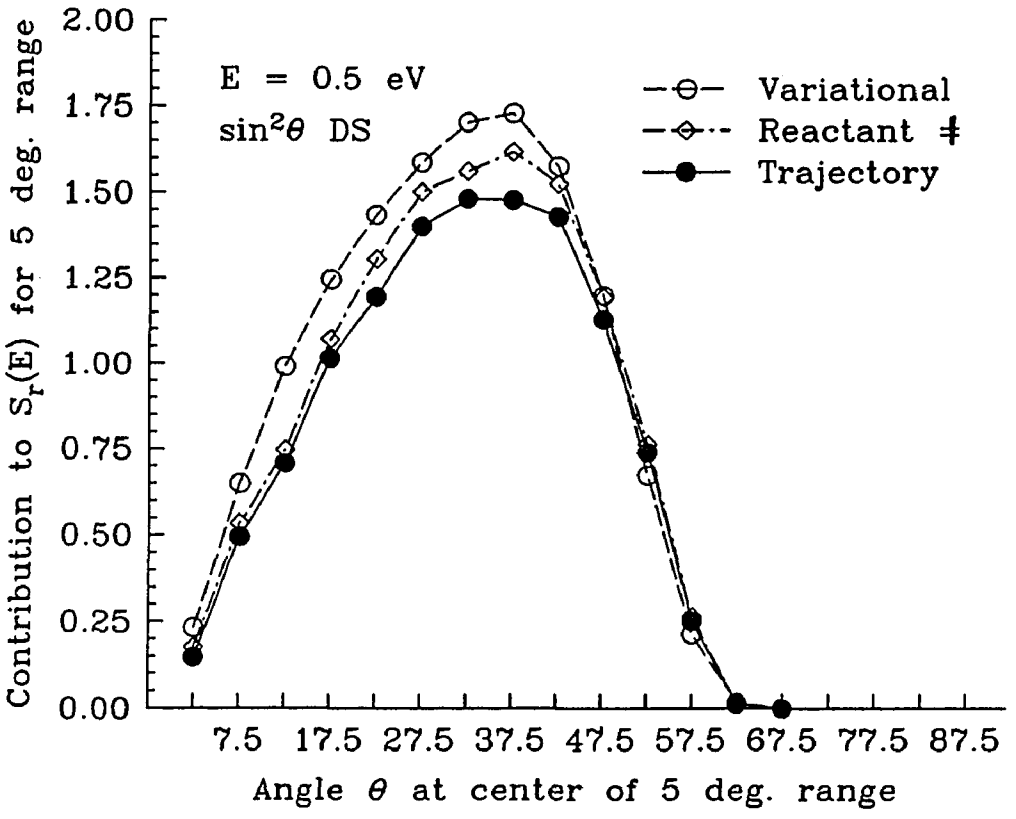

corresponds to 4.0 eV, rather than the energy for the microcanonical ensemble. This means that the potential energy at the end of the integration over R for fixed θ must be at least 4.0 eV; this condition must be satisfied for $0 < \theta < \pi$. This restriction does limit the flexibility of the DS. The values of the mean reaction cross section for this Q(E) DS and the Q(S) DS are 13.25 and 13.17 a. u., respectively. The variational theory distribution is very similar to that for the Q(N) linear θ distribution. The values of $<S_r(E)>^{CMT}$, $<S_r(E)>^{R\ddagger}$, and $<S_r(E)>^{VT}$ are 11.48$\pm$.37, 12.28$\pm$.39, and 13.25 a. u.; hence $\kappa = 0.935$, $\rho = 0.920$, and $\chi = 0.860$. The corresponding values of κ, ρ, and χ for the Q(N) linear θ DS are not markedly different; these values are 0.949, 0.960, and 0.910, respectively. The deviation of the trajectory distribution from the variational theory distribution appears to be skewed slightly toward low values of θ.

II. RESULTS FOR THE F + DH → FD(FH) + H(D) REACTIONS

Variational searches were performed for these reactions using the quadratic slope (Q(S)) restriction DS to obtain mean reaction cross sections at energies 0.1, .25, .5, and 1.0 eV. This formulation of the dividing surface is identical to the one used to study the F + H_2 reaction; however, the DS must now minimize the variational flux at each end of the heteronuclear reactant. The integration over θ to obtain the flux through the DS spans the range 0 to π. Since atoms B and C correspond to D and H, the collinear arrangements D–H–F and F–D–H correspond to θ values of 0 and π. The mean reaction cross sections are given in Table 16. The corresponding angular distributions of reactivity are shown in Fig. 72.

The canonical variational angular distributions of reactivity for temperatures of 300, 600, 1500, and 3000 K for the same DS are shown in Fig. 73. The canonical angular distributions for 300, 1500, and 3000 K resemble the microcanonical distributions for 0.1, 0.5, and 1.0 eV, respectively. The peaks for D–H–F and

TABLE 16

Comparison of total classical mechanical trajectory (CMT) and variational theory (VT) mean reaction cross sections for the F + DH → FD(FH) + H(D) reactions (total cross sections for the products of both reactions)

E	$\langle S_r(E) \rangle^{VT}$ quadratic $dr/dR > 0$	$\langle S_r(E) \rangle^{VT}$ 5–parameter unrestricted	$\langle S_r(E) \rangle^{CMT}$
(eV)	(a. u.)	(a. u.)	(a. u.)
0.10	1.358		
0.25	6.983		
0.50	15.862	15.390	11.63
1.0	29.02	26.17	20.01

FIGURE 72

Plots of energy dependent variational angular reactivity distributions for the F + DH reactions for the quadratic slope restriction dividing surface for energies 0.1, 0.25, 0.5, and 1.0 eV.

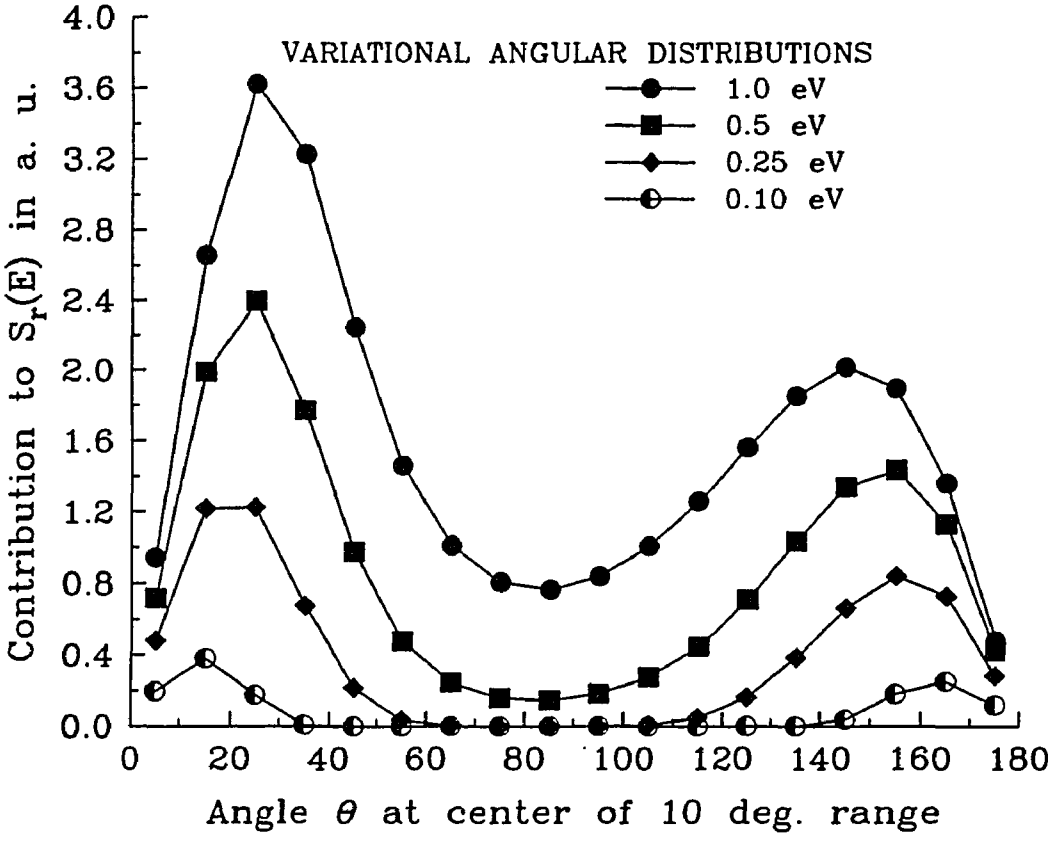

FIGURE 73

Plots of canonical variational angular reactivity distributions for the F + DH reactions for the quadratic slope restriction dividing surface for temperatures of 300, 600, 1500, and 3000 K.

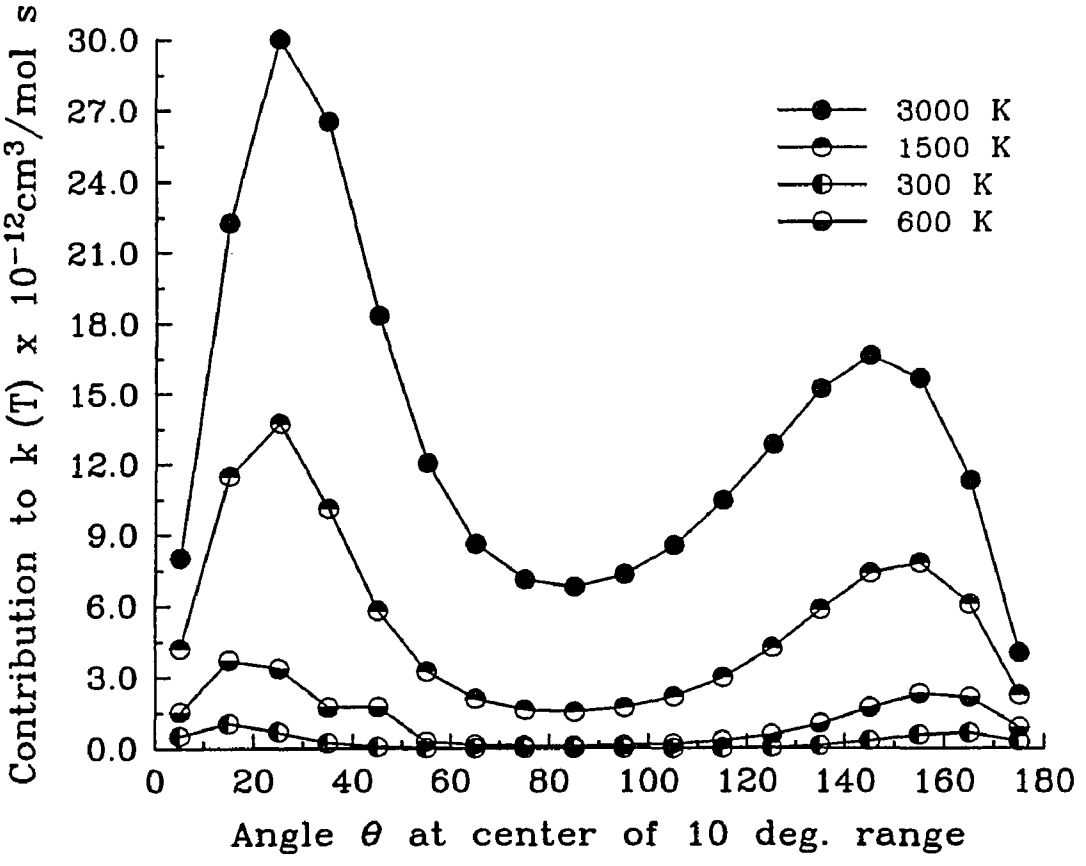

F–D–H configurations on the DS, at low and high θ, respectively, occur at approximately the same values of θ for these temperatures and corresponding energies.

Figs. 74 and 75 show angular distributions of reactivity for both variational and trajectory theories for the Q(S) DS at energies 0.5 and 1.0 eV. Note that it is impossible to obtain variational values of the mean reaction cross section for reaction at each end of DH, i. e., D + HF products for reaction at the H end near $\theta = 0$ and FD + H products for reaction at the D end near $\theta = \pi$ because the flux through the DS does not fall to zero for intermediate values of θ for energies of 0.5 and 1.0 eV. See the discussion of the requirement for obtaining practical variational values of the canonical rate constant for reaction at each end of a heteronuclear reactant in Ch. 4. The Q(S) DS for energies of 0.5 and 1.0 eV does not span high energy regions near the saddlepont of energy 2.31 eV at 81.5 deg. Figs. 76, 77, and 78 show intersections of Q(S) DSs for energies 0.5 and 1.0 eV with the r – R coordinate plane at orientation angles of 60, 81.5, and 120 deg., respectively. Neither DS spans high energy regions near angle dependent saddlepoints of the potential energy function near $\theta = 81.5$ deg.. Fig. 79 shows potential energy contours for the Q(S) DS at energy 0.5 eV. This figure shows that the 0.5 eV potential energy contours span the entire θ range ($0 < \theta < \pi$.)

Figs. 80 and 81 show variational angular distributions reactivity for the Q(S) and 5–parameter unrestricted DSs at energies 0.5 and 1.0 eV. Note that the distributions for the 5–parameter DS, which contains parameters which distinguish between reaction at each end of DH, plunge to zero flux near 81.5 deg. for both energies. Figs. 82, 83, and 84 show intersections of the 5–parameter DSs for energies of 0.5 and 1.0 eV with the r – R coordinate plane at orientation angles of 60, 81.5, and 120 deg., respectively. Note that only the DS for energy 1.0 eV appears in Fig. 82. For Figs. 82 and 84, the intersection of the DS with the r – R plane is plotted

FIGURE 74

Plots of energy dependent trajectory and variational angular reactivity distributions for the quadratic slope restriction dividing surface for energy 0.5 eV.

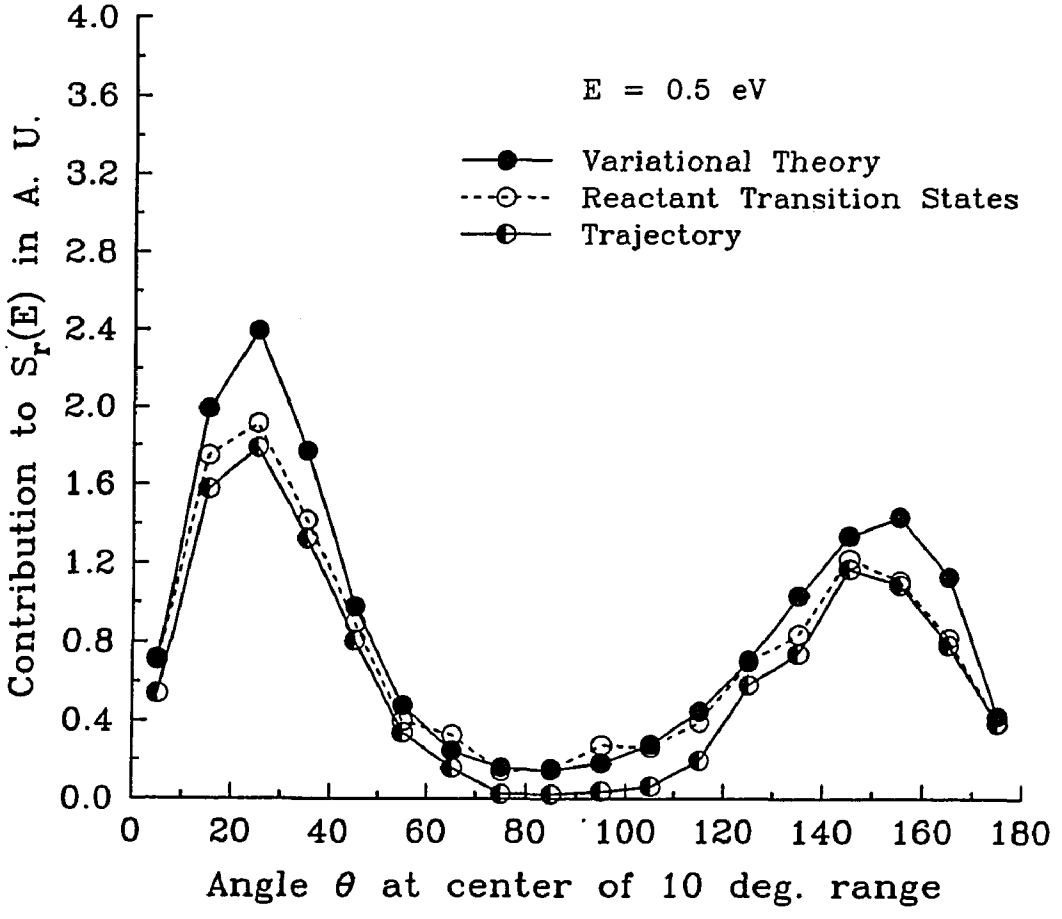

FIGURE 75

Plots of energy dependent trajectory and variational angular reactivity distributions for the quadratic slope restriction dividing surface for energy 1.0 eV.

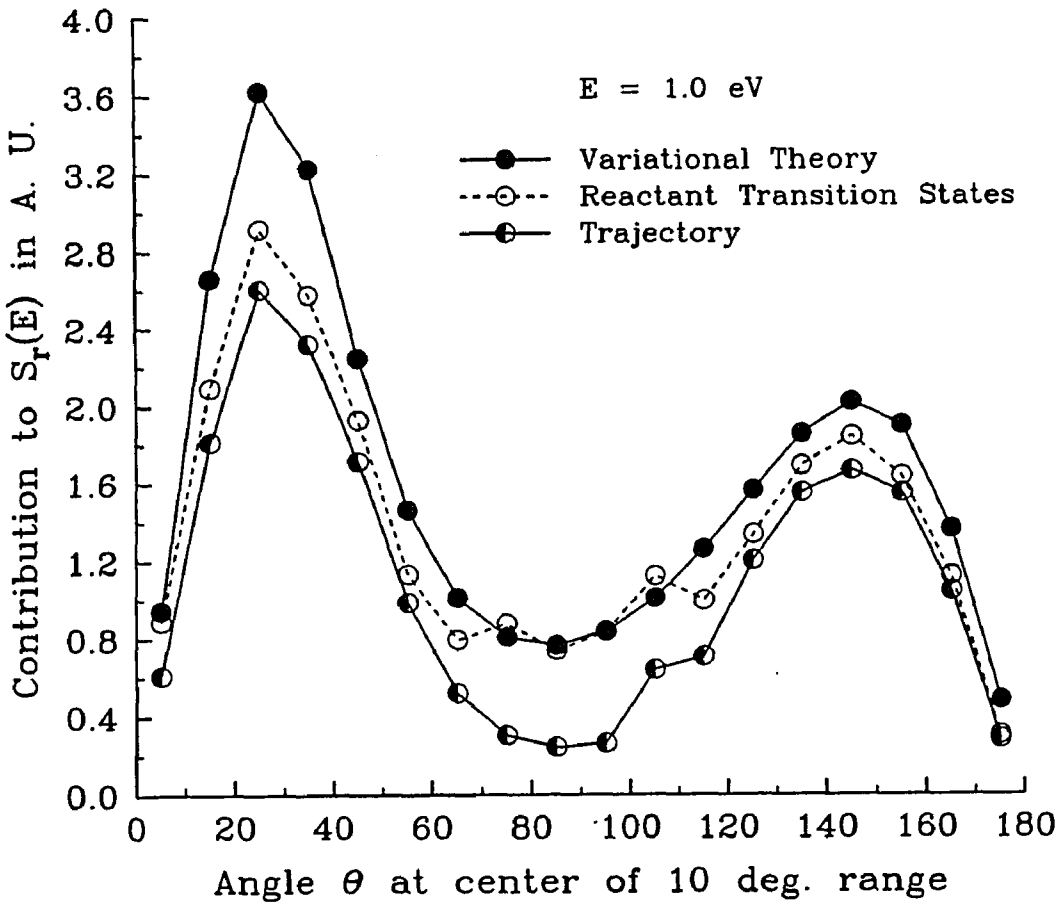

FIGURE 76

Potential energy contour map for $\theta = 60$ deg.. Intersections of energy dependent quadratic slope restriction dividing surfaces for 0.5 and 1.0 eV with the r – R plane are shown where the potential energy on the dividing surface is less than the microcanonical energy for the dividing surface.

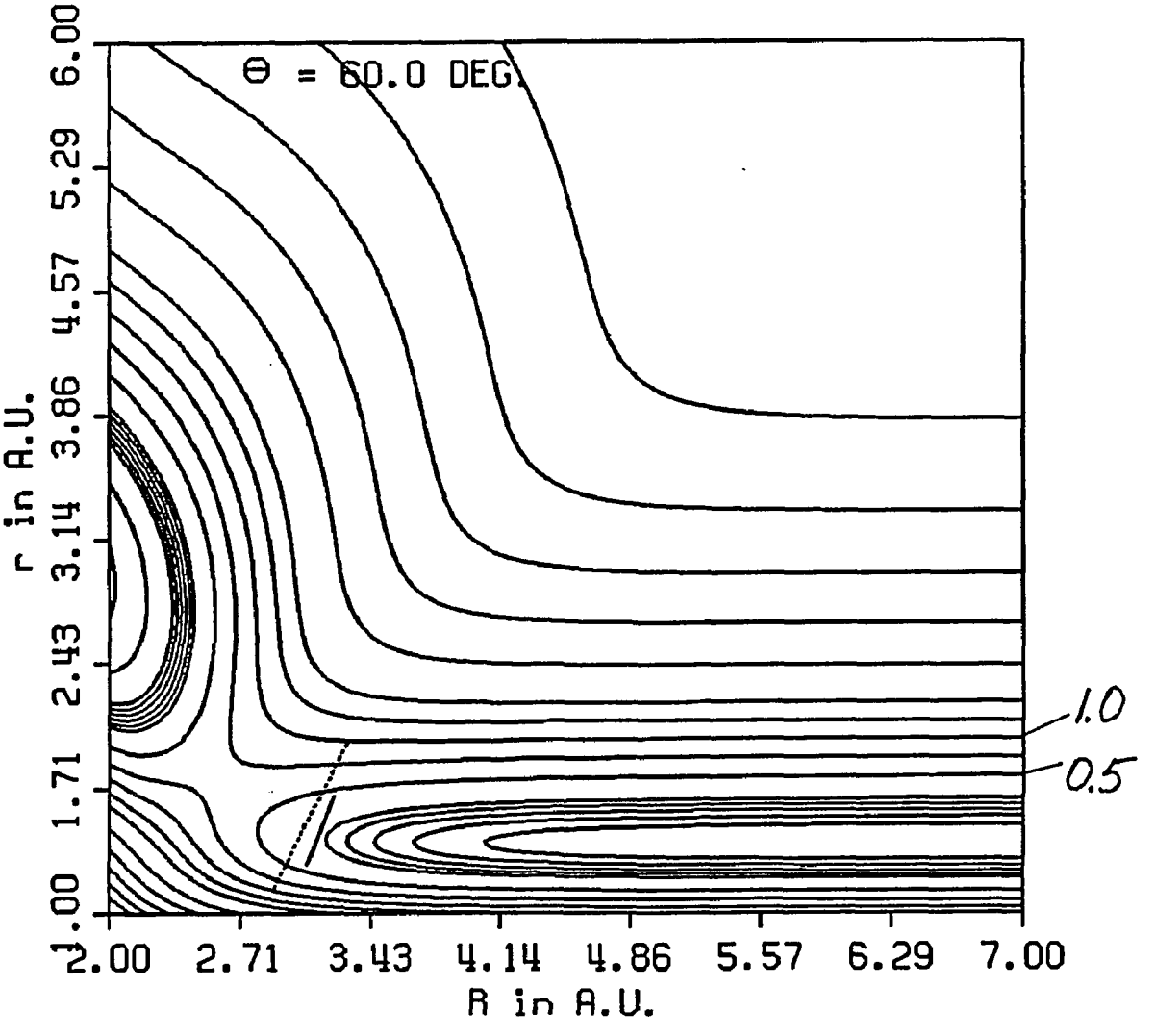

FIGURE 77

Potential energy contour map for $\theta = 81.5$ deg.. Intersections of energy dependent quadratic slope restriction dividing surfaces for 0.5 and 1.0 eV with the r – R plane are shown where the potential energy on the dividing surface is less than the microcanonical energy for the dividing surface.

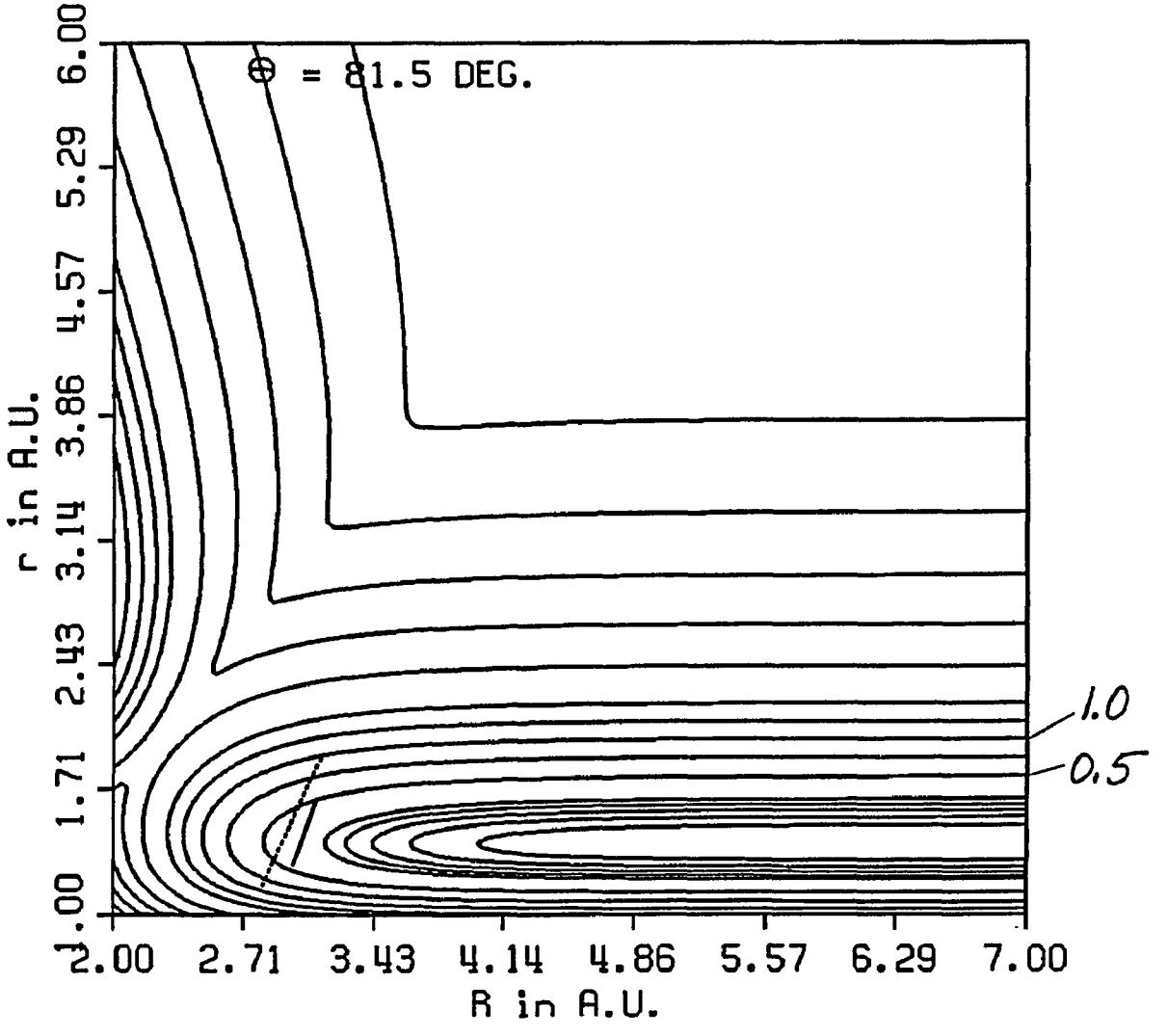

FIGURE 78

Potential energy contour map for $\theta = 120$ deg.. Intersections of energy dependent quadratic slope restriction dividing surfaces for 0.5 and 1.0 eV with the r – R plane are shown where the potential energy on the dividing surface is less than the microcanonical energy for the dividing surface.

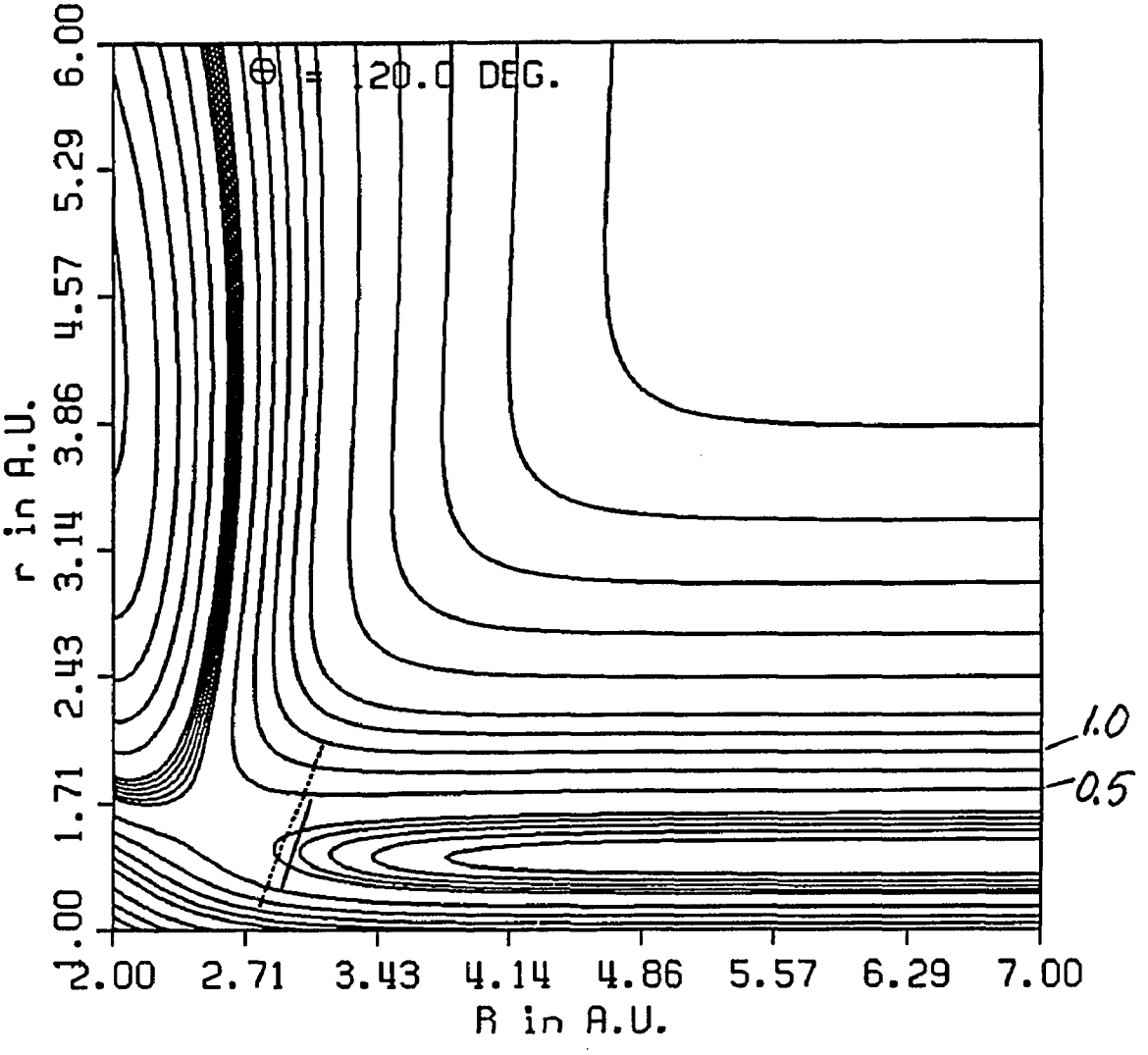

FIGURE 79

Potential energy contour map in polar coordinates for the energy dependent quadratic slope restriction dividing surface for energy 0.5 eV.

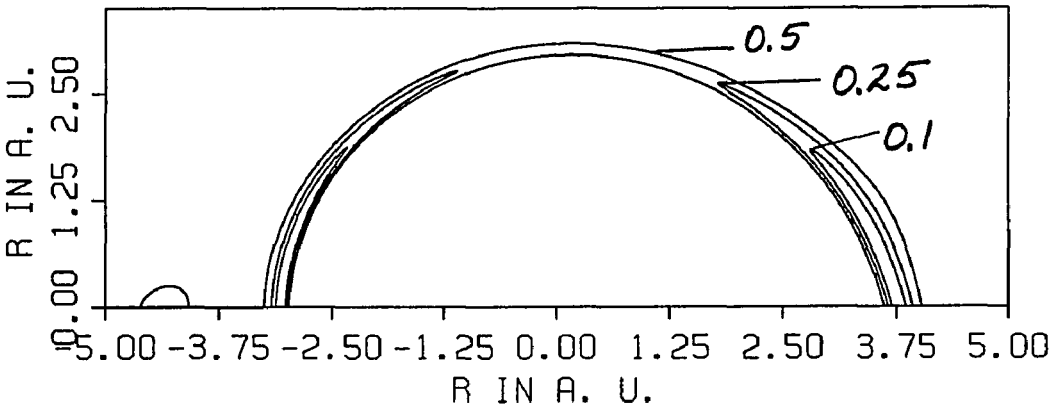

FIGURE 80

Plots of energy dependent variational angular reactivity distributions for the 6–parameter quadratic slope restriction (regular function) and 5–parameter (new function) dividing surfaces for energy 0.5 eV.

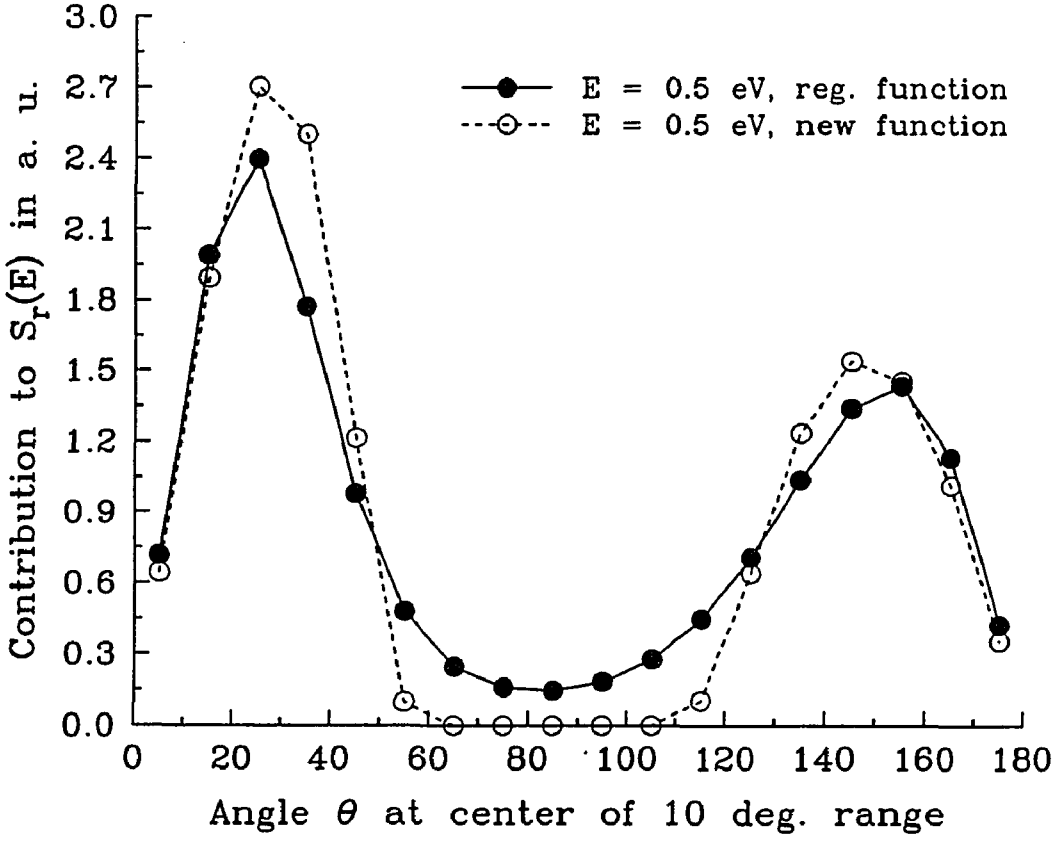

FIGURE 81

Plots of energy dependent variational angular reactivity distributions for the 6–parameter quadratic slope restriction (regular function) and 5–parameter (new function) dividing surfaces for energy 1.0 eV.

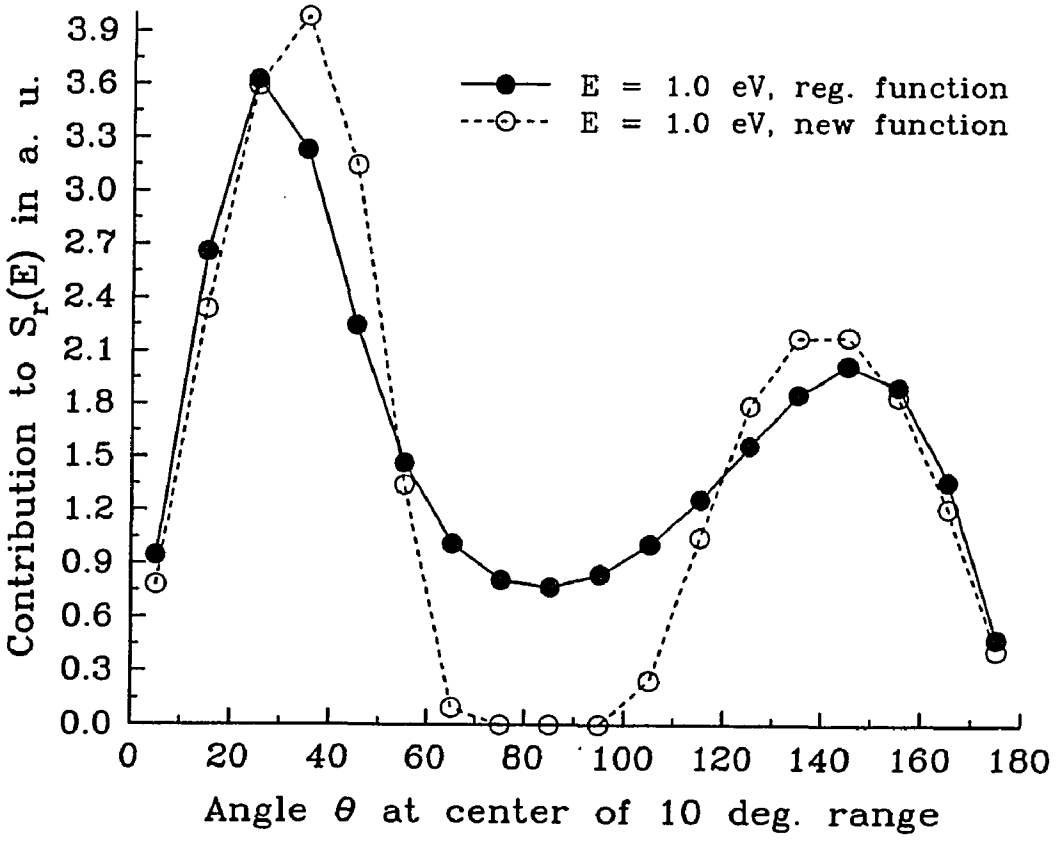

FIGURE 82

Potential energy contour map for $\theta = 60$ deg.. Intersections of energy dependent 5–parameter dividing surfaces for 0.5 and 1.0 eV with the r – R plane are shown where the potential energy on the dividing surface is less than the microcanonical energy for the dividing surface.

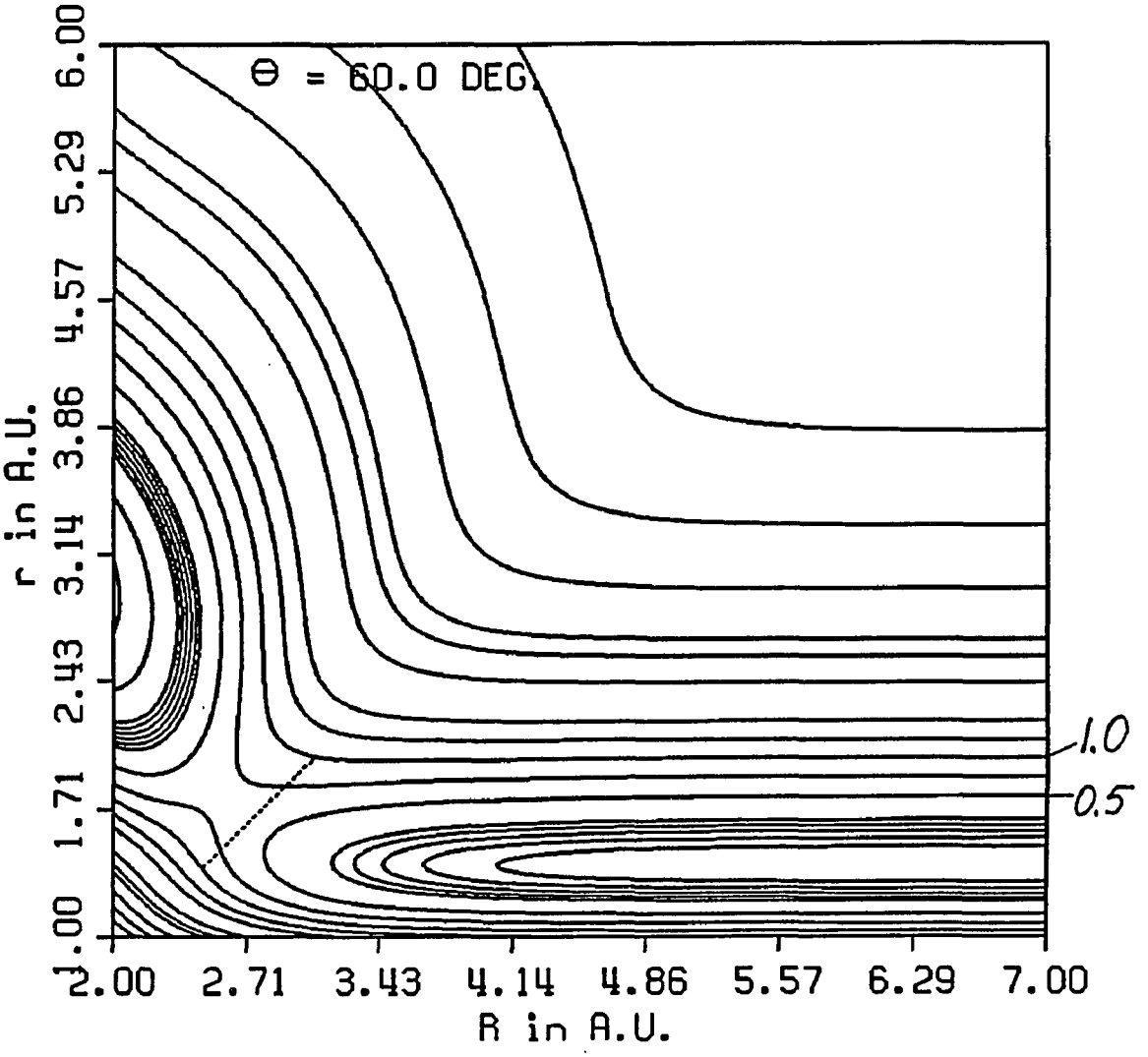

FIGURE 83

Potential energy contour map for $\theta = 81.5$ deg.. Intersections of energy dependent 5–parameter dividing surfaces for 0.5 and 1.0 eV with the r – R plane are shown where the potential energy on the dividing surface is less than 4.0 eV.

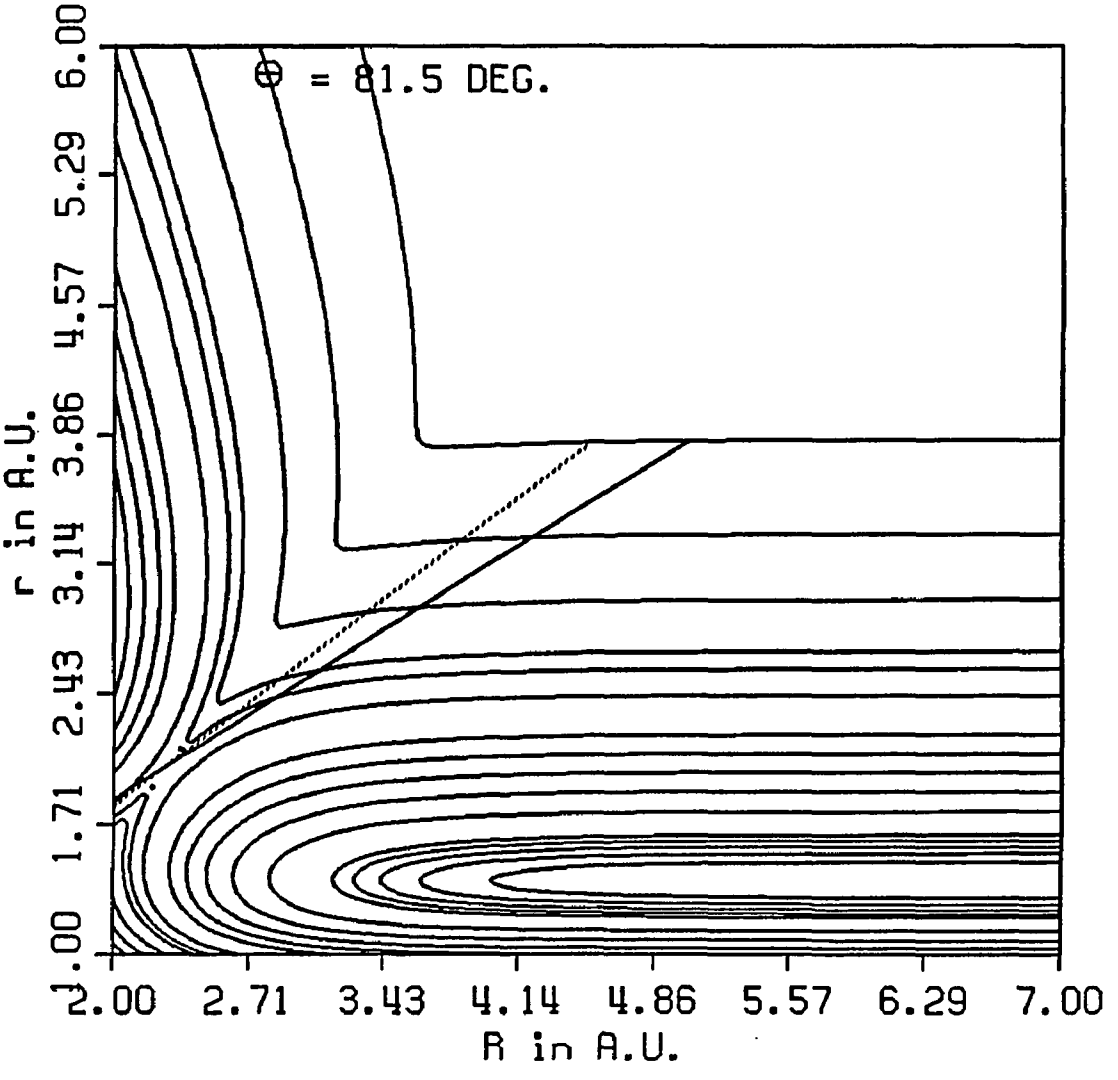

FIGURE 84

Potential energy contour map for $\theta = 120$ deg.. Intersections of energy dependent 5–parameter dividing surfaces for 0.5 and 1.0 eV with the r – R plane are shown where the potential energy on the dividing surface is less than the microcanonical energy for the dividing surface.

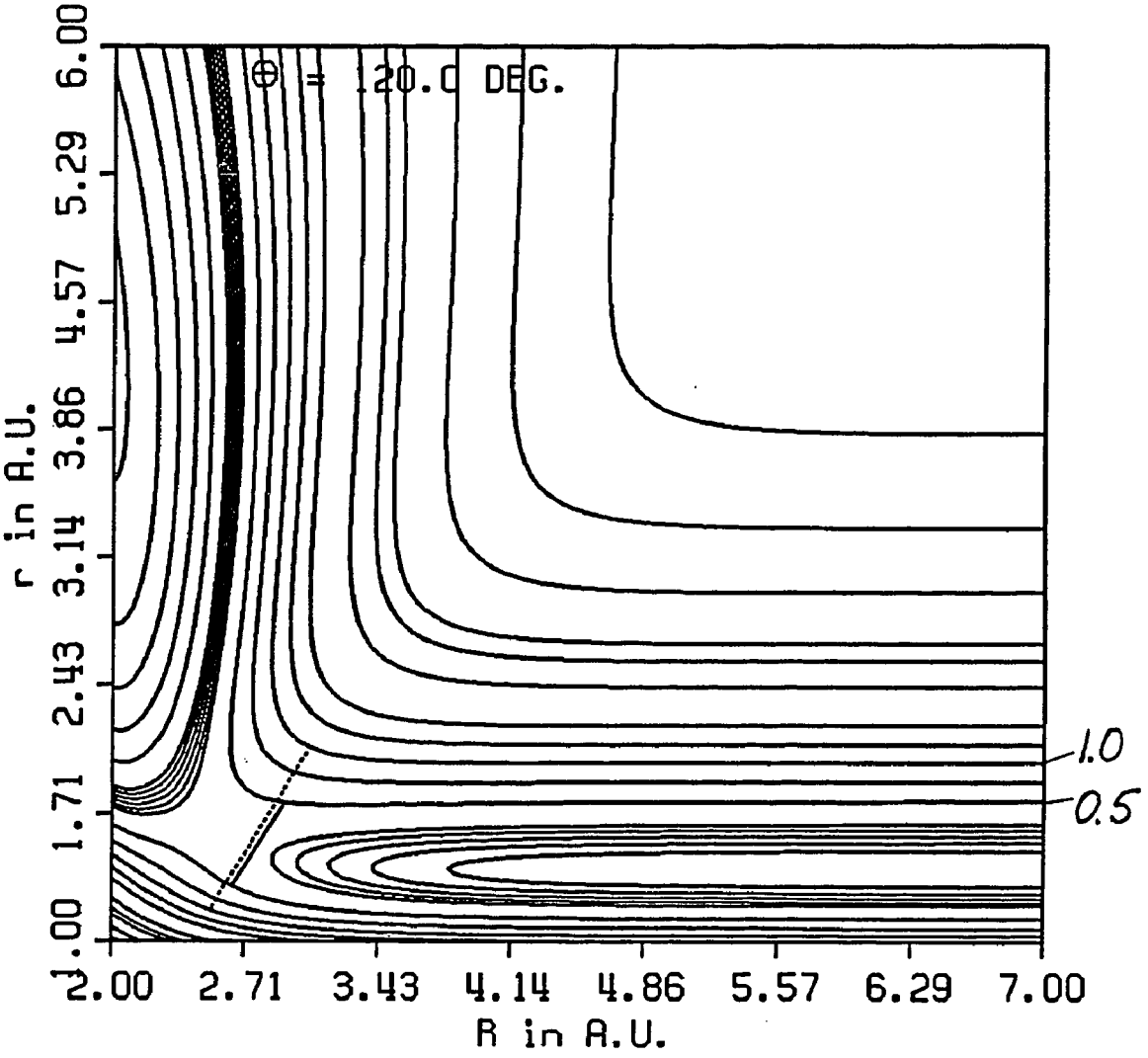

only when the potential energy is less than the specified microcanonical energy. The DS for 0.5 eV does not appear in Fig. 82 because the potential energy is higher than 0.5 eV for all points on the DS at $\theta = 60$ deg.. Both DSs appear in Fig. 84 for $\theta =$ 120 deg.. The DSs are plotted in a different way for $\theta = 81.5$ deg.. The DSs at this angle are plotted for all values of the potential energy up to 4.0 eV. If the DSs were only shown for values of the potential energy less that the microcanonical energies of 0.5 and 1.0 eV, no DSs would appear on this plot. Both DSs pass through the saddlepoint at 81.5 deg. as required. Fig. 85 shows potential energy contours for the 5–parameter unrestricted DS for energy 0.5 eV. The potential energy is greater than 0.5 eV over the θ range 58 to 110 deg.; the flux through the surface over this range is zero.

Results for variational Q(S) and 5–parameter DSs and trajectory mean reaction cross sections for energies 0.5 and 1.0 eV are summarized in Table 17. Variational theory correction coefficients for these DSs are summarized in Table 18. The total variational mean reaction cross sections for the 5–parameter DS are smaller than those for the 6–parameter Q(S) DS: 15.39 versus 15.86 a. u. at 0.5 eV and 26.17 versus 29.03 a. u. at 1.0 eV; total refers to the cross section for the formation of both products (D +HF and FD + H). The latter DS contains quadratic terms in R and θ; however it does not contain parameters which distinguish formally between reaction at each end of the heteronuclear reactant. Furthermore this DS is not forced to pass through the saddlepoint at 81.5 deg. and the flux at intermediate values of θ is not minimized effectively. Because the flux does not fall to zero at intermediate values of θ, it is impossible to divide the variational flux to obtain mean reaction cross sections for reaction at each end of DH to compare with trajectory values.

Variational theory correction coefficients for energies of 0.5 and 1.0 eV are summarized in Table 18. Trajectories were used to calculate the quantity

TABLE 17

Comparison of classical mechanical trajectory (CMT) and variational theory (VT) mean reaction cross sections for the F + DH → FD(FH) + H(D) reactions

Results for quadratic (6–parameter) $dr/dR > 0$ DS function for $0 < \theta < \pi$			
E (eV)	$\langle S_r(E)\rangle^{CMT}$ (a. u.)	$\langle S_r(E)\rangle^{R\neq}$ (a. u.)	$\langle S_r(E)\rangle^{VT}$ (a. u.)
0.50	11.63 (FH+FD) 6.58 (FH) 5.05 (FD)	13.71 (FH+FD)	15.86 (FH+FD)
1.0	20.01 (FH+FD) 10.89 (FH) 9.11 (FD)	24.81 (FH+FD)	29.03 (FH+FD)
Results for 5–parameter unrestricted DS function			
E (eV)	$\langle S_r(E)\rangle^{CMT}$ (a. u.)		$\langle S_r(E)\rangle^{VT}$ (a. u.)
0.50	11.63 (FH+FD) 6.58 (FH) 5.05 (FD)		15.39 (FH+FD) 9.05 (FH) 6.38 (FD)
1.0	20.01 (FH+FD) 10.89 (FH) 9.11 (FD)		26.17 (FH+FD) 15.26 (FH) 10.91 (FD)

TABLE 18

Variational theory correction coefficients for the

F + DH → FD(FH) + H(D) reactions

Results for quadratic (6–parameter) dr/dR > 0 DS function for $0 < \theta < \pi$			
E (eV)	κ(E) FH + FD	ρ(E) FH + FD	χ(E) FH + FD
0.50	0.848	0.864	0.733
1.0	0.806	0.855	0.689
Results for 5–parameter unrestricted DS function			
E (eV)	χ(E) FH + FD	χ(E) FH	χ(E) FD
0.5	0.756	0.727	0.797
1.0	0.764	0.714	0.835

κ(E) – transmission coefficient

ρ(E) – product coefficient

χ(E) – conversion coefficient

FIGURE 85

Potential energy contour map in polar coordinates for the energy dependent 5–parameter dividing surface for energy 0.5 eV.

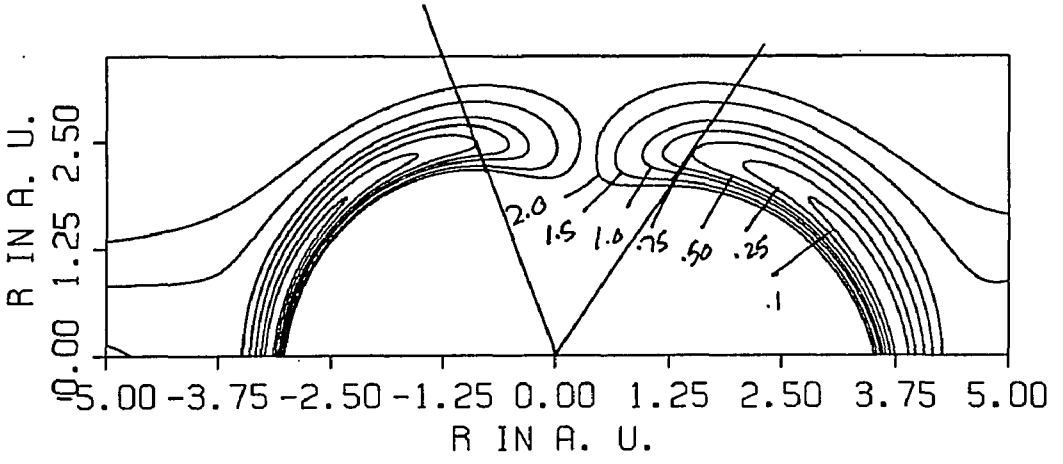

$<S_r(E)>^{R\ddagger}$ for the Q(S) DS, but this DS does not divide the flux into contributions for reaction at each end of DH. Hence the table gives total reaction values of $\kappa(E)$, $\rho(E)$, and $\chi(E)$. All three coefficients decrease when the energy increases from 0.5 to 1.0 eV as expected. The trajectory value of the mean reaction cross section is 26.7, and 31.1 percent smaller than the variational value at 0.5 and 1.0 eV, respectively. These percentages correspond to conversion coefficients of 0.733 and 0.689, respectively.

The 5–parameter DS does divide the flux into contributions for reaction at each end of DH, but trajectories were not used to evaluate the quantity $<S_r(E)>^{R\ddagger}$ for this DS. Hence, transmission and product coefficients cannot be calculated; however, conversion coefficients can be calculated for reaction at each end of DH. The total conversion coefficients for 0.5 and 1.0 eV, .756 and .764, respectively, are nearly equal. The trajectory total mean reaction cross sections are 24.4 and 23.6 percent smaller than the variational values at 0.5 and 1.0 ev, respectively. The conversion coefficient for FH + D decreases slightly and the conversion coefficient for FD + H increases slightly when the energy increases from 0.5 to 1.0 eV. The conversion coefficient for FH + D products is significantly smaller than for FD + H products at both energies: 0.727 versus 0.797 at 0.5 eV and 0.714 versus 0.835 at 1.0 eV. Yet the FH + D products are favored at both energies: the (FH + D)/(FD + H) trajectory cross section ratios are 1.30 and 1.20 at 0.5 and 1.0 eV, respectively. Trajectory and variational comparison studies are planned using the 5 and 10–parameter DS functions to characterize the angular variation of $\kappa(E)$ and $\rho(E)$ for both reactions and seek an explanation for the greater yields of FH + D products and more pronounced failure of the no–recrossing assumption at the H end of the DH reactant.

CHAPTER 6

SUMMARY AND CONCLUSIONS

Koeppl's formulation of the classical variational theory of reaction rates gives the rate as the equilibrium flux of reaction systems through a dividing surface in the configuration space of the reaction system. For atom – diatom reactions $A + BC \rightarrow AB(AC) + C(B)$, the dividing surface (DS) can be defined by a function of the internal coordinates which includes the orientation angle of reactants, that is, the angle between the internuclear axis of the diatomic reactant and a line from the center of mass of BC to the attacking atom.

The variational theory was applied to calculate canonical rate constants for the $F + H_2 \rightarrow FH + H$ reaction for three different potential energy surfaces (PES) at several temperatures. Two of the potential energy functions were introduced by others in an on–going effort to find a potential energy function which brings experimental and theoretical rate constants, and other dynamical properties, into agreement. The third was introduced by us to form a series of potential energy functions in which an important feature is varied in a systematic manner.

The potential energy may be expressed in terms of internal coordinates r, R, and θ where θ is the orientation angle defined above, r is the BC internuclear separation; and R is the distance between atom A and the center–of–mass of BC. Plots of potential energy contours in the reduced r – R space at fixed θ show a single saddle point for $0 < \theta < \pi$ for all of the functions. The value of the potential energy at the saddle point for a specified value of θ corresponds to the minimum potential energy for reaction at this value of θ. The barrier–orientation–angle profile shows a decreasing trend in the series of potential energy functions designated KR, T1, and T2, i. e., for the series KR → T1 → T2 the value of the potential energy at the angle

dependent saddle point for specified θ decreases over the entire range of θ ($0 < \theta < \pi$). We describe this behavior by saying that the "floppiness" of the potential energy function increases in the series KR → T1 → T2. Each of the potential energy functions represents a challenge for the variational theory because the value of R at the angle dependent saddle point varies markedly with θ. The DS must be able to span regions of configuration space near angle dependent saddle points where the potential energy is relatively high over the θ range where the reaction flux is relatively high. The DS must do this over the range in θ where the reaction flux is large in order to minimize the variational rate.

The downhill simplex algorithm was used to obtain variational values of the canonical rate constant at 300, 1500, and 3000 K for several formulations of the dividing surface for each of the three potential energy functions. The DS functions, in order of increasing flexibility, are designated truncated (TR), linear combination of internal coordinates (LCIC), quadratic (Q), and cubic (C). The TR DS function contains a linear R term and two variational parameters. The LCIC DS function contains linear terms in R and θ and three parameters. The Q DS function contains linear and quadratic terms in R and θ and six parameters. The C function contains linear, quadratic, and cubic terms in R and θ and 10 parameters.

For each potential energy function, the variational rate constant showed a decreasing (improving) trend with increasing flexibility of the DS. The largest improvement, i. e., decrease in rate constant, was obtained for the TR versus LCIC DS function. The TR DS function does not depend on θ and does a poor job of minimizing the reaction flux. When a reaction system is characterized by a floppy potential energy function and the value of R at the angle dependent saddle point varies markedly with θ, it is particularly important to include angle dependent terms in the formulation of the DS. The three potential energy functions used in the present work are all floppy in the sense that the angle dependent minimum

potential energy for reaction increases more gradually with θ than it does for other reaction systems which have been studied in similar detail, e. g., $H + H_2$. The LCIC versus TR and Q versus TR improvement in the variational rate increases for the potential energy function series KR → T1 → T2 at 300, 1500, and 3000 K. The improvement increases with increasing floppiness in the PES series because the ability of the DS to slant (LCIC) and curve (Q) toward the angle dependent saddle points where the potential energy is relatively high becomes increasingly important as the θ range over which the barrier is relatively low increases.

For the same DS formulation and temperature, the rate constant increases for the potential energy function series KR → T1 → T2. The barrier–angle profile falls over the entire θ range in this series. More reaction systems have enough energy to surmount the barrier over the entire θ range and the rate constant increases.

The LCIC versus Q DS improvement in the canonical rate constant is smaller than the LCIC versus TR improvement for the three potential energy functions. The C versus Q DS function improvement is relatively small. We concluded that the small improvement gained by using cubic formulations of DS was not worth the increased computational effort. We carried out a detailed study of the quadratic DS function which gives a rate constant which is close to the converged value.

The power series formulations of the dividing surface used in the present work (LCIC, Q and C) contain angle dependent terms. These terms make it possible to use the variational theory to characterize the dynamical sterochemistry of atom–diatom reactions in a new and useful way. This can be done by plotting contours of the variational flux through the angle dependent dividing surface. The variational flux can be displayed using contours which depend on internal coordinates θ and R; R is the distance between F and the center–of–mass of H_2. We call these plots reactivity relief maps. The dynamic stereochemistry can also be characterized by dividing the full range of orientation angle θ (0 to π) into equal

intervals and calculating the contribution to the canonical rate constant or energy dependent mean reaction cross section for each interval to show how this quantity varies with θ, i. e., show how the reactivity varies with the orientation angle. We used reactivity relief maps to study quadratic formulations of the DS and describe the dynamic stereochemistry of the F + H_2 reaction for the KR, T1, and T2 potential energy functions.

Variational searches for the Q DS function produced unusual results. Plots of intersections of the DS with the r – R coordinate plane for low values of θ showed that the DS curved toward the product valley and then abruptly back toward the reactant valley. These dividing surfaces did not proceed from a high energy region where the three nuclei are close to a low energy region where the reaction flux is large and then to a high energy region where the nuclei are far apart; they did not appear to divide configuration space into reactant and product regions in a way that would minimize the variational flux. Plots of reactivity relief maps showed "islands" of flux at large R near the reactant valley which represented superfluous contributions to the reactive flux. Attempts were made to find acceptable dividing surfaces by imposing restrictions on variational parameters during simplex searches. Restricted DS functions were obtained using the conditions: $\partial^2 r/\partial R^2 > 0$ (second derivative restriction); $\partial r/\partial R > 0$ for $0 < \theta < \pi/2$ (slope restriction); potential energy $V(r^*,R,\theta) > 4.0$ eV at R_{max} for $0 < \theta < \pi/2$ (energy limit restriction); and others. Dividing surfaces obtained in these restricted searches did not curve back toward the reactant valley. These dividing surfaces were acceptable, i. e., they proceeded from a high energy region where the nuclei are close to a high energy region where the nuclei are far apart over the entire θ range. However, "islands" were still present on reactivity relief maps because a DS which gives a rate constant close to the converged value must curve toward the product valley near the collinear orientation $\theta = 0$ and then turn abruptly to the high energy region, narrowly

missing the product valley. A great deal of work was done to show that contributions to the reactive flux associated with such islands were negligible.

Many variational searches were performed with restrictions on variational parameters in an attempt to improve the "appearance" of the DS. For example, although the energy limit DS is acceptable, this DS passes close to the product valley and makes an abrupt turn in the high energy region. This behavior resembles that for a DS found in an unrestricted search. The energy limit restriction forces the DS to terminate in the high energy region and prevents it from plunging into the reactant valley near the R integration limit. Extensive calculations for the $F + H_2$ reaction informed us that converged variational results for canonical rate constants obtained using different restrictions on parameters were not very different regardless of the appearance of the DS. For this reason and its appearance, the slope restriction Q DS was adopted as the standard for further study.

Energy relief maps for the $F + H_2$ reaction for restricted and unrestricted searches showed that the high reactive flux contours did not follow the path of angle dependent saddlepoints. The integral for the reactive flux through a DS contains the factor $\exp\{-\beta V(r^*,R,\theta)\}$; hence, if potential energy alone determines the variational DS, the DS will pass through angle dependent saddle points where the lowest potential energy on the DS for a specified θ is the highest and follow the path of steepest ascent from the saddle points over the full range of θ. Of course, the high flux contours may not follow the path of angle dependent saddle points because the variational DS is determined by entropic as well as enthalpic factors. Nevertheless, we decided to learn whether the quadratic formulation of the DS used in this work was capable of following the path of steepest ascent from angle dependent $F + H_2$ saddle points.

A least squares fit method was used to obtain parameters for a Q DS which passes through the saddle points and selected points on paths of steepest ascent

from them. This work met with limited success. By assigning large weights to saddle points, we were able to find a least squares (LS) fit DS which did a good job of passing close to the saddle points over the full range in θ; however, this DS did not do a good job of following the paths of steepest ascent from them. Consequently, we decided to examine another closely related DS in which θ is replaced with $\sin^2\theta$ wherever it appears in the Q DS function. This function gave a LS DS which did a better job of passing through the saddle points than the LS Q (linear θ) DS; still, this DS did not do a good job of following the path of steepest ascent from saddle points. Many sets of Q (linear θ) and Q ($\sin^2\theta$) LS DS parameters were obtained by using different sets of points and different weights for saddle points and points on paths of steepest ascent from them.

Canonical rate constants calculated using many sets of LS DS parameters for Q both linear θ and $\sin^2\theta$ DS functions were found to be 2 to 4 times larger than corresponding variational search values. Contours of the same value in reactivity relief maps span larger areas and are thicker in the direction of increasing R for LS than for variational DSs. Variational DSs follow the path of steepest ascent from points which are near the angle dependent saddle points better than the LS DSs over the θ range where the reactive flux is large; consequently, the rates are significantly lower. Many sets of simplex vertices based on LS DSs were used to initiate variational searches with and without restrictions on variational parameters. These searches converged to variational rate constants and DS parameters which were found using other methods to generate initial vertices for simplex searches.

It is of course possible that another DS function exists which can do a better job of following the path of ascent from angle dependent saddle points over the full range of θ, yield rate constants which are significantly lower than values for the Q linear θ and $\sin^2\theta$ DS functions, and give reactivity relief maps with high flux contours which follow angle dependent saddle points more closely than the Q linear

θ and $\sin^2\theta$ DS functions. This possibility could be investigated by formulating more DS functions and studying them as we did the Q $\sin^2\theta$ DS function. We chose instead to address this point by comparing variational and classical mechanical trajectory results for the Q DS functions already studied. If variational rate constants, energy dependent mean reaction cross sections, and angular distributions of reactivity are in good agreement with Monte Carlo trajectory results for the Q linear θ and $\sin^2\theta$ DSs, then these DSs are flexible enough to give accurate rate constants and mean reaction cross sections and provide an accurate description of the dynamic stereochemistry of the F + H_2 reaction. Agreement of these results would show that entropic factors are responsible for yielding variational DSs which do not follow the path of steepest ascent from angle dependent saddle points closely. This work is summarized later.

Canonical variational rate constants, reactivity relief maps, and angular distributions of rates were calculated for the reactions: F + DH → FD(FH) + H(D) for the T1 potential energy function and temperatures of 300, 600, 1500, and 3000 K. Results are presented for the same 6–parameter quadratic DS function used to study the F + H_2 reaction and for 5 and 10–parameter DS functions which contain parameters which distinguish between reaction at each end of the heteronuclear reactant. For the 6–parameter DS, the integration range for θ runs from 0 to π and variational values are reported for the total reaction rate constant, i. e., the sum of rates for reaction at both ends of the DH reactant. Because this DS does not span high enough energies at intermediate values of θ and divide the reactive flux into unambiguous contributions for reaction at each end of the DH reactant, variational rate constants cannot be obtained for the FH + D and FD + H product channels. The 5 and 10–parameter DS formulations define a continuous surface which passes through the angle dependent saddle point where the minimum potential energy for chemical reaction has its largest value at θ = 81.5 deg.. These DSs were used to

obtain practical variational rate constants for reaction at each end of DH for temperatures of 300, 600, and 1500 K. The FH + D products are slightly favored over FD + H; the ratio of the variational rate constants for these products for the 5 and 10–parameter DSs are 1.41 and 1.25, respectively, and the experimental value of this ratio is 1.42$\pm$.10.

The accuracy of the classical variational theory was studied by comparing values of the energy dependent mean reaction cross section with classical mechanical trajectory values. Quadratic rather than cubic formulations of the DS were used because of the small cubic versus quadratic gain in accuracy and the relative ease of a quadratic variational search. The accuracy of the variational theory was determined for quadratic rather than more restricted formulations of the DS because we wanted to know the accuracy when the rate constant or mean reaction cross section is close to its minimum value. Calculations were performed for the T1 potential energy function. The accuracy of the variational theory was determined by comparing variational and trajectory mean reaction cross sections rather than rate constants because the former could be calculated with a much smaller error than the latter in Monte Carlo calculations of the same number of trajectories. The accuracy of the variational theory was also studied by comparing angular distributions of contributions to the energy dependent mean reaction cross section with trajectory distributions.

For the F + H_2 reaction, variational and trajectory values of the mean reaction cross section were calculated for energies of 0.1, 0.25, 0.5, 0.75, 1.0, and 1.5 eV. We consider the agreement between these values to be excellent. The difference between these results increases with energy as expected; however, the difference at 1.0 and 1.5 eV amounts to only 18 and 25 percent, respectively and these energies are very high in the sense that the probability that reaction systems have these energies at temperatures commonly used in studies of gas phase reactions

is very small.

The difference between variational and trajectory values of the mean reaction cross section can be described by a factor known as the conversion coefficient(χ). Multiplication of the variational mean reaction cross section by the conversion coefficient gives the trajectory value. We further describe the difference between variational and trajectory values by expressing the conversion coefficient as the product of two factors, the transmission and product coefficient. The transmission coefficient(κ) applies the correction that most chemists believe transition state theory needs; this factor corrects for trajectories which originate in the reactant region and cross and then recross the DS and return to the reactant region, or cross the DS an odd number of times greater than or equal to 3 and contribute more than once (incorrectly) to the rate. Most chemists do not realize that another correction, the product coefficient(ρ), is required. This factor corrects for trajectories which originate in the product region and cross and recross the DS to contribute to the variational rate.

Transmission, product, and conversion coefficients were evaluated by calculating microcanonical ensembles of trajectories at energies of 0.1, 0.25, 0.5, and 1.0 eV. The results showed that the deviation between variational and trajectory cross sections for energies of 0.1, 1.0, and 1.5 eV caused by trajectories which start in the reactant region and cross the DS more than once was actually smaller than the deviation caused by trajectories which originate in the product region, i. e., $\kappa(E) > \rho(E)$ for these energies. For 0.5 eV, $\kappa(E)$ is approximately equal to $\rho(E)$.

Variational and trajectory distributions of contributions to the mean reaction cross section were compared for energies of 0.1, 0.5, 1.0 and 1.5 eV. We regard the agreement of these results as very good; the deviation between the distributions increases with energy as expected. The accuracy of the no–recrossing assumption of transition state theory has been the subject of many studies. The application of a

DS formulation which includes terms in θ makes it possible to determine how the accuracy of the no–recrossing assumption depends on the orientation angle. Our results show that that the accuracy of the no–recrossing assumption is lowest for intermediate values of θ. For collinear atom–diatom reactions, the correction factors decline more abruptly with increasing energy that for reaction in 3–dimensional space. On this basis, one expects deviations from the variational flux, i. e., small correction factors, to be skewed toward low values of θ. Only the distribution at the lowest energy, 0.1 eV, appears to skewed toward low values of θ.

Variational searches were performed for the F + DH → FD(FH) + H(D) reactions for the quadratic slope (Q(S)) restriction DS to obtain mean reaction cross sections at energies of 0.1, 0.25, 0.5, and 1.0 eV. Trajectory calculations were performed for energies of 0.5 and 1.0 eV. This 6–parameter DS is identical to the one used to study the F + H_2 reaction; however, the DS must now minimize the variational flux at each end of the reactant. The integration over θ is from 0 to π. Variational and trajectory angular distributions of contributions to the cross section were calculated for energies of 0.5 and 1.0 eV. The variational and trajectory distributions were in good qualitative agreement near the peaks at low and high θ values for FH + D and FD + H products, respectively. However, because the 6–parameter DS does not traverse high energy regions at intermediate values of θ, the DS does not divide the reactive flux into contributions for reaction at each end of the DH reactant, i. e., the flux does not fall to zero as it should for these energies. Hence, the 6–parameter DS yields a variational value of the mean reaction cross section for reaction at both ends, but not each end of the reactant. The values of the conversion coefficient for total reaction at 0.5 and 1.0 eV are 0.733 and 0.689, respectively.

Variational searches were performed for the 5–parameter DS function which forces the DS to pass through the saddle point at $\theta = 81.5$ deg. where the energy is

2.31 eV. Calculations were performed for energies of 0.5 and 1.0 eV. Angular distributions of contributions to the cross section were also calculated. The distributions plunge to zero at intermediate values of θ. The values of the conversion coefficient for total reaction at 0.5 and 1.0 eV are significantly higher for this DS, 0.797 and 0.835, respectively. Trajectory angular distributions of contributions to the cross section were not calculated for this DS because all good things must come to an end, including my thesis work. This worthwhile work will be continued by my adviser. The 5 and 10–parameter formulations of the DS will yield variational values of the cross section, and transmission, product, and conversion coefficients for reaction at each end of the diatomic reactant.

The general variational theory of chemical reaction rates will help chemists understand transition state theory in a new and richer way. If a chemist is asked to identify the transition state for a collinear reaction on a potential energy surface plot, he or she will probably point to the saddle point. A more informed chemist will draw a line or curve through the saddle point which follows the path of steepest ascent from it. A still more informed chemist will draw a curve which misses the saddle point and corresponds to a periodic orbit dividing surface. A variational DS defines a generalized transition state. A generalized variational DS for an atom–diatom reaction in 3–dimensional space which depends on the orientation angle provides a description of the dynamic stereochemistry of the reaction. The reactivity relief map shows how the reactive flux through the DS depends on the location on it. The differences between the three potential energy functions studied in our work on the $F + H_2$ reaction are subtle; yet, the reactivity relief maps were markedly different. They clearly showed how the reactive flux spread to higher values of θ in the series KR → T1 → T2. Reactivity relief maps can also be used to show how the field of reactivity that surrounds the reactant expands with increasing temperature and energy. Reactivity relief maps can be used to show how the field

of reactivity that surrounds a reactant depends on the identity of the attacking atom and how the field depends on the identity of the reactant for the same attacking atom. There is more work to be done.

APPENDICES

Appendices 1 – 23 contain variational and least squares fit dividing surface parameters for the $F + H_2$ reaction.

Appendices 24 – 40 contain variational and least squares fit dividing surface parameters for the $F + DH$ reactions.

When two rate constants are given, the upper and the lower entries correspond to Simpson's Rule and simple quadrature values, respectively.

Only the Simpson's Rule values are given in the Tables in Chapters 3 and 4.

APPENDIX 1

Truncated (A and B variational parameters) and linear combination of internal parameters (A, B, and C variational parameters) dividing surfaces for F + HH reaction. Rate constants (k(T)) are in 10^{12} $cm^3/mol \cdot s$, T is temperature.

T	300 K	1500 K	3000 K	6000 K
	Koeppl/Rutenburg potential energy surface			
k(T)	2.08165	54.5627	150.994	
	2.08055	54.5603	150.990	
A	2.22700	1.92287	1.63659	
C	–6.27525	–4.73934	–3.71810	
k(T)	1.88225	40.5168	111.071	
	1.88205	40.5155	111.068	
A	2.29638	2.09109	1.79741	
B	0.741223	1.19801	1.27753	
C	–6.78614	–5.92526	–4.96690	
	Truhlar 1 potential energy surface			
k(T)	3.38755	71.2417	176.644	422.706
	3.38763	71.2391	176.640	422.699
A	2.19365	1.91351	1.65370	1.28360
C	–6.03690	–4.66933	–3.76783	–2.50215
k(T)	2.80238	50.5703	128.430	338.059
	2.80219	50.5689	128.427	338.054
A	2.29760	2.10034	1.80488	1.22323
B	0.924215	1.30704	1.34775	1.09860
C	–6.79863	–5.98694	–5.01406	–2.92009
	Truhlar 2 potential energy surface			
k(T)	6.99299	95.3049	207.469	454.761
	6.99182	95.3020	207.465	454.753
A	2.15711	1.90786	1.67985	1.32558
C	–5.77437	–4.61574	–3.85759	–2.67538
k(T)	4.97077	64.8187	150.006	365.970
	4.97059	64.8173	150.003	365.964
A	2.30579	2.11173	1.81343	1.22947
B	1.13981	1.42567	1.42004	1.12948
C	–6.85943	–6.06298	–5.06653	–2.95157

APPENDIX 2

Quadratic linear θ dividing surfaces (DS) obtained with no restrictions (N), with second derivative (SD), slope (S), energy limit (E), energy limit and slope (ES) restrictions for Koeppl/Rutenburg potential energy surface for 300 K temperature (T) for F + HH reaction. Rate constants (k(T)) are in 10^{12} $cm^3/mol \cdot s$. A,B,C,D,E, and F are variational parameters.

DS	SD	S	S	N
k(300K)	1.79852 1.79844	1.69333 1.69926	1.6655643	1.6111752 1.6363926
A	1.89491	5.90939	6.4182364	12.751043
B	–9.49856	–7.07522	–5.0700338	–4.7566242
C	–5.25294	–13.9802	–15.467605	–28.659315
D	5.46059×10^{-9}	–0.844198	–0.91689059	–2.4102132
E	2.60189	1.79052	1.2560302	1.0305900
F	3.80603	5.22177	4.9433278	7.3871696

DS	E	E	E	ES
k(300K)	2.13582 2.13555	1.6706333 1.67056	1.6658379 1.66625	1.7231697 1.72315
A	2.08901	9.1022005	10.715023	6.9033126
B	–5.14231	–1.4309801	2.2969459	1.3160890
C	–4.52211	–21.365290	–24.838662	–16.999690
D	–0.231810	–1.5258053	–1.8865959	–0.98314693
E	1.569223	0.60340196	–0.41320905	–0.042018572
F	0.258220	1.4594334	1.1028120	–0.46721411

APPENDIX 3

Quadratic linear θ dividing surfaces (DS) obtained with no restrictions (N), with second derivative (SD), slope (S), energy limit (E), energy limit and slope (ES), energy limit or slope (E/S) restrictions for Koeppl/Rutenburg potential energy surface for 1500 K temperature (T) for F + HH reaction. Rate constants (k(T)) are in 10^{12} $cm^3/mol \cdot s$. A,B,C,D,E, and F are variational parameters.

DS	SD	S	E/S	N
k(1500K)	38.3643 38.3628	37.7694 37.7682	40.478121 40.4767	37.110426 37.1094
A	1.69423	5.34244	3.8481993	8.6667780
B	–6.72138	0.430803	2.1356097	–0.10783259
C	–4.26140	–12.4800	–9.0661459	–18.661766
D	1.69979×10^{-9}	–0.763205	–0.49337313	–1.6333065
E	1.81036	0.00908373	–0.23290134	–0.016744463
F	4.12305	1.92344	–0.27559683	3.5172186

DS	E	E	ES	ES
k(1500K)	43.036815 43.0348	37.387997 37.3868	41.117093 41.1144	39.283498 39.2822
A	2.0835903	7.3473403	2.8974978	5.3559277
B	–4.510856	0.42986753	–8.7793244	1.3395061
C	–4.3032847	–16.360357	–6.1459587	–12.781743
D	–0.25742202	–1.275331	–0.41951409	–0.76513225
E	1.6307188	–0.0081500487	2.8582176	0.10472132
F	0.29924037	2.3897947	0.96451109	–0.22305997

APPENDIX 4

Quadratic linear θ dividing surfaces (DS) obtained with no restrictions (N), second derivative (SD), slope (S), energy limit (E), energy limit and slope (ES), energy limit or slope (E/S) restrictions for Koeppl/Rutenburg potential energy surface for 3000 K and 6000 K temperatures (T) for F + HH reaction. Rate constants (k(T)) are in 10^{12} $cm^3/mol \cdot s$. A,B,C,D,E, and F are variational parameters.

DS	SD	S	S	N
k(3000K)	106.592 106.590	105.27064 105.268	104.514 104.511	103.47387 103.47601
A	1.48805	3.9409686	3.83355	6.0624697
B	–3.43987	1.1927327	–1.39631	–0.011789890
C	–3.52397	–9.1337370	–8.38953	–12.699461
D	8.95894×10^{-8}	–0.51283954	–0.546107	–1.1157988
E	0.887022	–0.22351130	0.313688	–0.051746961
F	3.08570	1.6006748	2.97638	2.8290490

DS	E	E	ES	ES
k(3000K)	115.26419 115.26049	103.93597 103.934	104.83360 104.831	104.22704 104.225
A	2.0921073	4.8310698	5.4553489	4.8128433
B	–4.3435875	–1.0970281	1.5227632	0.76492958
C	–4.4155555	–10.286669	–12.060218	–10.329423
D	–0.25830528	–0.80361997	–0.90945533	–0.79387008
E	1.6314241	0.22254993	–0.23677044	–0.18580959
F	0.3001093	3.0325195	1.2166516	1.9115189

DS	E/S	DS	SD
k(3000K)	107.46967 107.467	k(6000K)	306.553 306.548
A	4.2491989	A	1.15513
B	1.6032766	B	–0.297024
C	–10.085527	C	–2.37451
D	–0.57069142	D	6.46374×10^{-10}
E	–0.16192975	E	0.0928536
F	0.40125476	F	1.46857

APPENDIX 5

Quadratic linear θ dividing surfaces (DS) obtained with no restrictions (N), second derivative (SD), slope (S), energy limit (E), energy limit and slope (ES) restrictions for Truhlar 1 potential energy surface for 300 K temperature (T) for F + HH reaction. Rate constants (k(T)) are in 10^{12} $cm^3/mol \cdot s$. A,B,C,D,E, and F are variational parameters.

DS	SD	SD	S	S
k(300K)	2.65074 2.65039	2.56134 2.56116	2.56379 2.56351	2.5105424 2.51521
A	1.82836	6.90590	6.58301	6.3607896
B	−10.2862	1.12918	−1.12836	−3.1126676
C	−4.97827	−16.9458	−16.0877	−15.203410
D	4.91846×10^{-8}	−0.989586	−0.940430	−0.90868418
E	2.81703	0.0151712	0.650471	0.76162916
F	4.40004	0.262301	0.325714	4.2350450

DS	E	E	E	E
k(300K)	2.73034 2.73015	2.726398 2.7262	2.7245674 2.72437	2.4929685 2.49835
A	4.42193	4.3770321	4.4465037	8.2681903
B	−2.52226	−2.4810989	−2.1817055	−0.80445971
C	−10.2835	−10.169701	−10.364088	−19.148868
D	−0.631704	−0.62546304	−0.63461422	−1.3575748
E	0.862568	0.87815932	0.08639173	0.17595188
F	0.891022	0.91251436	0.79746314	3.3590399

DS	ES	N
k(300K)	2.5282860 2.53024	2.4549041 2.46241
A	5.8217754	11.930786
B	−1.7406906	2.0154167
C	−14.404856	−26.853614
D	−0.75590561	−2.2205023
E	0.46342087	−0.58547504
F	3.6997987	3.7676878

APPENDIX 6

Quadratic linear θ dividing surfaces (DS) obtained with no restrcitions (N), second derivative (SD), slope (S), energy limit (E), energy limit and slope (ES), energy limit or slope (E/S) restrictions for Truhlar 1 potential energy surface for 1500 K temperature (T) for F + HH reaction. Rate constants (k(T)) are in 10^{12} $cm^3/mol \cdot s$. A,B,C,D,E, and F are variational parameters.

DS	SD	S	E/S	N
k(1500K)	47.8037 47.8021	46.8892 46.8879	50.104059 50.1026	46.427523 46.426350
A	1.68332	4.94219	3.9986819	8.1785753
B	−6.84562	−2.45317	−1.7982992	−2.1624504
C	−4.20050	−11.2816	−9.1225998	−17.396928
D	5.90336×10^{-6}	−0.705466	−0.57124027	−1.5523433
E	1.82979	0.620685	0.91188093	0.51065598
F	4.38862	3.81868	0.32246567	4.2945376

DS	E	E	E	E
k(1500K)	48.330206 48.3288	48.309576 48.3082	47.583174 47.5819	47.024619 47.0234
A	3.8431331	3.8298400	4.5622862	5.9067795
B	−4.9894964	−5.5103384	−0.076267116	0.41226268
C	−8.1709091	−8.1457270	−10.393756	−13.584160
D	−0.6073744	−0.60459860	−0.64420261	−0.90363933
E	1.5731349	1.7267431	0.10970499	−0.01103032
F	2.2626151	2.3310401	2.0254648	2.4708945

DS	ES	ES	ES	E/S
k(1500K)	48.268306 48.2671	47.128804 47.127495	46.930039 46.9289	50.415073 50.4137
A	5.8401955	5.2195607	7.5267146	3.9796279
B	−1.8300234	0.37236567	1.8805672	2.3168046
C	−13.867953	−12.059189	−16.821482	−9.4484911
D	−0.83431348	−0.74026342	−1.3031610	−0.51572198
E	0.41109718	−0.12348565	−0.36621917	−0.23527803
F	4.9662610	2.9042197	1.8580592	−0.30558076

APPENDIX 7

Quadratic linear θ dividing surfaces (DS) obtained with no restrictions (N), second derivative (SD), slope (S), energy limit (E), energy limit and slope (ES), energy limit or slope (E/S) restrictions for Truhlar 1 potential energy surface for 3000 K and 6000 K temperatures (T) for F + HH reaction. Rate constants (k(T)) are in 10^{12} $cm^3/mol \cdot s$. A,B,C,D,E, and F are variational parameters.

DS	SD	S	S	N
k(3000K)	123.346 123.343	122.97353 122.97137	121.02559 121.023	119.86105 119.859
A	1.34911	4.8285306	4.0584273	5.9356106
B	−4.83930	0.39774950	−0.14892572	−0.12172908
C	−2.99461	−11.289816	−8.9834460	−12.388707
D	5.43692×10^{-8}	−0.68966607	−0.57977477	−1.0913540
E	1.22739	0.0052749060	0.0081361953	−0.026835859
F	3.69384	2.3842215	2.5793398	2.8499532

DS	E	E	E	E/S
k(3000K)	126.65903 126.656	123.89796 123.896	120.77428 120.772	123.60909 123.607
A	4.2186974	6.7165545	5.0149101	3.8094147
B	−2.7022989	1.6036039	0.386	1.9428501
C	−9.3013062	−15.315669	−10.904983	−9.0297934
D	−0.66858551	−1.1374564	−0.83091452	−0.48335502
E	1.0433396	−0.18737009	−0.017636769	−0.24424092
F	1.2801261	1.6267736	1.9728150	0.61160408

DS	ES	ES		SD
k(3000K)	122.73689 122.734	120.32880 120.326	k(6000K)	330.797 330.791
A	2.9717300	5.0806780	A	1.14911
B	−4.6253758	−0.085541418	B	−0.354466
C	−6.0598869	−10.891488	C	2.34730
D	−0.43897479	−0.84982478	D	2.37615×10^{-5}
E	1.3141696	−0.025770572	E	0.108236
F	2.8202651	2.7412203	F	1.50365

APPENDIX 8

Quadratic linear θ dividing surfaces (DS) obtained with no restrictions (N), second derivative (SD), slope (S), energy limit (E), energy limit and slope (ES) restrictions for Truhlar 2 potential energy surface for 300 K temperature (T) for F + HH reaction. Rate constants (k(T)) are in 10^{12} $cm^3/mol \cdot s$. A,B,C,D,E, and F are variational parameters.

DS	SD	S	S
k(300K)	4.65708 4.65693	4.64255 4.64271	4.5892637 4.58927
A	1.82884	2.57064	5.9077057
B	−10.0376	−5.84640	1.8849172
C	−4.94351	−6.95322	−14.702133
D	2.6631×10^{-7}	−0.0931646	−0.76476103
E	2.75592	1.55859	−0.27652311
F	4.67701	4.31173	0.89908462

DS	E	E	ES
k(300K)	5.57944 5.57919	5.0747441 5.07454	4.4898589 4.49033
A	1.85898	3.6037361	4.7522788
B	−0.956147	1.1727658	−13.138667
C	−4.48275	−8.6178252	−10.758215
D	−0.124509	−0.44120277	−0.71973159
E	0.511077	−0.1627808	3.6395605
F	0.258425	1.0842947	5.4099596

DS	E	E	N
k(300K)	4.5301085 4.53992	4.4141936 4.42078	4.3528455 4.3679319
A	7.6773438	9.8640399	11.369497
B	−3.9193558	−0.14114721	−4.8342726
C	−17.617159	−22.306600	−24.989832
D	−1.2425783	−1.7519447	−2.1649926
E	0.65016916	−0.024536514	1.1521852
F	8.3635326	4.2003878	6.3121047

APPENDIX 9

Quadratic linear θ dividing surfaces (DS) obtained with no restrictions (N), second derivative (SD), slope (S), energy limit (E), energy limit and slope (ES) restrictions for Truhlar 2 potential energy surface for 1500 K temperature (T) for F + HH reaction. Rate constants (k(T)) are in 10^{12} $cm^3/mol \cdot s$. A,B,C,D,E, and F are variational parameters.

DS	S	S	S
k(1500K)	61.1101 61.1089	60.723629 60.7224	60.274361 60.2730
A	5.08801	5.0611114	4.3698514
B	1.45204	0.95158659	−4.7276292
C	−12.1172	−11.924824	−9.7599915
D	−0.686799	−0.68714864	−0.62426074
E	−0.176041	−0.15983621	1.2690127
F	1.44315	2.2444849	4.2332233

DS	SD	E	ES
k(1500K)	61.2262 61.2246	62.4673 62.4660	61.956818 61.9555
A	1.67851	4.79085	4.9839964
B	−6.88722	0.181641	0.18139066
C	−4.16039	−11.3340	−11.709331
D	1.80511×10^{-6}	−0.684404	−0.71519912
E	1.82625	0.347000	0.32083109
F	4.63457	1.13428	1.0200494

DS	E	E	N
k(1500K)	59.93507 59.9337	59.934439 59.9331	59.845549 59.844485
A	6.3084163	6.2725131	8.5282840
B	−3.5160888	−3.4987127	0.92025020
C	−13.647809	−13.575413	−18.365573
D	−1.0889803	−1.0816653	−1.5960286
E	0.85387874	0.86584272	−0.29281933
F	4.7323066	4.6046313	3.4080885

APPENDIX 10

Quadratic linear θ dividing surfaces (DS) obtained with no restrictions (N), second derivative (SD), slope (S), energy limit (E), energy limit and slope (ES) restrictions for Truhlar 2 potential energy surface for 3000 K and 6000 K temperatures (T) for F + HH reaction. Rate constants (k(T)) are in 10^{12} $cm^3/mol \cdot s$. A,B,C,D,E, and F are variational parameters.

DS	SD	S	S	N
k(3000K)	143.836 143.833	142.39350 142.39115	141.69904 141.697	140.36934 140.36696
A	1.47736	3.8084681	4.0866658	5.7659694
B	−3.47236	0.89431249	−0.021258065	−0.45388271
C	−3.45807	−8.6128264	−9.0975284	−11.931201
D	7.35599×10^{-6}	−0.51202332	−0.57582448	−1.0642743
E	0.885076	−0.14227944	−0.035568315	0.051043118
F	3.28394	1.6242359	2.6942456	3.0130323

DS	E	ES	E	E
k(3000K)	147.921 147.919	143.68735 143.685	141.21547 141.213	140.90629 140.904
A	2.45218	2.1350720	4.55995029	5.1960218
B	0.584408	−0.82050808	−1.3744741	0.71881329
C	−5.78608	−5.1841385	−9.6966034	−11.209391
D	−0.233460	−0.10656149	−0.75002368	−0.86476329
E	0.158281	0.24772607	0.36705089	−0.22463426
F	0.472849	2.2759369	2.8398275	2.5139133

DS	SD
k(6000K)	362.194 362.189
A	0.962777
B	−1.26337
C	−1.76802
D	1.335×10^{-10}
E	0.452835
F	1.19260

APPENDIX 11

Quadratic $\sin^2\theta$ dividing surfaces (DS) obtained with no restrictions (N), second derivative (SD), slope (S), energy limit (E), energy limit and slope (ES) restrictions for Koeppl/Rutenburg potential energy surface for 300 K temperature (T) for F + HH reaction. Rate constants (k(T)) are in 10^{12} $cm^3/mol \cdot s$. A,B,C,D,E, and F are variational parameters.

DS	ES	SD
k(300K)	1.9653090	1.7909554
	1.9650230	1.7908159
A	3.1488580	2.1891842
B	−9.4535749	−18.947027
C	−7.2218466	−6.3243333
D	−0.38838724	$3.8817826 \times 10^{-10}$
E	2.5545678	5.7365847
F	12.014648	2.8875053

DS	S	E	N
k(300K)	1.6795128	1.6475354	1.5688250
	1.6850760	1.6741306	1.6114479
A	6.7038061	10.843558	12.180218
B	−0.54474065	−0.30868384	−17.335221
C	−16.302122	−25.055371	−27.150261
D	−0.95325956	−1.9180459	−2.3072410
E	0.35583167	0.033530042	4.6434370
F	6.0994949	12.453684	17.100029

APPENDIX 12

Quadratic $\sin^2\theta$ dividing surfaces (DS) obtained with slope (S) and energy limit (E) restrictions for Koeppl/Rutenburg potential energy surface for 1500 and 3000 K temperatures (T) for F + HH reaction. Rate constants (k(T)) are in 10^{12} $cm^3/mol \cdot s$. A,B,C,D,E, and F are variational parameters.

DS	S	E
k(1500K)	37.599162	37.578289
	37.597896	37.576951
A	5.2047898	6.4300632
B	−0.83633742	−0.25389324
C	−12.009861	−14.215105
D	−0.74342311	−1.0695117
E	0.54057188	0.15807073
F	3.3840881	5.1956802

DS	S	E
k(3000K)	105.69437	104.65673
	105.69185	104.65425
A	4.1073082	4.9746950
B	−0.55407360	−0.30599712
C	−9.0479854	−10.559625
D	−0.58675832	−0.83289100
E	0.13202336	0.10111865
F	5.0462093	4.5007306

APPENDIX 13

Quadratic $\sin^2\theta$ dividing surfaces (DS) obtained with no restrictions (N), second derivative (SD), slope (S), energy limit (E), energy limit and slope (ES) restrictions for Truhlar 2 potential energy surface for 300 K temperature (T) for F + HH reaction. Rate constants (k(T)) are in 10^{12} $cm^3/mol \cdot s$. A,B,C,D,E, and F are variational parameters.

DS	S	S	S	N
k(300K)	4.5206149 4.5215961	4.5082508 4.5118133	4.4605212 4.4611629	4.3851388 4.3897456
A	6.7353494	6.5069801	6.5679341	11.707846
B	2.2587616	−0.48266490	−9.4088385	−4.4634665
C	−16.340134	−15.606062	−15.895796	−25.904560
D	−0.96219277	−0.92956859	−0.93827630	−2.2225951
E	0.0091392047	0.34994829	3.2602551	1.9083745
F	−0.11928138	5.9230579	3.9314528	2.3135911

DS	SD	E/S	E
k(300K)	5.2171145 5.2168879	4.6058318 4.6056508	4.5002304 4.5054124
A	3.2099416	2.0174772	10.263819
B	3.2451331	−25.549887	0.54910012
C	−7.5662667	−5.6150226	−23.452206
D	−0.37152935	3.8530087×10^{-6}	−1.8178414
E	−0.60923612	7.4913742	0.033064518
F	0.86321040	10.358921	8.7200123

APPENDIX 14

Quadratic $\sin^2\theta$ dividing surfaces (DS) obtained with slope (S) and energy limit (E) restrictions for Truhlar 2 potential energy surface for 1500 and 3000 K temperatures (T) for F + HH reaction. Rate constants (k(T)) are in 10^{12} $cm^3/mol \cdot s$. A,B,C,D,E, and F are variational parameters.

DS	S	E
k(1500K)	60.646475	60.243300
	60.645132	60.242012
A	5.1673800	7.1899298
B	1.0174891	2.0018967
C	−11.863150	−15.771533
D	−0.73644044	−1.2502557
E	−0.011718478	−0.22440611
F	3.2744693	2.9988415

DS	S	E
k(3000K)	142.34553	144.03079
	142.34310	144.02848
A	4.0171762	4.2182967
B	0.60253559	4.8285202
C	−8.8377366	−9.5928942
D	−0.57388225	−0.58167622
E	3.9665599×10^{-5}	−0.97470742
F	3.1690709	0.28894929

APPENDIX 15

Quadratic least squares fit dividing surfaces for Koeppl/Rutenburg potential energy surface for 300, 1500, and 3000 K temperatures (T) for F + HH reaction. Rate constants (k(T)) are in 10^{12} $cm^3/mol \cdot s$. A,B,C,D,E, and F are variational parameters.

A	1.530263	1.531213
B	3.751047	3.757542
C	−4.314495	−4.318054
D	-3.408261×10^{-8}	-1.404546×10^{-6}
E	−0.5621243	−0.5633961
F	−0.7668458	−0.7705779
Response	0.2109372	0.2109368
k(300K)	2.8257477	2.8260626
	2.8254499	2.8257647
k(1500K)	51.789141	51.790324
	51.787333	51.788515
k(3000K)	128.14028	128.14136
	128.13736	128.13845

A	1.530902	1.887925
B	3.752689	4.271616
C	−4.31685	−5.091519
D	-5.835199×10^{-8}	−0.0806836
E	−0.5623405	−0.6836715
F	−0.7677233	−0.9389669
Response	0.2109367	0.2126263
k(300K)	2.8255592	2.8017943
	2.8252614	2.8014987
k(1500K)	51.783493	51.466237
	51.781685	51.464444
k(3000K)	128.12630	127.55217
	128.12338	127.54928

APPENDIX 16

Quadratic least squares fit dividing surfaces for Koeppl/Rutenburg potential energy surface for 300, 1500, and 3000 K temperatures (T) for F + HH reaction. Rate constants (k(T)) are in 10^{12} $cm^3/mol \cdot s$. A,B,C,D,E, and F are variational parameters.

A	0.3970045	1.132652
B	1.185821	3.766854
C	−1.602901	−3.667875
D	0.2205216	0.1199278
E	0.03680655	−0.5559697
F	0.2026214	−0.8501745
Response	0.2135047	0.2092699
k(300K)	2.9940886	2.8009466
	2.9937675	2.8006530
k(1500K)	53.347693	51.735671
	53.345739	51.733890
k(3000K)	130.46638	128.36302
	130.46322	128.36016

A	1.53101	−0.614939
B	3.754228	2.145731
C	−4.317052	−0.2302092
D	3.50851×10^{-9}	0.5635735
E	−0.5627459	−0.155141
F	0.7686377	−0.4451553
Response	0.2109368	0.2023083
k(300K)	2.8257923	2.8446980
	2.8254945	2.8444363
k(1500K)	51.784049	65.657425
	51.782242	65.721949
k(3000K)	128.12729	253.10821
	128.12438	253.04395

APPENDIX 17

Quadratic least squares fit dividing surfaces for Koeppl/Rutenburg potential energy surface for 300, 1500, and 3000 K temperatures (T) for F + HH reaction. Rate constants (k(T)) are in 10^{12} $cm^3/mol \cdot s$. A,B,C,D,E, and F are variational parameters.

A	2.096952	1.549945
B	4.214824	3.497866
C	−5.529544	−4.383273
D	−0.1293341	3.188127×10^{-9}
E	−0.6591693	−0.4887381
F	−0.8544921	−0.6260775
Response	0.1736400	0.1724613
k(300K)	2.7866409	2.8095499
	2.7863464	2.8092535
k(1500K)	50.948199	51.251282
	50.946411	51.249481
k(3000K)	126.21124	126.76256
	126.20834	126.75965

A	1.548836	1.549795
B	3.490836	3.495306
C	−4.379174	−4.382946
D	-1.184394×10^{-6}	1.367338×10^{-8}
E	−0.4870675	−0.4879203
F	−0.6230901	−0.6251881
Response	0.1724614	0.1724613
k(300K)	2.8101938	2.8097232
	2.8098973	2.8094267
k(1500K)	51.257792	51.252930
	51.255991	51.251128
k(3000K)	126.77276	126.76361
	126.76985	126.76070

APPENDIX 18

Quadratic least squares fit dividing surfaces for Koeppl/Rutenburg potential energy surface for 300, 1500, and 3000 K temperatures (T) for F + HH reaction. Rate constants (k(T)) are in 10^{12} $cm^3/mol \cdot s$. A,B,C,D,E, and F are variational parameters.

A	1.54906	−0.4007099	
B	3.493104	1.642566	
C	−4.380042	−0.5263967	
D	-2.33116×10^{-8}	0.4923835	
E	−0.4875928	−0.03231768	
F	−0.6242192	−0.1496243	
Response	0.1724613	0.1692725	
k(300K)	2.8101824	2.8631250	
	2.8098859	2.8628254	
k(1500K)	51.258436	52.416349	
	51.256635	52.414594	
k(3000K)	126.77480	136.61464	
	126.77189	136.61603	
A	1.135125	1.905479	$\sin^2\theta$
B	3.416924	4.462163	
C	−3.66678	−4.867395	
D	0.1184815	−0.100258	
E	−0.4577886	−0.5762206	
F	−0.6804277	−0.7707013	
Response	0.1719697	0.1110517	
k(300K)	2.8050906	2.3992976	
	2.8047952	2.3990819	
k(1500K)	51.424225	50.937588	
	51.422432	50.992531	
k(3000K)	127.30201	130.57324	
	127.29912	130.55272	

APPENDIX 19

Quadratic least squares fit dividing surfaces for Truhlar 2 potential energy surface for 300, 1500, and 3000 K temperatures (T) for F + HH reaction. Rate constants (k(T)) are in 10^{12} $cm^3/mol \cdot s$. A,B,C,D,E, and F are variational parameters.

A	1.480312	1.337144
B	3.264796	2.966692
C	−3.926126	−3.58251
D	−0.02767679	-8.524084×10^{-7}
E	−0.5168858	−0.4468228
F	−0.4066342	−0.3020464
Response	0.2702311	0.2694564
k(300K)	7.3499525	7.4201711
	7.3496584	7.4198737
k(1500K)	81.585169	81.975033
	81.583375	81.973218
k(3000K)	174.16566	174.65017
	174.16287	174.64732

A	1.466319	0.06651506
B	3.684101	2.006944
C	−4.06461	−1.274997
D	-3.999183×10^{-4}	0.3457766
E	−0.6103107	−0.1795707
F	−0.5941054	−0.1322868
Response	0.2700008	0.2420224
k(300K)	7.2118342	7.2779483
	7.2115480	7.2776495
k(1500K)	80.926438	82.162861
	80.924695	82.161053
k(3000K)	173.50132	175.03928
	173.49867	175.03647

APPENDIX 20

Quadratic least squares fit dividing surfaces for Truhlar 2 potential energy surface for 300, 1500 and 3000 K temperatures (T) for F + HH reaction. Rate constants (k(T)) are in 10^{12} $cm^3/mol \cdot s$. A,B,C,D,E, and F are variational parameters.

A	–0.7631037	1.242893	–0.4099375
B	–1.357181	1.850964	1.623957
C	1.031971	–3.183251	–0.5531667
D	0.4675676	–0.001308881	0.500394
E	0.573016	–0.1880087	–0.08176208
F	1.456515	0.2499761	0.05865252
Response	0.2208262	0.2205344	0.2083440
k(300K)	7.4217019	7.5205939	6.9053985
	7.4213783	7.5202953	6.9051183
k(1500K)	82.313583	80.665001	79.645010
	82.311603	80.663165	79.643462
k(3000K)	173.87985	170.90578	180.19100
	173.87985	170.90284	180.19200

APPENDIX 21

Cubic variational dividing surfaces (DS) obtained with second derivative (SD) and slope (S) restrictions for Koeppl/Rutenburg potential energy surface for 300 K temperature (T) for F + HH reaction. Rate constants (k(T)) are in 10^{12} $cm^3/mol \cdot s$. A,B,C,D,E,F,G,H,I,and J are variational parameters.

DS	SD	S
k(300K)	2.65115	2.65938
A	1.82045	4.903233
B	−10.3086	4.09211
C	−4.95702	−12.8180
D	6.40585×10^{-4}	−0.517948
E	2.83010	−0.820060
F	4.32192	−0.361936
G	5.5592×10^{-5}	-9.29815×10^{-6}
H	3.6692×10^{-5}	-8.23672×10^{-6}
I	-1.12237×10^{-5}	6.45316×10^{-4}
J	1.32845×10^{-4}	9.75131×10^{-4}

APPENDIX 22

Cubic variational, linear θ and $\sin^2\theta$, dividing surfaces obtained with slope restriction for Truhlar 2 potential energy surface for 300 K temperature (T) for F + HH reaction. Rate constants (k(T)) are in 10^{12} $cm^3/mol \cdot s$. A,B,C,D,E,F,G,H,I,and J are variational parameters.

	linear θ	$\sin^2\theta$
k(300K)	4.4540553	4.481133
	4.4540052	4.4810633
A	7.3096701	7.0278091
B	−2.6634661	−0.24549004
C	−16.441117	−16.505482
D	−1.3585214	−1.1240550
E	0.13634788	0.021366211
F	0.10511198	−0.06140020
G	0.089795812	0.034338647
H	0.29470305	0.2102959
I	1.4249434	1.4855530
J	0.039938182	1.4870286

APPENDIX 23

Cubic least squares fit, linear θ and $\sin^2\theta$, dividing surfaces for Truhlar 2 potential energy surface for F + HH reaction. Rate constants (k(T)) calculated for 300 K temperature (T) are in 10^{12} cm^3/mol·s. A,B,C,D,E,F,G,H,I,and J are variational parameters.

	linear θ	linear θ
A	1.586843	4.229681
B	3.075645	5.58877
C	−4.358422	−9.593151
D	-4.448633×10^{-3}	−0.6703786
E	−0.5029352	−1.130447
F	-1.472707×10^{-2}	−0.62335
G	-1.017828×10^{-3}	-1.996598×10^{-5}
H	-1.147339×10^{-3}	-1.111553×10^{-5}
I	-3.922883×10^{-4}	-6.654733×10^{-4}
J	1.247066×10^{-3}	1.559559×10^{-3}
k(300K)	6.8353612 6.8351068	384.13709 384.13328

	$\sin^2\theta$	$\sin^2\theta$
A	1.856448	2.121372
B	5.43826	5.247149
C	−5.19729	−5.593206
D	-2.043385×10^{-2}	−0.103556
E	−0.9345593	−0.922324
F	−0.3964916	-7.535236×10^{-2}
G	-3.437742×10^{-4}	2.148666×10^{-5}
H	2.261295×10^{-4}	1.021855×10^{-4}
I	8.200049×10^{-5}	7.863063×10^{-3}
J	3.061889×10^{-3}	5.423651×10^{-3}
k(300K)	5.9334133 5.9332125	5.8994553 5.8994046

APPENDIX 24

Quadratic least squares (LS) fit and variational dividing surfaces (DS) for 300 K temperature (T) for F + DH reaction. Variational DSs were obtained with no restrictions (N) and with slope (S) restriction; LS DSs were used to generate vertices for variational searches. Rate constants (k(T)) are in 10^{12} cm^3/mol·s. A,B,C,D,E, and F are variational parameters.

DS	LS	N*	S
k(300K)	15.095016	5.7339704	5.7105779
A	–0.18870620	–0.48882958	–0.43972902
B	1.3718260	–0.96446377	–0.85337329
C	0.21315970	0.16340649	–0.0015778036
D	0.22679580	0.41054203	0.40264202
E	0.13672640	0.55729829	0.56003189
F	–1.1049540	–0.41001320	–0.48982150

DS	LS	N*	S
k(300K)	16.68916	4.9911627	4.9911637
A	0.75675210	1.7202322	1.7202367
B	1.9035620	–0.44624889	–0.44550134
C	–1.8788690	–5.2931539	–5.2933552
D	-0.4005143×10^{-6}	-0.16096844×10^{-4}	-0.14934344×10^{-4}
E	0.15468230	0.52134958	0.52133122
F	–1.4692790	–0.57863600	–0.57905197

DS	LS	N	S
k(300K)	84.0729952	4.5213444	4.6351251
A	0.54003450	10.258728	5.4856948
B	1.3177210	1.9969031	0.16510790
C	–0.86189080	–24.232672	–13.966791
D	-0.2977213×10^{-6}	–1.8797585	–0.78366969
E	0.18073540	0.07190844	0.46624691
F	–1.1698480	–0.98651472	–0.73434535

N* – acceptable (no early bent, no need for corresponding slope)

APPENDIX 25

Quadratic least squares (LS) fit and variational dividing surfaces (DS) for 300 K temperature (T) for F + DH reaction. Variational DSs were obtained with no restrictions (N), with slope (S) and second derivative (SD) restrictions; LS DSs were used to generate vertices for variational searches. Rate constants (k(T)) are in 10^{12} cm^3/mol·s. A,B,C,D,E, and F are variational parameters.

DS	LS	N	*	S
k(300K)	19.951917	4.5228986	4.9519446	4.7285907
A	0.69040310	10.102008	2.86801942	5.2733377
B	1.7911690	1.5683755	0.62499639	–0.44251802
C	–1.4815730	–23.840782	–7.8512958	–13.190011
D	-0.5248976×10^{-6}	–1.85107183	–0.24495824	–0.75333396
E	0.057518710	0.18447459	0.22763830	0.48148902
F	–1.1979240	–0.95093633	–0.63295508	–0.3994592

DS	LS	N	SD	S
k(300K)	23.509826	4.5213444	5.1496033	4.6447601
A	–0.63474440	10.258553	1.7503301	5.4528224
B	0.81991400	1.9966817	0.58460917	0.015595558
C	1.4515680	–24.232256	–5.3587877	–13.830559
D	0.29533270	–1.8797242	0.65920218×10^{-11}	–0.77897461
E	0.22146000	0.071983857	0.20033481	0.46657040
F	–0.94890510	–0.98654039	–0.57790806	–0.63975276

DS	LS	N	SD	S
k(300K)	27.1124972	4.5237918	5.0080884	4.7948092
A	–0.81948840	10.073853	1.7102014	5.8495363
B	0.68527440	1.4539819	–0.62544823	1.2355763
C	1.8520240	–23.776219	–5.2000217	–15.364340
D	0.33861110	–1.8458211	0.84939796×10^{-4}	–0.83564790
E	0.24534230	0.21714555	0.51709585	0.45274984
F	–0.91611250	–0.94631328	–0.45248509	–1.3455198

N* – acceptable intermidiate value of 4.5228986(N) with no islands

APPENDIX 26

Quadratic least squares (LS) fit and variational dividing surfaces (DS) for 600 K temperature (T) for F + DH reaction. Variational DSs were obtained with no restrictions (N); LS DSs were used to generate vertices for variational searches. Rate constants (k(T)) are in 10^{12} $cm^3/mol \cdot s$. A,B,C,D,E, and F are variational parameters.

DS	LS	N
k(600K)	51.874651	21.870415
A	0.75675210	1.6790451
B	1.9035620	0.041759723
C	−1.8788690	−5.1555454
D	-0.40051430×10^{-6}	0.50148144×10^{-6}
E	0.15468230	0.50309505
F	−1.4692780	−0.82141838

k(600K)	LS	N
	57.729529	21.870412
A	0.69040310	1.6790494
B	1.7911690	0.041788470
C	−1.4815730	−5.1555562
D	-0.52489760×10^{-6}	-0.22598834×10^{-6}
E	0.057518710	0.50309234
F	−1.1979240	−0.82143169

APPENDIX 27

Quadratic least squares (LS) fit and variational dividing surfaces (DS) for 600 K temperature (T) for F + DH reaction. Variational DSs were obtained with slope (S) restriction; LS DSs were used to generate vertices for variational searches. Rate constants (k(T)) are in 10^{12} $cm^3/mol \cdot s$. A,B,C,D,E, and F are variational parameters.

DS	LS	S
k(600K)	63.030130	20.738847
A	–0.63474440	5.3796144
B	0.81991400	1.9888480
C	1.4515680	–13.730715
D	0.29533270	–0.76851632
E	0.22146000	0.12427389
F	–0.94890510	–1.1714694

k(600K)	LS	S
	49.602374	20.694364
A	–0.18870620	5.2096939
B	1.3718260	1.332828470
C	0.21315970	–13.2366352
D	0.22679580	–0.74424199
E	0.136726400	0.29030797
F	–1.1049540	–1.0974422

k(600K)	S (GK)	S (IR)
	20.981278	20.920403
A	4.8422413	4.7519632
B	0.18855897	0.16630175
C	–12.017161	–11.811115
D	–0.69174874	–0.67885189
E	0.45466821	0.49976750
F	–0.72497147	–0.82509890

GK – Koeppl's values obtained with 190 by 280 points grid

IR – Rutenburg's values obtained with 360 by 720 points grid used in this work; Koeppl's values were used as initial conditions

APPENDIX 28

Quadratic least squares (LS) fit and variational dividing surfaces (DS) for 1500 K temperature (T) for F + DH reaction. Variational DSs were obtained with no restrictions (N); LS DSs were used to generate vertices for variational searches. Rate constants (k(T)) are in 10^{12} $cm^3/mol \cdot s$. A,B,C,D,E, and F are variational parameters.

DS	LS	N
k(1500K)	154.46717	93.770471
A	0.75675210	1.5839356
B	1.9035620	0.729761383
C	−1.8788690	−4.8904310
D	-0.40051430×10^{-6}	0.13038164×10^{-5}
E	0.15468230	0.44716775
F	−1.4692780	−1.1204507

k(1500K)	LS	N
	163.75987	93.770489
A	0.69040310	1.5839268
B	1.7911690	0.72976013
C	−1.4815730	−4.8904103
D	-0.52489760×10^{-6}	0.30772507×10^{-5}
E	0.057518710	0.44716758
F	−1.1979240	−1.1204500

APPENDIX 29

Quadratic least squares (LS) fit and variational dividing surfaces (DS) for 1500 K temperature (T) for F + DH reaction. Variational DSs were obtained with slope (S) restriction; LS DSs were used to generate vertices for variational searches. Rate constants (k(T)) are in 10^{12} $cm^3/mol \cdot s$. A,B,C,D,E, and F are variational parameters.

DS	LS	S
k(1500K)	174.99064	91.610681
A	−0.63474440	4.4947089
B	0.81991400	2.0091216
C	1.4515680	−11.367076
D	0.29533270	−0.64210127
E	0.22146000	0.20442625
F	−0.94890510	−1.3594739

k(1500K)	LS	S
	154.64892	91.610655
A	−0.18870620	4.5147053
B	1.3718260	2.1036701
C	0.21315970	−11.405822
D	0.22679580	−0.64495790
E	0.136726400	0.16711664
F	−1.1049540	−1.3449734

k(1500K)	S (GK)	S (IR)
	94.371234	91.728875
A	3.6146794	4.4154167
B	0.32588262	1.7046384
C	−8.5989878	−11.181367
D	−0.5163860	−0.63077365
E	0.41293650	0.30784850
F	−0.76089663	−1.3745351

GK – Koeppl's values obtained with 190 by 280 points grid

IR – Rutenburg's values obtained with 360 by 720 points grid used in this work; Koeppl's values were used as initial conditions

APPENDIX 30

Quadratic least squares (LS) fit and variational dividing surfaces (DS) for 3000 K temperature (T) for F + DH reaction. Variational DSs were obtained with no restrictions (N); LS DSs were used to generate vertices for variational searches. Rate constants (k(T)) are in 10^{12} $cm^3/mol \cdot s$. A,B,C,D,E, and F are variational parameters.

DS	LS	N
k(3000K)	313.72073	239.84746
A	0.75675210	1.3731337
B	1.9035620	1.2332390
C	−1.8788690	−4.1469091
D	-0.40051430×10^{-6}	0.16070923×10^{-5}
E	0.15468230	0.31215782
F	−1.4692780	−1.1992651

k(3000K)	LS	N
	328.34496	239.84742
A	0.69040310	1.3731429
B	1.7911690	1.2332411
C	−1.4815730	−4.1469301
D	-0.52489760×10^{-6}	-0.43201791×10^{-6}
E	0.057518710	0.31215789
F	−1.1979240	−1.1992663

APPENDIX 31

Quadratic least squares (LS) fit and variational dividing surfaces (DS) for 3000 K temperature (T) for F + DH reaction. Variational DSs were obtained with slope (S) restriction; LS DSs were used to generate vertices for variational searches. Rate constants (k(T)) are in 10^{12} $cm^3/mol \cdot s$. A,B,C,D,E, and F are variational parameters.

DS	LS	S
k(3000K)	353.68291	235.64765
A	−0.63474440	3.4616987
B	0.81991400	1.8105969
C	1.4515680	−8.5079328
D	0.29533270	−0.49452838
E	0.22146000	0.18817255
F	−0.94890510	−1.2719780

k(3000K)	LS	S
	323.40066	235.53390
A	−0.18870620	3.5969363
B	1.3718260	2.1115355
C	0.21315970	−8.8955593
D	0.22679580	−0.51384772
E	0.136726400	0.11580405
F	−1.1049540	−1.3068950

k(3000K)	S (GK)	S (IR)
	241.73127	236.00357
A	2.6649164	3.4056656
B	0.30837955	1.7661116
C	−6.0398225	−8.2524825
D	−0.37404694	−0.48542972
E	0.38156257	0.13359240
F	−0.75284400	−1.1371776

GK – Koeppl's values obtained with 190 by 280 points grid

IR – Rutenburg's values obtained with 360 by 720 points grid used in this work; Koeppl's values were used as initial conditions

APPENDIX 32

Five–parameter least squares (LS) fit and variational dividing surfaces (DS) for 300 K temperature (T) for F + DH reaction. Variational DSs were obtained with no restrictions; LS DSs were used to generate vertices for variational searches. Rate constants (k(T)) are in 10^{12} $cm^3/mol \cdot s$. A, BAC, EAC, BAB, and EAB are variational parameters.

DS	LS	variational	LS	variational
k(300K)	7.3150126	5.1047472	7.5172632	5.1047472
A	0.86204100	0.40092300	1.0260790	0.40092300
BAC	–2.3856000	–4.6505110	–2.2365510	–4.6505111
EAC	0.22777180	0.97715923	0.13117960	0.97715924
BAB	–1.9540460	–6.3610307	–1.6937730	–6.3610304
EAB	0.30165200	1.7471427	0.18715490	1.7471426

DS	LS	variational	LS	variational
k(300K)	7.6683477	5.1047472	7.7096011	5.1047472
A	1.0450640	0.40094372	1.0289660	0.40092301
BAC	–2.1549980	–4.6504778	–2.0898300	–4.6505110
EAC	0.10316860	0.97714280	0.091689530	0.97715922
BAB	–1.60079100	–6.3609804	–1.6700870	–6.3610307
EAB	0.15482990	1.7471280	0.17947270	1.7471427

DS	LS	variational	LS	variational
k(300K)	8.0477613	5.1047472	9.0490737	5.1047472
A	1.0233740	0.40092283	1.2417800	0.40092063
BAC	–2.0802040	–4.6505112	–1.4949880	–4.6505089
EAC	0.090816840	0.97715934	–0.13845720	0.97715983
BAB	–1.3262830	–6.3610307	–0.99944570	–6.3610345
EAB	0.076871320	1.74714275	–0.070387440	1.7471443

APPENDIX 33

Five–parameter least squares (LS) fit and variational dividing surfaces (DS) for 300 K temperature (T) for F + DH reaction. Variational DSs were obtained with no restrictions; LS DSs were used to generate vertices for variational searches. Rate constants (k(T)) are in 10^{12} $cm^3/mol \cdot s$. A, BAC, EAC, BAB, and EAB are variational parameters.

DS	LS	variational	LS	variational
k(300K)	9.1216598	5.1047472	9.6603482	5.1047472
A	0.99557200	0.40092300	1.1132390	0.40104271
BAC	–1.6505420	–4.6505110	–1.1264300	–4.6503808
EAC	–0.012569250	0.97715922	–0.19113550	0.97708772
BAB	–1.0734810	–6.3610306	–1.6823240	–6.3608156
EAB	0.0066417990	1.7471427	0.16461720	1.7470546

DS	LS	variational	LS	variational
k(300K)	12.038319	5.1047472	12.867187	5.1047472
A	1.503987	0.40092301	1.2937370	0.40085656
BAC	–2.241668	–4.650511	–0.92544030	–4.6506818
EAC	–0.03431022	0.97715922	–0.30587100	0.97721413
BAB	0.4846572	–6.3610306	–0.028913680	–6.3611209
EAB	–0.5743715	1.7471427	–0.37410270	1.7471886

DS	LS	variational	LS	variational
k(300K)	80.375806	5.1047472	133.54949	5.1047472
A	1.0954760	0.40092302	0.87231540	0.40092300
BAC	0.25579610	–4.6505110	0.71670360	–4.6505110
EAC	–0.548122340	0.97715921	–0.59233090	0.97715922
BAB	–0.65461360	–6.3610306	–0.63516700	–6.3610306
EAB	0.14217710	1.7471426	–0.098061100	1.7471427

APPENDIX 34

Five–parameter least squares (LS) fit and variational dividing surfaces (DS) for 600 K temperature (T) for F + DH reaction. Variational DSs were obtained with no restrictions (N) and with slope (S) restriction DSs; LS DSs were used to generate vertices for variational searches. Rate constants (k(T)) are in 10^{12} $cm^3/mol \cdot s$. A, BAC, EAC, BAB, and EAB are variational parameters.

DS	LS	N	LS	S
k(600K)	34.802865	23.467340	30.251803	21.981156
A	0.99557200	0.52986014	1.0450640	0.53183608
BAC	–1.6505420	–4.3841054	–2.1549980	–4.3378702
EAC	–0.012569250	0.87492202	0.10316860	0.86601071
BAB	–1.0734810	–3.5579639	–1.6007910	–5.8923540
EAB	0.0066417990	0.88145455	0.15482990	1.6170660

DS	LS	S	LS	S
k(600K)	42.044656	21.981156	34.622777	21.981156
A	1.5039870	0.53183612	1.2417800	0.53183610
BAC	–2.2416680	–4.3378701	–1.4949880	–4.3378701
EAC	–0.034310220	0.86601068	–0.13845720	0.86601070
BAB	0.48465720	–5.8923577	–0.99944570	–5.8923540
EAB	–0.57437150	1.6170660	–0.070387440	1.6170660

DS	LS	N
k(600K)	42.044656	34.335167
A	1.5039870	2.3196577
BAC	–2.2416680	–2.3884174
EAC	–0.034310220	–0.31267227
BAB	0.48465720	0.48000000
EAB	–0.57437150	–0.75503572

APPENDIX 35

Five–parameter least squares (LS) fit and variational dividing surfaces (DS) for 1500 K temperature (T) for F + DH reaction. Variational DSs were obtained with no restrictions (N) and with slope (S) restriction; LS DSs were used to generate vertices for variational searches. Rate constants (k(T)) are in 10^{12} $cm^3/mol \cdot s$. A, BAC, EAC, BAB, and EAB are variational parameters.

DS	LS	S	LS	S
k(1500K)	125.14744	90.598337	113.28187	90.598337
A	0.99557200	0.69312537	1.0450640	0.69312537
BAC	–1.6505420	–3.8965085	–2.1549980	–3.8965085
EAC	–0.012569250	0.70825415	0.10316860	0.70825415
BAB	–1.0734810	–5.1861834	–1.6007910	–5.1861834
EAB	0.0066417990	1.4066468	0.15482990	1.4066468

DS	LS	S	LS	S
k(1500K)	139.837306	90.598337	124.26952	90.598337
A	1.5039870	0.69312538	1.2417800	0.69306570
BAC	–2.2416680	–3.8965085	–1.4949880	–3.8963898
EAC	–0.034310220	0.70825414	–0.13845720	0.70825839
BAB	0.48465720	–5.1861834	–0.99944570	–5.1861971
EAB	–0.57437150	1.4066468	–0.070387440	1.4066576

DS	LS	N
k(1500K)	139.83730	125.83237
A	1.5039870	2.1334963
BAC	–2.2416680	–2.5261995
EAC	–0.034310220	–0.22335097
BAB	0.48465720	0.48
EAB	–0.57437150	

APPENDIX 36

Five–parameter least squares (LS) fit and variational dividing surfaces (DS) for 3000 K temperature (T) for F + DH reaction. Variational DSs were obtained with slope (S) restriction; LS DSs were used to generate vertices for variational searches. Rate constants (k(T)) are in 10^{12} $cm^3/mol \cdot s$. A, BAC, EAC, BAB, and EAB are variational parameters.

DS	LS	S	LS	S
k(3000K)	278.99277	225.64809	258.97202	225.64809
A	0.99557200	0.78420330	1.0450640	0.78419885
BAC	–1.6505420	–3.4736721	–2.1549980	–3.4736752
EAC	–0.012569250	0.56000406	0.10316860	0.56000662
BAB	–1.0734810	–4.3507546	–1.6007910	–4.3507580
EAB	0.0066417990	1.1254670	0.15482990	1.1254696

DS	LS	S	LS	S
k(3000K)	304.27636	225.64809	276.70417	225.64809
A	1.5039870	0.78420331	1.2417800	0.78420256
BAC	–2.2416680	–3.4736721	–1.4949880	–3.4736731
EAC	–0.034310220	0.56000405	–0.13845720	0.56000465
BAB	0.48465720	–4.3507546	–0.99944570	–4.3507565
EAB	–0.57437150	1.1254670	–0.070387440	1.1254677

APPENDIX 37

Ten–parameter variational dividing surfaces (DS) obtained with slope (S) and energy (E) limit restrictions for 300 K temperature (T) for F + DH reaction. Rate constants (k(T)) are in 10^{12} cm^3/mol·s. A, EAC, BAC, EAB, BAB, D, FAC, HAC, FAB, and HAB are variational parameters.

DS	5–parameter	S #1	1500K S	S #2
k(300K)		4.50	84.07	4.5642
	in.vert. for	4.50	in.vert. for	4.5641
A	0.40	0.65377792	1.077238	1.0686535
EAC	–4.6	–11.119367	–8.8403282	–10.872891
BAC	0.98	3.7423976	2.8865812	3.5739874
EAB	–6.4	–12.970428	–9.8620056	–11.014253
BAB	1.7	4.9651041	3.9381221	4.0717566
D	0.0	–0.026679610	–0.13562938	–0.15243191
FAC	0.0	–0.015997257	–0.25630110	–0.31606439
HAC	0.0	–0.58153124	–0.42520578	–0.51073262
FAB	0.0	–0.044341476	–0.73696869	–0.75831177
HAB	0.0	–0.74143717	–0.57320151	–0.48436163

DS	E = 1.5 eV	E = 3.0 eV #1	E = 3.0 eV #2	E = 3.5 eV
k(300K)		4.3627955	4.3736656	4.374212
	in.vert. for	4.3627315	in.vert. for	4.374147
A	0.58	0.79701523	0.90693661	0.90692209
EAC	–16.	–16.469412	–15.803704	–15.791407
BAC	6.2	6.2294236	5.8784144	5.8714191
EAB	–14.	–15.571533	–15.516222	–15.455465
BAB	5.3	6.3228029	6.2586661	6.2352802
D	–0.059	–0.055530752	–0.09137408	–0.090761220
FAC	–0.021	–0.025933114	–0.02269297	–0.022552659
HAC	–1.1	–1.1537448	–1.062775	–1.0612496
FAB	–0.12	–0.15926600	–0.14197866	–0.14184244
HAB	–0.8	–1.0808865	–1.0572509	–1.0534842

S #1 has big islands
S #2 has no islands, is given in tables
All E have no islands
E = 3.0 eV #1 and E = 3.5 eV are given in tables

in.vert. – values used to generate vertices for variational search (initial vertices)

APPENDIX 38

Ten–parameter variational dividing surfaces (DS) obtained with slope (S) and energy (E) limit restrictions for 600 K temperature (T) for F + DH reaction.

Rate constants (k(T)) are in 10^{12} $cm^3/mol \cdot s$. A, EAC, BAC, EAB, BAB, D, FAC, HAC, FAB, and HAB are variational parameters.

DS	5–parameter	S #1	1500K S	S #2
k(600K)		20.006715	84.07	19.7613
	in.vert. for	20.006410	in.vert. for	19.7610
A	0.53	0.45925352	1.0772380	0.99378230
EAC	–4.3	–10.601927	–8.8403282	–10.000711
BAC	0.87	3.6875264	2.8865812	3.2908024
EAB	–5.9	–7.3645357	–9.8620056	–10.752419
BAB	1.6	2.3507898	3.9381221	4.1157636
D	0.0	0.083432710	–0.13562938	–0.13700965
FAC	0.0	–0.094687590	–0.25630110	–0.17875959
HAC	0.0	–0.63156720	–0.42520578	–0.47360105
FAB	0.0	–0.020198738	–0.73696869	–0.68173205
HAB	0.0	–0.18798259	–0.57320151	–0.53336400

DS	E = 3.0 eV	E = 3.0 eV	E = 3.0 eV	E = 3.5 eV
k(600K)		19.5	19.442295	19.1312
	in.vert. for	19.5	in.vert. for	19.1310
A	0.8	1.1702046	1.1553479	0.98238510
EAC	–16.	–16.446363	–16.193686	–15.044753
BAC	6.	6.0955918	6.016783	5.6731278
EAB	–16.	–15.390818	–15.617061	–15.468104
BAB	6.	6.3527521	6.43494956	6.5669600
D	–0.1	–0.14701804	–0.13202109	–0.036845324
FAC	–0.03	–0.032237866	–0.02740227	–0.027775032
HAC	–1.	–1.1091442	–1.1045700	–1.0896685
FAB	–0.1	–0.11815952	–0.11960874	–0.11876498
HAB	–1.	–1.1290873	–1.1455636	–1.2475515

S #2 is given in tables
All three E have no islands
E = 3.5 eV is given in tables

in.vert. – values used to generate vertices for variational search (initial vertices)

APPENDIX 39

Ten–parameter variational dividing surfaces (DS) obtained with slope (S) and energy (E) limit restrictions for 1500 K temperature (T) for F + DH reaction. Rate constants (k(T)) are in 10^{12} $cm^3/mol \cdot s$. A, EAC, BAC, EAB, BAB, D, FAC, HAC, FAB, and HAB are variational parameters.

DS	5–parameter	S		E = 3.0 eV #1
k(1500K)		84.07	83.747861	83.00
	in.vert. for	84.07	in.vert. for	83.00
A	0.69	1.1271424	1.0772380	1.3137707
EAC	–3.9	–11.0116721	–8.8403282	–12.558664
BAC	0.71	3.9653903	2.8865812	4.6439291
EAB	–5.2	–8.7596162	–9.8620056	–9.9135266
BAB	1.4	3.4061123	3.9381221	3.8378812
D	0.0	–0.16121366	–0.13562938	–0.18771692
FAC	0.0	–0.33309180	–0.25630110	–0.38636358
HAC	0.0	–0.67665847	–0.42520578	–0.93673573
FAB	0.0	–1.0720990	–0.73696869	–0.23573261
HAB	0.0	–0.41438957	–0.57320151	–0.57375507

DS		E = 3.0 eV #2		E = 3.5 eV
k(1500K)		82.57	← used as	82.605801
	in.vert. for	82.57	in.vert. for	82.605268
A	0.96	0.97549528		0.98458065
EAC	–12.	–12.047854		–12.018236
BAC	4.7	4.5084214		4.4551247
EAB	–14.	–14.117744		–14.188567
BAB	6.3	6.4481747		6.4355136
D	–0.088	–0.090590545		–0.088631171
FAC	–0.28	–0.27826224		–0.26519951
HAC	–0.87	–0.83416907		–0.81538534
FAB	–1.6	–1.0268748		–0.98158043
HAB	–1.2	–1.2706586		–1.2591824

S and E = 3.0 eV #1 are given in tables

in.vert. – values used to generate vertices for variational search (initial vertices)

APPENDIX 40

Ten–parameter variational dividing surfaces (DS) obtained with slope (S) and energy (E) limit restrictions for 3000 K temperature (T) for F + DH reaction. Rate constants (k(T)) are in 10^{12} cm^3/mol·s. A, EAC, BAC, EAB, BAB, D, FAC, HAC, FAB, and HAB are variational parameters.

DS	5–parameter	S #1	1500K S	S #2
k(3000K)		221.800	84.07	215.4
	in.vert. for	221.800	in.vert. for	215.4
A	0.78	1.4823691	1.0772669	0.96779026
EAC	–3.4	–4.5470957	–8.8396900	–7.6295509
BAC	0.56	0.86278393	2.8863062	2.4682394
EAB	–4.3	–4.1223493	–9.8622525	–8.2069382
BAB	1.1	0.86869277	3.9384380	3.2455816
D	0.0	–0.21176665	–0.13549864	–0.083332004
FAC	0.0	–0.20201530	–0.25623334	–0.22808266
HAC	0.0	–0.0060200261	–0.42526101	–0.39121714
FAB	0.0	0.081930572	–0.73713930	–0.62280712
HAB	0.0	0.088928791	–0.57332825	–0.49366407

DS		E eV	1500K E	E = 3.0 eV
k(3000K)		208.58504	83.00	212.45
	in.vert. for	208.58382	in.vert. for	212.45
A	2.6	4.7835280	1.2969858	1.2224399
EAC	–5.0	–6.0212654	–12.4319040	–9.9321680
BAC	0.62	0.020085600	4.6016381	3.5381662
EAB	–4.0	–4.6172632	–9.7995753	–9.4916158
BAB	0.56	0.45525527	3.8056902	4.0400463
D	–0.49	–0.83120327	–0.16681016	–0.15401664
FAC	1.2	4.6905715	–0.38372831	–0.21652424
HAC	0.028	0.0082838693	–0.84076762	–0.64176413
FAB	0.55	1.9224960	–0.23685991	–0.23589615
HAB	0.15	–0.010876691	–0.58047772	–0.78396810

S #2 is given in tables
E = 3.0 eV is given in tables

in.vert. – values used to generate vertices for variational search (initial vertices)

REFERENCES

1. H. Pelzer and E. Wigner, Z. Physik. Chem. **B 15**, 445 (1932).
2. J. Horiuti, Bull. Chem. Soc. Jpn. **13**, 210 (1938).
3. J. C. Keck, J. Chem. Phys. **29**, 410 (1958); **32**, 1035 (1960).
4. J. C. Keck, Adv. Chem. Phys. **13**, 85 (1967).
5. R. A. Marcus, J. Chem. Phys. **41**, 2614, 2624 (1964); **43**, 1598 (1965).
6. G. W. Koeppl, J. Am. Chem. Soc. **96**, 6539 (1974); D. I. Sverdlik and G. W. Koeppl, Chem. Phys. Lett. **59**, 449(1978).
7. G. W. Koeppl, J. Chem. Phys. **87**, 5746 (1987).
8. Pechukas in *Dynamics of Molecular Collisions, Part B*, edited by W. H. Miller (Plenum, New York, 1976), p 239.
9. P. Pechukas, Ann. Rev. Phys. Chem. **32**, 159 (1981).
10. P. Pechukas, Ber. Bunsenges. Phys. Chem. **86**, 372 (1982).
11. E. Pollak, in *The Theory of Chemical Reaction Dynamics*, edited by M. Baer (Chemical Rubber, Boca Raton, FL, 1984).
12. D. G. Truhlar, W. L. Hase, and J. T. Hynes, J. Phys. Chem. **87**, 2664 (1983).
13. D. G. Truhlar and B. C. Garrett, Ann. Rev. Phys. Chem. **35**, 159 (1984)
14. D. G. Truhlar, A. D. Isaacson, and B. C. Garrett, in *The Theory of Chemical Reaction Dynamics*, edited by M. Baer (Chemical Rubber, Boca Raton, FL, 1984)
15. W. J. Chesnavich and M. T. Bowers, in *Gas–Phase Ion Chemistry*, edited by M. T. Bowers, (Academic, New York, 1979), p 119.
16. W. J. Chesnavitch and M. T. Bowers, *Prog. React. Kinet.* **11**, 137 (1982).
17. R. B. Walker and J. C. Light, Ann. Rev. Phys. Chem. **31**, 401 (1980).
18. M. Menendez, L. Banares, J. Alonso and G. Urena, Chem. Phys. **120**, 273–289 (1988).

19. R. D. Levine, Chem. Phys. Lett. **175**, 331–337 (1990).

20. D. G. Truhlar and B. C. Garrett, J. Phys. Chem. **96**, 6515–6518 (1992).

21. R. J. Frost and I. W. M. Smith, J. Chem. Soc, Faraday Trans. **84**, 1825 (1988).

22. G. A. Voth, D. Chandler, and W. H. Miller, J. Chem. Phys., **91**, 7749 (1989).

23. R. Hernandez and W. H. Miller, Chem. Phys. Lett **214**, 129–136 (1993).

24. W. H. Miller, Acc. Chem. Res. **26**, 174–181 (1993).

25. E. Pollak and D. Proselkov, Chem. Phys. **170**, 265–273 (1993).

26. W. H. Miller, Ber. Bunsenges. Phys. Chem. **95**, 389–393 (1991).

27. H. Eyring, J. Chem. Phys. **3**, 107 (1935).

28. S. Glasstone, K. J. Laidler, and H. Eyring, *Theory of Rate Processes* (McGraw–Hill, New York, 1941).

29. M. C. Evans and M. Polanyi, Trans. Faraday Soc. **31**, 875 (1935).

30. G. W. Koeppl, J. Am. Chem. Soc. **96**, 6539 (1974).

31. J. O. Hirschfelder, Int. J. Quant. Chem. **IIIS**, 17–31 (1969).

32. P. Pechukas and F. J. McLafferty, J. Chem. Phys. **58**, 1622 (1973).

33. K. Morokuma and M. Karplus, J. Chem. Phys. **55**, 63 (1971).

34. G. W. Koeppl and M. Karplus, J. Chem. Phys. **55**, 4667 (1971).

35. D. L. Martin and L. M. Raff, J. Chem. Phys. **77**, 1235 (1982).

36. D. I. Sverdlik and G. W. Koeppl, J. Chem. Phys. **91**, 250–270 (1989).

37. I. Schecter, R. D. Levine, and R. B. Bernstein, J. Phys. Chem. **91**, 5466–5471 (1987).

38. I. Schecter, M. G. Prisant, and R. D. Levine, J. Phys. Chem. **91**, 5472–5480 (1987).

39. J. N. L. Connor, J. C. Whitehead, and W. Jakubetz, J. Chem. Soc., Faraday Trans. **83**, 1703–1718 (1987).

40. J. N. L. Connor and W. Jakubetz, J. Chem. Soc., Faraday Trans. **89**,

1481–1486 (1993).

41. C. F. Bender, B. J. Garrison, and H. F. Schaefer, J. Chem. Phys. **62**, 1188–1190 (1975).
42. M. J. Frisch, B. Liu, J. S. Binkley, H. J. Schaefer, and W. H. Miller, Chem. Phys. Lett. **114**, 1–5 (1985).
43. D. G. Truhlar, B. C. Garrett, and N. C. Blais, J. Chem. Phys. **80**, 232 (1984).
44. D. W. Schwenke, R. Stekler, F. B. Brown, and D. G. Truhlar, J. Chem. Phys. **84**, 5706–5710 (1986).
45. F. Brown, R. Stekler, D. W. Schwenke, D. G. Truhlar, and B. C. Garrett, J. Chem. Phys. 82, 188 (1985).
46. R. Stekler, D. G. Truhlar, and B. C. Garrett, J. Chem. Phys. **82**, 5499 (1985).
47. C. W. Bauschlicher, Jr., S. P. Walch, S. R. Langhoff, P. R. Taylor, and R. L. Jaffe, J. Chem. Phys. **88**, 1743–1751 (1988).
48. G. C. Lynch, R. Stekler, D. W. Schwenke, A. J. C. Varandas, D. G. Truhlar, and B. C. Garrett, J. Chem. Phys. **94**, 7136 (1991).
49. T. Takayanagi and S. Sato, Chem. Phys. Lett. **144**, 191 (1988).
50. S. L. Mielke, G. C. Lynch, D. G. Truhlar, and D. W. Schwenke, Chem. Phys. Lett. **213**, 10–16 (1993).
51. J. T. Muckerman, J. Chem. Phys. **54**, 1155 (1971).
52. A. Persky, J. Chem. Phys. 59, 5578–5584 (1973).
53. M. J. Berry, J. Chem. Phys. **59**, 6229–6253 (1973).
54. R. K. Sparks, C. C. Hayden, K. Shobatke, D. M. Neumark, and Y. T. Lee, "Horizons of Quantum Chemistry", K. Fukui and B. Pullman (Eds.), D. Reidel Publishing Co. (1980).
55. R. F. Heidner, J. F. Bott, C. E. Gardner, and J. E. Melzer, J. Chem. Phys. **72**, 4815 (1980)
56. E. Wurzburg and P. L. Houston, J. Chem. Phys. **72**, 4811 (1980).

57. J. T. Muckerman, in *Theoretical Chemistry*, D. Henderson, Ed., Vol. 6A,Academic Press, N. Y., (1981)

58. K. T. Lee and J. M. Bowman, J. Phys. Chem. **86**, 2289–2291 (1982).

59. K. Tsukiyama, B. Katz, and R. Bersohn, J. Chem. Phys. **83**, 2889–2893 (1985).

60. E. Pollak, Chem. Phys. Lett. **119**, 98 (1985).

61. I. Schecter and R. D. Levine, Int'l. Chem. Kin. **18**, 1023 (1986).

62. H. Kornweitz, A. Persky, and R. D. Levine, Chem. Phys. Lett. **128**, 443–448 (1986).

63. D. R. Herschbach, R. B. Berstein, and R. D. Levine, J. Phys. Chem. **91**, 5365 (1987).

64. H. R. Mayne, J. Phys. Chem. **92**, 6289–6293 (1988).

65. F. E. Budenholzer and D. C. Jeng, Chem. Phys. Lett., **156**, 411–414 (1989).

66. M. A. Ioffe, Y. M. Gershenzou, V. B. Rozenshtein, and S. Y. Umanskii, Chem. Phys. Lett. **154**, 131–134 (1984).

67. C. Yu, Y. Sun, D. J. Kouri, P. Halvick, D. G. Truhlar, and D. W. Schwenke, J. Chem. Phys. **90**, 7608–7609 (1989).

68. M. D'Mello, D. E. Manolopoulos, and R. E. Wyatt, Chem. Phys. Lett., **168**, 113–118 (1990).

69. D. E. Manolopoulos, M. D'Mello, R. E. Wyatt, and R. B. Walker, Chem. Phys. Lett., **169**, 482–488 (1990).

70. T. Toshiyuki, S. Tsunoshimo, and S. Sato, J. Chem. Phys. **93**, 2487–2492 (1990).

71. G. W. Johnston, H. Kornweitz, I. Schecter, A. Persky, B. Katz, R. Bersohn, and R. D. Levine, J. Chem. Phys. **94**, 2749–2756 (1990).

72. G. C. Lynch, P. Halvick, M. Zhao, D. G. Truhlar, C. Yu, D. J. Kouri, and D. W. Schwenke, J. Chem. Phys. **94**, 7150–7158 (1991).

73. A. Lazarides, D. Neuhauser, and H. Rabitz, J. Chem. Phys. **99**, 6653–6666 (1993).

74. J. D. Kress, J. Chem. Phys. **98**, 5106 (1993).

75. D. E. Manolopoulos, K. Stark, H. J. Werner, D. W. Arnold, S. E. Bradforth, and D. M. Neumark, Science **262**, 1852 (1993).

76. G. C. Schatz, Science **262**, 1828 (1993).

77. F. J. Aoiz, V. T. Herrero, M. M. Nogueira, and V. S. Rabanos, Chem. Phys. Lett. **211**, 72–81 (1993).

78. F. J. Aoiz, V. T. Herrero, M. M. Nogueira, and V. S. Rabanos, Chem. Phys. Lett. **204**, 359–367 (1993).

79. F. J. Aoiz, L. Banares, V. T. Herrero, and V. S. Rabanos, Chem. Phys. Lett. **218**, 422–432 (1994).

80. W. H. Miller, J. Chem. Phys. **61**, 1823 (1974).

81. B. C. Garrett and D. G. Truhlar, J. Chem. Phys. **70**, 1593 (1979).

82. W. H. Miller, J. Chem. Phys. **65**, 2216 (1976); Acc. Chem. Res. **9**, 306 (1976).

83. J. B. Anderson, J. Chem. Phys. **58**, 4684 (1973); **60**, 2566 (1974); **67**, 2446 (1975).

84. E. Pollak and P. Pechukas, J. Am. Chem. Soc. **100**, 2984 (1978).

85. D. R. Coulson, J. Am. Chem. Soc. **100**, 2992 (1978).

86. R. N. Porter, D. L. Thompson, L. M. Raff, and J. M. White, J. Chem. Phys. **62**, 2429 (1975).

87. B. C. Garrett and D. G. Truhlar, J. Phys. Chem. **83**, 1052 (1979)

88. M. Karplus, R. N. Porter, and R. D. Sharma, J. Chem. Phys. **43**, 3259 (1965).

89. K. Morokuma, B. C. Eu, and M. Karplus, J. Chem. Phys. **51**, 5193 (1969).

90. M. A. Eliason and J. O. Hirschfelder, J. Chem. Phys. **30**, 1426 (1959).

91. J. Ross and P. Mazur, J. Chem. Phys. **35**, 19 (1961).

92 L. A. Pipes, *Applied Mathematics for Engineers and Physicists* (McGraw–Hill,

New York, 1946).

93. F. London, Z. Elektrochem. **35**, 552 (1929).

94. H. Eyring and M. Polanyi, Z. Phys. Chem. **B12**, 279 (1931).

95. S. Sato, Bull. Chem. Soc. Jap. **28**, 450 (1955); J. Chem. Phys. **23**, 592, 2465 (1955).

96. P. J. Kuntz, E. M. Nemeth, J. C. Polanyi, S. D. Rosner, and C. E. Young, J. Chem. Phys. **44**, 1168 (1966).

97. J. A. Nelder and R. Mead, Computer J. **7**, 308 (1965).

98. W. H. Press, B. P. Flannery, S. A. Tevkolsky, and W. T. Vetterling, *Numerical Recipes* (Cambridge University Press, Cambridge, 1986).

99. E. Pollak and P. Pechukas, J. Chem. Phys. **69**, 1218 (1978).

100. D. I. Sverdlik, G. P. Stein, and G. W. Koeppl, Chem. Phys. Lett. **67**, 87 (1979).

101. G. P. Stein, Ph. D. Dissertation, The City University of New York, 1977.

102. B. C. Garett, D. G. Truhlar, J. Am. Chem. Soc. **101**, 4534 (1979).

103. B. C. Garett, D. G. Truhlar, and R. S. Grev, J. Phys. Chem. **85**, 1569 (1981).

104. W. J. Chesnavich, Chem. Phys. Lett. **53**, 300 (1978).